AFCRL-65-258

A STUDY OF PS CONVERTED WAVES

Kenneth L. Cook and John K. Costain

University of Utah
Salt Lake City, Utah

Contract No. AF19(628)-201

Project No. 8652

Task No. 865202

FINAL REPORT

April 30, 1965

WORK SPONSORED BY ADVANCED RESEARCH PROJECTS AGENCY

Project VELA UNIFORM

ARPA Order No. 180-16, Amendment 2
Project Code No. 8100, Task 2

Prepared
for
AIR FORCE CAMBRIDGE RESEARCH LABORATORIES
OFFICE OF AEROSPACE RESEARCH
UNITED STATES AIR FORCE
BEDFORD, MASSACHUSETTS

AFCRL-65-258

A STUDY OF PS CONVERTED WAVES

Kenneth L. Cook and John K. Costain

University of Utah
Salt Lake City, Utah

Contract No. AF19(628)-201

Project No. 865

Task No. 865202

FINAL REPORT

April 30, 1965

WORK SPONSORED BY ADVANCED RESEARCH PROJECTS AGENCY

Project VELA UNIFORM

ARPA Order No. 180-16, Amendment 2
Project Code No. 8100, Task 2

Prepared
for
AIR FORCE CAMBRIDGE RESEARCH LABORATORIES
OFFICE OF AEROSPACE RESEARCH
UNITED STATES AIR FORCE
BEDFORD, MASSACHUSETTS

NOTICES

Request for additional copies by agencies of the Department of Defense, their contractors, and other government agencies should be directed to:

DEFENSE DOCUMENTATION CENTER (DDC)
CAMERON STATION
ALEXANDRIA, VIRGINIA 22314

Department of Defense Contractors must be established for DDC services or have their "need-to-know" certified by the cognizant military agency of their project or contract.

All other persons and organizations should apply to the:

U.S. DEPARTMENT OF COMMERCE
OFFICE OF TECHNICAL SERVICES
WASHINGTON 25, D. C.

CONTENTS

CONTENTS (con't)

ONTENTS (con't) Page

APPENDICIES

EXHIBITS

ILLUSTRATIONS

ILLUSTRATIONS (con't.)

ILLUSTRATIONS (con't.)

ILLUSTRATIONS (con't.)

Tables

CHAPTER I

INTRODUCTION

The purpose of this investigation was to make a detailed study of the fundamental properties of PS converted waves to ascertain whether they can be detected consistently on seismograms from both underground nuclear explosions and earthquakes and whetner they can be used to help distinguish underground nuclear explosions from earthquakes. The study included:

a. Theoretical considerations of the amplitudes of PS and other converted waves as compared to observed amplitudes.

b. Harmonic analysis of seismograms to aid in the interpretation.

c. Analysis of seismograms of underground nuclear explosions and large, distant earthquakes recorded at the University of Utah seismograph stations and other selected stations to develop dependable criteria for recognition of PS converted waves on seismograms.

d. The analysis of selected seismograms from underground nuclear explosions for recognition of PS converted waves recorded by vertical- and horizontal-component seismometers at the Geotech field stations.

General background

A PS converted wave is a seismic body wave which results from the conversion of an incident parent P wave at a boundary within the earth's crust or upper mantle to a refracted vertically polarized shear wave, SV. Other types of conversion are also possible, as for example, the conversion of an incident SV wave to a P wave.

Although this study was originally intended to concentrate on the P to S conversion, it was recognized during the course of the investigation that other types of conversion within the earth's crust and upper mantle are also of importance in seismology and therefore also in the problem of distinguishing earthquakes and underground nuclear explosions. Consequently this study was expanded to include some of these other types of conversions. It should be emphasized, however, that our study is concerned principally with those types of conversions that would arrive before the conventional body shear wave and for the most part within approximately one minute after the arrival of the initial P wave.

Most of the previous work by Soviet and American investigators on P to S conversions has been summarized and evaluated by Cook, Algermissen, and Costain (1962, p. 4775). As of 1962, the tentative results of the research on PS converted waves, principally for epicentral distances less than 400 km, can be summarized as follows:

1. The amplitude of the PS converted waves were usually several times greater than that of the first arrival of the P wave, but not without exception.

2. The successively later arrivals of PS converted waves from successively deeper horizons showed progressively greater ground-velocity amplitudes.

3. For blasts, the periods of the various PS converted waves were approximately the same as those of the parent P wave (Schwind and others, 1960); whereas for earthquakes, the periods of the PS converted waves were 1.3 to 1.7 times larger than those of the parent P wave (Kuz'mina, 1959).

It should be emphasized that it is desirable to compile particle-motion diagrams or similar aids to the identification of the PS converted waves. As of 1962, particle-motion diagrams in PS converted waves studies had been published only by the American workers (Schwind and others, 1960). Of the Soviet workers, Kuz'mina (1959) was the only one who reported compiling particle-motion diagrams, but his were not published.

The tentative interpretations that have been made in the limited time available on this research project indicate that converted body waves may constitute a recognizable part of the early arriving seismic energy within about 30 sec after the first arrival of the energy of the compressional P wave and before the arrival of the conventional body shear wave at epicentral distances up to about 10,000 km. We include in converted waves the energy that is both refracted and reflected at boundaries within the earth's crust and upper mantle.

Data necessary in the study of PS converted waves

To facilitate the identification of PS converted waves in particular and converted waves in general, it is desirable to know the crustal section and velocities in the region of study. Even with this information available, considerable difficulty may be experienced with multiple reflections. This problem has been discussed briefly by Cook, Algermissen, and Costain (1962, p. 4776).

Particle-motion diagrams greatly facilitate the identification of PS converted waves. Often, the beginning of a phase on a seismogram is difficult to determine without the aid of a particle-motion diagram. In a comparison of observed data with theory, such factors as near-surface layering and instrument response must be considered.

CHAPTER II

EQUIPMENT AND INSTRUMENTATION

Permanent seismograph stations

Most of the seismograms from permanent seismograph stations used for analysis in this study were recorded at the three seismograph stations of the University of Utah. Table 2-2 gives the principal facts of these stations and pertinent information concerning the instrumentation, including the magnifications. The Portable Benioff seismographs at all three stations, the Wood-Anderson seismographs at Dugway and Price, and allied instrumentation were funded largely from this project; and this instrumentation was installed prior to October 1, 1963.

Some seismograms used for analysis, especially during the earlier part of the study, were recorded at other permanent seismograph stations. Table 2-2 gives the available principal facts and pertinent information concerning the instrumentation of these stations.

For the analyses of seismograms from the permanent seismograph stations, the seismograms were usually used from vertical and horizontal seismometers which were matched and which also had essentially the same magnification. In those cases in which the magnifications of the matched instruments differed, the digitized values as measured on the seismograms were normalized.

Table 2-1-- Seismograph stations of the University of Utah

Dugway, Utah* (DUG)

Latitude: 40° 11.7' N Longitude: 112° 49.0' W
Elevation: 1481 meters Bedrock: Rhyolite-quartz dacite flow (Tertiary)
Locality: The vault is located 5 miles southwest of Dugway, Utah and is underground.
Time: Standard timing system of the World-Wide Seismograph System, Model 10700, The Geotechnical Corporation, Garland, Texas. Time signal impressed every 6 hours.
Instruments: Standard Benioff three-component seismographs (Z,N.E)**; To = 1 sec, Tg = 0.75 sec, Mag. = 400,000#, trace speed 60 mm per minute; Portable Benioff three-component seismographs (Z,N,E)***, To = 1 sec, Tg = 1.5 sec, Mag. = 100,000#, trace speed 60 or 120 mm/min; Wood-Anderson horizontal torsion seismographs (N,E)***, To = 0.8 sec, Mag. = 2,800, trace speed 60 mm per minute.

Price, Utah (PCU)

Latitude: 39° 36.4' N Longitude: 110° 48.3' W
Elevation: 1714 meters Bedrock: Mancos shale (Cretaceous)
Locality: The vault is located on the campus of Carbon College, Price, Utah
Time: Simplex Master Clock calibrated against WWV. Time signals impressed manually twice daily.
Instruments: Portable Benioff three-component seismographs (Z,N,E)****; To = 1 sec, Tg = 1.5 sec, Mag. = 36,100 (Z) and 14,000 (N,E), trace speed 60 or 120 mm/min; Wood-Anderson horizontal torsion seismographs (N,E); To = 0.8 sec, Mag. = 2,800, trace speed 60 mm/min.

* One of the stations in the World-Wide Network of Standardized Seismographs operated in conjunction with the U. S. Coast & Geodetic Survey.

** Instruments placed in operation May 6, 1962.
*** Instruments placed in operation on September 30, 1963.
**** Instruments placed in operation on May 16, 1962.

All three components (Z,N,E).

Table 2-1(continued)-- Seismograph stations of the University of Utah

Salt Lake City, Utah (SLC)

Latitude: 40° 45.9' N Longitude: 111° 50.9' W
Elevation: 1425 meters Bedrock: Quaternary alluvium
Locality: The vault is located on the campus of the University of Utah, Salt Lake City, Utah
Time: IBM Master Clock, calibrated against WWV. WWV receiver equipped with radio time-signal converter and amplifier for impression of time signals directly on each seismogram. Time signal impressed twice daily.
Instruments: Portable Benioff three-component seismographs (Z,N,E)*****; To = 1 sec, Tg = 1.5 sec, Mag. = 30,000 (Z) and 25,000 (N,E), trace speed 60 or 120 mm/min.

***** Instruments placed in operation on April 8, 1962.

Table 2-2-- Other permanent seismograph stations, from which seismograms were used in this study.

Boulder City, Nevada (BCN)

Latitude: 35° 58' 51" N
Longitude: 114° 50' 02" W
Elevation: 776 meters

Instrumentation January 15, 1962 (written communication Jan. 15, from Capt. R. A. Earle, U. S. Coast and Geodetic Survey)

3 Benioff Moving Coil Short Period

	Z	E-W	N-S
Tg	0.45 sec	0.45 sec	0.45 sec
To	1.4 sec	1.4 sec	1.4 sec
Seismometer damping	Near critical	Critical	Critical
Magnification (Operating)	100,000 ca	50,000 ca	50,000 ca

Note: The above applies to film magnified 8 times.

Flaming Gorge, Utah (FGU)

Latitude: 40° 55' 35.5" N
Longitude: 109° 23' 10.3" W
Elevation: 1982.5 meters

Instrumentation January 8, 1962 (written communication January 8, 1962 from Capt. R. A. Earle, U. S. Coast and Geodetic Survey)

3 Benioff Moving Coil Short Period

	Z	E-W	N-S
Tg	0.33 sec	0.58 sec	0.35 sec
To	1.06 sec	1.48 sec	1.41 sec
Galv. Damping	6:1	Near critical	3:1
Seismo. Damping	Near critical	3:1	Near critical
Magnification (Operating)	150,000 ca	65,000 ca	65,000 ca
Relative dial setting Mag.	60	60	60

Note: Avove applies to film magnified 8 times.

Table 2-2(continued).-- Other permanent seismograph stations, from which seismograms were used in this study.

La Paz, Bolivia (LPB)

Latitude: 16° 31' 57.6" S
Longitude: 68° 05' 54.1 W
Elevation: 3292 meters

Instrumentation: Standardized seismographs, World-wide network of U. S. Coast and Geodetic Survey
Magnification of Z, E-W, and N-S: approximately 50,000 at 1 cps.

La Palma, El Salvador (LPS)

Latitude: 14° 17' 32.0" N
Longitude: 89° 09' 43.0 W
Elevation: 1000 meters

Instrumentation: Standardized seismographs, World-wide network of U. S. Coast and Geodetic Survey

Magnification of Z, E-W, and N-S: approximately 100,000 at 1 cps.

Stations of the Long-Range Seismic Measurements Program
(Geotech stations)

Sites in the western part of the United States recording underground nuclear explosions at the Nevada test site are shown in Figure 5-1 . These sites are occupied as part of the Long-Range Seismic Measurements (LRSM) program and are operated by the Geotechnical Corporation as part of the VELA UNIFORM program.

Data are recorded in the field on an Ampex 14-channel magnetic-tape system, Model 314, and are frequency-modulated with a 270-cps center-frequency carrier. Field recordings are made at a tape speed of 0.3 ips.

Selected segments of data from each of these LRSM stations for each event are re-recorded onto a single reel of tape to form a magnetic tape composite of a single event. A typical composite contains data from about forty stations, recorded in the order of increasing distance from the signal epicenter. Approximately 30 minutes of data are recorded from each station. Both short-period and long-period data are recorded.

Three short-period seismometers at each LRSM site, either large or small Benioff seismometers, are oriented in vertical, radial and transverse directions with respect to the azimuth to the epicenter. The response of the short-period system peaks at about 2.6 cps. Magnifications varied from site to site.

We have further edited the magnetic tape composites of certain underground nuclear explosions, and put the well-recorded short-period data on new composites, which were later digitized. This is discussed more fully in Chapter IV.

CHAPTER III
THEORETICAL STUDIES

Energy and amplitude ratios of converted waves

A study was made of amplitude ratios, energy ratios, and phase angles of reflected and refracted P and SV waves derived from SV waves or P waves incident on a plane interface. All computations were programmed in FORTRAN for the IBM 7040 and 1620 systems. These programs are listed in the Appendix; Program 18 deals with incident P waves and Program 19 with incident SV waves. Incident angles were varied from 0° to 88°. Both real and imaginary coefficients were considered in the calculations. Reflection and transmission coefficients were calculated for P and SV waves for various velocity and density ratios.

Results of a plane SV wave incident on a plane interface are described in Costain, Cook and Algermissen (1963; 1965) and by Costain and Cook (1965). In these publications, energy ratios from Knott's energy equation and amplitude ratios and phase angles from the Zoeppritz equations were calculated for a plane SV wave incident on a plane elastic discontinuity using Program 19. Incident angles were varied from 0° to 88° in increments of 2° except near the critical angles, and near phase changes of 180° in the real domain, where the ratios were calculated in increments of 0.25°. Compressional velocity ratios (transmitted/incident) of 0.7, 0.8 and 0.9, and density ratios (transmitted/incident) of 0.7, 0.8, 0.9 and 1.0 were used. Poisson's ratio was 0.25 for each medium. Some calculations for a Poissons ratio of 0.400 are given in Costain and Cook (1965).

A layered crustal section was investigated and a FORTRAN program written (Program 9A) to calculate the theoretical amplitudes to be expec-

ted from converted and unconverted P and S waves on the basis of reflection coefficients from the Zoeppritz equations. The program assumes layer thicknesses large compared with the wavelength involved. Some results are presented in Costain, Cook and Algermissen (1963).

Theoretical travel-time curves

Theoretical travel-time curves were computed (using Program DR-13 listed in the Appendix) for many crustal models in the western part of the United States. These curves include all P and S head waves from each interface, and converted head waves such as PPPSS, SSPSS, SSPPP, etc. The models are based on seismic refraction studies by the United States Geological Survey, University of Utah, and others. The travel-time curves were used to aid in the interpretation of the events on the seismograms out to the arrival of the body S-wave. In addition, certain reflected and multiply reflected phases were added to the travel-time curves (Appendix: Programs 5 and 21).

Other theoretical work was primarily of a nature to aid in the interpretation of the early part of the seismogram, and included:

a) Computation of the power density spectrum from the cosine transform of the autocorrelation function (Program No. DR 12-B).

b) Computation of head wave coefficients for a PPP head wave using the method of Zvolinskii (Program No. 1).

A complete list of the theoretical, utility, and data analysis programs is contained in the Appendix.

Theoretical Particle-Diagram Motion

Particle-motion in an infinite, homogeneous, isotropic medium was examined theoretically for certain simple combinations of P and S motion. The following diagrams were constructed according to the diagram of Figure 3-1a.

Fig. 3-1b: Two P waves of amplitudes A_1 and A_2 ($A_1 = 10$; $A_2 = 12$) arriving at a point at different angles of incidence, i ($\Delta i = 10°$). Both wave trains have the same frequency (1 cps), but differ in phase by an amount $\pi/6$. The x-component of motion is given by:

$$x = 10 \sin (2\pi t) \sin 10° + 12 \sin (2\pi t + \pi/6) \sin 70°.$$

The vertical, or y-component of motion is given by:

$$y = 10 \sin (2\pi t) \cos 10° + 12 \sin (2\pi t + \pi/6) \cos 70°$$

The resultant motion is shown in Figure 3-1b.

Fig. 3-1c: Pure P and pure S arriving simultaneously with the S-amplitude ($A_s = 15$) greater than the P-amplitude ($A_p = 10$). The two wave trains arrive at the same angle of incidence (i = 20°) but differ in phase by an amount $\pi/6$. Both have a frequency of 1 cps. The equations that describe the x- and y- components of motion are

$$x = 10 \sin (2\pi t) \cos 20° - 15 \sin (2\pi t + \pi/6) \sin 20°$$

$$y = 10 \sin (2\pi t) \sin 20° + 15 \sin (2\pi t + \pi/6) \cos 20°$$

The resultant motion is shown in Figure 3-1c.

Fig. 3-1d: Pure P and pure S arriving simultaneously with continuously decreasing amplitudes, the amplitude of S decreasing faster than the amplitude of P. Initially $A_s > A_p$. Both wave trains arrive at the same angle of incidence (i = 30°) and have the same frequency (1 cps), but differ in phase by an amount $\pi/6$.

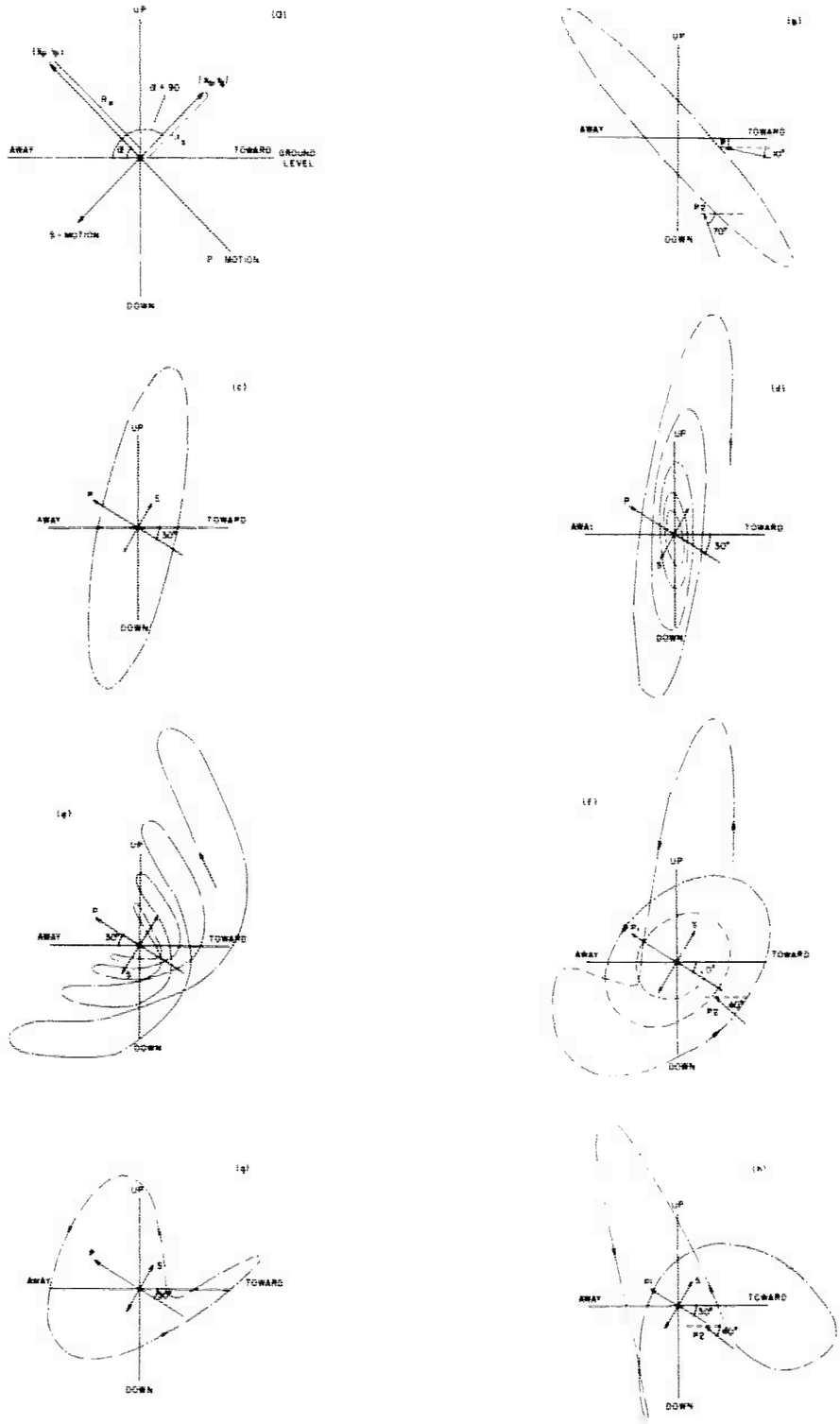

Figure 3-1. Theoretical vertical particle-motion diagrams.

$$x = (20/e^{0.4t}) \sin (2\pi t) \cos 30° - (50/e^{0.6t}) \sin (2\pi t + \pi/6) \sin 30°$$

$$y = (20/e^{0.4t}) \sin (2\pi t) \sin 30° + (50/e^{0.6t}) \sin 2\pi t + \pi/6) \cos 30°$$

The resultant motion is shown in Figure 3-1d.

Fig. 3-1e: P and S both decreasing in amplitude at different rates ($A_S > A_P$), arriving at the same angle of incidence, differing in phase by an amount $\pi/6$, and with the frequency of the P-wave equal to twice the frequency of the S-wave.

$$x = (20/e^{0.4t}) \sin (4\pi t) \cos 30° - (50/e^{0.6t}) \sin (2\pi t + \pi/6) \sin 30°$$

$$y = (20/e^{0.4t}) \sin (4\pi t) \sin 30° + (50/e^{0.6t}) \sin (2\pi t + \pi/6) \cos 30°$$

The resultant motion is shown in Figure 3-1e.

Fig. 3-1f: P_1 and S arriving simultaneously followed by P_2 after a time t (t = 0.45 sec).

A_s decreases faster than A_{p2} which decreases faster than A_{p1}.

P_1 and S arrive at the same angle of incidence; P_2 arrives at a slightly different angle. All arrivals have the same frequency but differ in phase. This example is shown in Figure 3-1f.

Fig. 3-1g: P and S arriving at same angle of incidence. Both waves have the same constant amplitude ($A_s = A_p$) but differ in phase and frequency (frequency of S = 6/5 cps; frequency of P = 4/5 cps).

$$x = 10 \sin (8\pi t/5) \cos 30° - 10 \sin (12\pi t/5 + \pi/6) \sin 30°$$

$$y = 10 \sin (8\pi t/5) \sin 30° - 10 \sin (12\pi t/5 + \pi/6) \cos 30°$$

This example is shown in Figure 3-1g.

Fig. 3-1h: P_1, P_2 and S all with the same constant amplitude.

P_1 and S arrive at the same angle of incidence.

P_1 and P_2 are in phase with each other, but out of phase with S.

All have different frequencies (P_1 = 4/5 cps; P_2=8/5 cps; S = 6/5 cps).

$$x = 10 \sin (8\pi t/5) \cos 30° - 10 \sin (12\pi t/5 + \pi/6) \sin 30° + 10 \sin (16\pi t/5) \cos (\pi/4.5)$$

$$y = 10 \sin (8\pi t/5) \sin 30° + 10 \sin (12\pi t/5) + \pi/6) \cos 30° + 10 \sin (16\pi t/5) \sin (\pi/4.5)$$

The plots in Figure 3-1 are representative of at least a few of the types of particle-motion diagrams that can be expected in the simplest cases. The examples described above do not include the effects of instrument response, the effects of a free surface, the effects of layering, inhomogeneities, or anisotropy. Diagrams similar to those in Figure 3-1 are frequently observed on actual particle-motion diagrams of ground motion. However, this should not imply that the theoretical and observed particle-motion diagrams that resemble each other have a common origin. The simple theoretical study shows that differences in wave type, frequency, phase, and rates of change of amplitude of phases arriving simultaneously at a point does give a combined affect which resembles actual particle-motion diagrams in many instances. Further study is necessary to determine the relative importance of each of these effects, as well as the effects of a layered half-space.

Figure 3-2 shows four representative particle-motion diagrams that in some respects closely resemble the theoretical diagrams of Figure 3-1. All four diagrams show motion in a vertical-radial plane. Diagrams (a), (b), (c), and (d) of Figure 3-2 are to be compared with diagrams (e), (g), (d) and (h), respectively, of Figure 3-1.

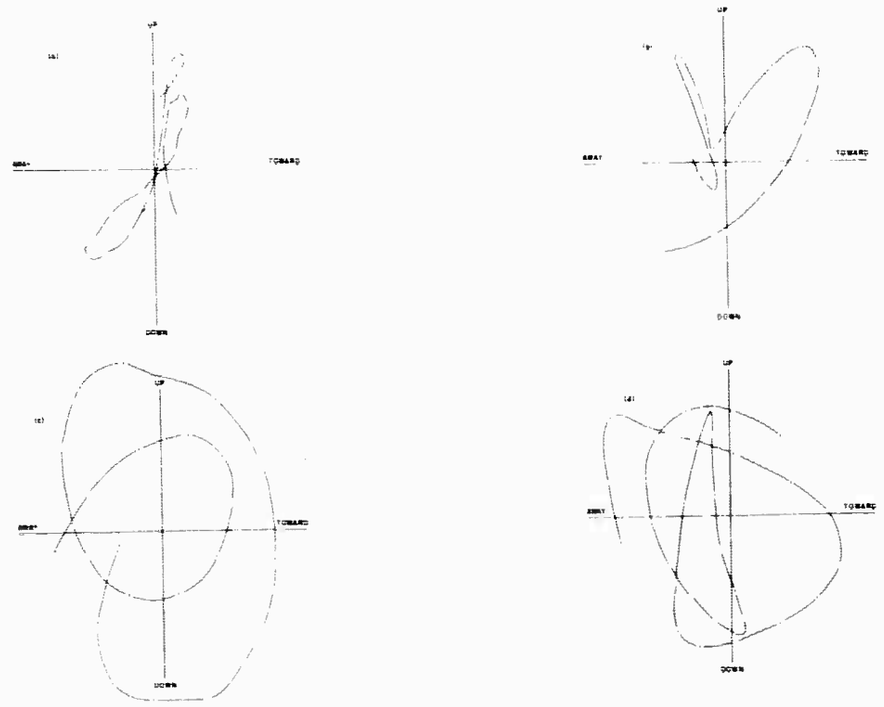

Figure 3-2. Observed vertical particle-motion diagrams.

(a) Particle-motion diagram of the AARDVARK event as recorded at station MNNV. Time: P_n + 16.95 sec.

(b) Particle-motion diagram of the STILLWATER event as recorded at station WINV. Time: P_n + 15.96 sec.

(c) Particle-motion diagram of the STILLWATER event as recorded at station WINV. Time: P_n + 24.24 sec.

(d) Particle-motion diagram of the STILLWATER event as recorded at station WINV. Time: P_n + 18.04 sec.

CHAPTER IV

METHOD OF ANALYSIS OF DATA RECORDED BY THE GEOTECH FIELD STATIONS

Data available for analysis

Data recorded by the Geotech field teams were received from several sources. Data in digital form on 1/2" IBM-compatible computer tapes were received from the Seismic Data Laboratory in Alexandria, Virginia. These data included:

Explosion	Station
AARDVARK	MVCL
AARDVARK	FMUT
AARDVARK	LCNM
AARDVARK	DRCO
AARDVARK	MNNV
AARDVARK	PMWY
FISHER	WINV
FISHER	MVCL
FISHER	FMUT
FISHER	MNNV
FISHER	LCNM
GNOME	LCNM
GNOME	TPNV
GNOME	SVAZ
GNOME	FSAZ
GNOME	WMAZ

In addition to the above, a total of seventeen analog 1" FM magnetic tape composites, each containing 20 to 40 analog FM recordings of a single explosion recorded at different stations, were edited and spliced, and a new composite made. Editing was done by the Geophysics Department, University of Utah; splicing and playback to get the final new composite was done by Space Technology Laboratories, Redondo Beach, California. The original seventeen tape composites were copies of recordings made by the Geotech field teams across the United States for the following seventeen explosions:

STOAT	GNOME
FISHER	AARDVARK

MAD	CHINCHILLA
FEATHER	PLATYPUS
CODSAW	HARDHAT
AGOUTI	CIMMARON
CHENA	ARMADILLO
MINK	STILLWATER
PAMPAS	

Time segments containing the best short-period data from the above seventeen explosions were recombined on a new composite. The new composite reduced the number of 1" reels from seventeen to three. These three reels contain all of the best short-period data for each of the above seventeen explosions. Short-period calibration data were put on two additional composite reels. The signal composite also contains long-period data since the original 1" analog FM magnetic tapes were fourteen-track recordings of both short-period and long-period data; however, when editing, emphasis was placed on the short-period data.

Digitizing intervals used

The three 1" analog FM composite reels were then digitized and the digitized data placed on 1/2" computer tape for subsequent processing on the IBM 7040 digital computer. The digitizing was done by

a) Hercules Powder Co., Salt Lake City, Utah
(digitizing interval 0.02 sec)

b) Space Technology Laboratories, Redondo Beach, Calif.
(digitizing interval 0.03 sec)

A description of the contents of the three composite analog FM magnetic tapes made by the University of Utah and Space Technology Laboratories is on the following pages.

Composite Analog Tapes
of Data Recorded by
The Geotech Field Teams

Composite Analog Reel No. 1

GNOME

LCNM, POTX, SSTX, TCNM, SMTX, MLNM, LPTX, SVAZ, HBOK, AMOK, TOOK, FSAZ, WMAZ, KNUT, WNSD, SFAZ, DRCO, SJTX, PMWY, MPAR, VNUT, FMUT, LMNV, CWAR, WRAR, JSTN, MMTN, CPCL, TPNV, MNNV, HLID, CVTN, WINV, MVCL, NGWS, BLWV, DHNY, BGME.

AARDVARK

LMNV, MNNV, ATNV, KNUT, TFCL, FMUT, WINV, CPCL, FSAZ, MVCL, VNUT, VTOR, HLID, DRCO, LCNM, PTOR, PMWY, HSNB, WNSD, LPTX, TOOK, SEMN, MPAR, CNWS, MMTN, BLWV, GLTX, SJTX, CWAR, JSTN, NGWS, DANY, BGME.

FISHER

LMNV, MNNV, KNUT, WMAZ, FMUT, WINV, CPCL, FSAZ, MVCL, SFAZ, HLID, TCNM, VNUT, MLNM, LCNM, PMWY, SSTX, AMOK, LPTX.

MAD

TPNV, KNUT, WMAZ, WINV, LMNV, MNNV, FMUT, CPCL, FSAZ, MVCL, VNUT, HLID, PMWY, SSTX, WNSD, SMTX, MPAR, BLWV.

FEATHER

MNNV, KNUT, WMAZ, FMUT, WINV, CPCL, MVCL, VNUT, DRCO, PMWY, SSTX, WNSD, HBOK.

MINK

WINV, VNUT, MNNV, BFCL, FMUT, FSAZ.

CHENA

MNNV, CPCL, FSAZ, MVCL, VNUT, HLID.

Composite Analog Reel No. 2 [1]

HARDHAT

DVCL, MNNV, ATNV, KNUT, TNCL, WMAZ, FMUT, WINV, CPCL, FSAZ, MVCL, SFAZ, SFAZ-CC, VNUT, VTOR, SVAZ, HLID, DRCO, MLNM, TCNM, BFCL, LCNM, EPTX, TCNM, PTOR, PMWY, RTNM, EFTX, GNNM, BMTX, SSTX, LPTX.

PAMPAS

DVCL, MNNV, ATNV, ATNV-CC, BFCL, KNUT, TNCL, TNCL-CC, WMAZ, FMUT, WINV, CPCL, FSAZ, SFAZ, VTOR, HLID, TCNM, MVCL, VNUT, SVAZ, DRCO, LCNM, KNUT-CC, WMAZ-CC, SVAZ-CC, PTOR, EPTX, EFTX, SSTX.

CIMARRON

DVCL, ATNV, BFCL, KNUT, TNCL, WMAZ, FMUT, WINV, FSAZ, SFAZ, VTOR, HLID, MNNV, CPCL, MVCL, VNUT, SVAZ, DRCO, TCNM, PTOR, LCNM, EPTX, EFTX.

AGOUTI

DVCL, MNNV, MNNV-CC, ATNV, ATNV-CC, KNUT, TNCL, TNCL-CC, WMAZ, FMUT, WINV, FSAZ, SFAZ, DVCL-CC, BFCL, KNUT-CC, WINV-CC, CPCL, MVCL, VNUT, SVAZ, HLID, TCNM, BFCL-CC, FMUT-CC, CPCL-CC, FSAZ-CC, MVCL-CC, HLID-CC, DRCO, DRCO-CC, MLNM, KLNM-CC, TCNM-CC, LCNM, LCNM-CC, GNNM.

---

[1] CC - denotes cavity collapse

Composite Analog Reel No. 3 [1]

ARMADILLO

DVCL, DVCL-CC, MNNV, ATNV, ATNV-CC, KNUT, KNUT-CC, TNCL, TNCL-CC, WMAZ, WMAZ-CC, FMUT, FSAZ, VTOR, WINV, MNNV-CC, BFCL, FMUT-CC, CPCL, MVCL, SFAZ, VTOR-CC, HLID, TCNM, WINV-CC, CPCL-CC, FSAZ-CC, MVCL-CC, SFAZ-CC, HLID-CC, MLNM, MLNM-CC, TCNM-CC, PTOR, PTOR-CC, LCNM, LCNM-CC, PMWY, PMWY-CC, EPTX, EPTX-CC, GNNM, GNNM-CC, BMTX, VNUT, VNUT-CC, SVAZ, SVAZ-CC, DRCO, DRCO-CC, BFCL-CC.

CODSAW

DVCL, MNNV, KNUT, TNCL, WMAZ, WINV, VTOR, BFCL, FSAZ, SFAZ, HLID, TCNM, DVCL-CC, MNNV-CC, KNUT-CC, TNCL-CC, WMAZ-CC, FMUT, WINV-CC, CA-CPCL, CPCL, MVCL, VNUT, VTOR-CC, SVAZ, DRCO, LPTX.

CHINCHILLA

DVCL, ATNV, KNUT, TNCL, WMAZ, WINV, VTOR, MNNV, CW-BFCL, BFCL, FMUT, CW-FSAZ, FSAZ, CW-SFAZ, SFAZ, CW-HLID, CS-TCNM, TCNM, CPCL, CW-MVGL, MVCL, CW-VNUT, VNUT, CW-SVAZ, SVAZ, HLID, CW-DRCO, DRCO, LCNM, EPTX, SSTX.

STILLWATER

DVCL, MNNV, ATNV, ATNV-CC, KNUT, TNCL, WMAZ, FMUT, WINV, VTOR, MNNV-CC, BFCL, KNUT-CC, TNCL-CC, WINV-CC, FSAZ, MVCL, SFAZ, HLID, BFCL-CC, FMUT-CC, CPCL, CPCL-CC, FSAZ-CC, MVCL-CC, SFAZ-CC, VNUT, VNUT-CC, VTOR-CC, SVAZ, HLID-CC, DRCO, MLNM, MLNM-CC, TCNM, TCNM-CC, LCNM, EFTX, SSTX, DHNT.

STOAT

DVCL, KNUT, WMAZ, FMUT, WINV, MNNV, CPCL, FSAZ, MVCL, SFAZ, HLID, TCNM, VNUT, SVAZ, KLNM, DRCO, LCNM.

PLATYPUS

DVCL, MNNV, ATNV, WMAZ, FSAZ, SSTX.

---

[1] CC - denotes cavity collapse.

The new analog composite was not completed in time to process more than a small fraction of the data on the three reels. Most of the data that were processed were studied using the alphanumeric and CalComp particle-motion plots described below.

Other data recorded by the Geotech field teams which were received but not processed by us in any way because of insufficient time include:

a) Eighteen underground explosions on reels of 1" FM magnetic tape received in March 1964 from the Seismic Data Laboratory.

b) Sixteen earthquakes and underground explosions recorded by the Geotech recording teams and digitized by the Seismic Data Laboratory. These data are in digital form on 1/2" IBM-campatible computer tape.

Only underground explosions were studied from the recordings made by the Geotech field teams.

Particle-motion diagrams were made directly from digitized data. No corrections for instrument response other than magnification were made. The particle-motion diagrams were displayed by one of the following methods:

a) Hand plots. The diagrams were plotted by hand during the early stages of the project since machine methods were not readily available to us. The following particle-motion diagrams were constructed using this method:

Explosion	Station
AARDVARK	MNNV, ATNV, KNUT, TFCL, FMUT, WINV, CPCL, FSAZ, MVCL, VNUT, FTOR, HLID, DRCO, LCNM, PTOR, PMWY, MNNV, LCHI, MVCL, VTOR, NCID
FISHER	KNUT, MVCL, LCNM
GNOME	MMTN, LPTX, WNSD, SJTX, POTX, SSTX, TCNM, SMTX, MLNM, LPTX, SVAZ, AMOK, FSAZ, WMAZ, KNUT, PMWY, MPAR, VNUT, FMUT, CWAR, WRAR, JSTN

b) Alphanumeric plots - These are machine plots done on the IBM 7040 system with an IBM 1403 printer as output. This method greatly increased plotting efficiency over the hand plots, but the computer facilities required for obtaining this type of plot were not available to us until March 1964. The program itself was not operational until September 1964. The method prints out a known, preselected sequence of letters and numbers on the IBM 1403 printer at positions on the paper corresponding to the digitized data. The known sequence of symbols is then connected by hand to get the final particle-motion diagram. The data for the particle-motion diagrams are read directly from digitized data on magnetic tape or from cards, using Program DR-18FP1 or Program DR-18FP2 respectively, described in the Appendix. An example of an alphanumeric plot is shown in Figure 4-1

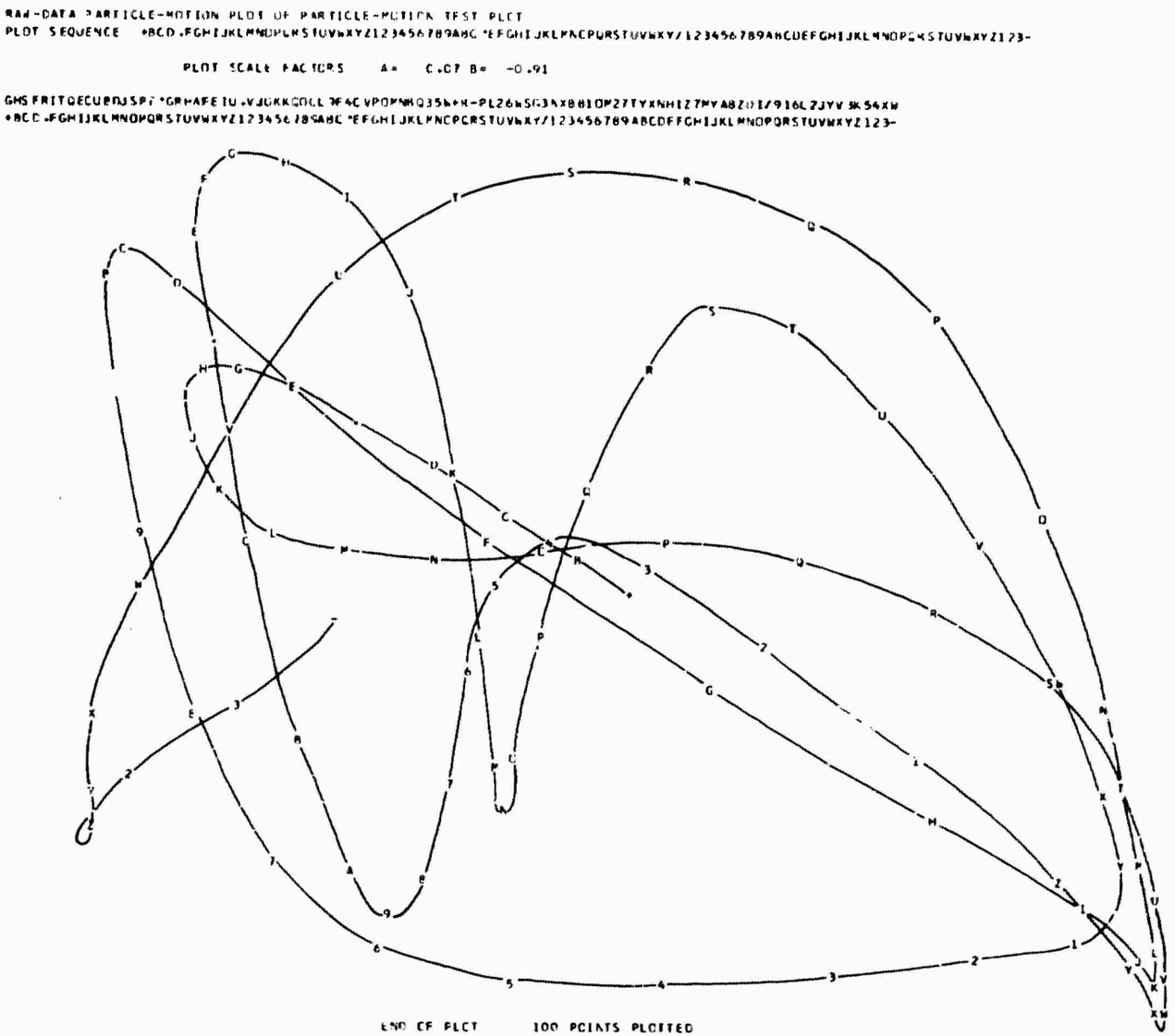

Figure 4-1. Particle-motion diagram illustrating the alphanumeric type of plot.

Table 4-1 Summary of particle-motion plots of data recorded at the Geotech stations

Explosion	Station	Epicentral Distance (KM)	Plot[1]	Gain[2]	Yield (KT.)	Seis[3]	Plot Interval (Sec.)	Magnification (K) Vertical	Radial	Trans
AARDVARK	FMUT	417	H		38 ± 5					
ARMADILLO	FMUT	413.7	A	H	6.6 ± 0.7		38.46	55.0	29.0	30.
CIMARRON	FMUT	417.0	A	H	11.0 ± 2.0	L	36.90			
HARDHAT	FMUT	403.4	A	H	5.9 ± 1.9		37.04	25.9	30.4	30.
PAMPAS	FMUT	413.1	A	H	?		20.00	44.0	25.6	25.
STOAT	FMUT	417.0	A	H	4.8 ± 0.60	S	31.20	72.0	38.0	38.
AARDVARK	MNNV	219	A	L	38 ± 5	L	37.84			
CHINCHILLA	MNNV	242.0	A	H	1.8		37.00	26.6	25.2	32.
CODSAW	MNNV	236.0	A	H	?		20.20	26.6	25.2	32.
STOAT	MNNV	218.7	A	H	4.8 ± 0.60	L	23.84	67.8	54.3	53.
AGOUTI	WINV	475.4	A	H	6.0 ± 0.6	L	36.00	470.0	354.0	360.
CHINCHILLA	WINV	493.2	A	H	1.8		8.40			
STILLWATER	WINV	484.3	A	H	2.6 ± 0.30		34.40	414.0	409.5	385
STOAT	WINV	475.4	A	H	4.8 ± 0.60	L	29.20			
AARDVARK	CPCL	494			38 ± 5					
AGOUTI	CPCL	493.9	A	H	6.0 ± 0.6	L	32.00	388.0	331.0	347
AGOUTI	SFAZ	597.4	A	H	6.0 ± 0.6	L	8.60	228.0	230.0	246
ARMADILLO	SFAZ	577.3	C	H	6.6 ± 0.7					
AARDVARK	FSAZ	499	H		38 ± 5					
ARMADILLO	FSAZ	479.2	C		6.6 ± 0.7					

Notes:

1. H denotes hand plot; A denotes alphanumeric plot; C denotes CalComp plot.
2. H denotes high-gain channel; L denotes low-gain channel.
3. L denotes large Benioff seismometer; S denotes small Benioff seismometer.

The following particle-motion diagrams were constructed using this method:

Explosion	Station
CIMMARON, HARDHAT, PAMPAS, STOAT	FMUT
AARDVARK, CHINCHILLA, CODSAW, STOAT	MNNV
AGOUTI, CHINCHILLA, STILLWATER, STOAT	WINV
AGOUTI (Cavity collapse)	ATNV
AGOUTI	CPCL
AGOUTI	SFAZ

c) CalComp plots. The University of Utah Computer Center acquired an IBM 1627 (CalComp) plotter in October 1964, and plotting techniques using data on magnetic tape were perfected in December 1964. This method is, of course, preferable to either of the above for displaying particle-motion diagrams.

The following particle-motion diagrams were constructed using this method:

Explosion	Station
ARMADILLO	FSAZ, SFAZ, WMAZ

In general, particle-motion diagrams were constructed only for the first 20 to 30 seconds of motion after the arrival of the initial P wave. In a few cases particle-motion diagrams were made for the time interval around the expected arrival of the body S-wave to help identify this S phase.

Particle-motion diagrams were always made for both a horizontal plane and a vertical-radial plane.

A typical sequence of particle-motion diagrams plotted on a CalComp plotter is shown in Chapter 5, Figure 5-10.

A summary of all particle-motion plots for the Geotech stations for which we have at least two events per station is given in Table 4-1.

CHAPTER V

INTERPRETATION OF DATA RECORDED AT THE GEOTECH FIELD STATIONS

Introduction

A limited study of the theoretical amplitudes of P to S and S to P conversions was made during the early part of this project. This is discussed in Chapter III. The theory dealt with plane waves, but more significantly, with wave lengths that were small compared with layer thicknesses. More recent results of the Haskell-Thompson matrix method have shown the importance of thin, low-velocity surface layers on the motion at the surface arising from a plane compressional wave incident at the base of a layered half-space. In particular, Hannon (1964) has constructed a number of theoretical seismograms using frequency-dependent transmission coefficients which may be computed by the Haskell-Thompson matrix method. The method determines the ratio of the vertical and horizontal motions at the surface to the total amplitude (or the amplitudes of the components) of the plane wave incident at the bottom interface of the layered system (Haskell, 1953; Hannon, 1964).

The amplitude ratios are functions of frequency, angle of incidence, layer thickness, compressional and shear velocities in each layer, and densities of the layers. The steady-state transmission coefficients give the amplitude and phase of the vertical and horizontal surface motion to the motion of the steady-state plane wave incident at the bottom interface. They include the important effects of frequency and layer thickness on the transmission coefficients, as well as the angle of incidence, velocities, and densities of the layers that affect the amplitude ratios as computed from the Zoeppritz equations (Chapter III, this report).

Hannon (1964) used four crustal models with varying thicknesses of alluvial layers ranging from zero to 30, to 730 to 1430 meters in thickness. It is worthwhile here to summarize his conclusions (Hannon, 1964, p. 2072):

1) The presence of less than 100 feet of sediments causes the surface amplitudes to increase by a factor of two for the source functions used by him. Ringing was a predominant feature.

2) For thicker alluvial sections, the surface motion amplitudes were even greater, and reached values three times those for the model with no alluvium.

3) "The near surface layering exerts a greater influence on the horizontal component than on the vertical, causing the horizontal component to have a more irregular shape. This emphasizes the importance of converted SV waves. This effect is further illustrated by the fact that the arrival times predicted by ray theory...do not agree...as well for the horizontal as they do for the vertical. Thus the presence of layering may produce elliptical particle motion."

4) "The different character introduced by the multiple and converted waves tends to introduce a longer period oscillation in the record which is dependent on the structure rather than on the source."

It is apparent from Hannon's work that care must be used in interpreting shear motion on a particle-motion diagram, and in particular, in identifying the shear on the basis of its amplitude relative to other observed phases on the seismogram. The effect of layered structure may drastically affect both the amplitude of the shear, and the apparent

arrival-time on a component seismogram. As Hannon showed, for the pulse widths he used, the near-surface layering exerted a greater influence on the horizontal component than on the vertical, thus emphasizing the importance of converted SV waves.

In the interpretations discussed in this Chapter, the amplitudes of certain of the converted waves, for example, PPS, seem larger than would be expected for the assumed velocity contrasts in the simplified crustal sections used. However, the crustal models assumed are a first approximation only, based on refraction data recorded at relatively widely separated stations in many cases, and more resolution may be required to detect and explain the effects of thin, near surface layering on the amplitudes of the arrivals, although the models used do agree with the arrival times of the phases interpreted on the seismograms, in most cases. Also, it is apparent that "ringing" is present on many of the seismograms, which may override a weaker PS converted wave following a stronger P phase.

In view of the theoretical work discussed above which takes into account the frequency content of the pulse as well as the layer velocities, densities and incident angles, the interpretations presented in this Chapter must be regarded as provisional, especially where the interpretation of shear arriving before the body S wave is concerned. True shear arrivals during this time would have to be a result of P to S conversion somewhere along the transmission path. The effect of the recording station location and the layering beneath the station on the amplitudes of the arrivals is now recognized as having an important effect on the character of the seismogram. Quantitative measurements of amplitude ratios of S to P or P to S or even P to P from particle-motion diagrams must be made with care. Further study of the enhancement of the amplitudes of early shear arrivals as a function of frequency content of the pulse is warranted.

General Discussion

Figure 5-1 shows the geographic locations of the Geotech recording teams in the western part of the United States with respect to the Nevada test site (NTS). We were not able to interpret all of the data we have on magnetic tape in digital form recorded at these stations. A few events recorded at selected stations are discussed in this chapter.

Figure 5-2 shows the locations of all of the underground explosions in the Nevada test site for which particle-motion diagrams were made at at least one Geotech field recording station for this study. Table 5-1 lists some of the pertinent data for each of these eleven explosions. Emphasis was placed on Geotech stations at which two or more underground explosions were recorded at the same site from the same approximate source, that is, the Nevada test site. Particle-motion diagrams were also made for the GNOME event in New Mexico, but no other data are available for the same source area and epicentral distances, and so these particle-motion diagrams are not presented herein.

Figure 5-3 shows CalComp plots of three underground nuclear explosions recorded at Winnemucca, Nevada (WINV) by the Geotech field recording teams. The signals fom the underground nuclear explosions STOAT and AGOUTI are very similar. The digital-to-analog playbacks of each of these two recordings are shown in Figure 5-4 on an expanded scale. The traces are almost identical phase for phase for the entire fifteen seconds of the signal. Beyond that, the signal as shown is poor because of clipping in the digitizing electronics were the FM analog tapes were digitized. The third explosion, STILLWATER, in Figure 5-3, does not have the same degree of similarity in the first fifteen seconds, but the epicenter for this explosion was approximately nine kilometers from STOAT and AGOUTI.

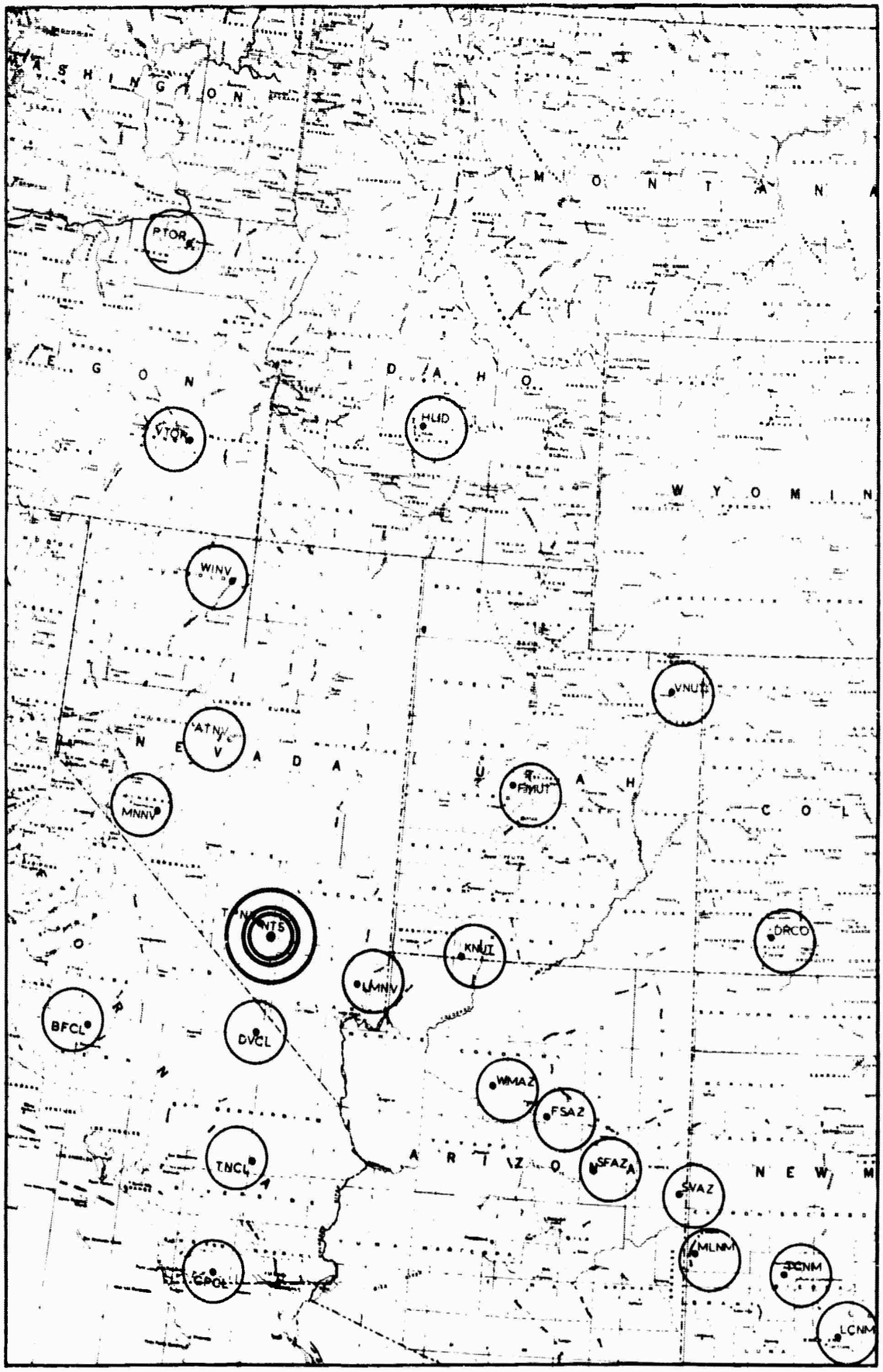

Figure 5-1. Location map of LRSM recording stations in the western part of the United States.

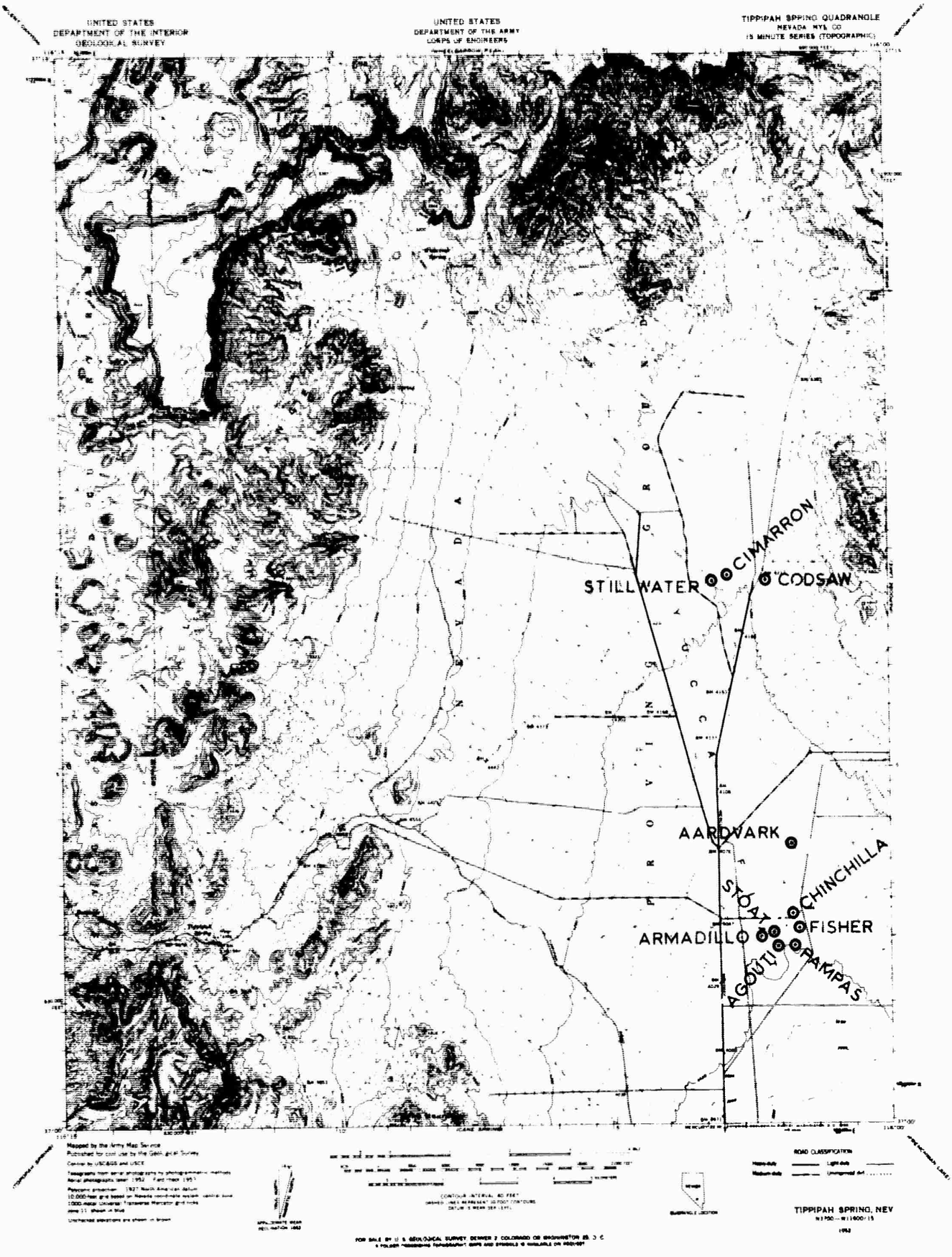

Figure 5-2. Location map of underground nuclear explosions at the Nevada test site.

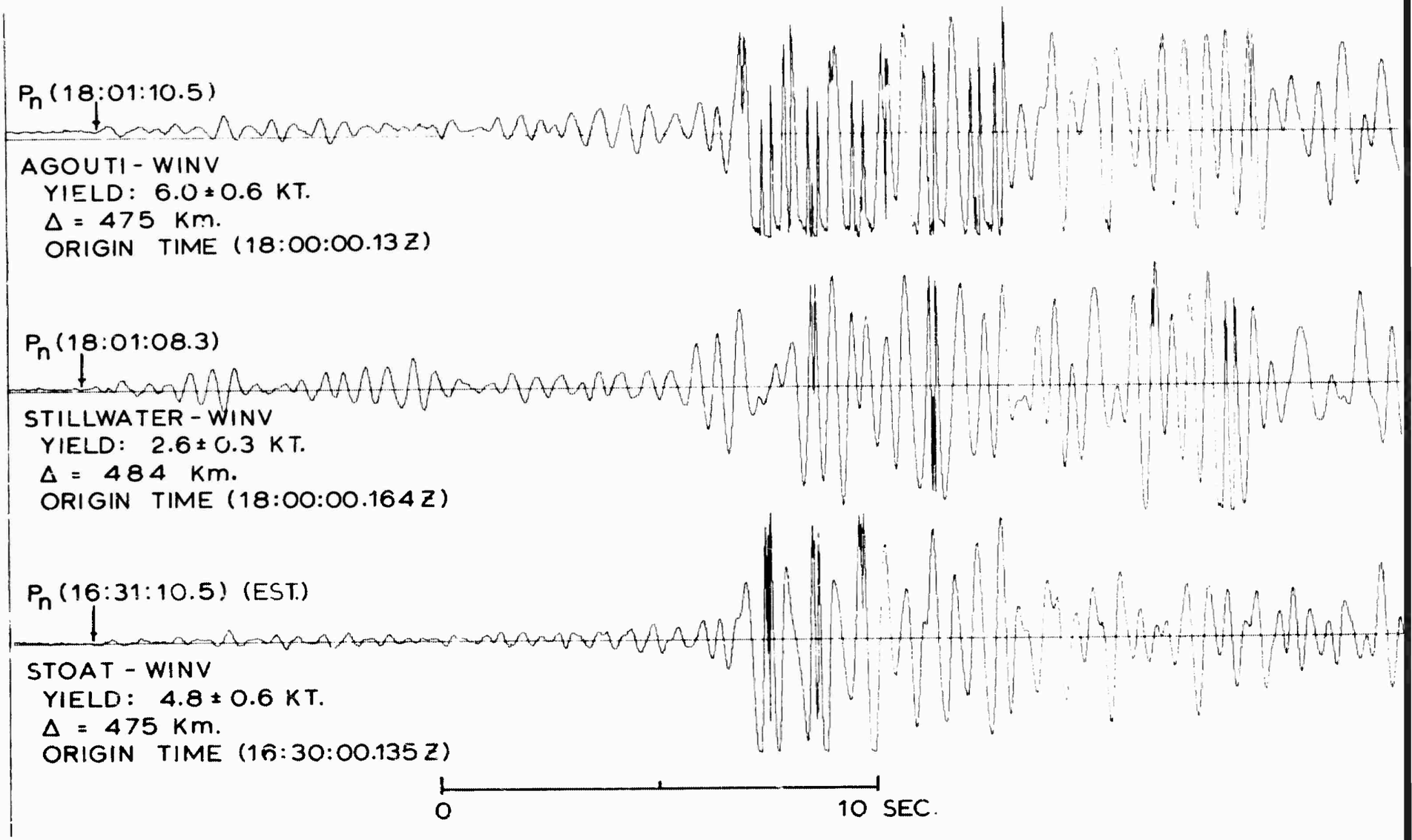

Figure 5-3. CalComp digital-to-analog playback of the events AGOUTI, STILLWATER and STOAT as recorded at station WINV.

Table 5-1.-- Data pertaining to certain underground nuclear explosions at the Nevada test site.

Event	Date	Time of Origin	Yield (kt)	Latitude	Longitude	Environment
FISHER	12/3/61	23:04:59.63z	13.5 + 1.1-1.6	37° 02' 41" N (Site area 3-U3ah)	116° 01' 40" W	Geologic Medium (A Shot Depth Surface Elevation Shot Elevation
STOAT	1/9/62	16:30:00.135z	4.5 ± 0.6	37° 02' 41" N (Site U3ap)	116° 02' 06" W	Geologic Medium (A Shot Depth Surface Elevation Shot Elevation
AGOUTI	1/18/62	18:00:00.13z	6.0 ± 0.6	37° 02' 50.1" N (Site Area 3-U3ao)	116° 02' 03.7" W	Geologic Medium (A Shot Depth Surface Elevation Shot Elevation
STILLWATER	2/8/62	18:00:00.164z	2.7 ± 0.3	37° 07' 38" N (Site U9c)	116° 03' 09" W	Geologic Medium (A Shot Depth Surface Elevation Shot Elevation
ADILLO	2/9/62	16:30:00.125z	6.6 ± 0.6	37° 02' 37" N (Site U3ar)	116° 02' 20" W	Geologic Medium (A Shot Depth Surface Elevation Shot Elevation
HARDHAT	2/15/62	18:00:00.100z	5.9 ± 0.5	37° 13' 35" N (Site U15a)	116° 03' 34" W	Geologic Medium (G Shot Depth Surface Elevation Shot Elevation
CHINCHILLA	2/19/62	16:30:00.132z	1.8 ± 0.25	37° 02' 57" N (Site U3ag)	116° 01' 46" W	Geologic Medium (A Shot Depth Surface Elevation Shot Elevation

Table 5-1.-- (Continued)

Event	Date	Time of Origin	Yield (kt)	Latitude	Longitude	Environment
CODSAW	2/19/62	17:50:00.159z	?	37° 07' 39" N (Site UGg)	116° 02' 13" W	Geologic Medium (Allu Shot Depth 6 Surface Elevation 42 Shot Elevation 35
CIMARRON	2/23/62	18:00:00.160z	11.2 ± 2.0	37° 07' 44" N (Ugh)	116° 02' 54" W	Geologic Medium (Allu Shot Depth 10 Surface Elevation 42 Shot Elevation 32
PAMPAS	3/1/62	19:10:00.091z	?	37° 02' 30" N (U3aL)	116° 01' 45" W	Geologic Medium (Allu Shot depth 11 Surface Elevation 40 Shot Elevation 28
AARDVARK	5/12 ~~3/25~~/62	19:00:00.103z	38 ± 0.5	37° 03' 55" N	116° 01' 49" W	Geologic Medium (T Shot Depth 14

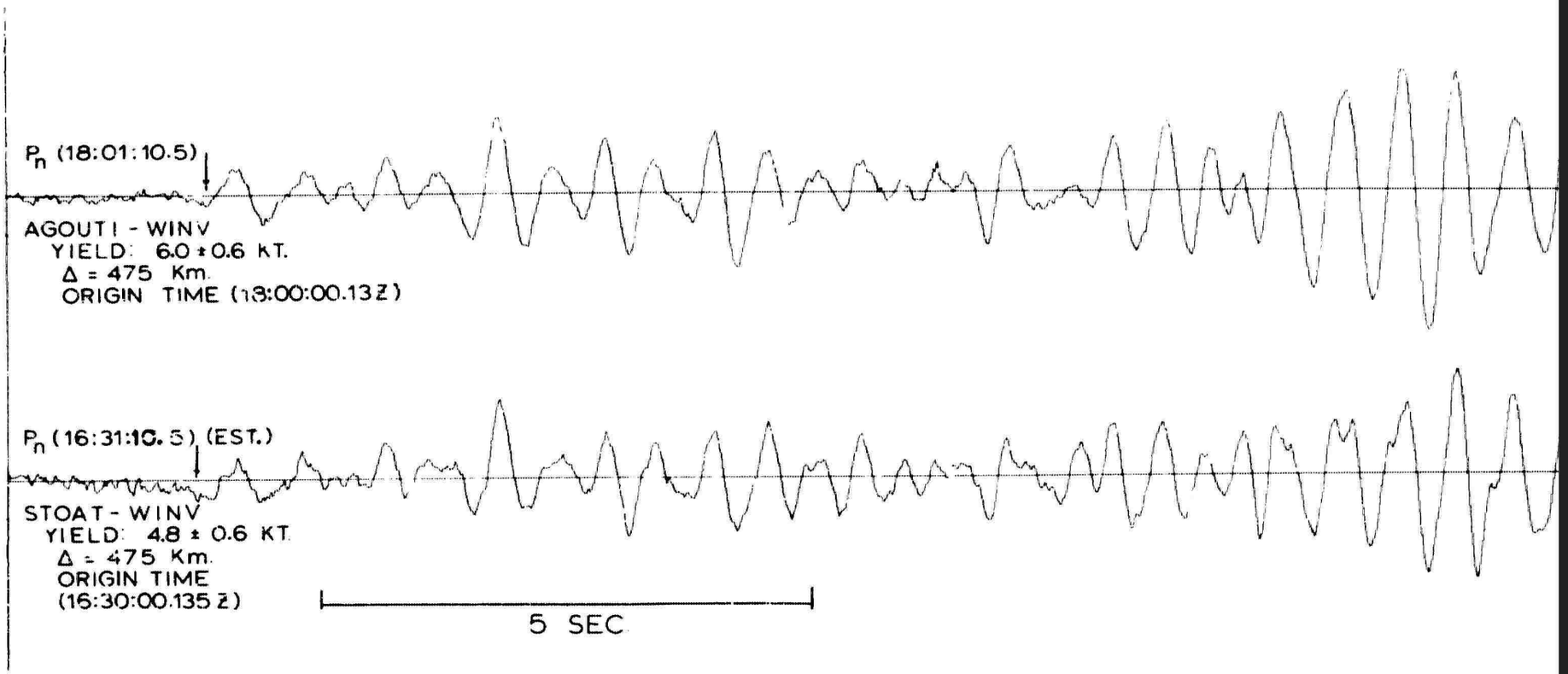

Figure 5-4. CalComp digital-to-analog playback of the AGOUTI and STOAT events as recorded at station WINV. First 15 sec only.

See Fig. 5-2. Other considerations such as yield, depth of burial, geological environment at the source, etc. would also be expected to affect the source function.

Figure 5-5 shows an annotated version of Figure 5-3 for AGOUTI, STILLWATER, and STOAT as recorded at WINV. Several things are apparent on the seismograms:

1) Patterns resembling beat frequency patterns or possibly "ringing" are well developed during the first 15 seconds of the seismogram for STILLWATER. The patterns are still evident after 15 seconds in the stronger arrivals. Envelopes have been drawn in to accentuate the patterns. Such patterns are also observed for AGOUTI but are less well developed. Also, clipping in the digitizing electronics has obscured the patterns after the first 15 seconds of the AGOUTI seismogram.

2) For the seismogram of STILLWATER, the wave train labeled ABCDEFG at approximately 17.5 seconds after the arrival of P_n is very similar in appearance to the wave train labeled A'B'C'D'E'F'G' at approximately 24.5 seconds after the arrival of P_n. Examination of the particle-motion diagrams for these two wave trains show the ground motion for cycle A to be S-like and prograde, whereas the ground motion for A' is P-like and prograde. Cycles C, D, C, F, and G show prograde P-motion, but C', D', E', and F' show prograde S-motion, for the most part. The first wave train, then, is predominantly P-motion, the later wave train is predominantly S-motion. Both wave trains are of approximately the

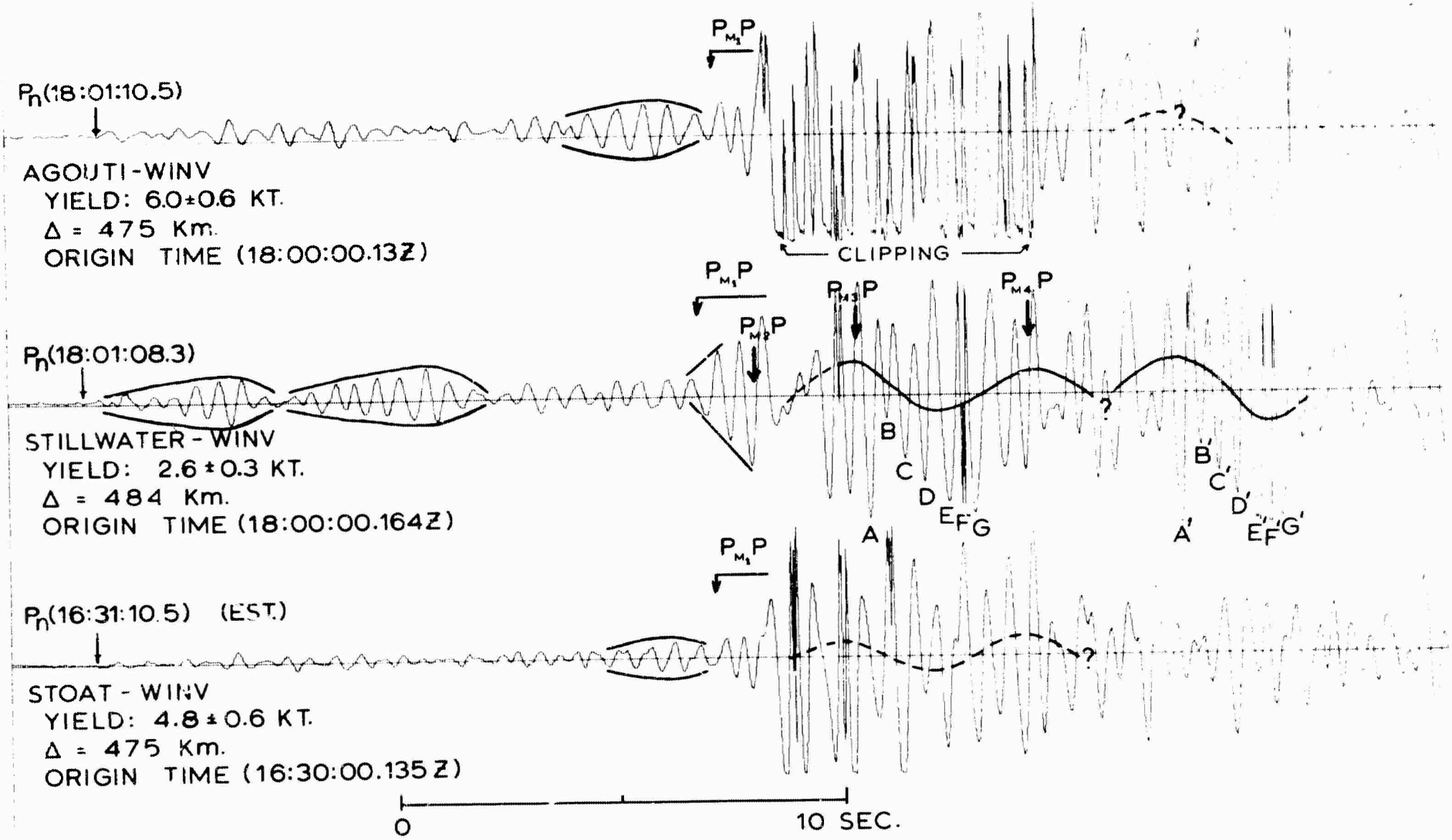

Figure 5-5. CalComp digital-to-analog playback of the events AGOUTI, STILLWATER and STOAT as recorded at station WINV. Annotated.

same amplitude, as shown on the seismogram recording the vertical component of ground motion.

3) Wave trains A...G and A'...G' on the STILLWATER seismogram are parts of short-period events which modulate another wave whose period is approximately four seconds. The amplitude of the "carrier" wave seems to decrease slightly with increasing time and the wave modulated by the A'...G' wave train does not appear to be a simple continuation of the one modulated by wave train A...G. The time of onset of the wave modulated by wave train A...G appears to be at approximately 15.5 seconds after the arrival of P_n at WINV.

4) A spectral analysis plot of STILLWATER-WINV shows two dominant peaks in the frequency spectrum, one at 1.8 cps and one at 2.3 cps. These two peaks seem to be associated primarily with approximately the first 14 seconds, and with the last 14 seconds, respectively, of the seismogram.

Many of the main features discussed above appear in other seismograms obtained by the Geotech stations that we have studied to date. The modulated low frequency "carrier" waves can be seen for both STOAT and AGOUTI (Figure 5-5) but clipping in the digitizing electronics for AGOUTI makes the wave difficult to see. These low-frequency waves are recorded over the interval of time during which multiple reflections are arriving from the base of the crust. The wave as sketched in for the STOAT seismogram appears to be of higher frequency than that for either STILLWATER or AGOUTI.

Figure 5-6 shows an annotated series of three underground nuclear explosions recorded at Fillmore, Utah (FMUT). The "beat" frequency patterns and low frequency waves are not as well developed as they are for STILLWATER-WINV. The sites for the three explosions were widely separated at the Nevada test site (see Figure 5-2), and the seismograms bear little resemblance to one another.

Wave trains after $P_{M1}P$ (or $\overline{P}$?) on the vertical seismograms for CIMARRON and HARDHAT on Figure 5-6 for station FMUT are similar to wave trains recorded for STILLWATER at WINV (Figure 5-5). However, the CIMARRON-HARDHAT group is not as well developed later on the same seismogram. The crustal tranmission paths are probably quite different in detail for STILLWATER-WINV and CIMARRON-FMUT. There is a decrease in amplitude for first-motion and later arrivals arriving at FMUT from the Nevada test site as compared with corresponding epicentral distances in Arizona and Nevada.

The beat-frequency patterns may be a resonance effect due to the presence of a low-velocity sedimentary surface layer for which the reflection coefficient is effectively unity at the top of the layer. Van Nostrand (1964) has shown that "resonance is the most important factor in signal amplitude variation resulting from changes in near surface geology". The maximum signal amplitude occurs when the thickness of the low-velocity surface layer approaches a quarter-wavelength. For frequencies of 1 cps in a low-velocity sedimentary layer having a P-wave velocity of 3.0 km per second, maximum signal amplitudes will be obtained for layer thicknesses of 775 meters, or about 2,500 feet. These quarter-wavelength resonant thicknesses will considerably distort the signal shape, which then becomes a function of the thickness of the thickness of the surface layer. Van Nostrand (1964) shows the original input signal considerably increased in amplitude for a surface layer whose thickness is $\lambda/4$, and considerably lengthened

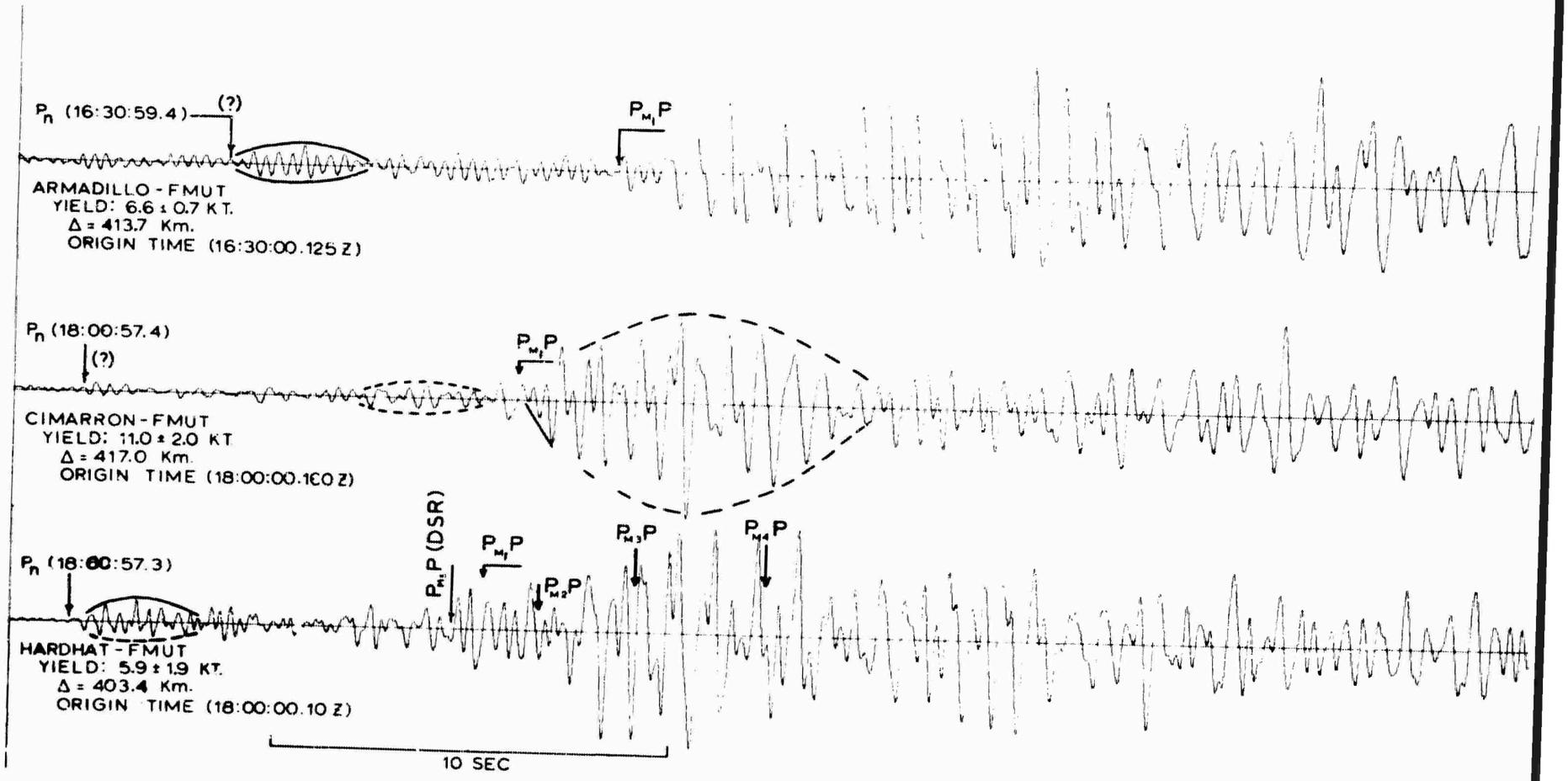

Figure 5-6. CalComp digital-to-analog playback of the events ARMADILLO, HARDHAT and CIMMARON as recorded at FMUT.

in time for a surface layer whose thickness is $3\lambda/4$.

The resonance effect will seriously interfere with the identification of weak arrivals closely following stronger ones, since an original two-cycle event may be drawn out into as many as eight cycles by the resonance effect.

From the time of arrival of P_n on the seismogram of STILLWATER-WINV out to about four seconds, the motion is predominantly P-like. The amplitude increased gradually almost in a linear fashion out to approximately 3.5 seconds. Some of this may be a resonance effect due to "ringing" associated with a low-velocity sedimentary layer beneath the station.

Table 5-2 lists theoretical arrival times for some "phases" which were searched for on the seismogram of STILLWATER-WINV.

The interval from 4.5 sec to 6.5 sec after the arrival of P_n is characterized by about four cycles of predominantly S-like motion with the attitude of the major axis of the motion in a vertical plane gradually increasing until the motion is nearly vertical. The amplitude increases in a linear fashion during the interval of $\triangle t$ = 4.5 sec to $\triangle t$ = approximately 7.5 sec.

The motion for the first five cycles in this interval is alternately prograde and retrograde for each cycle. This behavior may indicate the simultaneous arrival of wave trains of different type and frequency. The alternating prograde and retrograde behaviour in the theoretical particle-motion diagrams was a characteristic of the simultaneous arrival of wave trains of slightly different frequency content.

At about 6.5 sec after the first motion, the motion becomes large in amplitude and nearly vertical and remains prograde for the next 11 cycles until approximately 12 sec after the arrival of P_n. The amplitudes reach a maximum at about 7.5 sec after the arrival of P_n.

Table 5-2.--Theoretical arrival times of certain phases for the crustal section of Figure 5-7a (STILLWATER-WINV)

Phase	Description	Theoretical Arrival Time (Sec)	Phase-P_n Arrival Time, t, sec
P_n	First arrival, head wave	67.7	-
$S\underline{P}P$ and $P\underline{P}S$	Head waves, converted at base of crust	71.9	4.2
$S\underline{P}S$	Head wave, up and down paths shear	76.1	8.4
P_g	Direct wave	80.2	12.6
$P_{M1}P$ (or $\overline{P}$?)	P-wave reflected once from base of crust (or a guided wave in the crust)	80.9	13.2
$P_{M1}PP\underline{P}P$	P-wave reflected once from base of crust at critical angle, then reflected from the surface of earth back to base of crust where it continues as a P head wave	73.6	5.9
$P_{M2}P$	P-wave reflected twice from base of crust	82.6	14.9
$P_{M3}P$	P-wave reflected three times from base of crust	85.2	17.5
$P_{M4}P$	P-wave reflected four times from base of crust	88.7	21.0
$P_{M2}PP\underline{P}P$	P-wave reflected twice from base of crust and continuing as a head wave	79.6	11.9
$S_{M1}P$ and $P_{M1}S$	S-wave (or P-wave) converted on reflection at base of crust to a P-wave (or S-wave)	90.27	22.6

BLANK PAGE

The phase SPP theoretically should arrive about 4.2 sec after the arrival of P_n. See table 5-2. This is also the approximate arrival time of PPS. The PPS head wave is probably of lower amplitude than SPP but it may take several cycles before the SPP becomes dominant on the particle-motion diagrams. The vertical trace of STILLWATER shows a linear increase in amplitude for the wave group in the interval $\Delta t = 4.5$ sec to $\Delta t = 7.5$ sec. It has not yet been determined whether the linear increase in amplitude is associated with a "beat" or is a buildup of a particular phase, or is the combined effect of two or more arrivals, or is a resonance effect. Some evidence in favor of a resonance effect is the repetition of the phenomenon on the seismogram several times in the first 20 seconds. The linear increase in amplitude seems to be common to the P_n group, the SPP group, and the P_MP group, suggesting a common station effect which promotes resonance for all significant arrivals, regardless of the transmission path.

The theoretical travel-time of an SPS phase based on the model of Figure 5-7a is 76.1 sec, or 8.4 seconds after the arrival of P_n. There is some indication of shear on the particle-motion diagram at the expected arrival time for SPS and it is possible that this phase is present. The motion is predominantly S-like for several seconds after the expected arrival time of SPS. However, the motion is not clear-cut and it is not possible to estimate the time of onset of the phase.

The dominant prograde motion changes to a single cycle of retrograde motion at about 12 seconds after P_n. Following this change are several cycles of well-developed shear motion just preceding the arrival of $P_{M_1}P$.

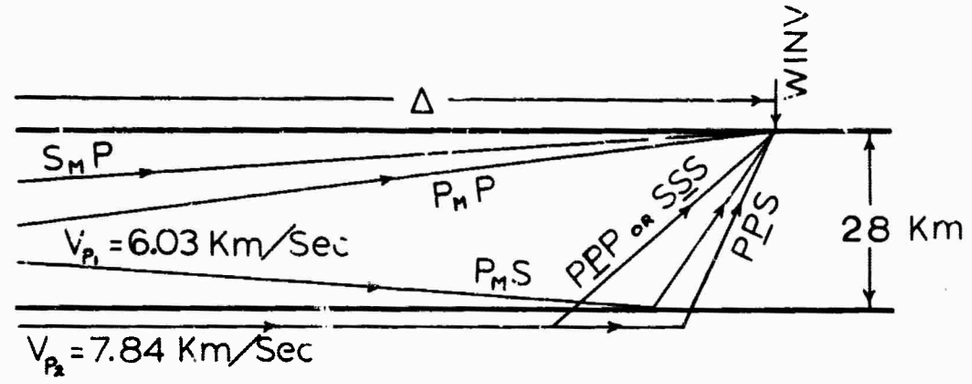

STILLWATER–WINV (Δ=484 Km.)
AGOUTI –WINV (Δ=475 Km.)
STOAT –WINV (Δ=475 Km.)

a. CRUSTAL SECTION – N. CENTRAL NEVADA

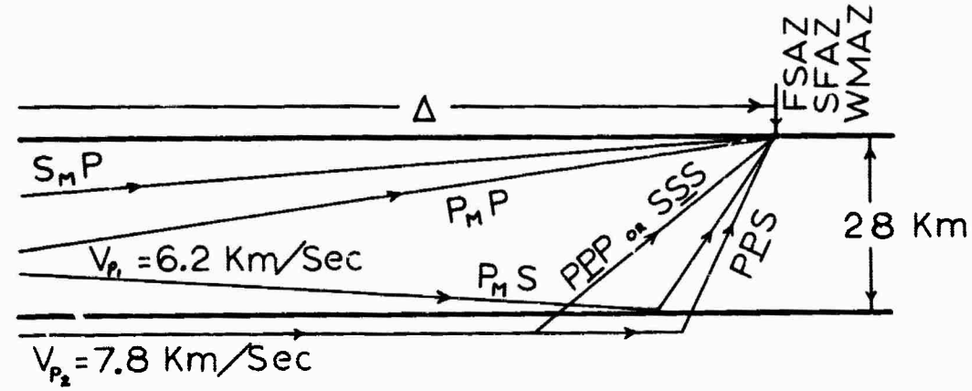

ARMADILLO–FSAZ (Δ = 479.2 Km.)
ARMADILLO–SFAZ (Δ = 577.3 Km.)
ARMADILLO–WMAZ (Δ = 387.9 Km)

b. CRUSTAL SECTION – NORTHERN ARIZONA

Figure 5-7. Simplified crustal sections

(a) North central Nevada
(b) Northern Arizona

$P_{M_1}P$ appears to become well developed at approximately 14 seconds after the arrival of P_n. This agrees well with the theoretical arrival time for $P_{M_1}P$ but it would probably also agree with the approximate travel time of a guided wave in the crust, usually called $\bar{P}$. This phase is the most distinctive arrival on most of the seismograms.

The S-like motion proceding $P_{M_1}P$ (or $\bar{P}$) for STILLWATER-WINV is very well developed and is prominent on the radial seismometer trace. However, the observed arrival time of 12.0 sec after P_n does not coincide with any arrival which could be expected to have a large amplitude for the crustal section being used. The S-like motion may be the result of the complex interaction of crustal layering, the arrival of low amplitude portions of the $P_{M_1}P$ phase, and other phases such as SPS(?). The S-like motion preceding $P_{M_1}P$ for STILLWATER-MNNV is not as well developed on other seismograms for other explosions.

The portion of the seismogram after the arrival of $P_{M_1}P$ (or $\bar{P}$?) out to approximately 27 seconds is believed to be due mainly to multiple reflections from the base of the crust, or multiple reflections of $\bar{P}$. This energy may also include $S_{M_1}P$, that is shear energy converted to P on reflection at the Mohorovicic discontinuity. No attempt has been made to identify the onset time of each multiple on the seismograms. The approximate expected arrival times for $P_{M_1}P$ (i=2, 3, 4) have been noted in parentheses on STILLWATER-WINV.

There is well developed S-like motion appearing on the particle-motion diagrams at approximately 22.5 sec which coincides with the expected arrival time of $P_{M_1}S$.

Discussion of the ARMADILLO event as recorded at WMAZ, FSAZ and SFAZ

Stations WMAZ, FSAZ and SFAZ are in northern Arizona and in line with the Nevada test site. Epicentral distances from NTS for WMAZ, FSAZ and SFAZ are 387.9, 479.2 and 577.3 km, respectively. Inspection of Figure 5-8 shows some of the events which make up the early part of the seismogram at each station. Arrival times are shown as measured from the arrival of P_n.

At WMAZ, using the crustal section of Diment, Stewart and Roller (1961), the first good indication of shear on the particle-motion diagrams is at 4.4 sec after the first motion. This coincides well with the expected arrival of PI, a converted head wave from the base of the crust. It is also apparent from the particle-motion diagrams that the observed shear motion is "riding" on P energy of much larger amplitude which could be the SPP phase.

For this crustal model, SPS and $P_{M_1}P$ should both arrive at approximately 8.5 sec after P_n. Inspection of the particle-motion diagrams around this time shows a strong P-arrival at about 7.7 sec. Several cycles of large amplitude P-motion follow. The P-motion is prograde. This P-motion is believed to be due to the arrival of $P_{M_1}P$, a reflection from the base of the crust, or $\overline{P}$, a guided wave in the crust. There is also some indication of shear at about 8.0 sec lasting for about a cycle which may indicate the SPS arrival. At approximately 10 sec there are several cycles of good S-like motion. This motion does not coincide with the expected arrival time of any of the phases in Figure 5-8. The motion is retrograde.

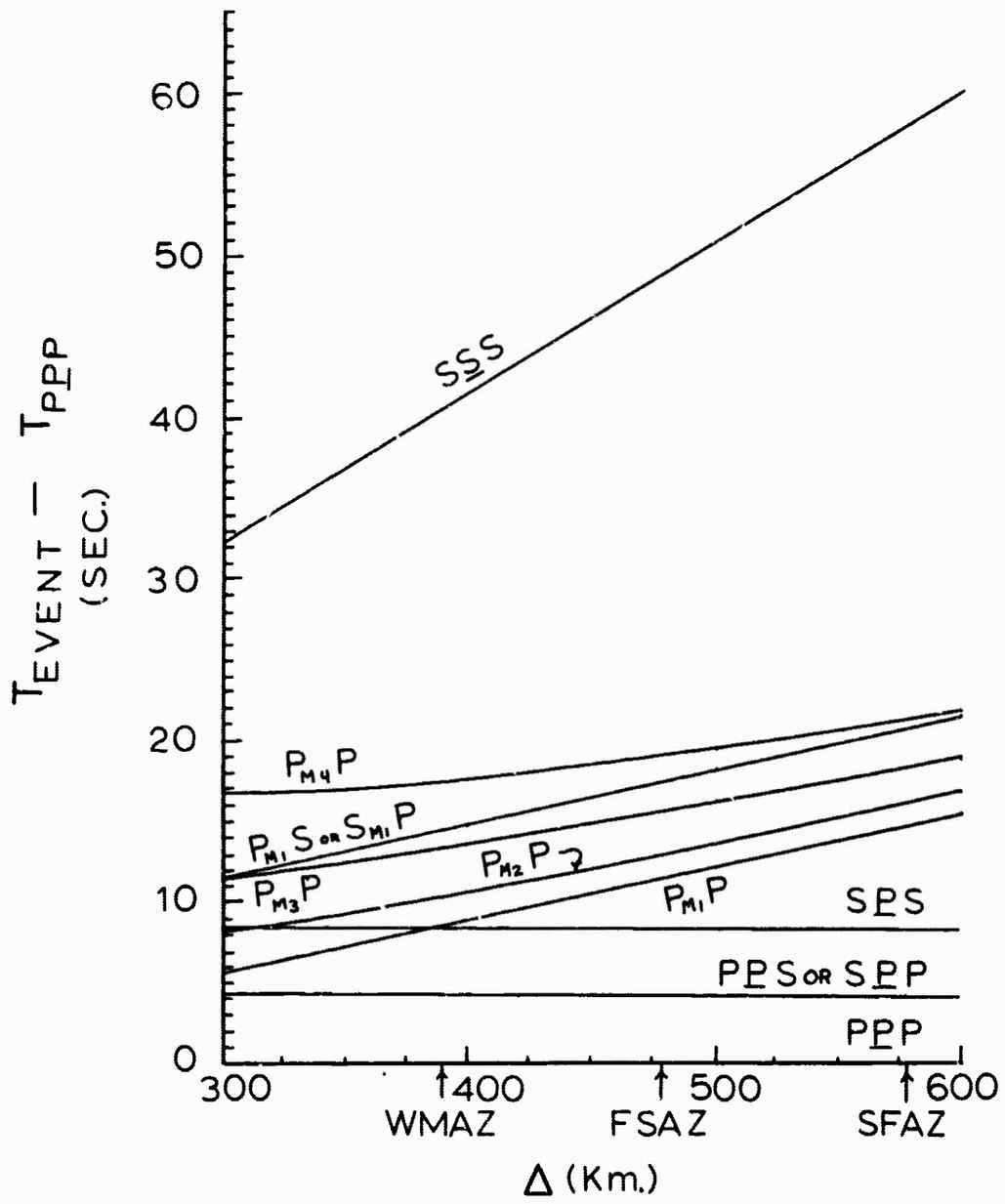

Figure 5-8. Travel-time curves based on the crustal section of Figure 5-7b.

After the arrival of $P_{M_1}P$(or $\bar{P}$), the seismogram out to approximately 25 sec, at least, is probably due to multiple reflections from the base of the crust, or multiple reflections of $\bar{P}$.

It is possible that some intermediate layering would provide a velocity structure giving a travel-time of about 10.0 sec for a phase that could be called SPS, as in the Berg, Cook, Narans, and Dolan (1960) model where SPS is generated from the base of the 9 km layer.

It is difficult to draw positive conclusions from a study of a single event such as ARMADILLO recorded at a single station such as WMAZ. However, shear motion is apparent on the particle-motion diagrams at 4.4 sec and 8 sec which does coincide approximately with the expected arrival time for PPS and SPS, respectively. Further, except for the shear at 10 sec, these are the only intervals of shear apparent on the particle-motion diagrams out to about 10 sec. The SPS motion is considerably larger than the PPS motion.

There is S-like motion recorded at FSAZ at about 4.2 sec after the arrival of P_n. This coincides very well with the expected arrival time for the PFS head wave from the base of the crust (see Figure 5-7b and Figure 5-8. There are no intervals of shear preceding this on the seismogram. The S-like motion lasts for approximately one second and is followed (at 5.5 sec after P_n) by 3 cycles of larger amplitude P-motion lasting to almost 8 sec after P_n on the seismogram. Most of this P-motion is probably associated with the SPP phase. At approximately 8 sec after P_n, several cycles of higher frequency S-like motion are apparent on the particle-motion diagrams, coinciding very well with the theoretical arrival time of SPS from the base of the crust. The theoretical arrival time of $P_{M_1}P$ (or $\bar{P}$) at FSAZ from the Nevada test site using the crustal

section of Diment, Stewart, and Roller (1961) is approximately 11.2 sec. This coincides almost exactly with the arrival of high-amplitude prograde P-like motion (see Figure 5-10), and it is almost certainly due to the arrival of $P_{M_1}P$ (or $\bar{P}$). Following this arrival are the usual large amplitudes due to multiple reflections from the base of the crust.

Station SFAZ recording the ARMADILLO event shows frequencies considerably higher than those recorded at FSAZ for the same event (see Figure 5-9). This is probably a station effect. The signal appears to show the effects of reverberations. The motion is P-like with a small minor axis. No S-like motion is evident until approximately 6 seconds after P_n when several cycles of S-like motion appear lasting approximately two seconds. This S-like motion does not coincide with any expected S arrival-time on Figure 5-8. Ringing may have a severe effect on body-wave arrivals at this station for this event. P-motion resumes at approximately 8 seconds after P_n. Shear-motion is again apparent beginning approximately 10 seconds after P_n and continuing approximately 2 seconds. This interval of shear coincides well in arrival-time with a similar interval recorded at station WMAZ and noted above. The S-like motion is not as well developed on the seismogram recorded at FSAZ for the ARMADILLO event, for this time interval, but the particle-motion does indicate that some shear is also present in the dominant P-like motion associated with the arrival of $P_{M_1}P$.

The theoretical arrival time of $P_{M_1}P$ at SFAZ for the ARMADILLO event based on the crustal section of Diment, Stewart, and Roller is approximately 15 seconds after P_n. This time on the record (see Figure 5-9) does not coincide with the arrival of a large amplitude P-phase. The large amplitudes usually associated with $P_{M_1}P$ (or $\bar{P}$) are not seen until about

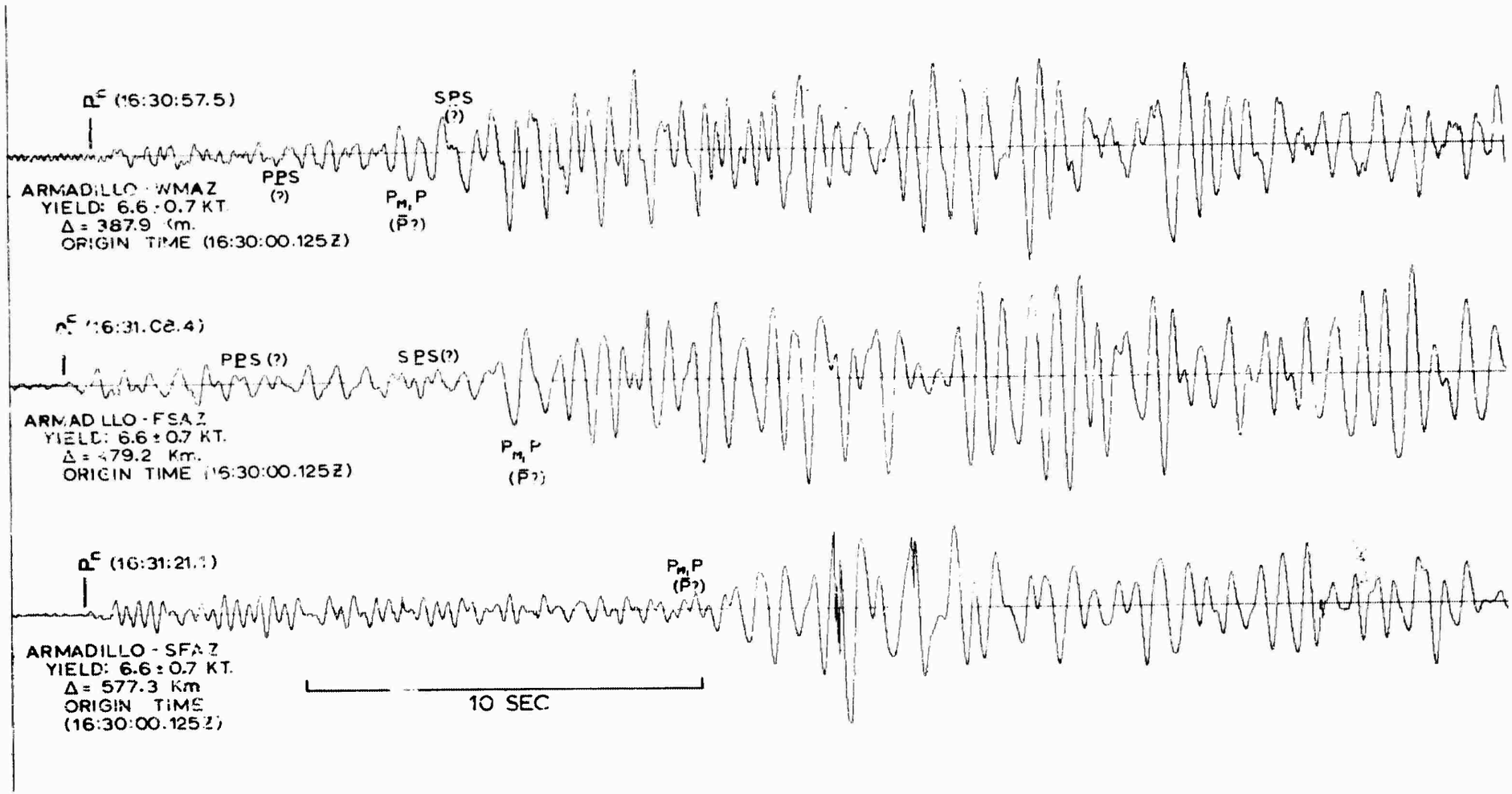

Figure 5-9. CalComp digital-to-analog playback of the ARMADILLO event as recorded at WMAZ, FSAZ, and SFAZ.

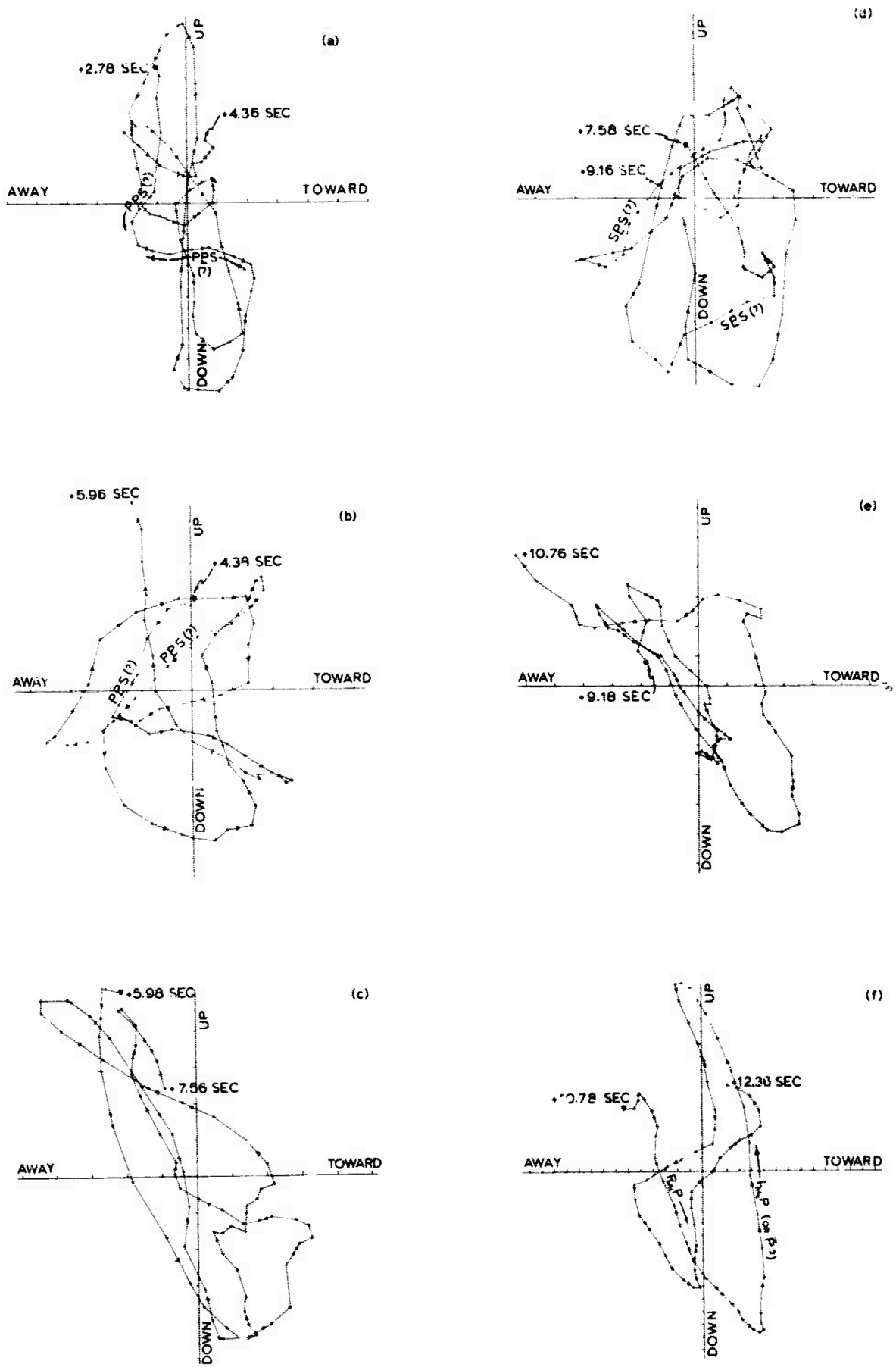

Figure 5-10. Particle-motion in a vertical plane from +2.78 to +12.36 sec after P_n for the ARMADILLO event as recorded at FSAZ.

16 seconds after P_n. The arrival of $P_{M_1}P$ (or $\bar{P}$) would then seem to be approximately one second late at SFAZ for the ARMADILLO event. It is to be noted, however, that the usual high amplitude following $P_{M_1}P$ for at least 10 or 15 seconds which we associate with multiple reflections from the base of the crust are not present either, on this seismogram (see Figure 5-9).. Therefore, evidently less P-energy has traveled as a guided wave for this event as compared with FSAZ and WMAZ, and the actual onset of $P_{M_1}P$ at SFAZ probably occurs about a second before the larger amplitudes appear at 16 seconds after the arrival of P_n at SFAZ. The station is about 100 km from FSAZ and attenuation in the crustal wave guide will made the onset of $P_{M_1}P$ more difficult to pick for SFAZ. It can be seen on the seismogram for SFAZ in Figure 5-9 that the signal appears to be modulated by a low-frequency wave that begins at the expected time of arrival of $P_{M_1}P$ (or $\bar{P}$?).

CHAPTER VI

METHOD OF ANALYSIS OF DATA RECORDED AT PERMANENT SEISMOGRAPH STATIONS

Data available for analysis from permanent seismograph stations

Table 6-1 summarizes the available seismic data from permanent seismograph stations that were used in the present investigation. A total of 159 events are listed. The methods of analysis of these data will be given in a later section.

Table 6-1 Data from permanent seismograph stations that were digitized in the present investigation

STATION CODE:

BCN	- Boulder City, Nevada
FGU	- Flaming Gorge, Utah
PCU	- Price, Utah
SLC	- Salt Lake City, Utah
DUG	- Dugway, Utah (world-wide station) Heavy Mass Benioffs
DUG (Port)	- Dugway, Utah Portable Benioffs
SPB	- Bolivia - (world-wide station)
LPS	- El Salvador - (world-wide station)

SYMBOL KEY

*	- Seismic event.
**	- Event digitized at 9.5 minute angle from recorded base line.
+	- Event originally * and later confirmed in the February, 1964 edition of "The Effects of Nuclear Weapons".
#	- Event has IBM computer display.

DATE	STATION	SECONDS DIGITIZED	REMARKS
9-19-57	BCN	10	RAINIER
10-8-58	BCN	10	Confirmed Blast
1-16-59	BCN	10	Central California
2-27-59	BCN	6	Central Utah
3-16-59	BCN	11	Central Nevada
3-23-59	BCN	10	Central Nevada
4-1-59	BCN	10	West Nevada
7-24-59	BCN	10	N. California
10-13-59	BCN	10	Central Arizona
10-17-61	FGU	10	Central Utah

	DATE	STATION	SECONDS DIGITIZED	REMARKS
	5-12-62	DUG	15	AARDVARK
	6-1-62	DUG	18	# RACOON (twice)
	6-6-62	DUG	15	# PACKRAT
	6-13-62	DUG	13	# DESMOINES
	6-21-62	DUG	20	# DAMAN I
	6-30-62	DUG	15	# SACRAMENTO
	7-4-62	SLC	15	Bingham Blast
	7-6-62	SLC	10	Bingham Blast
	7-6-62	DUG	14	SEDAN
**	7-6-62	DUG	14	# SEDAN
	7-13-62	DUG	7	MERRIMAC
**	7-13-62	DUG	15	# MERRIMAC
	7-24-62	DUG	15	Mexico
	7-27-62	DUG	16	# WICHITA
	8-3-62	PCU	10	N. Chile
	8-3-62	SLC	10	N. Chile
	8-24-62	DUG	18	# BOBAC
	9-6-62	SLC	11	Magna, Utah
	9-14-62	DUG	20	# HYRAX
	9-16-62	DUG	20	Mexico
	9-24-62	DUG	14	Hokkaido, Japan
	9-28-62	DUG	15	W. Columbia
	9-29-62	DUG	18	# Confirmed Blast
**	10-5-62	DUG	9	MISSISSIPPI
	10-12-62	DUG	20	# ROANOKE
	10-19-62	DUG	16	# Confirmed Blast
	10-19-62	DUG	12	Mexico
**	10-19-62	DUG	31	Mexico
	10-24-62	DUG	12	Mexico
	10-27-62	DUG	15	# Confirmed Blast
	11-12-62	DUG	12	Andreanof Island
	12-7-62	DUG	14	# Confirmed Blast
	12-11-62	DUG	15	Central Utah
	12-12-62	DUG	20	# NUMBAT
	12-29-62	DUG	15	N. Chile
	1-6-63	DUG	15	Kurile Islands
	1-27-63	SLC	15	Central Utah
**	2-22-63	DUG	25	North Pole
**	2-22-63	DUG	28	Dominican Republic
**	2-24-63	DUG	25	Guatemala

	DATE	STATION	SECONDS DIGITIZED	REMARKS
**	3-1-63	DUG	14	# *
	3-7-63	DUG	15	South Chile
**	3-15-63	DUG	17	# *
	4-24-63	PCU	5	Price, Utah
	4-24-63	SLC	15	Price, Utah
	5-4-63	DUG	15	Andreanof Islands
	5-6-63	PCU	15	Price, Utah
	5-6-63	DUG	15	Price, Utah
	5-16-63	PCU	15	Price, Utah
	5-17-63	DUG	15	Kurile Islands
	5-22-63	DUG	24	Mexico
	5-25-63	DUG	15	Denver
	5-25-63	PCU	15	Denver (bad)
	5-27-63	SLC	15	Fox Island
	6-1-63	DUG	15	Samoa
	6-3-63	DUG	18	Honshu
	6-3-63	DUG	15	Columbia
**	6-5-63	DUG	12	+ YUBA
**	6-6-63	DUG	20	#+ HUTIA
	6-10-63	DUG	15	Kamchatka
**	6-14-63	DUG	14	+ MATACO
	6-24-63	DUG	15	Fox Island
	6-25-63	SLC	15	Yellowstone
	6-25-63	DUG	15	Yellowstone
**	6-25-63	DUG	13	+ KENNEBEC
	7-2-63	DUG	15	Denver
	7-4-63	SLC	20	Tonga Islands
	7-4-63	DUG	20	Tonga Islands
	7-8-63	DUG	15	N. California
	7-15-63	DUG	15	Kamchatka
	7-16-63	DUG	15	Georgia, USSR
	7-17-63	DUG	15	West Nevada
**	7-20-63	DUG	12	S. Nevada
	8-8-63	DUG	15	Fox Island
**	8-12-63	DUG	15	#+ PEKAN
	8-13-63	DUG	15	Kodiak Island
	9-8-63	SLC	20	Fiji Islands
**	9-13-63	LPS	35	# BILBY
**	9-13-63	LPB	37	BILBY
	9-13-63	SLC	20	BILBY

	DATE	STATION	SECONDS DIGITIZED		REMARKS
**	10-11-63	DUG	15	+	GRUNION
**	10-16-63	PCU	20	+	CLEARWATER
**	10-16-63	SLC	17	+	CLEARWATER
**	10-16-63	DUG (Port.)	17	+	CLEARWATER
**	10-26-63	DUG	20	#	SHOAL
	10-26-63	DUG	20		SHOAL
**	11-14-63	DUG	14	#+	ANCHOVY
	11-19-63	DUG	14		Bingham Blast
	11-19-63	SLC	20		Bingham Blast
**	11-22-63	DUG	12	+	GREYS
**	12-6-63	DUG	18		Mono County, Calif.
**	12-10-63	DUG	35		West Bolivia
**	12-12-63	DUG	13	+	EAGLE
**	12-14-63	DUG	37		Central Alaska
**	12-16-63	DUG	26		Ecuador
**	12-19-63	DUG	32		Argentina
**	12-20-63	DUG	32		N. Peru
**	12-21-63	DUG	45		Tonga Islands
**	12-29-63	DUG	40		N. Chile
**	12-30-63	DUG	34		Kurile Islands
**	1-10-64	DUG	25		Kurile Islands
**	1-16-64	SLC	20	*	
**	1-19-64	DUG	25		Solomon Islands
**	1-23-64	DUG	12	*	
**	1-30-64	DUG	20	*	
**	2-1-64	DUG	31		Fox Island
**	2-6-64	DUG	30		Columbia
**	2-9-64	DUG	25		Fiji Islands
**	2-13-64	DUG	25		Bolivia-Brazil
**	2-13-64	DUG	12	*	
**	2-19-64	DUG	29		N. Chile
**	2-20-64	DUG	24		Kurile Islands
**	2-22-64	DUG	30		Kurile Islands
**	3-12-64	DUG	20	*	
**	3-15-64	DUG	20	#*	
**	3-23-64	DUG	20	#	Walker Lake, Nevada
**	3-24-64	DUG	20	#	Walker Lake, Nevada
**	3-31-64	DUG	25	#	Kurile Islands
**	4-7-64	DUG	20	#	Walker Lake, Nevada
**	4-8-64	DUG	40		Kurile Islands

DATE	STATION	SECONDS DIGITIZED	REMARKS
** 4-9-64	DUG	35	El Salvador
** 4-14-64	DUG	14	#*
** 4-14-64	DUG	33	Kurile Islands
** 5-14-64	DUG	13	#*
** 5-15-64	DUG	15	#*
** 6-11-64	DUG	20	#*
** 6-12-64	DUG	20	*
** 6-18-64	DUG	20	*
** 6-20-64	DUG	20	Mexico
** 6-25-64	DUG	12	*
** 6-30-64	DUG	14	*
** 7-7-64	DUG	33	Oregon Coast
** 7-16-64	DUG	12	#*
** 7-19-64	DUG	25	#*
** 8-8-64	DUG	30	Nicaragua
** 8-10-64	DUG	40	S. Peru
** 8-18-64	DUG	40	Peru-Brazil
** 8-24-64	DUG	30	Montana
** 9-23-64	DUG	19	Las Vegas, Nevada
** 10-22-64	DUG	35	SALMON

Data processing

Each of the traces of the vertical-component and two horizontal-component paper seismograms was hand-digitized for a total length of 15 to 40 sec; the length of the digitizing of each event usually depended on the clarity of the record and the quality of amplitudes of the events. The digitizing interval was 0.05 sec. The digitizing was done with a Gaertner microscope xy-coordinate comparator (Fig. 6-1). The readings were corrected for the tilt of the zero reference line of the seismogram trace by drawing a straight construction line at an angle of 9.5 minutes of arc counter-clockwise from the recorded base line at the beginning of the time interval to be digitized. For a recorder-drum speed of 60 mm/min, the error in amplitude involved in using this construction line as the corrected zero reference line is only 0.055 mm and 0.110 mm at times of 20 and 40 sec, respectively, after the start of digitizing; and this error in amplitude was considered negligible in this study.

The events that were digitized in this manner are given in table 6-1. In the early part of our work some seismograms, as for example those from the Boulder City station, were digitized at 0.1-sec intervals; and also some of these were not corrected for tilt. However, these were not used in the later detailed analysis discussed later in this section.

All paper seismograms that were digitized were carefully checked for differential shrinkage of the paper by measuring, with the Gaertner microscope xy-coordinate comparator, the distance between the corresponding successive minute marks on the Z, E-W, and N-S seismograms in that portion of each seismogram analyzed. For essentially all of the

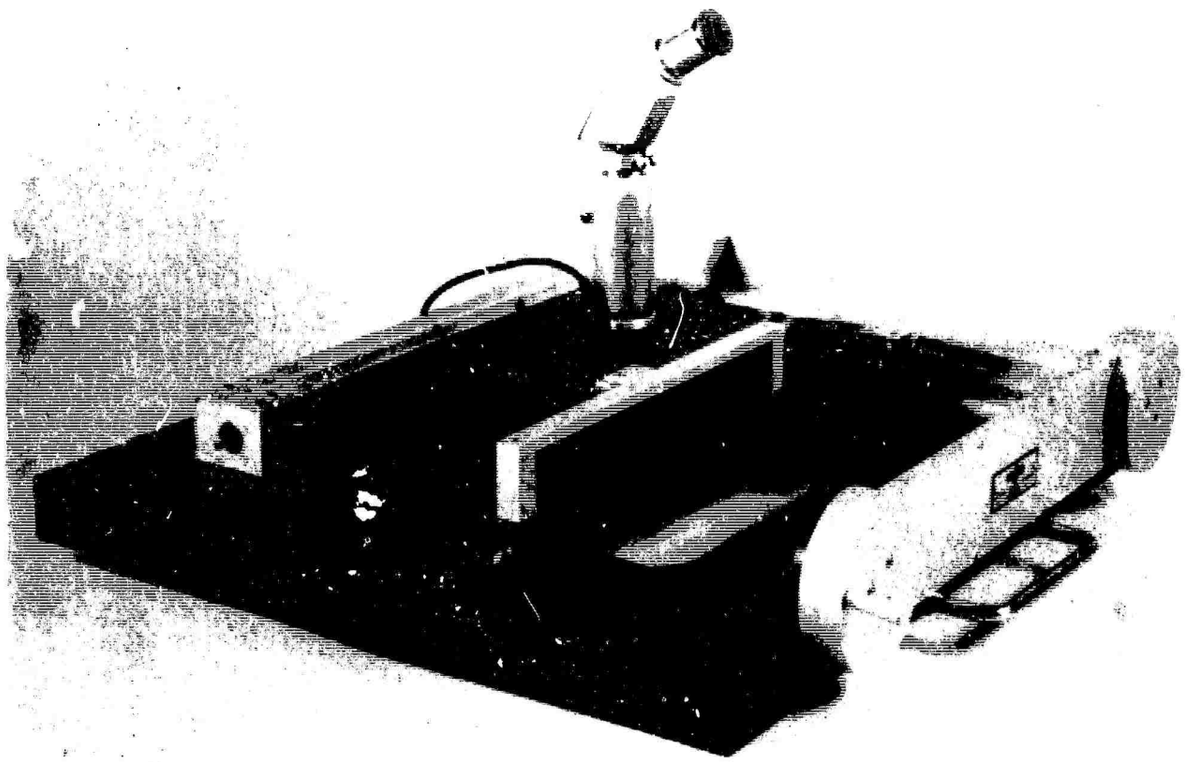

Figure 6-1. Gaertner microscope xy-coordinate comparator used for hand-digitizing seismograms.

seismograms digitized out to a total time interval of about 20 sec (20 mm for a recorder-drum speed of 60 mm/min), the differential paper shrinkage between the three-component records was less than 0.03 sec and hence considerably less than one digitizing interval (0.05 sec) and therefore considered negligible. For some of the seismograms digitized out to 40 sec (40 mm), however, the differential paper shrinkage slightly exceeded 0.05 mm; and proper adjustments in the reading procedures were made so that corresponding points on the three-component traces could be read and therefore compared with an accuracy of one digitizing interval (0.05 sec).

It had been determined from graphical synthesis that an error in the digitizing interval of 0.05 sec for seismic waves of 1.0-sec period would not appreciably change the character of the particle-motion diagram.

The digitized data for the Z, E-W, and N-S components were punched on IBM cards for subsequent data processing on either the IBM 7040 or IBM 1401, or both, which were available at the University of Utah Computer Center. Various computer programs were used in the presentation of the data and the subsequent analyses of the data that will now be described.

The computer also computed and printed out the values of epicentral distances (using the Richter method of calculations for short distances and Turner's method (Macelwane and Sohon, 1932, p. 285-287, for teleseismic distances) and printed out various forms of data presentation that were used in the analysis of the data.

Particle-motion diagrams

To facilitate the compilation of the particle-motion diagrams, the computer computed and printed out (from the E-W and N-S component values) the resolved radial-horizontal component value as measured along a horizontal azimuth toward the epicenter. The particle-motion diagrams were at first hand-plotted. Later, the data were processed with the computer so that the particle-motion diagrams were plotted automatically on a CalComp plotter. For each event, particle-motion diagrams were plotted in (1) a vertical plane along the azimuth toward the epicenter and (2) a horizontal plane; in this report these will be designated as vertical and horizontal particle-motion diagrams, respectively.

Other presentations of data

The computer printed out, in the form of a closely spaced dot presentation (at 0.05-sec intervals) on the abscissa the following four traces (Fig. 6-2):

(1) The values of the resolved radial-horizontal component (Fig. 6-2D).

(2) The values of the vertical component (Z) (Fig. 6-2E).

(3) The values of the horizontal north-south component (NS) (Fig. 6-2F).

(4) The values of the horizontal east-west component (EW) (Fig. 6-2G).

Figure 7-8 also shows an example of this type of presentation for the underground nuclear explosion DAMAN I, in which trace D is at the top of the diagram and traces E, F, and G are successively below it.

To facilitate the recognition of the various phases, three types of closely spaced dot presentations were printed out by the computer:

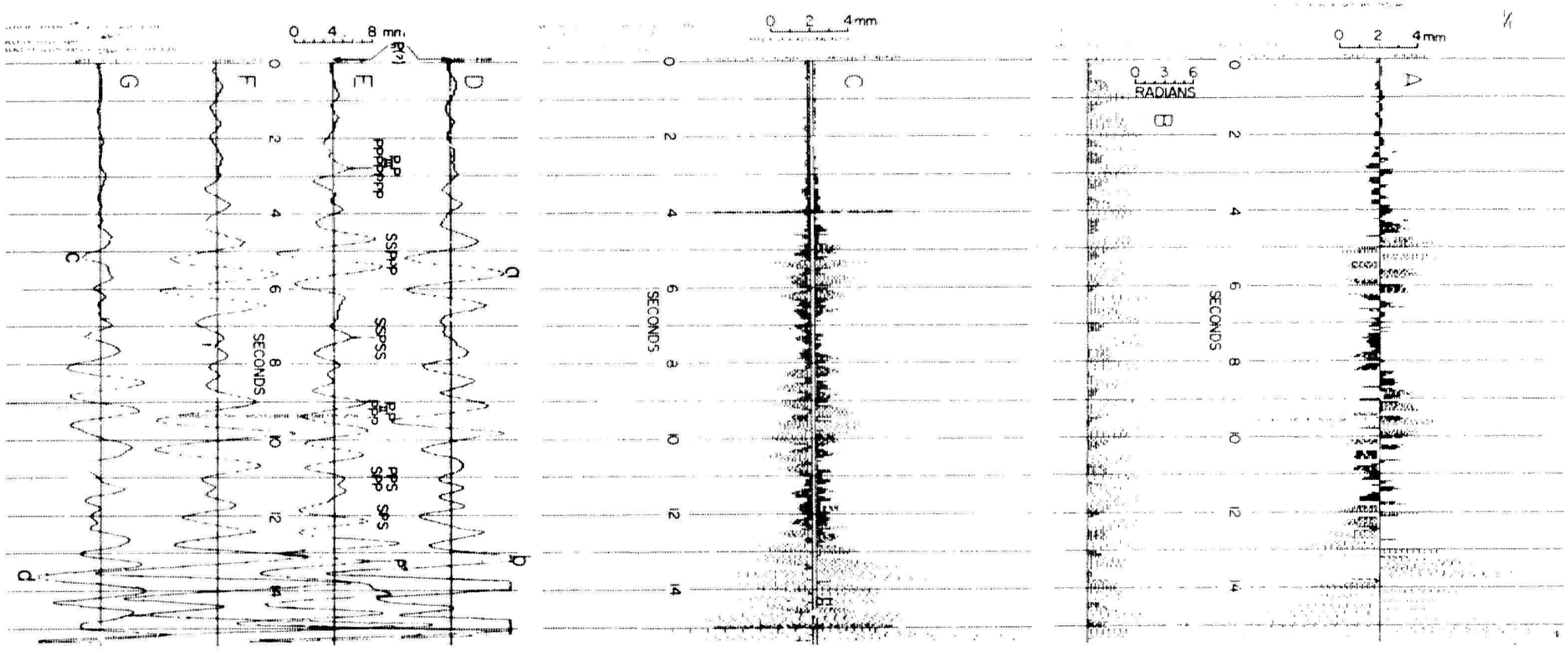

Figure 6-2. Various presentations of data for DAMAN I underground nuclear explo ion, Nevada test site, June 21, 1962: dot presentations to help listinguish character of ground motion--(A) S- and P-like, (B) prograde and retrograde, (C) linear and elliptical; and (D to E) digital-to-analog seismograms.

A. A presentation to distinguish between P-like and S-like motion. Figure6-3 shows how this presentation is obtained. On the vertical particle-motion diagram (Fig. 6-3 A), "P-like" (points a and b) and "S-like" (points c and d) motion, respectively, are shown between two successive points digitized at 0.05-sec intervals. The absolute magnitudes of these particle-motion vectors are then drawn to scale (in mm) as ordinate (Fig. 6-3 C) so that P-like and S-like motion will be plotted above and below the reference line, respectively, at intervals of time corresponding to the digitizing interval. A predominance of the length and number of dots above the abscissa during a given time interval indicates P-like motion and a predominance of the length and number of dots below the abscissa indicates S-like motion. Figure 6-2 A gives an example of this type of presentation for DAMAN I.

B. A presentation to distinguish between prograde and retrograde motion. As shown on the vertical particle-motion diagram (Fig. 6-3 A), the value of the angle of orientation of the line between two successive points, as measured counterclockwise from the horizontal line in the direction toward the epicenter, is either 0 to $\pi/2$ or π to $3\pi/2$ radians for S-like motion and either $\pi/2$ to π or $3\pi/2$ to 2π for P-like motion. The value of α is drawn to scale (in radians) as ordinate (Fig. 6-3 D) above the abscissa at intervals of time corresponding to the digitizing interval. This presentation indicates the direction of apparent rotation of the motion on the vertical particle-motion diagram: (1) if the values of the loci of the top of the dots increase as time increases, the motion is prograde (counterclockwise); and (2) if the values of the loci of the top of the dots decrease as time increases, the motion is retrograde (clockwise). It should be noted that for $\alpha = 0$, the

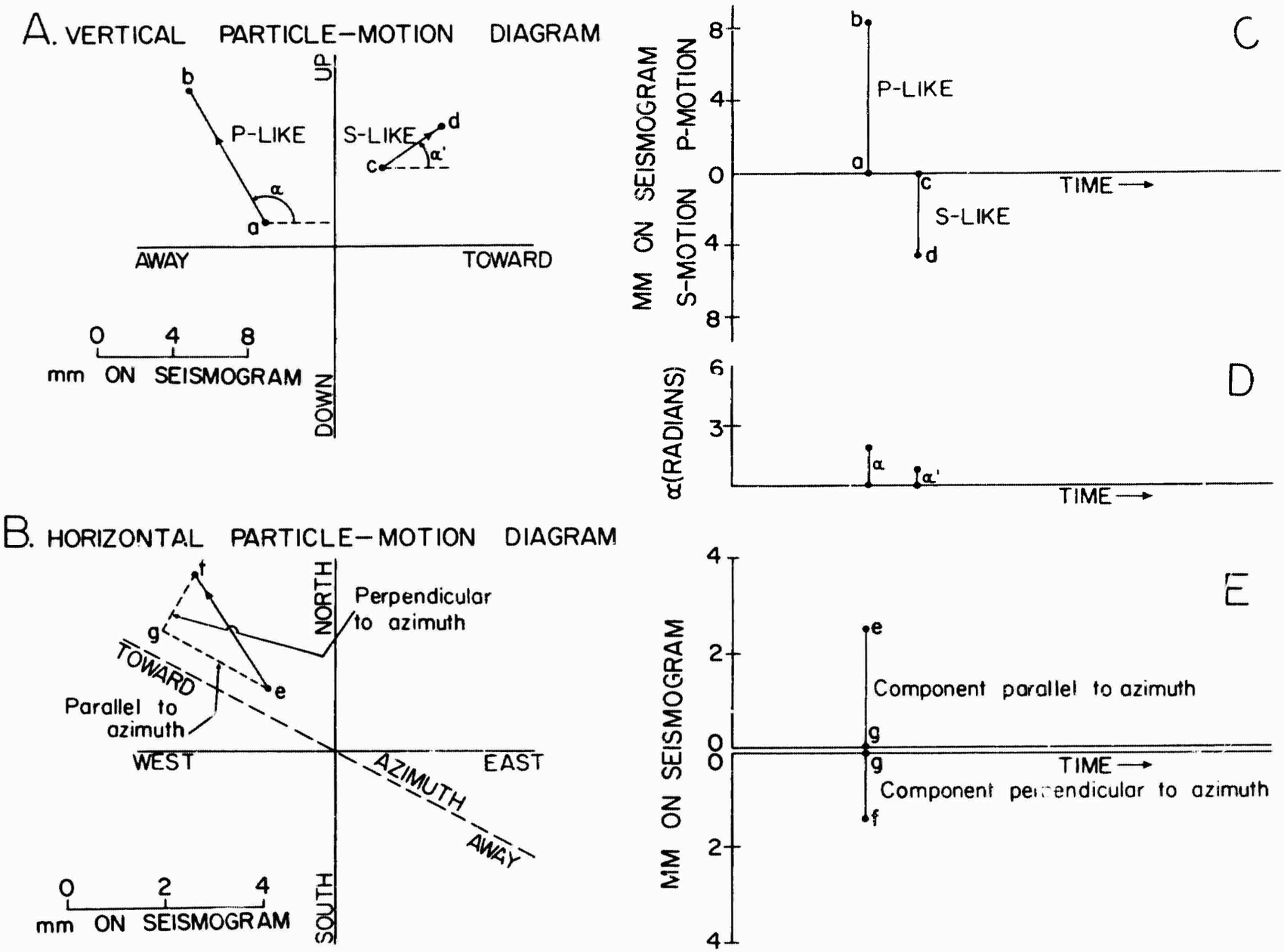

Figure 6-3. Portion of (A) vertical particle-motion diagram and (B) horizontal particle-motion diagram to show method of compiling dot presentations to help distinguish character of ground motion--(C) S- and P-like; (D) prograde and retrograde (measurement of angle α), and (E) linear and elliptical.

direction of motion is toward the epicenter. Figure 6-2B gives an example of this type of presentation for DAMAN I.

C. A presentation to distinguish between linear and elliptical motion. On the horizontal particle-motion diagram (Fig. 6-3 B), the length of the resultant line of two successive points (e and f) is projected on both (a) the horizontal azimuthal direction away from the epicenter, for which the component value is plotted to scale (in mm) above the reference line (Fig. 6-3 E) (this component is the resolved radial-horizontal component value) and also (b) the direction perpendicular to the azimuthal direction, for which the component value is plotted to scale (in mm) below the reference line (Fig. 6-3 E). In this presentation, a purely compressional (P) wave or shear (SV) wave polarized in a vertical plane along an azimuthal direction from the epicenter would have values in the direction of the azimuth only (dots above the abscissa only). Thus a preponderance of dots above the abscissa indicate linear-type motion; and a number of dots below the abscissa indicate a corresponding amount of elliptical-type motion in the horizontal plane. Figure 6-2C gives an example of this type of presentation for DAMAN 1.

It should be emphasized that the motions indicated by these presentations are ground surface motions only, and that caution must be used when relating this motion to body waves.

In Figure 6-2, for DAMAN I underground nuclear explosion, these dot presentations are displayed together with the digital-to-analog seismograms and vertically above them in the same time sequence. This type of composite presentation affords a powerful method of analysis of the phases.

CHAPTER VII

INTERPRETATION OF DATA RECORDED AT PERMANENT SEISMOGRAPH STATIONS

Consistency of the character of body-wave phases of underground nuclear explosions from Nevada test site and recorded at Dugway, Utah

Investigators of refraction seismic studies of earth crustal structure have long recognized the similarity of the seismograms obtained at a given station when shots are repeated at the same or near-by shotpoints. For example, for seismograms observed from the underground nuclear explosions LOGAN and BLANCA at an epicentral distance of 1610 km, Romney (1959, Fig. 2, p. 1492) recognized the similarity of the waveforms from both shots; he reported that "each of the HARDTACK underground nuclear explosions produced almost identical waveforms at a given station". To our knowledge, however, little quantitative analysis has ever been made of this similarity.

We will first discuss the striking consistency of the body-wave phases after the arrival of the first P energy, and later show how this consistency can be used for the positive detection and identification of certain underground nuclear explosions from the Nevada test site as recorded at the Dugway, Utah station.

Available data

The seismograms used in this study were obtained at the Dugway seismograph station, Utah (Fig. 7-1), which is one of the stations in the University of Utah network. The instrumentation is the type used in the standardized world-wide network operated in cooperation with the U.S. Coast and Geodetic Survey. The three-component system is matched, with a magnification of 400,000 for each of the three seismometers, namely the vertical (Z), and the two horizontal (EW and NS) seismometers. The drum speed of the recorder is 60 mm/min.

Figure 7-1. Map showing Nevada test site (NTS) and Dugway, Utah seismograph station. Δ = 437 to 448 km. Bearing of NTS from Dugway = S. 40° W.

The seismograms for a total of 22 announced underground nuclear explosions at the Nevada test site (NTS) were used for this study. Figure 7-2 shows the locations of 15 of these explosions, for which the latitudes and longitudes have been declassified. The announced Richter magnitudes of these events were 3.9 to 5.8. In addition, several other events which have not yet been declassified but which are believed to be underground nuclear explosions from NTS, were analyzed; however, these are not included in this report.

Tables 7-1 and 7-2 give unclassified pertinent data incident to the announced nuclear explosions studies: table 7-1 gives principal facts that facilitate the intepretation; and table 7-2 includes data either observed on the seismograms or computed therefrom.

Comparison of underground nuclear explosions

In the present study, an analysis was made of seismograms obtained at a single permanent seismograph station, namely Dugway, Utah, from (1) 22 announced underground nuclear explosions at the Nevada test site (NTS) and (2) various other events which, on the basis of a brief examination of the original seismograms only, were considered tentatively to be possible explosions from the NTS and therefore worthy of detailed study.

During this analysis, a striking consistency in the character of the phases of the body waves during the first 15 to 20 sec after the first P arrival was discovered for several of the confirmed underground nuclear explosions and for several of the events that we now consider to be positively, but as yet unclassified, underground nuclear explosions. The consistency of the character of the phases is so striking that now only can some of the body phases, including certain provisionally interpreted con-

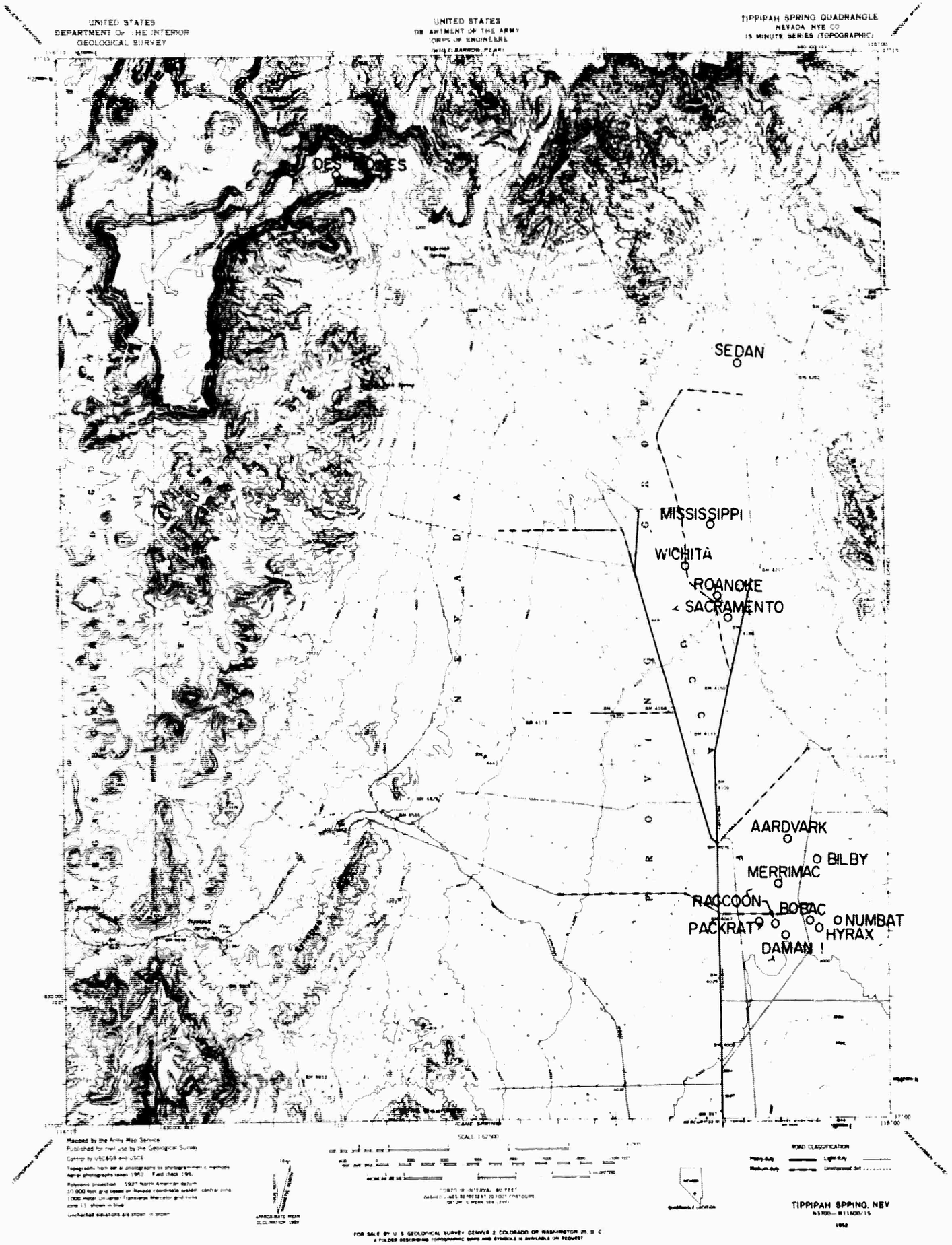

Figure 7-2. Topographic map (U.S. Geological Survey) of Yucca Flat at Nevada test site and the names and locations of 15 of the 22 announced underground nuclear explosions included in this study.

December 11, 1963, from Lieut. Robert E. Riecker, U.S. Air Force, who obtained this information from published data.

Date (GCT)	Name	Magnitude (Richter scale)	Yield [1] (Kt)	Epicentral distance to Dugway, Utah (km)	Time of detonation (GCT) hr:min:sec	Latitude (North)	Longitude (West)	Type of material	Shot Depth (feet)
5-12-62	AARDVARK	4.9	38	446.1	19:00:00.103#	37°03'55"	116°01'49"	Tuff	1,434 (1,424)**
6-1-62	RACOON	-	Low	448.0	17:00:00.137#	37°02'44"	116°02'04"	Alluvium	550 (539)**
6-6-62	PACKR	4.4 ± 0.5	Low	448.2	17:00:00.122#	37°02'45"	116°02'21"	Alluvium	869 (860)**
6-13-62	DES MOINES	4.4	Low	440.1	21:00:00.116#***	37°13'20"	116°09'44"	Tuff	655 (1,424)** (1,205) [2]
6-21-62	DAMAN I	-	Low	448.0	17:00:00.131#	37°02'35"	116°01'50"	Alluvium	860 (854)**
6-30-62	SACRAMENTO	4.1 ± 0.4	Low	449.5	21:30:00.155#	37°07'03"	116°02'51"	Alluvium	500
7-6-62	SEDAN	4.9 ± 0.4	100	437.3	17:00:00.147	37°10'37"	116°02'43"	Alluvium	600 (635)**
7-13-62	MERRIMAC	4.6 ± 0.3	Low	447.1	16:00:00.2#	37°03'18"	116°02'00"	Alluvium	1,370 (1,356)**
7-27-62	WICHITA	4.1 ± 0.6	Low	442.0	21:00:00.2#	37°07'47"	116°03'23"	Alluvium	750 (493)**
8-24-62 (2nd expl.)	BOBAC	4.0 ± 0.5	Low	447.4	17:00:00.13#	37°02'46"	116°01'26"	Alluvium	680 (675)**
9-14-62	HYRAX	4.1 ± 0.7	Low	447..	17:10:00.1#	37°02'38.8	116°01'16.0"	Alluvium	718 (720)**
9-29-62	ALLEGHENY*	-	Low	-	17:00:00.2##	-	-	Tuff**	692**
10-5-62	MISSISSIPPI	-	Intermed**	440.8	17:00:00.15#	37°08'22"	116°03'01"	Tuff	1,620**
10-12-62	ROANOKE	3.9 ± 0.3	Low	442.2	15:00:00.155#	37°07'22"	116°03'03"	Alluvium (Tuff)	514 (510)**
10-19-62	BANDICOOT*	-	Low	-	18:00:00.08#]	-	-	Alluvium**	800**
10-27-62	SANTEE*	-	Low	-	15:00:00.14##	-	-	Alluvium**	1,050**
12-7-62	TENDRAC*	-	Low	- -	19:00:00.09##	-	-	-	-
12-12-62	NUMBAT	4.3 ± 0.5	Low	446.9	18:45:00.1***	37°02'46.0"	116°00'56.2"	Alluvium	775
6-6-63	HUTIA	-	Low**	-	14:00**	-	-	Alluvium	442**
8-12-63	PEKAN*	-	Low	-	23:45**	-	-	Alluvium**	997**
9-13-63	BILBY	5.8	200	446.0	17:00:00.13	37°03'38"	116°01'18"	Tuff	2,314 (2,413)**
10-26-63	SHOAL	-	About 12**	-	17:00:00.100 [4]	39°12'01" [4]	118°22'49" [4]	Granite**	1,205**
11-14-63	ANCHOVY*	-	Low	-	16:00**	-	-	Alluvium	853**

[1] Low yield means less than 20 kilotons; intermediate means 20 to 999 kilotons, inclusive. All yield data taken from Glasst

[2] Depression is subsidence of earth into underground cavity, as distinguished from crater by throw-out of earth. All depress

[3] Excavation experiment; formed crater about 1,280 ft. diameter, 320 ft. maximum depth (Glasstone, 1964).

[4] Written communication from C. C. Bates to T. W. Caless, Oct. 14, 1964; also Caless, 1965, p 1-1.

#(1) Written communication December 11, 1963 from Lieut. Robert E. Riecker, U.S. Air Force and (2) written communication, July 9 March 29, 1963 from Major General A. W. Betts, U.S. Atomic Energy Commission.

Written communication, July 9, 1962, October 8, 1962 and March 29, 1963 from Major General A. W. Betts, U.S. Atomic Energy

* Written communication from Dixon Stewart, U.S. Atomic Energy Commission, received October 21, 1964.

** Glasstone, Samuel (editor), 1964, The effects of nuclear weapons: published by U.S. Atomic Energy Committee, April 1962, A February 1964. Some shot-depth data differ somewhat from those originally given us by Lieut. R. E. Riecker.

*** The detonation times of 2200 and 1745 for DES MOINES and NUMBAT, respectively, on p. 6776 of Glasstone are incorrect (writ from Brigadier General D. L. Crowson, U.S. Air Force).

A

nd nuclear explosions at Nevada test site (NTS). All data, unless otherwise noted, were obtained in written communication, Robert E. Riecker, U.S. Air Force, who obtained this information from published data.

	Yield [1] (kt)	Epicentral distance to Dugway, Utah (km)	Time of detonation (GCT) hr:min:sec	Latitude (North)	Longitude (West)	Type of material	Shot Depth (feet)	Surface Elevation (feet)	Shot Elevation (feet)	Depression [2] (Diam. & Depth (feet)
	38	446.1	19:00:00.103#	37°03'55"	116°01'49"	Tuff	1,434 (1,424)**	4,072	2,638	924;?2
	Low	448.0	17:00:00.137#	37°02'44"	116°02'04"	Alluvium	550 (539)**	4,021	3,471	314;24
	Low	448.2	17:00:00.122#	37°02'45"	116°02'21"	Alluvium	869 (860)**	4,022	3,153	598;40
	Low	440.1	21:00:00.116#***	37°13'20"	116°09'44"	Tuff	655 (1,424)** [4] (1,205) [4]	5,652	4,997	None
	Low	448.0	17:00:00.131#	37°02'35"	116°01'50"	Alluvium	860 (854)**	4,016	3,156	556;96
	Low	442.5	21:30:00.155#	37°07'03"	11 02'51"	Alluvium	500	4,240	3,740	356;41
	100	437.3	17:00:00.147	37°10'37"	116°02'43"	Alluvium	600 (635)**	4,317	3,657	[3]
	Low	447.1	16:00:00.2#	37°03'18"	116°02'00"	Alluvium	1,370 (1,356)**	4,041	3,671	662;50
	Low	442.0	21:00:00.2#	37°07'47"	116°03'23"	Alluvium	750 (493)**	4,239	3,489	390;36
	Low	447.4	17:00:00.13#	37°02'46"	116°01'26"	Alluvium	680 (675)**	4,013	3,333	425;45
	Low	447.4	17:10:00.1#	37°02'38.8	116°01'16.0"	Alluvium	718 (720)**	4,016	3,298	474;100
	Low	-	17:00:00.2##	-	-	Tuff**	692**		-	100;10
	Intermed**	440.8	17:00:00.15#	37°08'22"	116°03'01"	Tuff	1,620**		2,609	425;125
	Low	442.2	15:00:00.155#	37°07'22"	116°03'03"	Alluvium (Tuff)	514 (510)**	4,197	3,683	80;5
	Low	-	18:00:00.08#[1]	-	-	Alluvium**	800**	-	-	300;100
	Low	-	15:00:00.14##	-	-	Alluvium**	1,050**	-	-	400;20
	Low	-	19:00:00.09##	-	-	-	-	-	-	-
	Low	446.9	18:45:00.1***	37°02'46.0"	116°00'56.2"	Alluvium	775	4,030	3,255	500;40
	Low**	-	14:00**	-	-	Alluvium	442**	-	-	300;20
	Low	-	23:45**	-	-	Alluvium**	997**	-	-	550;60
	200	446.0	17:00:00.13	37°03'38"	116°01'18"	Tuff	2,314 (2,413)**	4,074	1,760	1800;80
	About 12**	-	17:00:00.100 [4]	39°12'01" [4]	118°22'49" [4]	Granite**	1,205**	5,248 [4]	-	-
	Low	-	16:00**	-	-	Alluvium	853**	-	-	600;65

20 kilotons; intermediate means 20 to 999 kilotons, inclusive. All yield data taken from Glasstone, 1964.

f earth into underground cavity, as distinguished from crater by throw-out of earth. All depression data taken from Glasstone, 1964.

ed crater about 1,280 ft. diameter, 320 ft. maximum depth (Glasstone, 1964).

C. C. Bates to T. W. Caless, Oct. 14, 1964; also Caless, 1965, p I-1.

ber 11, 1963 from Lieut. Robert E. Riecker, U.S. Air Force and (2) written communication, July 9, 1962, October 8, 1962, and General A. W. Betts, U.S. Atomic Energy Commission.

9, 1962, October 8, 1962 and March 29, 1963 from Major General A. W. Betts, U.S. Atomic Energy Commission.

Dixon Stewart, U.S. Atomic Energy Commission, received October 21, 1964.

, 1964 The effects of nuclear weapons: published by U.S. Atomic Energy Committee, April 1962, Appendix B; revised edition reprinted depth data differ somewhat from thoseoriginally given us by Lieut. R. E. Riecker.

30 and 1745 for DES MOINES and NUMBAT, respectively, on p. 6776 of Glass ne are incorrect (written commu ication, January 18, 1965, L. Crowson, U.S. Air Force).

B

Table 7-2.-- Observed travel times and other pertinent data of announced underground nuclear explosions, Nevada test site (NTS).

Date (GCT)	Name	Epicentral Distance to Dugway, Utah (km)	Time of Detonation (GCT) h m s	Time# of Start of Digitizing (GCT) h m s	Observed (or Estimated) Time# of Arrival of P_n (GCT) h m s	Observed (or Estimated) Travel Time of P_n (sec)	Time of P_n(?) arrow to Left (L) or Right (R) of 0.00 on Digital-to-Analog Seismogram (sec)	Length of Time Digitized (sec)
10-26-63	SHOAL	489.8	17 00 00.100	17 01 08.8	17 01 08.8	68.7	0.0	
6-6-62	PACKRAT	448.2	17 00 00.122	17 01 02.1	(17 01 02.5)	(62.4)	0.4 to R	15
6-21-62	DAMAN I	448.0	17 00 00.131	17 01 02.1	(17 01 02.0)	(61.9)	0.1 to L	20
6-1-62	RACCOON	448.0	17 00 00 137	17 01 03.8	*	*	*	18
8-24-62	BOBAC	447.4	17 00 00.13	17 01 02.1	(17 01 02.3)	(62.2)	0.2 to R	18
9-14-62	HYRAX	447.4	17 10 00.1	17 11 02.1	(17 11 02.5)	(62.4)	0.4 to R	20
7-13-62	MERRIMAC	447.1	16 00 00 2	16 01 01.0	(16 01 02.2)	(62.0)	1.2 to R	15
12-12-62	NUMBAT	446.9	18 45 00.1	18 46 02.1	(18 46 02.4)	(62.3)	0.3 to R	20
5-12-62	AARDVARK	446.1	19 00 00.103	19 01 02.5	19 01 02.4**	62.3(?)	0.1 to L	14
9-15-63	BILBY	446.0	17 00 00.13	17 01 02.2	17 01 02.3	62.2	0.1 to R	
6-30-62	SACRAMENTO	442.5	21 30 00.155	21 31 02.0	(21 31 01.8)	(61.6)	0.2 to L	15
10-12-62	ROANOKE	442.2	15 00 00.155	15 01 02.1	(15 01 01.8)	(61.6)	0.3 to L	20
7-27-62	WICHITA	442.0	21 00 00.2	21 01 02.1	(21 01 01.7)	(61.5)	0.4 to L	16
10-5-62	MISSISSIPPI	440.8	17 00 00.15	17 01 02.1	(17 01 02.0)	(61.9)	0.1 to L	9
7-6-62	SEDAN	437.3	17 00 00.147	17 01 01.1	(17 01 01.3)	61.2	0.2 to R	14
6-13-62	DES MOINES	440.1	21 00 00.116	21 01 02.1	(21 01 01.2)	(61.1)	0.9 to L	13
9-29-62	ALLEGHENY		17 00 00.2	17 01 02.1	(17 01 01.6)	(61.4)	0.5 to L	18
10-19-62	BANDICOOT		18 00 00.08	18 01 02.1	(18 01 02.6)	(62.5)	0.5 to R	16
10-27-62	SANTEE		15 00 00.14	15 01 02.1	*	*	*	15
12-7-62	TENDRAC		19 00 00.09	19 01 03.6	(19 01 02.6)	(62.5)	1.0 to L	14
6-6-63	HUTIA		14 00	14 01 03.8	*	*	*	20
8-12-63	PEKAN		23 45	23 46 02.3	(23 46 02.3)	(62.2(?))[1/]	*	15
11-14-63	ANCHOVY		16 00	16 01 05.3	(16 01 02.4)	(62.3(?))[1/]	2.9 to L	14

* Amplitude too small for accurate determination.
** On EW seismogram only (vertical seismogram has a considerable amount of local noise. P_n may have arrived slightly earlier than indicated on this seismogram, which also had a considerable amount of local noise

Corrected for any necessary clock correction.

1/ Assumes that the time of detonation was about 00.1 sec after the minute indicated in the "Time of detonation" column.

BLANK PAGE

verted waves, be recognized, but also certain underground nuclear explosions can be positively detected and identified by this similarity.

In the present report, this consistency of the character of the phases of certain underground nuclear explosions will be described; and an interpretation of the recognizable body-wave phases and a comparison of their relative amplitudes will be given.

Crustal models and possible body-wave phases for area of investigation

The crustal model of Berg and others (1960) for the eastern part of the Basin and Range province, as determined from chemical explosions at Promontory and Lakeside, Utah and from underground nuclear explosions at the Nevada test site, comprises (1) a top 9-km-thick layer with a velocity of 5.73 km/sec; (2) a 16-km-thick layer with a velocity of 6.33 km/sec; and (3) a 47-km-thick layer with a velocity of 7.59 km/sec overlying a mantle at a depth of 72 km with a velocity of 7.97 km/sec. The crustal model of Pakiser and Hill (1963), which was obtained with an unreversed northward-trending seismic refraction profile from underground nuclear explosions at the Nevada test site that extended northward to Elko, Nevada and beyond, comprises essentially a one-layer crust with a velocity of 6.03 km/sec overlying the mantle at a depth of 28 km and with a velocity of 7.84 km/sec. Pakiser and Hill (1963, p. 5763) cite definite evidence for an intermediate layer of velocity 6.7 km/sec along reversed profiles extending from Elko, Nevada.

The epicentral distance of the events for most of the seismograms investigated in this phase of the study was 437 to 448 km (table 7-2). For these epicentral distances and using the earth crustal model of Berg and others (1960) for the eastern part of the Basin and Range province, Figure 7-3 shows the ray paths and some of the various phases hat could theoretically be expected to arrive at Dugway from NTS. Listing them in the order of expected arrival at Dugway, we have:

P_n (i.e., PPPPP)	The refraction from the 25-km-depth boundary.
PPPPPPP and/or $P_{III}P$	The refraction from the 72-km-boundary. The reflection off the 72-km-depth boundary.
SSPPP	A P phase, which is a head waves which originated at the explosion as shear and which was converted to P at the 25-km-depth boundary, and continued on as P.
SSPSS	An S wave which is converted to P at the 25-km-depth boundary and travels back up through the crust as S.
PPP and/or $P_{II}P$	The refraction from the 9-km-depth boundary. The reflection off the 25-km-depth boundary.
PPS and SPP	Head-wave conversions from the 9-km-depth boundary.
SPS	A shear phase, which originated at the explosion as shear and which was converted to P at the 9-km-depth boundary, and then converted back to S.
$\bar{P}$ '	A channel wave in the upper part of the crust.

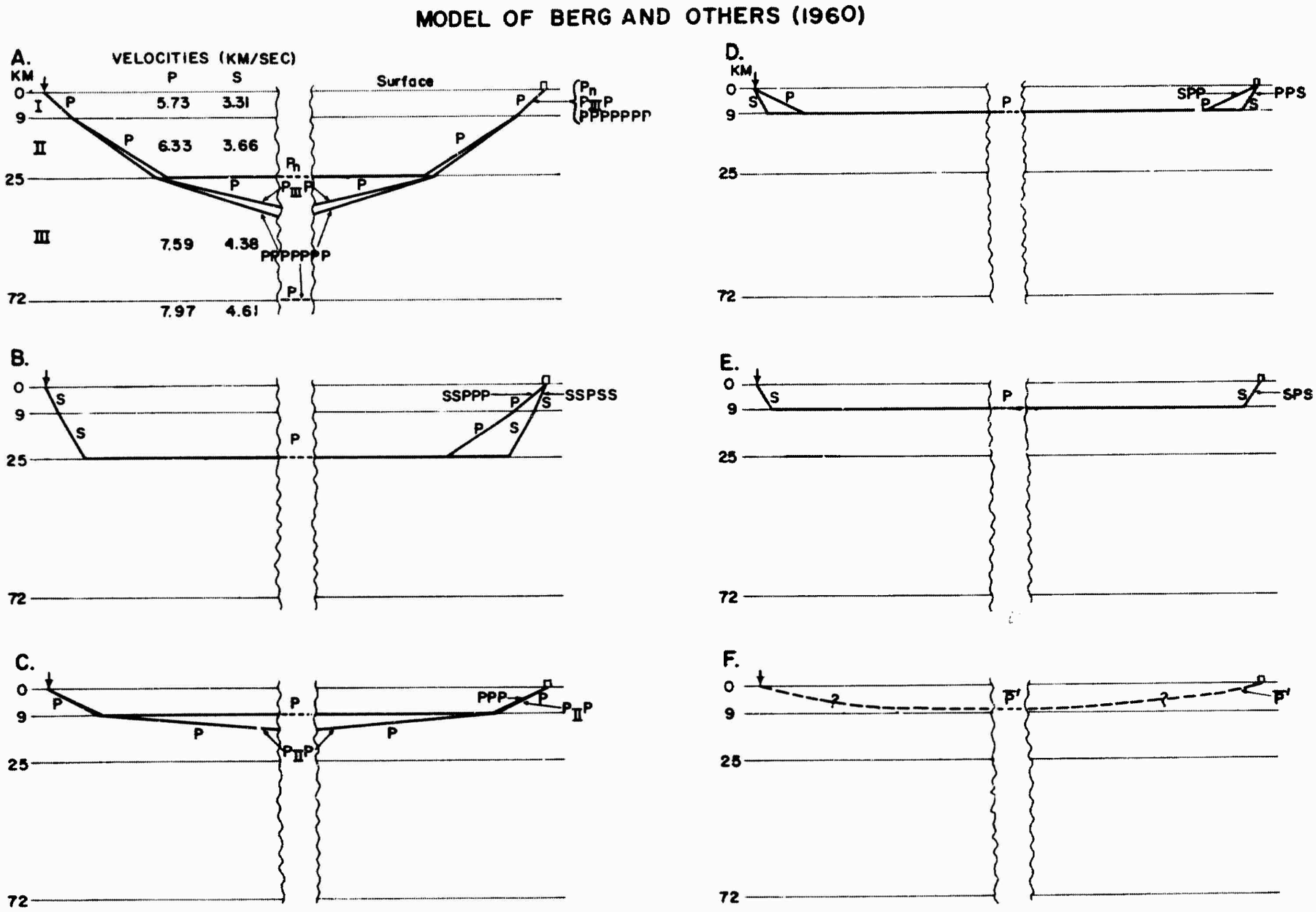

Figure 7-3. Ray paths of some possible phases traveling from Nevada test site to Dugway, assuming horizontal layers and earth crustal model of Berg and others (1960).

Using the model of Berg and others (1960), Figure 7-4 shows the true angles at which some of these phases should arrive at Dugway from NTS. For this same model, Figure 7-5 shows the travel-time curves for these phases. It should be noted that for an epicentral distance of about 448 km, for example, the various phases arrive at intervals of about 2 to 4 sec after each other; at a couple of times, however, there is a possible overlapping of the phases.

Using the digitized data, both vertical particle-motion diagrams (that is, in a vertical plane along the great-circle azimuth away from the explosion) and horizontal particle-motion diagrams (that is, in a horizontal plane) were plotted--at first by hand-plotting and later in the project with a CalComp plotter.

Figure 7-6 shows the vertical particle-motion diagrams for DAMAN I underground nuclear explosion. The scale, in mm on the original seismogram, are shown; the scale may change from one diagram to the next. Also note that "toward" and "away" from the explosion are to the right and left, respectively--which is opposite to the usual convention. "Up" and "down" motion are as indicated. P-like motion would be dominantly in quadrants II and IV, whereas S-like motion would be dominantly in quadrants I and III. The dots are at the 0.05-sec digitizing intervals, and the numbers are in seconds after the start of digitizing.

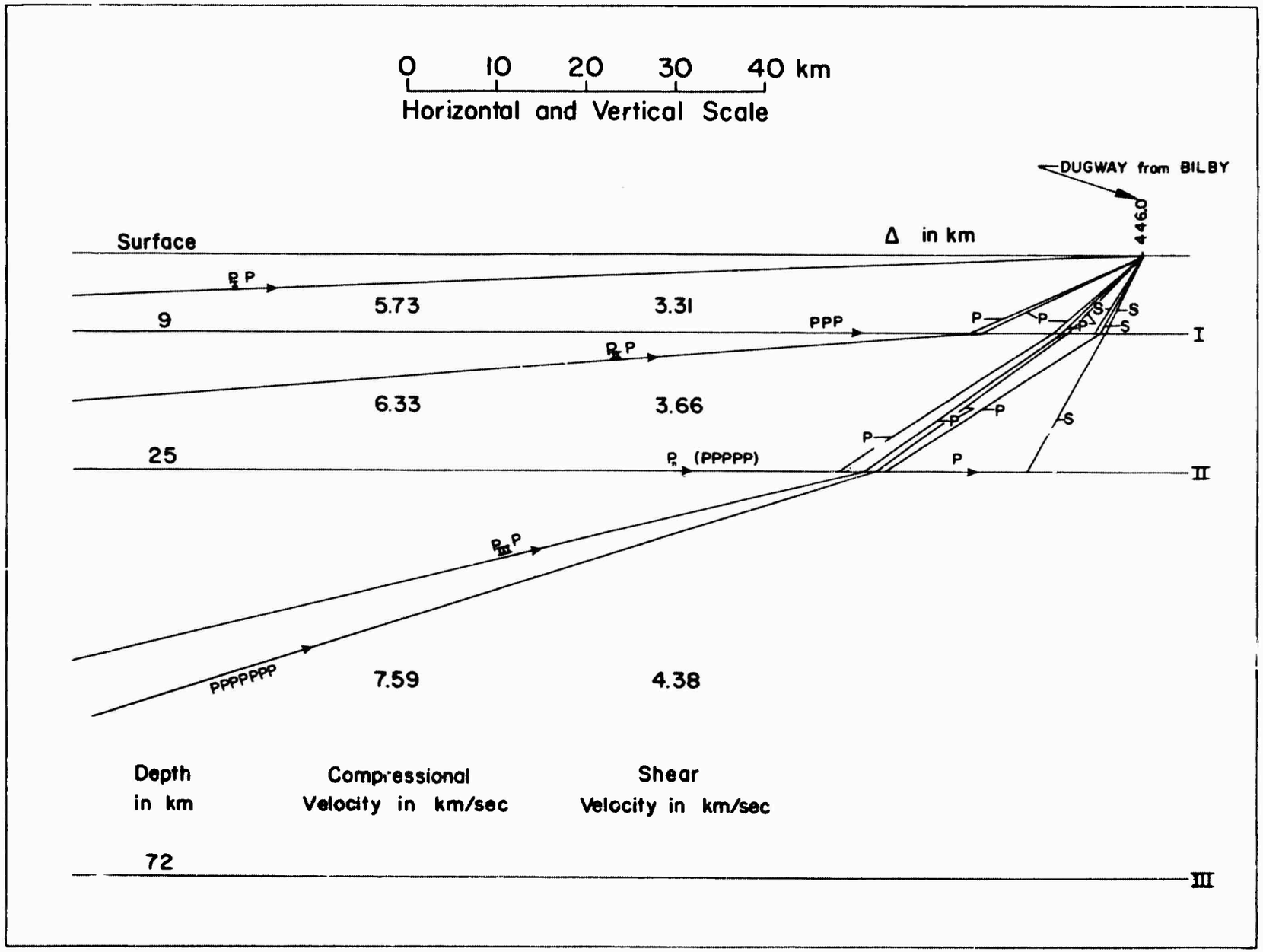

Figure 7-4. Ray paths of some possible phases arriving at Dugway from BILBY underground nuclear explosion, Nevada test site, September 13, 1963 assuming horizontal layers and earth crustal model of Berg and others (1960).

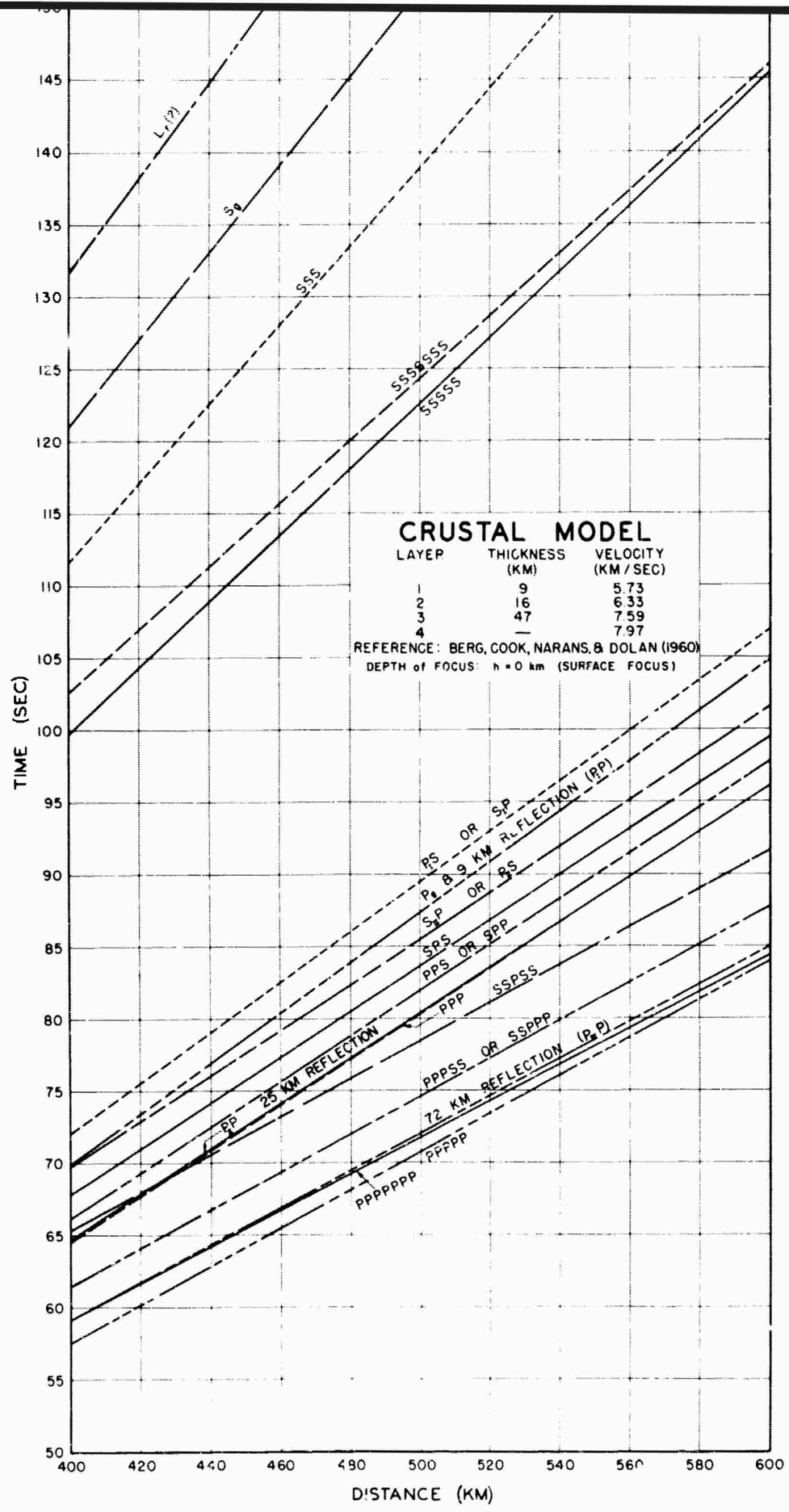

Figure 7-5. Theoretical travel-time curves for various refracted, reflected, and converted waves using the earth crustal model of Berg and others (1960) for the eastern part of the Basin and Range province. Horizontal layering is assumed.

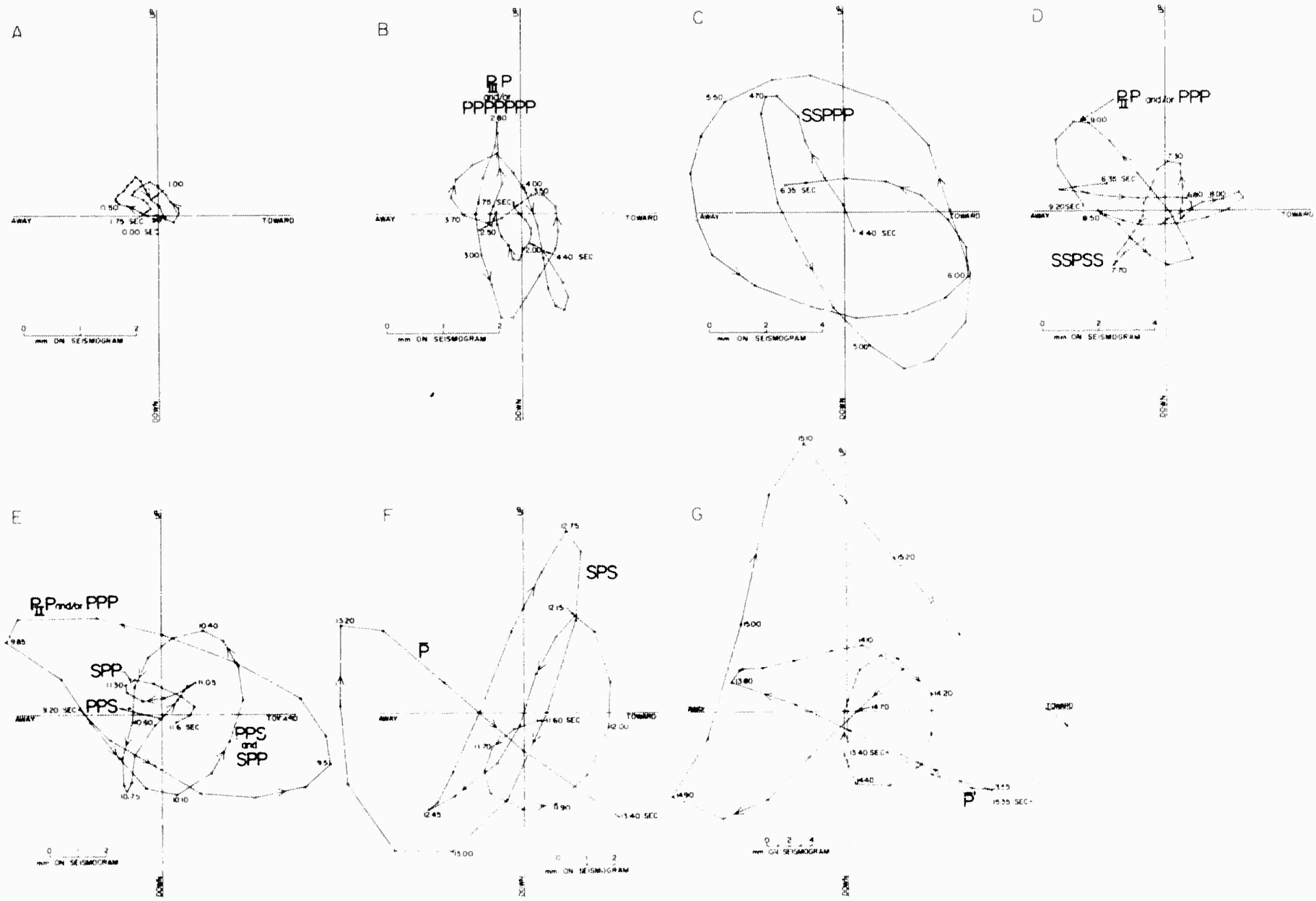

Figure 7-6. Vertical particle-motion diagrams, DAMAN I underground nuclear explosion, Nevada test site, June 21, 1962, time interval 0.00 to 15.35 sec; 0.00 = 17h 01m 02.1s GCT.

Using the same crustal model of Berg and others (1960) just described, we provisionally interpret the phases indicated on this particle-motion diagram as follows:

Approximate time (sec)	Phase
(Not seen on this record--amplitude too small)	P_n
2.5	$P_{III}P$ and/or PPPPPPP
4	SSPPP
7 1/2	SSPSS
8	$P_{II}P$ and/or PPP
10.1	PPS and SPP
11 1/2	SPS
13	$\bar{P}$; or a Multiple of P

The phases correspond well in arrival time with those shown in table 7-3 for this model. However, there are still some problems in identifying positively several of the phases that need to be resolved.

Table 7-3 shows the theoretical travel times of early-arriving body-wave phases, including certain converted head waves and certain reflected waves, for an epicentral distance of 448 km (Nevada test site to Dugway, Utah) for the crustal models of Pakiser and Hill (1963) and Berg and others (1960). The time interval Δt, is the calculated time of arrival of each phase after the arrival of P_n as based on each model.

Although the travel times for some of the phases differ markedly between the model, the travel times for other of the phases are essentially the same.

Table 7-3. Theoretical travel times of early-arriving body-wave phases, including certain converted head waves and certain reflected waves, for an epicentral distance of 448 km (Nevada test site to Dugway, Utah) for the crustal models of Pakiser and Hill (1963) and Berg and others (1960). Time Δt is the calculated time of arrival of each phase after the arrival of P_n, as based on the model.

Phase	Crustal model: Pakiser and Hill (1963) Travel Time (sec)	Pakiser and Hill (1963) Δt (sec)	Berg and others (1960) Travel Time (sec)	Berg and others (1960) Δt (sec)
P_n	63.0	0.0	63.9 [1/]	0.0
PPPPPPP	--	--	65.2	1.3
$P_{III}P$	--	--	65.3	1.4
SSPPP	67.3	4.3	67.8	3.9
SSPSS	71.6	8.6	71.7	7.8
PPP** and/or $P_{II}P$	75.2	12.4	72.3	8.4
PPS and/or SPP	--	--	74.0	10.1
SPS	--	--	75.7	11.8
P_g	74.6	11.6	78.3	14.4
$P_{II}S$ or $S_{II}P$	81.3	18.3	77.3	13.4
S_n (SSSSS)	109.3	46.5	110.7	46.8
S_g	128.5	65.7	135.5	71.6

[1/] The travel time of the first arrival shown on Fig. 7 of Berg and others (1960, p. 525) is 62.9 sec, which is in excellent agreement with that of Pakiser and Hill (1963).

** PPP is for model of Berg and others (1960) only.

Figures 7-7 and 7-8 show the digital-to-analog seismograms of BILBY and DAMAN I, respectively. In each figure, from top to bottom, are:

D. The resolved radial-horizontal component

E. The Z component

F. The north-south component

G. The east-west component

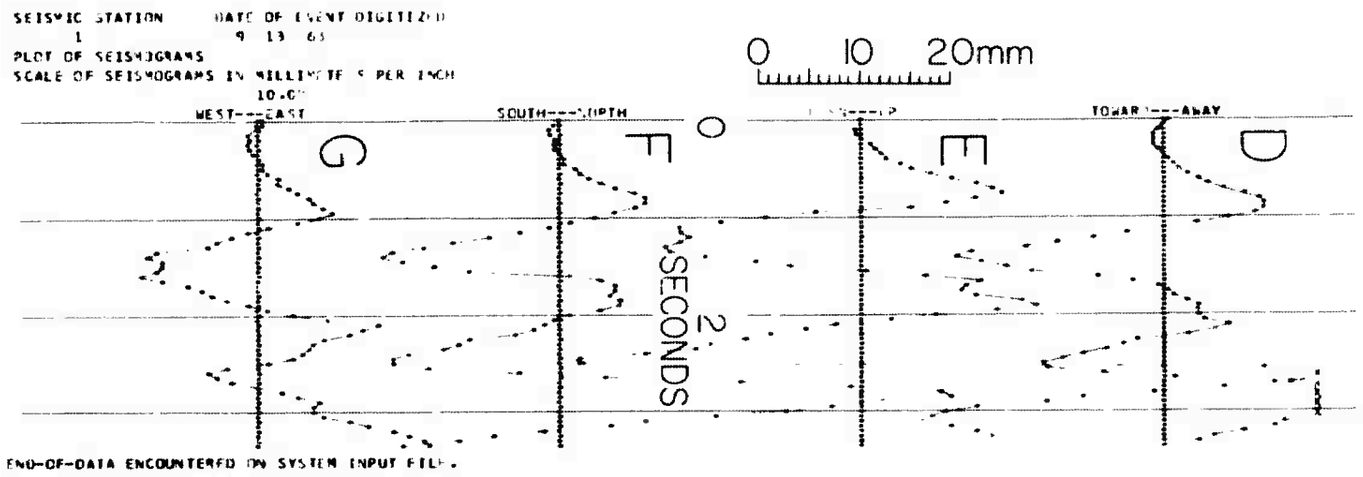

Figure 7-7. Digital-to-analog seismogram, BILBY underground nuclear explosion, Nevada test site, September 13, 1963; 0.00 = 17h 01m 02.2 GCT.

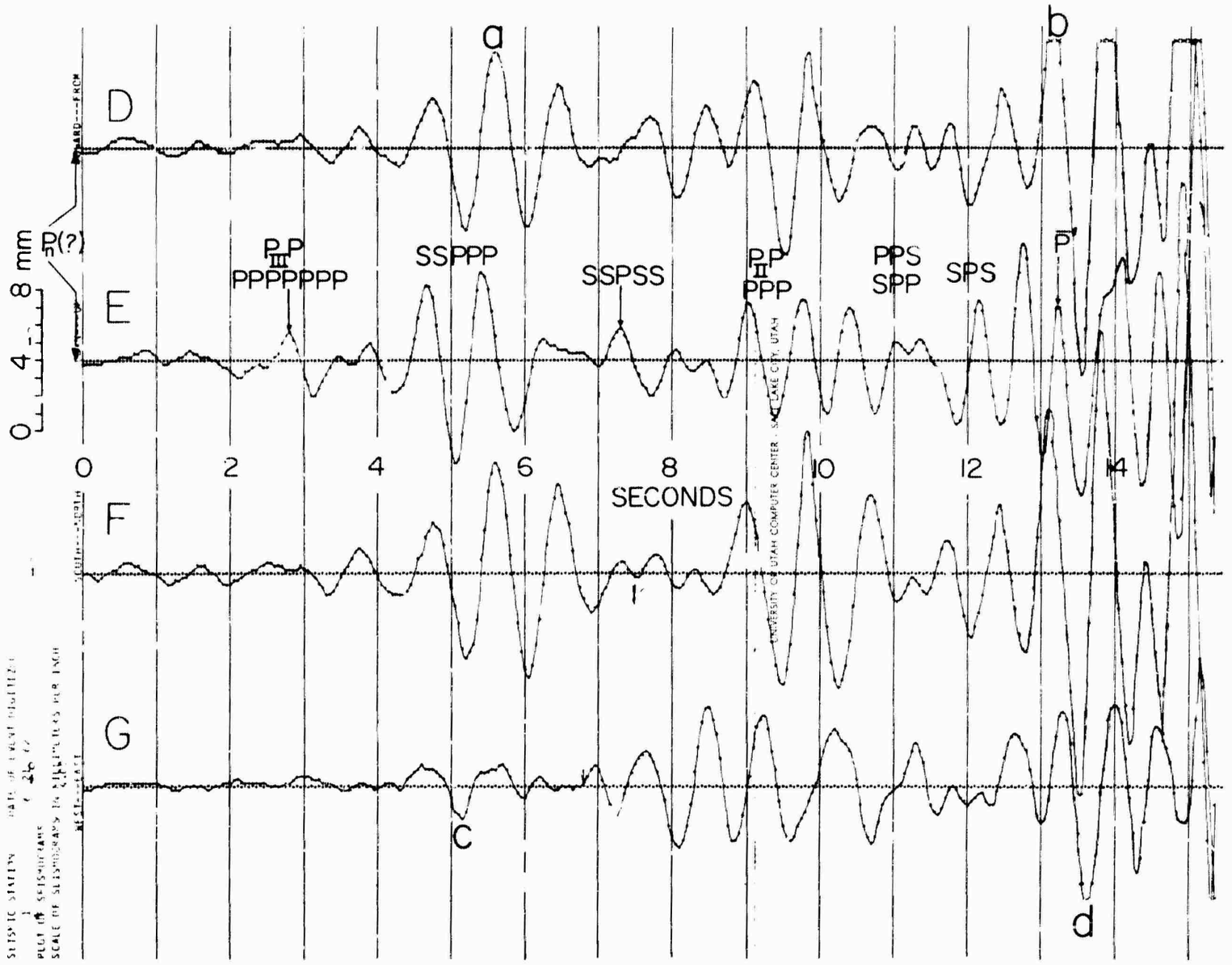

Figure 7-8. Digital-to-analog seismogram, DAMAN I underground nuclear explosion, Nevada test site, June 21, 1962; 0.00 = 17h 01m 02.1s GCT.

Arrival of P_n-- P_n (the first arrival of P, as a refraction off the 25-km-depth layer, also designated as PPPPP) was observed at Dugway with certainty for BILBY only. BILBY gave an excellent first P-motion, and its observed travel time of 62.2 sec (table 7-2) is believed accurate to within 0.2 sec. For an epicentral distance of 446.0 km, this value of travel time compares favorably with the value of (1) 62.7 sec taken from the travel-time curve of Pakiser and Hill (1963) for eastern Nevada and (2) 62.9 sec taken from the travel-time curve of Berg and others (1960, p. 525), provided the first-arrival curve on Figure 7 of Berg and others is used. It should be noted that although at an epicentral distance of 448 km, the observed travel-time curve of Berg and others (1960, p. 524; Fig. 7, p. 525) for the underground nuclear explosion BLANCA indicates a value of 62.9 sec,[-/] the computed travel time from the formula for their crustal model is 63.9 sec because their formula was obtained by averaging data other than that from BLANCA alone. This 1-sec discrepancy, however, is reflected in the travel-time curves of the crustal model of Berg and others (1960) in Figure 7-5 by a 1-sec delay in the absolute time of arrival of P_n. Other minor variations can therefore also be expected in comparing the theoretical (based on the crustal model) and observed values of the time intervals, Δt, after the first arrival of P_n (i.e., PPPPP in Figure 7-5).

-/ One of the portable stations (9B) used in the measurements from BLANCA was in Skull Valley, Utah within about 20 miles from the Dugway station.

The observed travel times of the first arrivals at Dugway from the underground nuclear explosions SEDAN, AARDVARK, and MISSISSIPPI (table 7-1) give partial confirmation for the observed travel time for BILBY, provided their different epicentral distances are taken into account. It is found, however, that the discrepancy in travel times between BILBY and these 3 explosions may be as large as half a second; and this discrepancy is attributable largely to the inaccuracy of picking the first arrival amidst the microseismic or local noise on the seismograms of these 3 explosions.

For essentially all of the seismograms used in this study, the arrival of P_n was not definitely observed on the seismograms, even with our microscope, as it was usually masked by microseismic noise. However, to study the consistency of the body-wave phases, it is not necessary to observe the first arrival of P_n on all seismograms.

Because of the similarity of the character of the early body-wave phases, especially as observed on the ditial-to- analog seismograms (as discussed below), the positive determination of the arrival of P_n on the BILBY digital-to-analog seismograms permitted an estimation to be made of the probable time of the arrival of P_n on each of the other digital-to-analog seismograms--even though the P_n arrival could not actualiy be observed on these othe' seismograms. The probable time of the arrival of P_n on each of the other digital-to-analog seismograms was determined by (1) matching them, over a light table, with the digital-to-analog seismograms of BILBY, and marking on them the position where the arrival of P_n would be expected. On the reproductions in this paper, this position is indicated with "P_n (?)" and a vertical arrow. In using this procedure, the assumption is made that the time interval between the

arrival of P_n and the very early body-wave phases that are observed (even when P_n is not observed) does not vary appreciably from seismogram to seismogram for many (but not necessarily all) underground nuclear explosions that occur within perhaps 10 km of each other within NTS. This assumption is believed valid; but its validity is still being tested.

It should be noted that the accuracy of any predicted time of detonation of an event that is detected and identified as an underground nuclear explosion within NTS will be predicated principally on the accuracy of the determination of the arrival time of P_n for BILBY.

Phases after P_n.-- When the digital-to-analog records, which are printed out by the IBM 1403 printer, are compared by placing any two records over each other on a light table, the consistency of the character of the body phases during the first 15 to 20 sec after the arrival of P_n is striking.

During approximately the first 2 sec after the arrival of P_n in the seismograms used in this study, little consistency is generally observed because of microseismic background noise; if any is seen, one must interpret it with caution. Beginning with about 2 1/2 sec and thereafter for most of the digital-to-analog traces included in this study, the amplitudes of the body phases are generally sufficiently above the microseismic noise level so that consistencies of the character of the phases can be recognized when they exist.

$P_{III}P(?)$ and/or PPPPPPP(?) (table 7-4).-- A small but distinct P arrival that was observed at a time interval, Δt, of about 2 1/2 sec after P_n from essentially all of the nuclear explosions of Richter magnitude 4.1 or greater is provisionally interpreted as a reflection or refraction from the 72-km-depth boundary postulated by Berg and others (1960) in the eastern part of

the Basin and Range province. The distance for critical reflection from the 72-km layer of the model of Berg and others (1960) is about 350 km.

SSPPP(?).-- The phase tentatively identified as SSPPP is a prominent phase that occurs on essentially all the 22 seismograms recorded at Dugway from underground nuclear explosions detonated at NTS. The phase arrives about 4 to 4 1/2 sec after the arrival of P_n, is usually characterized by a W-shape on the digital-to-analog seismogram, is much larger than P_n, and is prominent even when P_n is too small to be identified. The SSPPP phase is designated for energy which apparently originates as a shear wave at NTS, travels down through the two upper crustal layers as a shear wave to the 25-km-depth boundary, travels as a P head-wave along this boundary, and then travels up through the two-layer crust as a P wave.

The phase shows about equal amplitudes of deflection on the vertical and north-south components (table 7-4). Particle-motion diagrams of this interval show the motion to be P-like with an apparent incident angle (from the vertical) of about 30°. For reasons as yet unexplained, the east-west component shows little motion although the energy from NTS should be arriving at about equal amplitude on both horizontal components.

On seismograms with energies appreciably above the microseism level, a very symmetrical envelope can be drawn around the peaks of the SSPPP(?) phase (see DAMAN I and MERRIMAC). This envelope suggests that the SSPPP(?) phase may start at a time interval Δt as early as 4.4 sec (after P_n), which is close to the theoretical times of arrival of 3.9 and 4.3 sec for the models of Berg and others (1960) and Pakiser and Hill (1963), respectively. The particle-motion diagram at about 4 1/2 sec shows a very strong dis-

tinctive arrival of a P-like wave; this P-like wave is perhaps the most striking characteristic found when comparing all records and is probably the start of the SSPPP phase.

The evidence seems strong that the phase starting at about 2 1/2 sec is not the start of the high amplitude deflections between 4 1/2 and 7 sec (the SSPPP phase). The apparent gradual build-up of the north-south component suggests that the opposite may be possible. In most cases the amplitude on the Z component decreases after 2 1/2 sec, indicating an arrival of different energy at 4 1/2 sec, although a destructively interfering phase causing this decrease cannot be ruled out. However, the particle-motion diagrams show that the P energy at 2 1/2 sec has a much steeper angle of incidence than the P phase at 4 1/2 sec; and on many particle-motion diagrams, there is intervening S-like motion.

If this phase is correctly identified as SSPPP, the large amplitude of this phase indicates that a large amount of shear energy must be generated by some underground nuclear explosions. The large amount of shear energy that corresponds approximately with the theoretical times of S_n (i.e. SSSSS--see below) on this model also give additional supporting evidence. If this presumption of a large amount of shear energy generated by some underground nuclear explosions is incorrect, however, the phase designated SSPPP may be caused by a channeling effect that has not yet been recognized to date by the refraction work, or by a ringing effect of the Dugway station.

SSPSS(?).-- The phase designated SSPSS(?) is an S wave which is converted to P at the 25-km-depth boundary and travels back up through the crust as S. Except for this last leg, its path is identical to that of SSPPP(?). The phase arrives about 7 to 7 1/2 sec after P_n and is much

smaller than SSPPP(?). (table 7-4) This phase apparently corresponds with the phase tentatively identified as SPS(?) by Pakiser and Hill (1963, p. 5761), who observed the phase arriving about 8 sec after P_n and by Ryall and Stewart (1963, p. 5821), who observed the phase arriving about 10 sec after P_n.

$P_{II}P(?)$ and/or PPP(?).-- A prominent P phase arrives consistently about 8 1/2 sec after P_n; it, too, is sometimes characterized by a W-shape on the digital-to-analog seismograms. The amplitude of the deflection on the N-S component is usually about twice that on either the vertical or E-W component (table 7-4). On some seismograms, as for example, on the N-S component of DAMAN I, the shape of the phase closely resembles that of the SSPPP(?) phase. Also a striking comparison was found in the first deflection of both phases, if present, immediately after 4 1/2 and 8 1/2 sec. The first peaks of these phases line up perfectly on nearly all records regardless of any other characteristics on the record or the locataion (within NTS) or magnitude of the explosion.

On some traces, there is some evidence of "ringing". A consistent oscillation or "ringing" on the east-west component starts at 7.6 to 7.8 sec after P_n, and gradually increases in amplitude to persist for approximately 4 sec. This appears on 13 of the 17 records in Area I and 3 of the 6 in Area II. At 9 sec, this component is sometimes still large enough to influence the particle-motion diagram and may explain the inconsistent analysis of the type of motion (S-like or P-like) due to this phase as observed on the vertical and north-south components.

This phase is apparently the same as $\bar{P}$ (after Mohorovičić) observed by Ryall and Stuart (1963, p. 5821) and interpreted by them as a phase "associated with waves reflected beyond the critical angle, from the base of the crust". In our notation, this phase is designated $P_{II}P$.

head-wave conversions from the 9-km-depth layer that arrive about 10 to 10 1/2 sec after P_n. On some particle-motion diagrams, good S-like motion is observed; on others, elliptical-type S motion is observed; and on still others, inconsistencies are observed that suggest that these two phases may be intermixed. The amplitudes of these phases are generally much smaller than $P_{II}P$ and/or PPP.

SPS(?).-- A prominent phase, tentatively identified as SPS, occurs at about 11 1/2 sec after P_n (table 7-4); it usually comprises 2 cycles on the record. This phase was observed in essentially all the records studied. On the particle-motion diagrams, the S-like motion is usually distinct and large.[1]

The validity of our interpretation of the PPP, PPS, SPP, and SPS phases rests on the existence of an intermediate layer at a depth of about 9 km, which was not found conclusively by Pakiser and Hill (1963) beneath the Nevada test site.

$\bar{P}$; or Multiple P.-- A large-amplitude phase arrives consistently about 13 sec after P_n (table 7-4). This phase may be (1) a multiple reflection of P from the 25-km-depth boundary (which goes back to the surface, then back to the same boundary and finally back to the surface) or (2) a guided or trapped wave in the upper part of the crust. The theoretical arrival times for such a multiple reflection is 10.4 and 14.5(?) sec for the crustal models of Berg and others (1960) and Pakiser and Hill (1963), respectively.

S_n (i.e., SSSSS).-- At the time interval Δt (after P_n) of 50 to 53 sec, large amplitudes (table 7-4). on the horizontal components are observed. This time is approximately the theoretical time for a body S_n (i.e., SSSSS) wave. These large amplitudes give strong support to the hypothesis that a large amount of shear energy is generated in most of the underground nuclear explosions studied. However, particle-motion diagrams were not made on these seismograms at this time interval.

---

[1] It is difficult to explain why the amplitude of SPS(?) is proportionally so much larger than that of SPP(?).

Table 7-4-- Peak-to-peak amplitudes (in mm) of some body-wave phases as measured on the (Z) vertical, (NS) north-south, and (EW) east-west horizontal components of seismograms obtained at Dugway, Utah from underground nuclear explosions, Nevada test site

Date	NAME	Magnitude	Epicentral Distan. °	Time	Z	EW	NS	Time	Z	EW	NS	Time	Z	EW	NS	Time	Z	EW	NS	Time	Z	EW	NS	Time	Z	Eh	Ns	Time	Z	Eh
5-13-62	AARDVARK	4.9	448.1	1:30	20	3	20	3.4	26	4	23	4.05 to 4.4 ?	60	19	77	6 80	30	35	28	8 40 ?	30	25	Indistinct	8 70 to 9 ?	48	50	69	Not recognized				Not recognized				13.3	145	66	89			
6-1-62	RACCOON	?	448.0	Noise				Noise				Noise				Noise				8 40 ?	3 0	1 2	2	Not discernable				Not discernable				11.3	11	5.5	5	12.75	22 5	16	20	53.		
6-6-62	PACKRAT	4.4 ± 0 5	448.2	2.80	3	1+	2.5	3.20	4	1	3	4.45	8.5	2.2	6	7.15	5.5	6	9	8.65	3	4	2	8 80	2+	4	2 5	10.5 ?	11	5.5	8	Not discernable				12 85	22	17 5	12	51		
6-21-62	DAMAN 1	?	448.0	2.60	4	1+	2	Not checked				4.45	10	3	12	6 85	4	8	4	8.55	5.5	6	5	8.70	6 5	7	10	10.50	4	6	6	11.55	7 Poor	9	5 5	12.85	1+	11 0	21 5	$1?		
-6-62	SEDAN	4.7 ± 0.4	437.3	2.50	9	2	6	3.55	8	2	6	5.00	33	5	25	7.00	7	10	5	8 45	16	10	12	8.75	17	12	21	?				?				12.80	46	29	58			
7-13-62	MERRIMAC	4.8 ± 0.3	447.1	2.60	5	1+	3	3.70	4	3	4	4.40	13	5.5	14	7.10	4	12	5.5	8.60	10.5	9	5 5	8.75	1 5	9	1.2	10.60	12	51	6.5	11.35	7	11	2	12 85	26	20	25	52		170
8-24-62 (second explosion)	BOBAC	4.0 ± 0.5	447.4	Not discernable (Noise)				Not discernable (Noise)				4.45	4	2	4	7.05	1	2	2	8 45	4	3 5	3	8.85	4	3	4	10.45	4	3	3	11 45	2.5	1	1 5	12 85	8	3.5	4 5			
9-14-62	MYRAK	4.1 ± 0.7	447.4	2 65	3	1+	1+	Not discernable				4 35	8.5	3	6.5	7.35	1.5	3 5	1	8 40	6.5	5	2 7	8 75	5	6.5	6.5	Not discernable				11.45	65	5	6	12 85	9	4	13	53		96
10-5-62	MISSISSIPPI	?	440.8	2 55	36	4	28	3.65	27	9	28	4.25	82	28	22	Questionable because digitizing stops shortly after				Not digitized					N D.			N. D.					N.D.				N.D.			90		200+
10-19-62	BANDICOOT	?	?	2.60	Poor	2.3	2	3.65	2	1	2	4.40	11	2.5	13	7.10	9	4	8	Questionable				8 80	8	8	14 5	10.60	4	13	10	Not discernable				12 90	13	6	24	53		36
12-7-62	Confirmed Nuclear exp.	?	?	2.50	1.5	1	1.75	Not checked				4 40	12	3	12.5	7.10	3.5	8 5	2.0	8.40	?	8	5	8 85	5	8.5	12	10 60	12	11	6 5	11 45	0	?	2	12 85	11 5	12	26	54		120
12-12-62	HUMRAT	4.3 ± 0.5	446.9			Poo.	Record	Phases too questionable to pick times.																																
3-1-63	Suspected Explosion	?	?	2 60	4	1-	2	3.65	2	1-	2	4.40	13	4	15	7.15	7	8	7	Questionable				8.85	11	10	21												51 bad phase		190
9-13-63	BILBY	5.8	446 0	2.50	78	20	56	Not digitized																				10:60	11	12	14	11:30	9	8	7	13.00	10	9	48	52	---	
11-14-63	Suspected explosion	?	?	Missing, late start digitizing				Missing				4 60	8	3	8	7 15	4	6	7	Not discernable				Not discernable				Not discernable				Not discernable				13.30	4	?	27		---	

ALL TIMES AFTER BLUE P_n ARRIVAL

Consistency of patterns

Figures 7-8, 7-9, and 7-10 show the digital-to-analog seismograms for 3 announced underground nuclear explosions within NTS. On each figure, the 4 letters "a, b, c, and d" are placed on key peaks or troughs that occur consistently on all the seismograms shown; and these key peaks and troughs can be used to match the seismogram of one explosion against another. Once they are matched (over a light table, for example), there are literally tens or scores of other consistencies that can be found between these underground explosions.

The first explosion, DAMAN I, is known to be located within 1 1/2 km of the second, MERRIMAC, as their latitudes and longitudes have been declassified. The character of the seismogram of the third explosion is so consistent with that of the other two that it was probably detonated in the same general area within NTS as the other two.

It should be emphasized that certain other announced underground nuclear explosions detonated in this same area (area I) within NTS as the previous 3 examples do <u>not</u> show the excellent consistency shown by these 3 examples. The main point is, however, that if we do observe a seismogram essentially identical to these three, we believe we can correctly detect and identify it as positively an underground nuclear explosion from this area within NTS.

Similar comparisons have been made on other seismic events which are believed to be underground nuclear explosions from the Nevada test site but which have not yet been declassified.

Figure 7-11 shows the digital-to-analog seismogram for SEDAN, which was detonated in another area (area II) within NTS. In detail, its character is

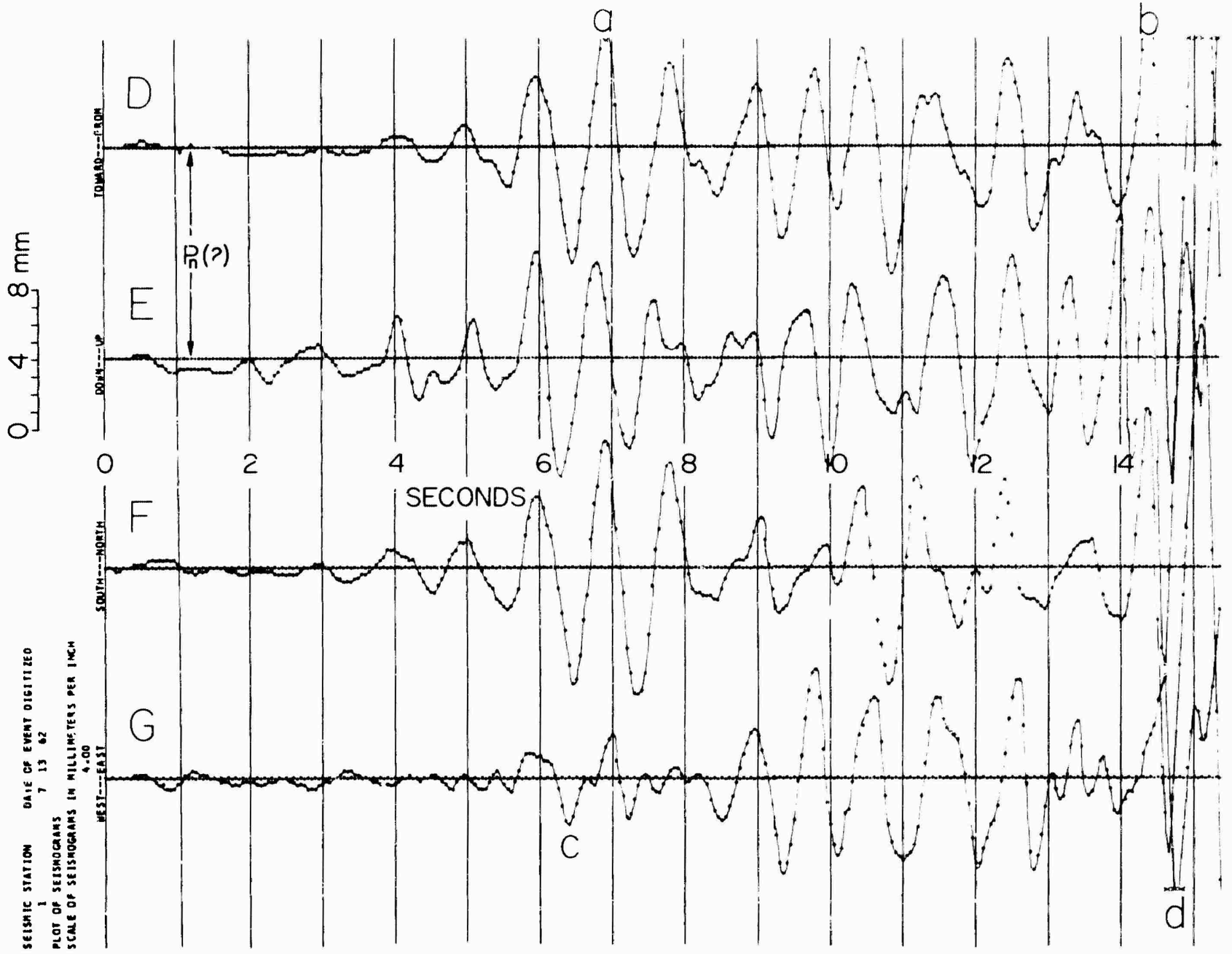

Figure 7-9. Digital-to-analog seismogram, MERRIMAC underground nuclear explosion, Nevada test site, July 13, 1962; 0.00 = 16h 01m 01.0s GCT.

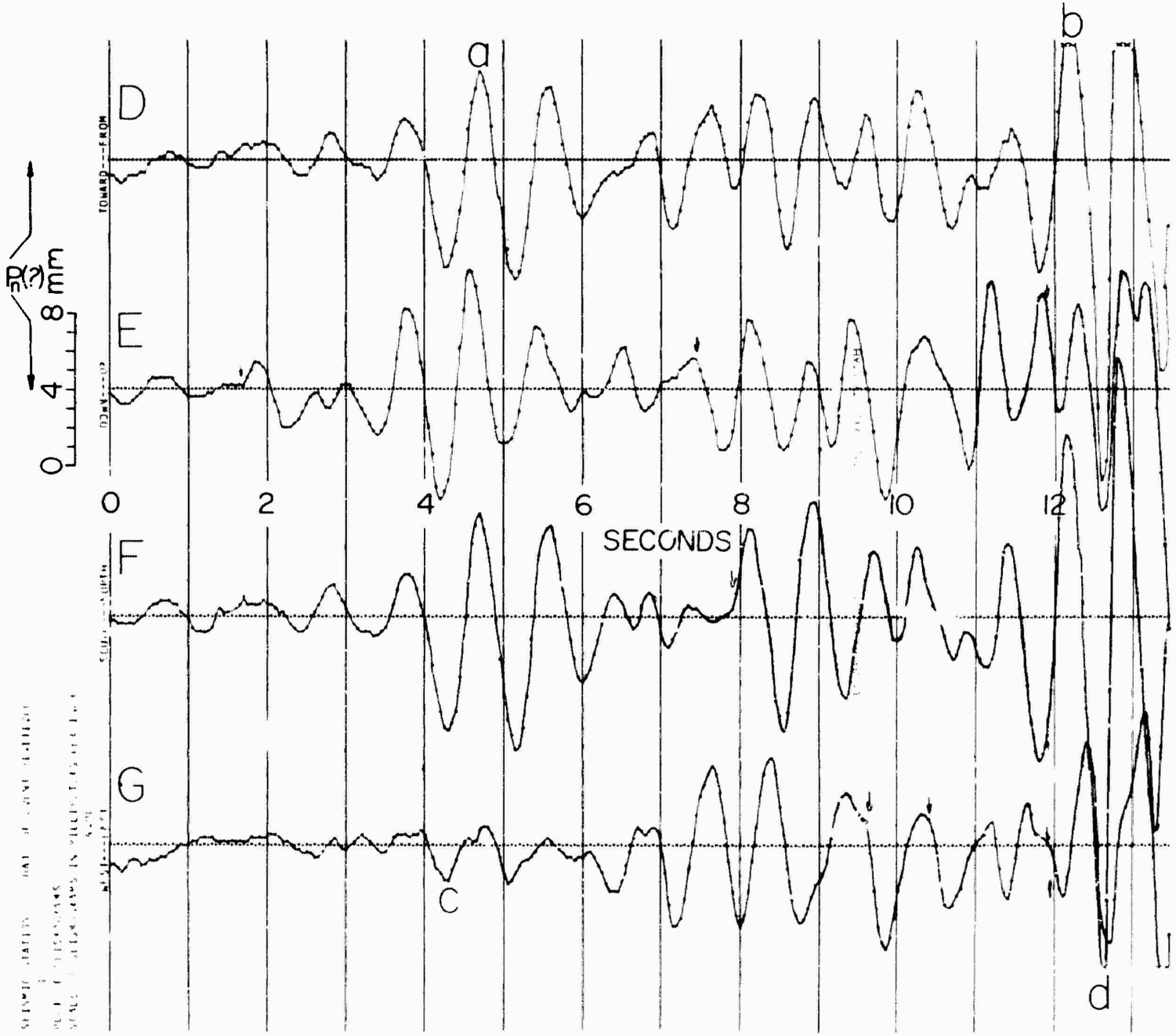

Figure 7-10. Digital-to-analog seismogram, announced underg nd nuclear explosion, Nevada test site.

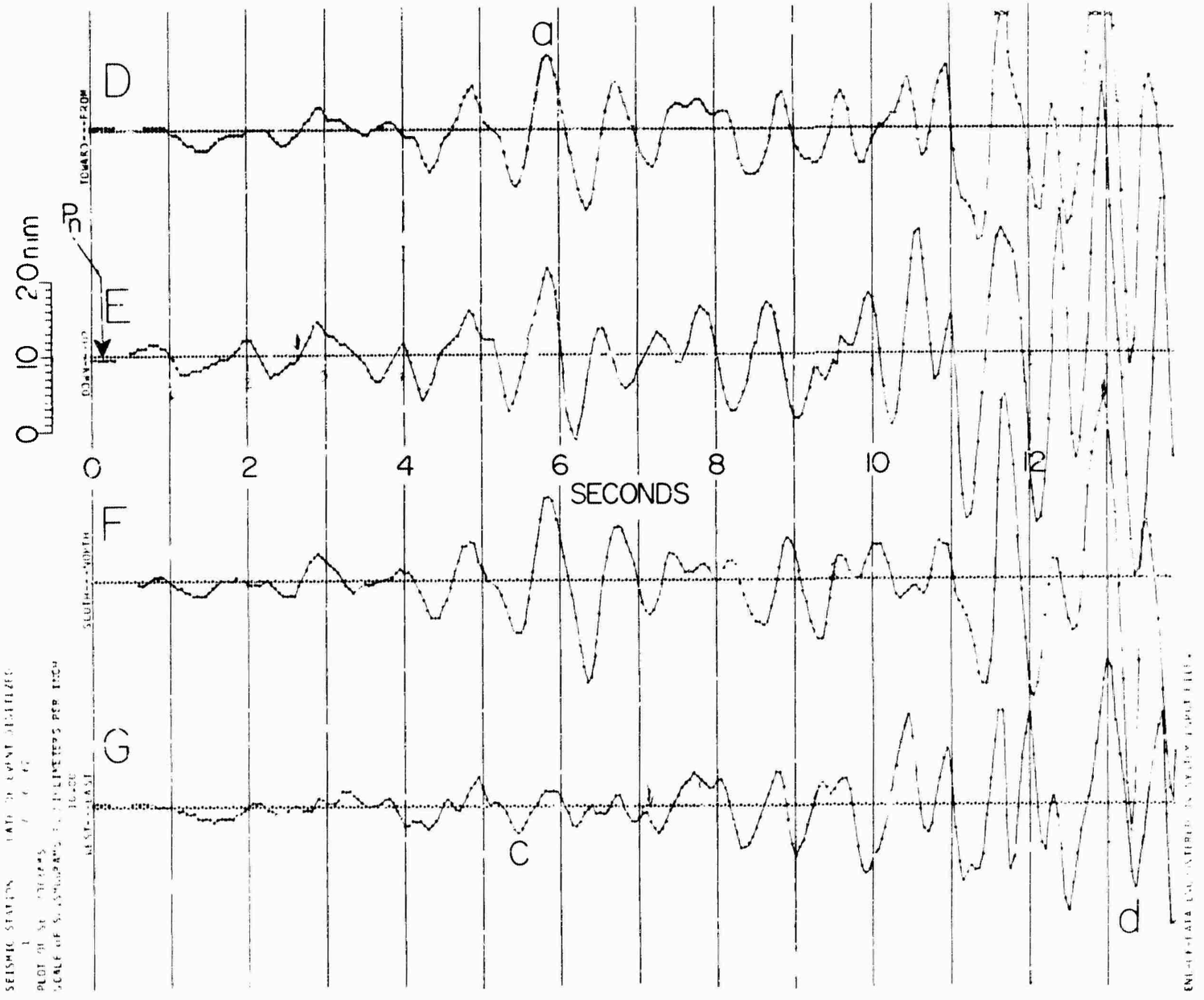

Figure 7-11. Digital-to-analog seismogram, SEDAN underground nuclear explosion, Nevada test site, July 6, 1962; 0.00 = 17h 01m 01.1s GCT.

markedly different from that of the p

ever, some of the corresponding phases can be recognized.

Figure 7-12 shows the digital-to-analog seismogram for DES MOINES, (area III) which was detonated in yet a third area within NTS. Its character is markedly different from any of the preceding seismograms. For example, it has a much higher frequency content. Also some ringing may be present.

Positive detection and identification of certain underground nuclear explosions from Nevada test site

From our study we conclude as follows:

Provided the explosions occurred in the same area, the various presentations indicate a striking consistency of the body-wave phases from some (but not universally from all) underground explosions within that area. The characteristics of the body-wave patterns vary from three different areas of detonation within the Mercury test site, presumably because of different source functions (depending on rock type, geologic environment, degree of coupling, yield, etc.). This striking consistency has been used successfully for the positive detection and identification of certain underground nuclear explosions detonated at the Nevada test site and recorded at Dugway, Utah and to correctly determine, within a few kilometers, the area of the detonation within NTS; and it is believed that the times of detonation of these certain explosions can be correctly predicted within one second usually and within a few tenths of a second sometimes.

We doubt that an earthquake within the NTS area could give the exactly identical character as that from DAMAN I or MERRIMAC, for example, but we have no data from earthquakes within NTS to prove it.

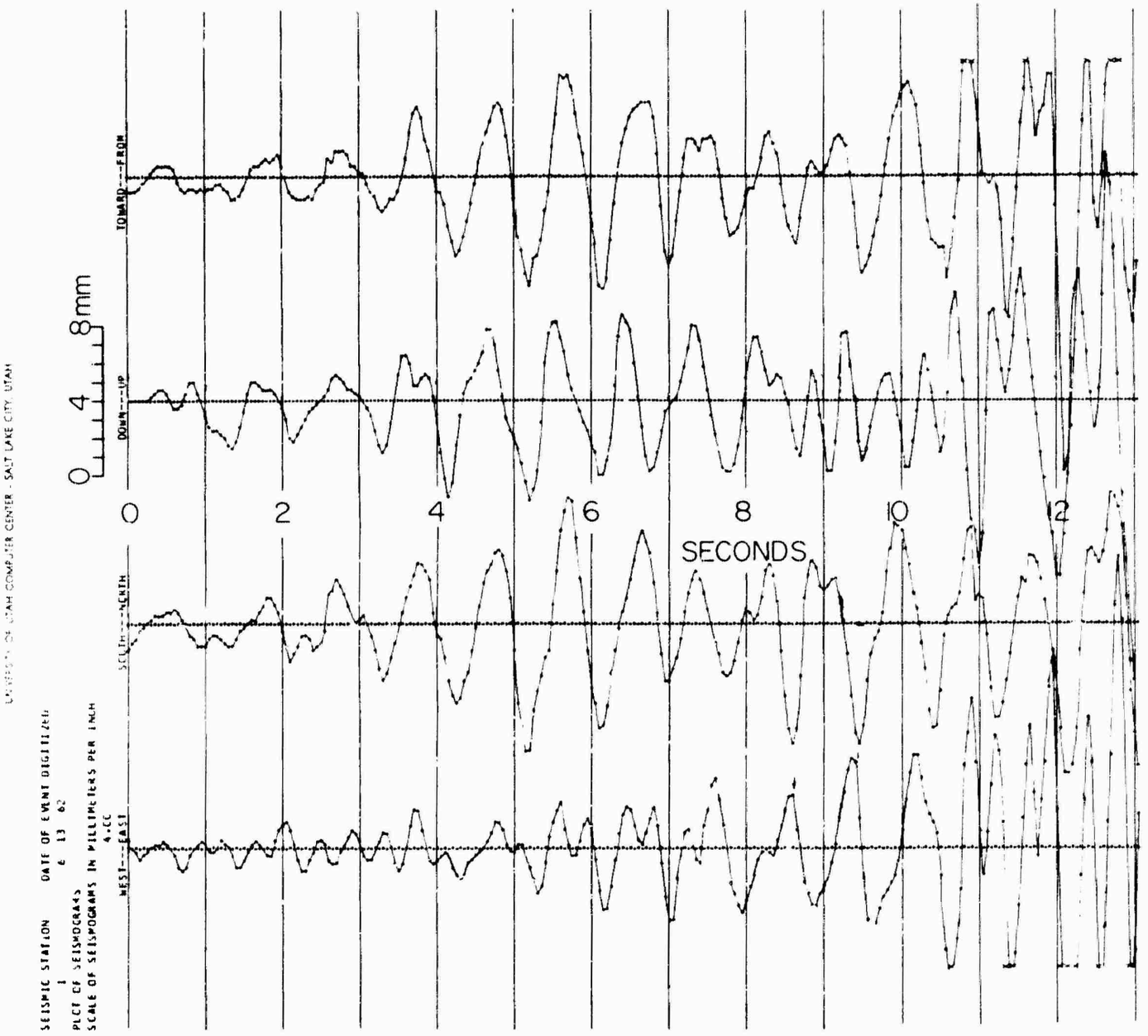

Figure 7-12. Digital-to-analog seismogram, DES MOINES underground nuclear explosion, Nevada test site, June 13, 1962; 0.00 = 21h 01m 02.1s GCT.

We next will compare seismograms from 4 probable underground explosions in the Semipalatinsk area, USSR, again as recorded at Dugway, Utah. The Richter magnitudes of the events, as reported by the U.S. Coast and Geodetic Survey preliminary epicenter cards, were 5.6 or greater: and the epicentral distance was about 9,800 km (about 90°).

The 4 Soviet probable underground explosions have many striking consistencies. In particular, the events of May 16, 1964 and July 19, 1964 are almost identical in many respects. As given by the U. S. Coast and Geodetic Survey[/] (table 7-5), their latitudes are identically the same and their longitudes are the same within 0.2°. On Figures 7-13 and 7-14, which show the digital-to-analog seismograms of the 2 explosions, the 4 letters "a, b, c, and d" are placed on key peaks or troughs that occur consistently on all the seismograms shown; and these key peaks and troughs can be used to match the seismogram of one explosion against another. Once they are matched (over a light table for example,) there are literally tens or scores of other consistencies that can be noted between the seismograms.

The excellent consistency of these 2 seismograms indicates that the events are from the same area and have essentially the same source functions. We doubt that any earthquake in this area would give a pattern as nearly identical to these as they are to each other.

The seismograms of the other two Soviet probable underground explosions are also very similar to these two; in particular, essentially all the major characteristics are present. The slight differences in character

---

[/] The U. S. Coast and Geodetic Survey preliminary epicenter determination cards show all 4 of these Soviet events as "zero depth" events.

Table 7-5.-- Pertinent data incident to probable large underground explosions[1/] in the Semipalatinsk area, USSR

Date (GCT)	Magnitude[1/] (Richter scale)	Epicentral distance to Dugway Utah (degrees) (km)	Origin Time[1/] (GCT) h m s	Latitude[1/] (north)	Longitude[1/] (east)
March 15, 1964	5.6	90° 00' (10,000)	07 59 58.0	49.7	78.0
May 16, 1964	5.6	89° 46' (9,974)	06 00 58.1	49.9	78.3
July 19, 1964	5.5	89° 48' 9,977	05 59 58.9	49.9	78.1
Nov. 16, 1964	6.0	90° 00' (10,000)	05 59 57.4	49.7	78.0

[1/] U.S. Coast and Geodetic Survey preliminary epicenter determination cards, which indicate these events as zero-depth events.

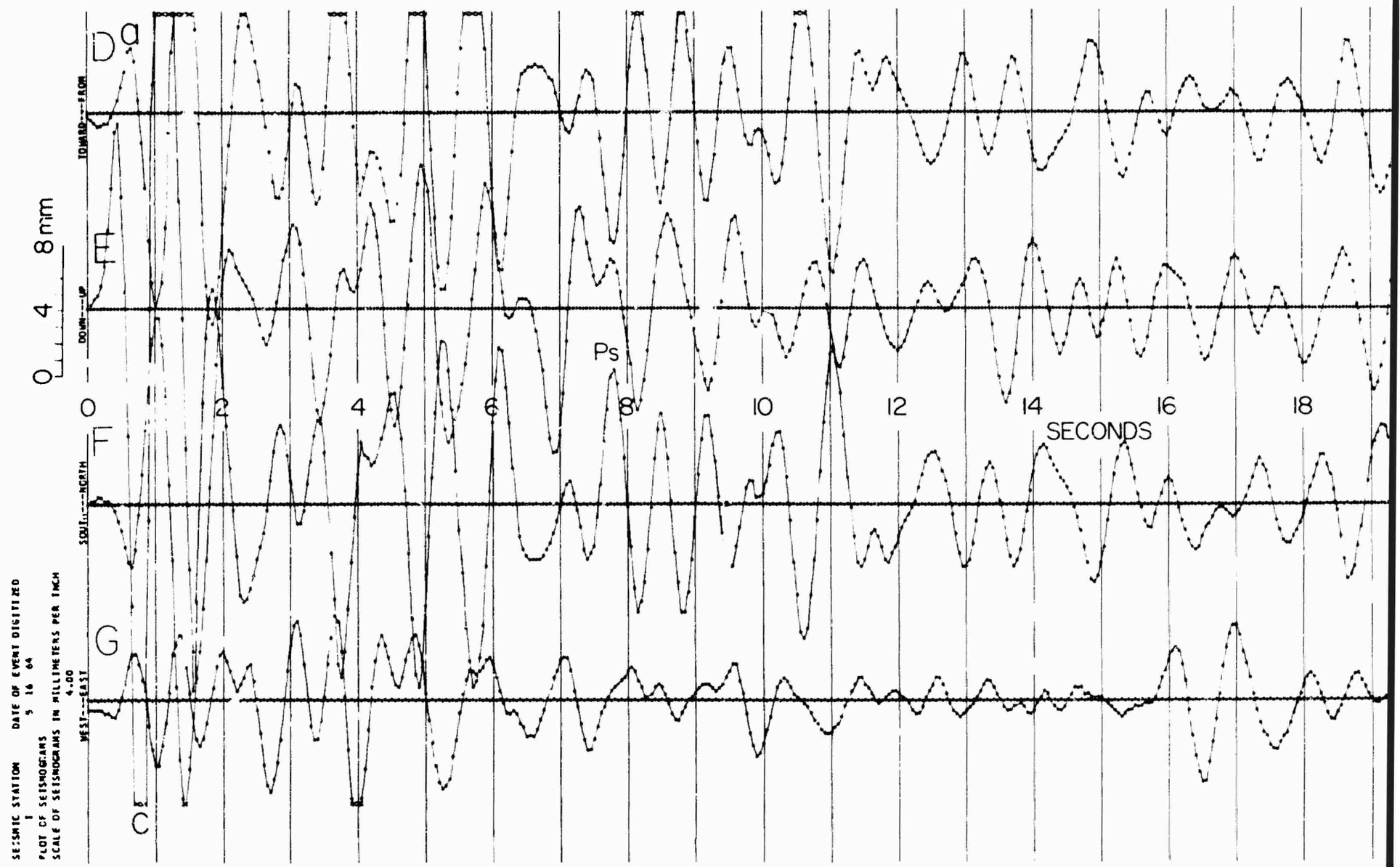

Figure 7-13. Digital-to-analog seismogram of probable underground explosion in the Semipalatinsk area, USSR, May 16, 1964; 0.00 = 06h 14m 00.7s GCT.

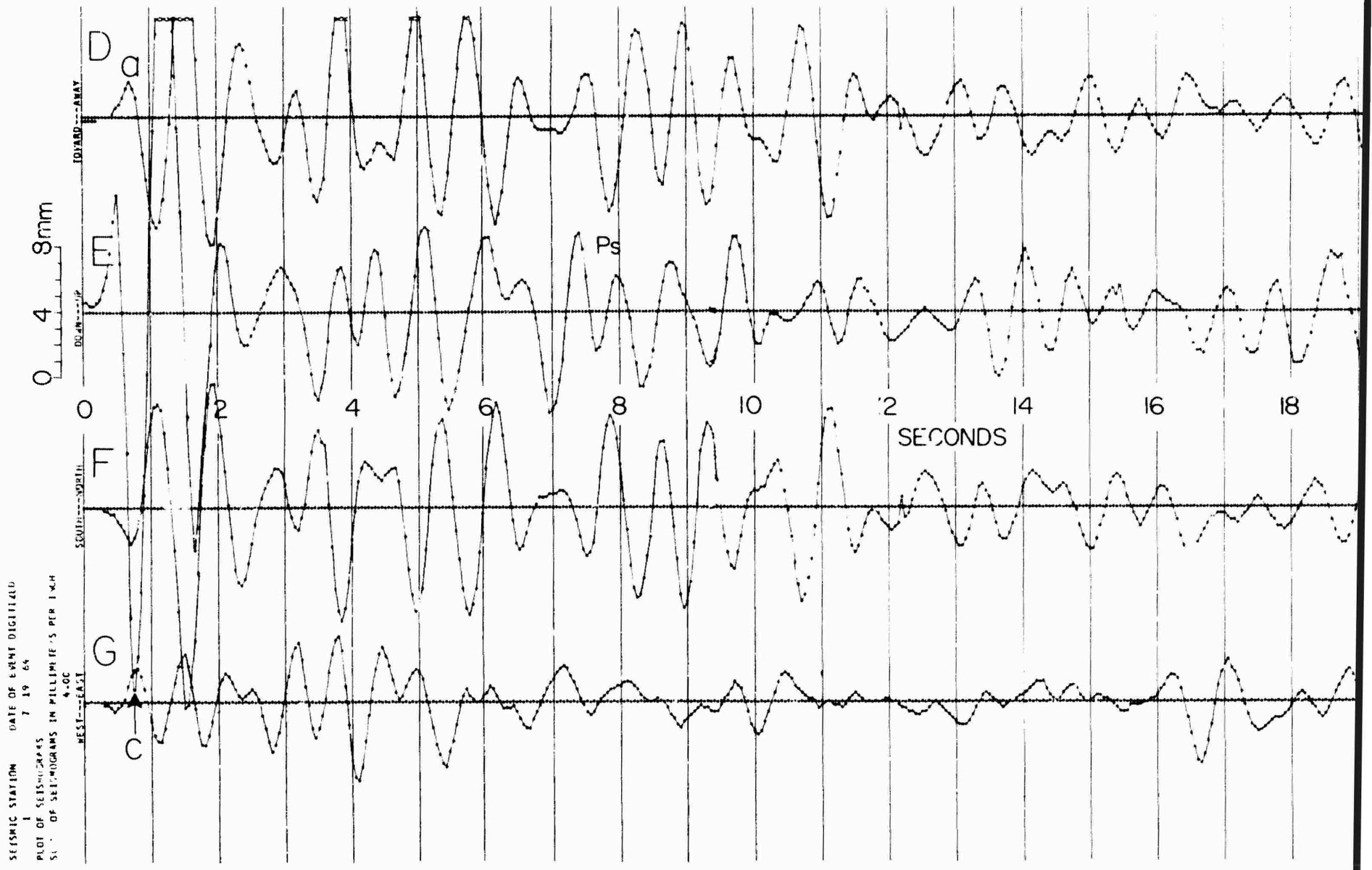

Figure 7-14. Digital-to-analog seismogram of probable underground explosion in the Semipalatinsk area, USSR, July 19, 1964; 0.00 = 06h 13m 01.4s GCT.

may be because they have slightly different source functions or they may be from slightly different areas.

PS converted waves from earthquakes and large underground explosions at epicentral distances of 2,000 to 10,000 kilometers

In this section we will demonstrate that PS converted waves have been observed from earthquakes and large underground explosions at epicentral distances of 2,000 to 10,000 kilometers. In doing this, we will also be able to explain certain events on the seismogram that contribute to the complexity of the coda of P. The study will be restricted to events from the teleseismic distances just given.

Available data

All the seismograms to be discussed were recorded by the Benioff short-period matched seismometers (magnification 400,000) at Dugway, Utah. The seismograms were hand-digitized and analyzed in a manner identical to that discussed in the previous sections.

The seismograms of 10 earthquakes were studies: 4 from the Kurile Islands, 2 from Japan, one from the Tonga Islands, and 3 from Mexico. (See table 7-6) In addition, four Soviet probable underground nuclear explosions from the Semipalatinsk area were studied.

Expected arrival time of PS converted waves

The time of arrival of a PS converted wave will generally be expressed in terms of the time interval, Δt, after the first arrival of P. To confirm the travel time of a given body-wave phase, however, the Jeffreys-Bullen tables of 1958 have been used.

Table 7-7, which was compiled from data given in the Jeffreys-Bullen tables of 1958, gives the time interval, Δt (in sec), after the initial P, at which various body phases will arrive from epicentral distance, Δ, of 10° (1,111 km) to 90° (10,000 km). The phases studied are:

P - the first arrival
pP
sP
PcP

The tables include the data for different depths of focus: (1) zero depth; (2) 33-km depth; (3) 96-km depth; and (4) 159-km depth.

Figure 7-15 shows the earth crustal model of Berg and others (1960), the Dugway station, and the approximate ray paths for the two extreme ranges of epicentral distances of the events studied. The angles of incidence assumed at the base of the crust were computed with a formula by Gutenberg (Richter, 1958). Also shown on this diagram are the P to S conversions at the 25- and 72-km-depth boundaries.

Using the assumptions of this model, and assuming further that a PS converted wave is generated at the postulated 72-km-depth boundary of Berg and others (1960), the time interval, Δt, of the arrival of such a PS converted wave after the first arrival of P would be about 8.7 sec from a shallow earthquake in Mexico and about 7.7 sec from an underground explosion in central USSR.

Arrivals of shear (SV) waves that are observed at these time intervals after P in this study are identified as PS converted waves generated at the 72-km-depth boundary.

Figure 7-16 shows a graph of the time interval, Δt, after the initial P, at which a PS converted wave should arrive from an assumed one-layer earth crustal model for various assumed velocities. The assumed

Epicenter	Date	Latitude [1] (degrees)	Longitude [1] (degrees)	Depth [1] of focus (km)	Origin [1] time (GCT) h m s	Observed time of first P Arrival (GCT) h m s	Time of start of digitizing (GCT) h m s	Epicentral distance (degrees) (km)	Richter [1] magnitude	Directi A
Kurile Islands	Feb. 20, 1964	44.6N	150.0E	50	09 53 51.1	10 04 43.7	10 04 43.6	67.3° (7,480)	5.2 (C.G.S.)	-.619 +
Kurile Islands	May 17, 1963	45.3N	150.8E	33	04 06 36	04 17 26.7	04 17 26.6	66.6° (7,400)	5.9 (C.G.S.)	-.617 +
Kurile Islands	Feb. 22, 1964	48.5N	154.9E	60	17 50 56.2	18 01 16.6	18 01 16.6	62.6° (6,960)	5.0 (C.G.S.)	-.604 +
Kurile Islands	Jan. 6, 1963	47.4N	155.9E	33	21 20 56.5	21 31 19.8	21 31 19.8	62.6° (6,960)	none given	-.620 +
Hokkaido, Japan	Sept. 24, 1962	42.8N	145.3E	33	14 38 21	14 49 40 5	14 49 40.2	71.4° (7,930)	none given	-.605 +
Honshu, Japan	June 3, 1963	34.2N	138.7E	43	07 35 54	07 48 06.3	07 48 06.3	80.9° (8,990)	5.3 (C.G.S.)	-.624 +.5
Tonga Islands	July 4, 1963	26.3°S	177.7°W	158	10 58 13	11 10 54.8	11 10 54.5	89.6° (9,990)	6 3/4 (Pas) 6 3/4-7 (Bks) 6½ (CGS)	-.897 -.
Mexico	Oct. 19, 1962	19.8°N	108.3°W	53	21 21 48	21 26 26.4	21 26 75.3	70.8° (2,310)	none given	-.296 -.8
Mexico	May 22, 1963	17.7N	106.0°W	33	04 24 29	04 29 35.5	04 29 35.6	23.3° (2,590)	4.6	-.263 -.9
Mexico	June 20, 1964	18.5°N	105.5°W	28	17 12 15	17 17 14.4	17 17 14.0	22.7° (7,520)	5.5 (C.G.S.)	-.754 -.91

* The picking of an individual phase listed to 0.1 sec does not imply that the onset of that phase can be identified on the seismogram to wi

[1] Data taken from U.S. Coast and Geodetic Survey preliminary epicenter cards.

eis

Direction Cosines A	B	C	Identified Phase	Maximum Peak-Peak Amplitude (mm)	Time Interval After Initial P (sec)*	Phase Intervals (Jeffreys Bullen Tables 1958)	P Travel Time (Jeffreys Bullen Tables) 1958	Observed P Travel Time
-.619	+.357	+ 700	pP	14	13.1-16.6	15.0		
			pPs	5	16.6-17 8		m s	m s
			sP	18	18.1-21.5	20.1		
			pPs	9	21.2-22.7			
			sPs	8	22.6-24.0?		10:51.6	10:52.6
-.617	+.344	+.705	P	54	0-03.1			
			Ps	18	3.1-05.7			
			pP	15	9.8-11.2	10.0	10:49.1	10:50.7
			pPs (?)	24	13.2-13.6			
-.604	+.284	+.745	pP	20	15.2-17.3	16.4	10:20.9	10:20.4
			pPs	11	18.0-20.0			
			sP	7	21.0-22.4	23.0		
			pPs	9	22.4-25.8			
-.620	+.278	+.734	pP	8	9.5-10.5	10.0	10:23.2	10:23.3
-.605	+.419	+.677	pP	33	9.3-12.0	10.0		
			pPs	9	12.0-14.6			
			sP	68	14.6-19.9	14.0	11:18.7	11:19.5
			sPs	10	17.5-18.0			
			PcP	32	21.2-23.1	20.2		
			PcPs (?)	19	23.1-25.0			
			PcPs (?)	10	28.0-29.0			
-.624	+.547	+.560	PcP	22	7.9-10.0	7.1		
			pP	8	10.5-11.6	12.4		
			pPs	6	13.4-14.2			12:12.3
			sP	23	14.2-17.4	17.5		
			sPs	10	17.4-20.0?		12:11.2	
-.897	-.036	-.441	PcP	80	1.2-4.3	1.5		
			PcPs	28	4.3-5.9		12:40.5	12:41.8
			P	50	0-4.5			
-.296	-.895	+.337	Ps	14	4.5-5.0			
			Ps	21	8.3-9.6.			
			pP	30	13.7-19.1.	13.5		
			pPs	12	19.2-20.2			
			sP	52	20.2-23.9		4:39.1	4.38.4
			sPs	15	24.0-24.9			
			sPs	18	30.0-?			
-.263	-.915	+.302	P	25	0-4.9			
			Ps	8	5.4-6.6			
			pP	15	10.3-12.0	10.0	5:05.7	5:06.5
			sP	20	12.5-14.9	14.0		
			sPs	9	14.9-16.0			
-.254	-.915	+.316	pP	12	10.2-12.3	8.5	5:00.6	4:59.4
			sP	9	13.1-14.7	12.0		

eismogram to within 0.1 sec.

B

Table 7-7.-- Teleseismic Phases Significant In The First 35 seconds for $10 \leq \Delta \leq 90^{\circ}$
Reference: Jeffreys and Bullen, 1958, Seismological tables, Office of the British Association, Burlington House, London, 50p.

DEPTH OF FOCUS (h) in Km.		ALL TIME INVERVALS IN SEC. Δt								
	Δ Degrees	10	20	30	40	50	60	70	80	90
	Δ Km	1,111	2,222	3,333	4,444	5,556	6,667	7,778	8,889	10,000
0 (surface)	PP-P	8	19	57.5						
	PPP-P	15	28	715						
	pP-P									
	sP-P									
	PcP-P	371.0	256.0	182.4	125,8	80.3	45.9	22.4	7.9	1.5
33 Km	PP-P	8.6	19.5	58.3						
	PPP-P	15.6	28.5	72.3						
	pP-P	10	10	10	10	10	10	10	10	10
	sP-P	12	13	14	14	14	14	14	14	14
	PcP-P	369.2	255.1	181.9	125.4	79.9	45.6	22.3	7.7	1.5
96 Km	PP-P	10.8	23.9	61.4						
	PPP-P		33.9	77.4						
	pP-P	20	21	22	23	23	24	25	25	26
	sP-P	26	32	33	34	34	35	35	36	36
	PcP-P	363.4	252.5	180.0	124	78.8	44.8	21.7	7.4	1.4
159 Km	PP-P			64.3						
	PPP-P			82.3						
	pP-P		27	34	35	36	38	39	40	41
	sP-P	39	49	52	54	54	55	56	57	58
	PcP-P	357.1	249.9	178.2	122.5	77.8	44.1	21.2	7.2	1.3

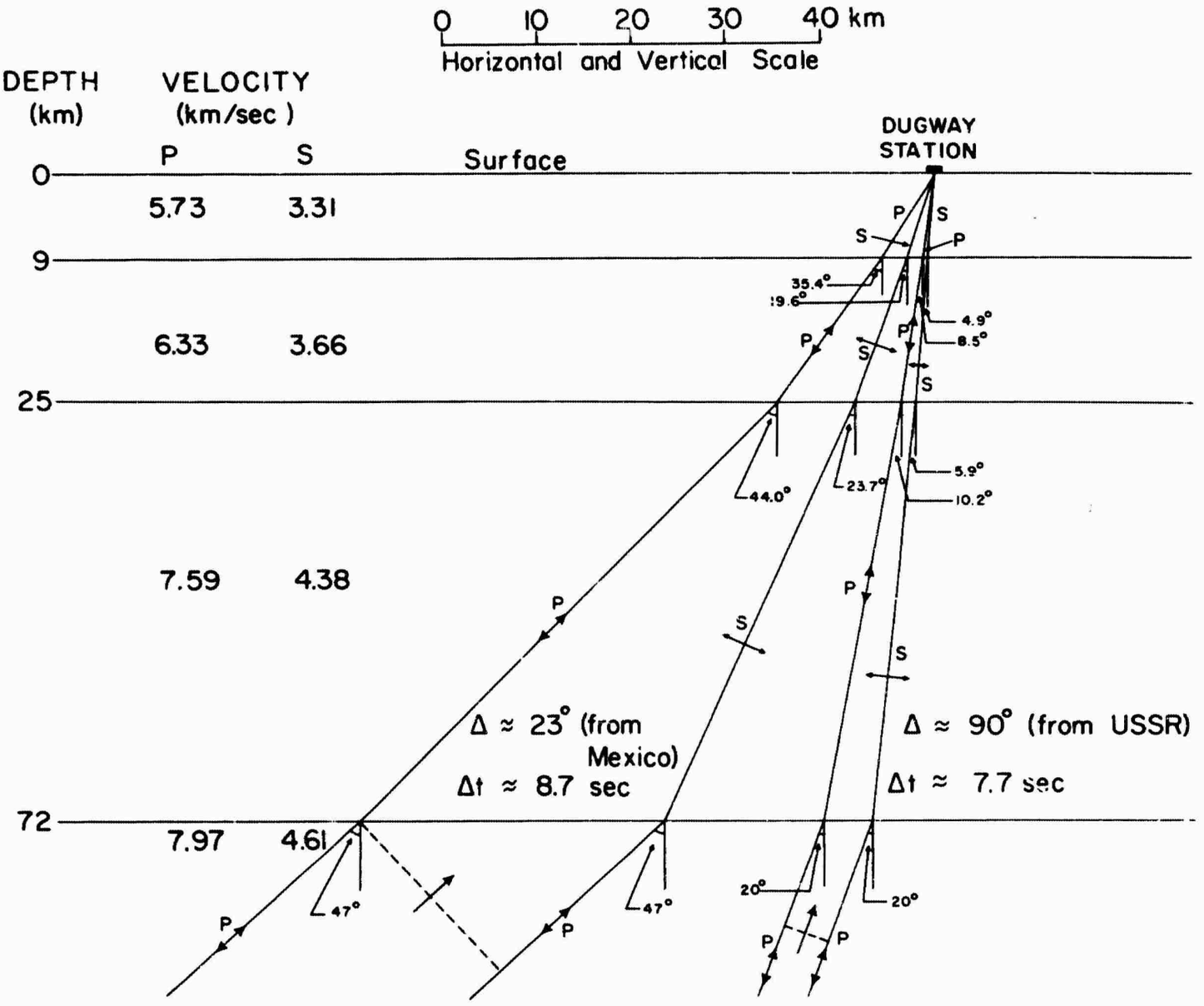

Figure 7-15. Ray paths of P waves and PS converted waves penetrating the assumed earth crustal model of Berg and others (1960) at angles of incidence for epicentral distances (Δ) appropriate for events from Mexico (left) and USSR (right) studied. Δt = time interval between PS converted wave and P.

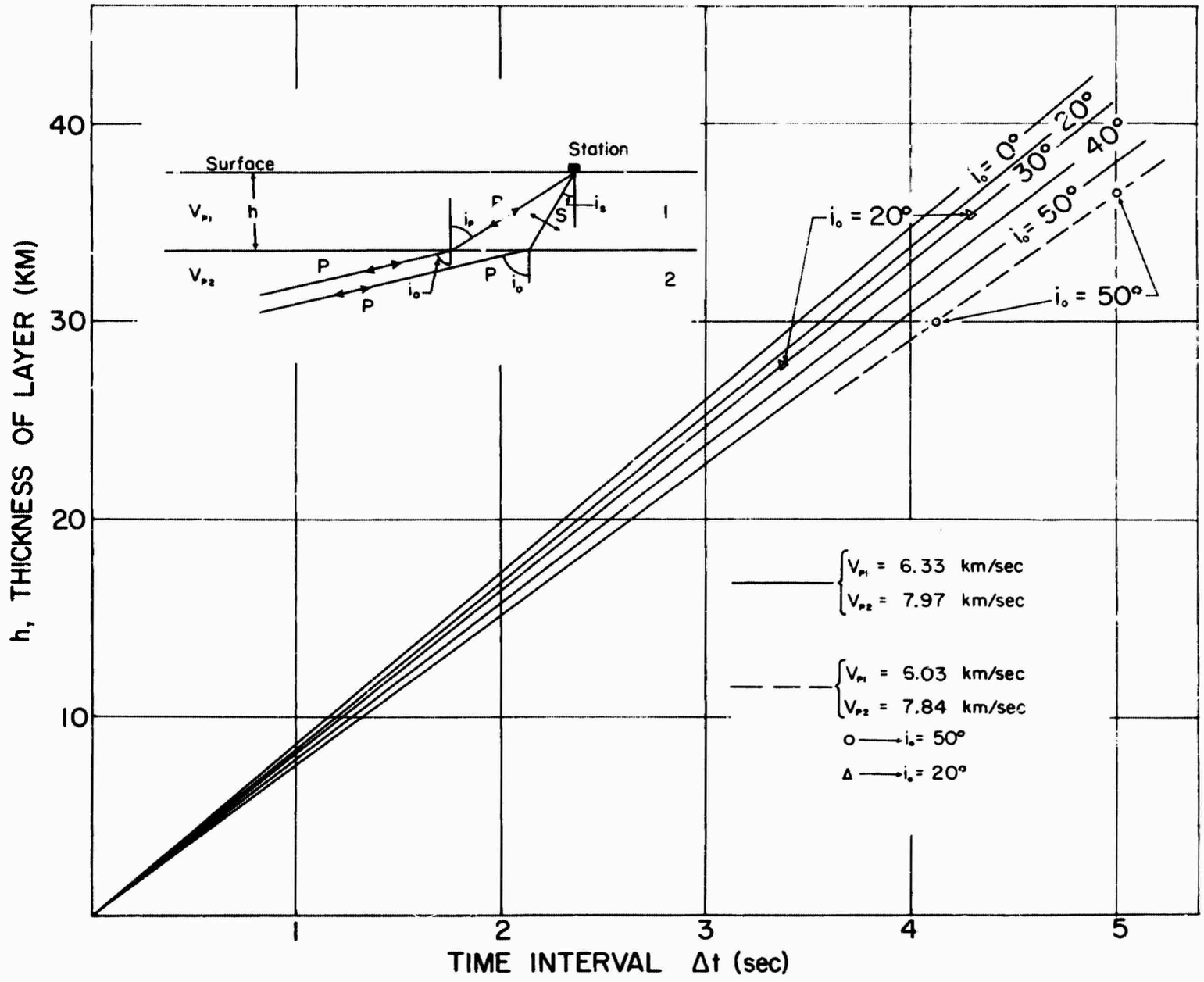

Figure 7-16. Relationship of time interval, Δt, between PS converted wave and P wave for an assumed one-layer crust with different thicknesses, h, and for various angles of incidence, i_c', at the base of the crust. Data are for two sets of compressional-velocity values.

velocities are those included in the earth crustal models of (1) Berg and others (1960) and (2) Pakiser and Hill (1963). To obtain the approximate range of values of Δt involved, various thicknesses of the crust and various angles of incidence, i_o, at the base of the crust are assumed.

In the eastern part of the Basin and Range province, a major and persistent discontinuity at a depth of 25 to 28 km has been confirmed independently by several teams of investigators (Berg and others, 1960; Pakiser and Hill, 1963; Ryall and Stewart, 1963). The principal use of this diagram is to show that any PS converted wave generated at the 25-km-depth boundary can be expected to arrive about 3 to 3 1/2 sec after the first P arrival. It should be noted that for a P to S conversion at a depth of 25 km, there is a dependency of Δt on the angle of incidence that theoretically should be observable on seismograms. For example, the time interval Δt for an angle of incidence of about 50° is nearly 1/2 sec greater than the Δt for an angle of incidence of 20°.

Arrivals of shear (SV) waves that are observed at these time intervals after P in this study are identified as PS converted waves generated at the 25-km-depth boundary.

Earthquakes

Figure 7-17 shows the vertical particle-motion diagram for an earthquake (magnitude not given by U.S.C.&G.S.) from Mexico on Oct. 19, 1962, with a depth of focus of 53 km. The first P arrival (Fig. 7-17 A) has an apparent angle of incidence at the surface of about 30° with the vertical, which is in accord with theory. The P motion is essentially linear and prograde.

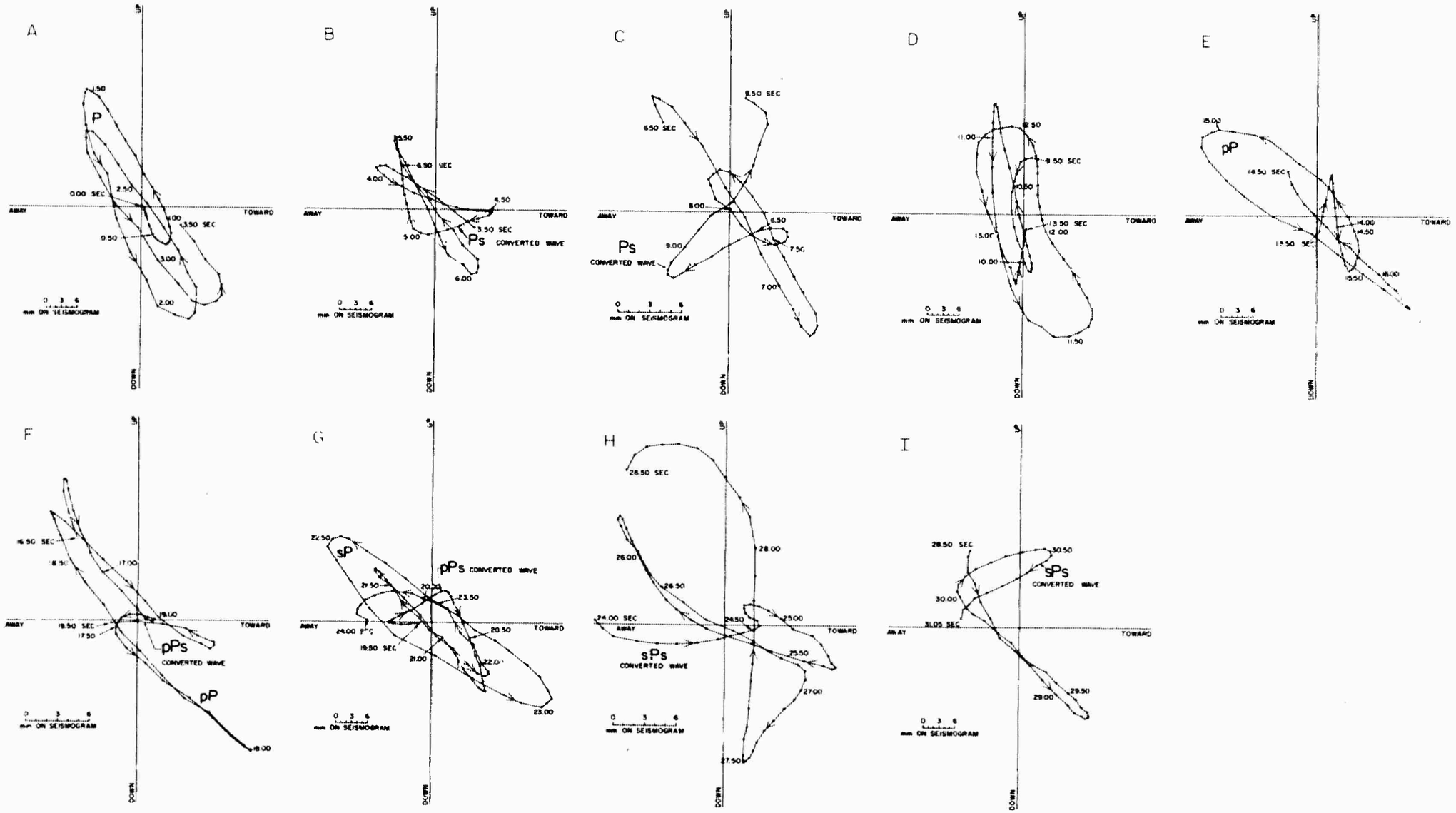

Figure 7-17. Vertical particle-motion diagrams, Mexico earthquake, Oct. 19, 1962, time interval 0.00 to 31.05 sec after first P arrival; 0.00 = 21h 26m 2[illegible].3s GCT.

In Figure 7-17B, the PS converted wave apparently generated at the 25-km-deep layer begins manifesting itself at about 3.5 sec by changing noticeably the slope of the segment of the line on the particle-motion diagram; and after "phasing in" for about 1 sec, becomes pronounced at about 4.50 sec and shows excellent S-like motion for half a second. The peak-to-peak amplitude of the shear motion, as measured on the vertical-particle-motion diagram, is about one-third that of the P, similarly measured. It should be noted that the P wave starts its large-amplitude motion about 1 sec after the first arrival of P energy; consequently, the PS-converted-wave energy similarly starts its large manifestation at 4.50 sec.

In Figure 7-17C the PS converted wave apparently generated at the 72-km-depth boundary begins manifesting itself at about 7.95 sec by changing noticeably the slope of the segment of the line on the particle-motion diagram; and after "phasing in" for about half a second, it becomes pronounced at about 8.50 sec and shows excellent S-like motion for about 1 sec thereafter. The peak-to-peak amplitude of the shear motion, as measured on the vertical particle-motion diagram, is about one-third that of the P, similarly measured.

From this same earthquake, the PS converted wave in Figure 7-17G is apparently generated at the 25-km-depth boundary from the pP body wave in Figure 7-17E. Also the PS converted waves in Figure 7-17H and 7-17I are apparently generated at the 25- and 72-km-depth boundaries, respectively, by the sP body wave in Figure 7-17G. Moreover, the PS converted wave in Figure 7-17H may conceivably include some shear energy generated at the 72-km-depth boundary by the pP body wave in Figure 7-17E, as this is the time at which this energy should arrive.

Figure 7-18 shows the horizontal particle-motion diagrams for the same time period for the same Mexico earthquake. During the early arrivals, the motion is essentially linear and essentially along the direction of a great circle to the epicenter; later, however, the motion is intermittently elliptical and near-linear. There is a tendency for some of the PS converted wave arrivals to initiate some elliptical motion, which suggests that the converted wave is not a simple SV wave but is complex.

Figure 7-19 shows the vertical particle-motion diagrams for an earthquake on May 17, 1963 from the Kurile Islands with a Richter magnitude of 5.9 and a depth of focus of 33 km. The PS converted wave shown in Figure 7-19B is apparently generated at the 25-km-depth boundary. Its peak-to-peak magnitude is about one-third that of P, as measured on these diagrams.

No recognizable PS converted wave generated at the 72-km-depth boundary was observed from this earthquake.

Figure 7-20 shows the P- and S-like motion dot presentation and the digital-to-analog seismogram of this Kurile Islands earthquake. The excellent character of the shear motion in the PS converted wave generated at the 25-km-depth boundary and with a time interval, $\triangle t$, of about 4 sec after P, is shown on (1) the dot presentation (A) and (2) the radial horizontal motion trace (B) and the vertical trace (C), wherein the two traces (B and C) are 180° out of phase.

Figure 7-21 shows the vertical particle-motion diagram for an earthquake on Feb. 20, 1964 from the Kurile Islands with a Richter magnitude of 5.2 and a depth of focus of 50 km. The PS converted waves in diagrams C and F are apparently generated at the 25- and 72-km-depth

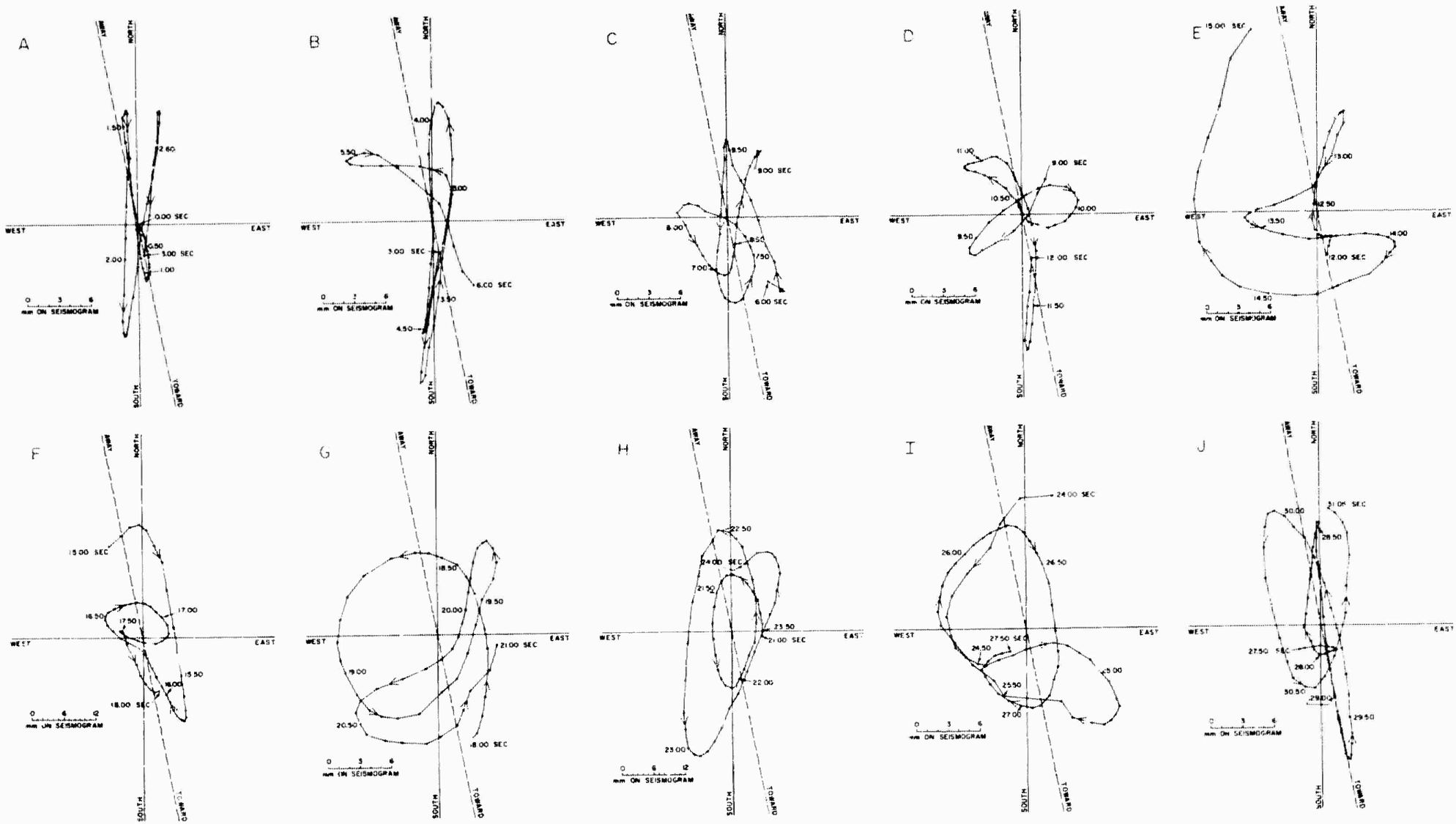

Figure 7-18. Horizontal particle-motion diagrams, Mexico earthquake, Oct. 19, 1962, time interval 0.00 to 31.05 sec after first P arrival; 0.00 = 21h 26m 26.3s GCT.

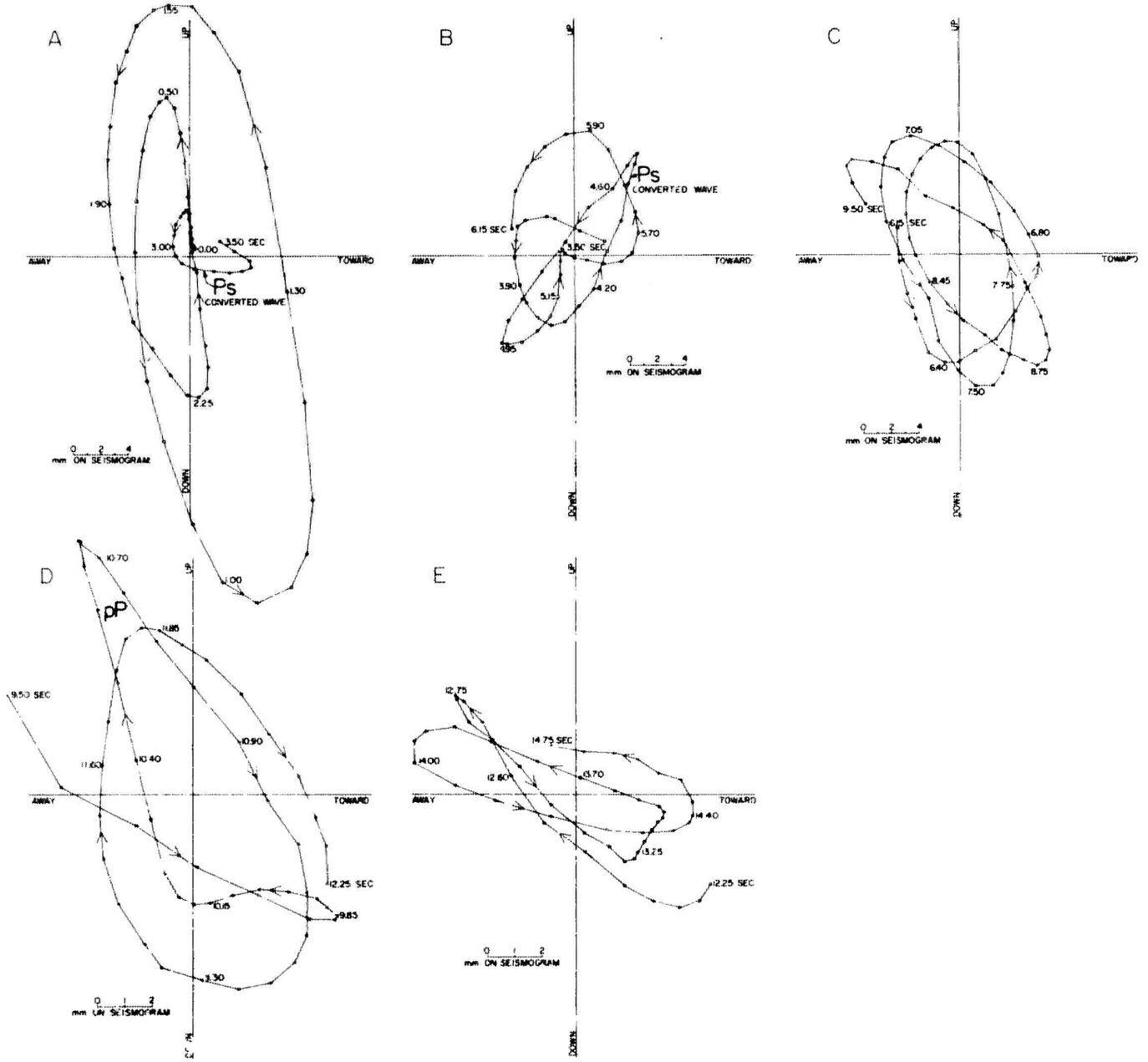

Figure 7-19. Vertical particle-motion diagrams, Kurile Islands earthquake, May 17, 1963, time interval 0.00 to 14.75 sec after first P arrival; 0.00 = 04h 17m 26.6s GCT.

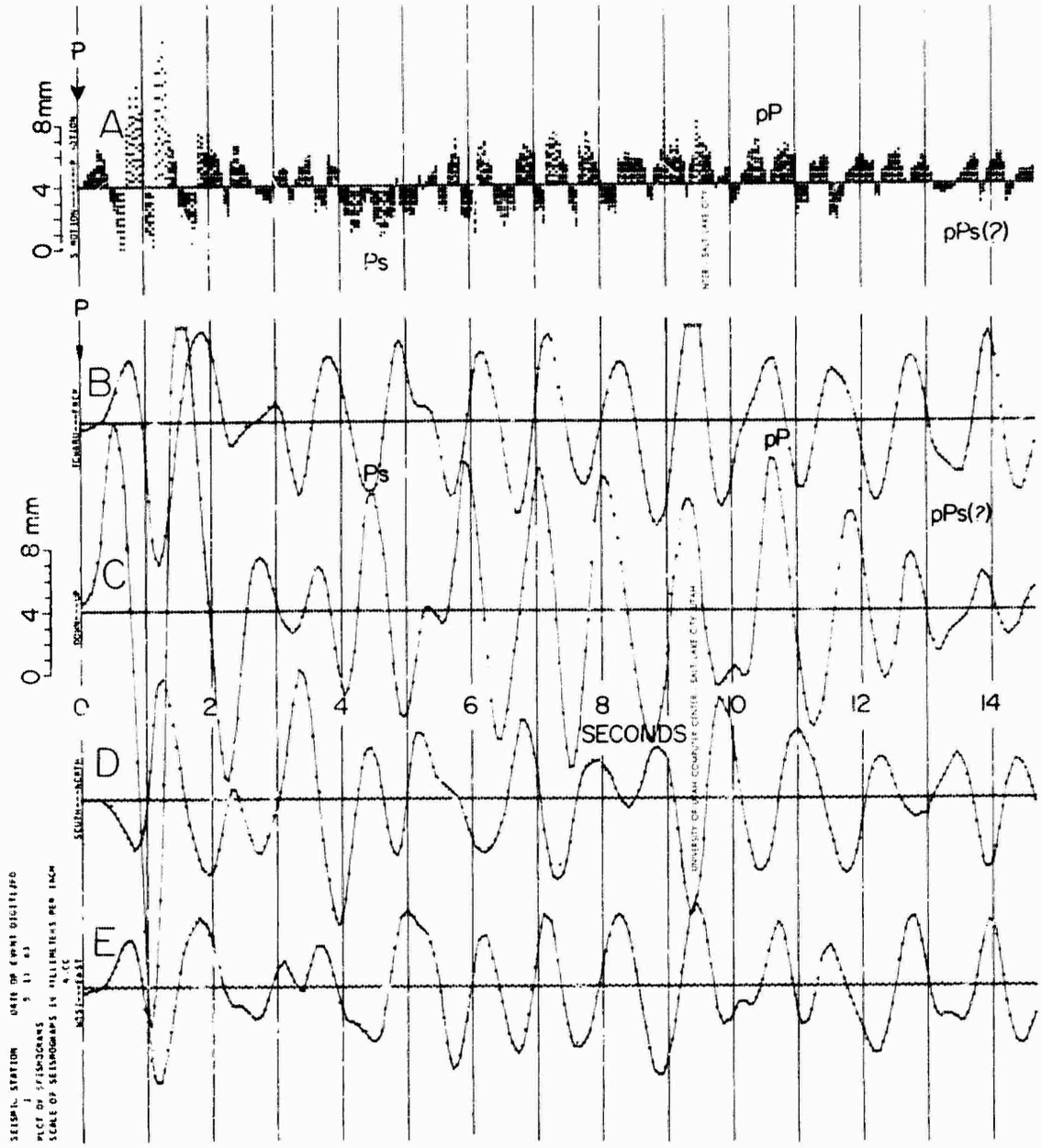

Figure 7-20. (A) P- and S-like-motion dot presentation and (B to E) digital-to-analog seismogram of Kurile Islands earthquake, May 17, 1963, time interval 0.00 to 14.60 sec after first P arrival; 0.00 = 04h 17m 26.6s GCT.

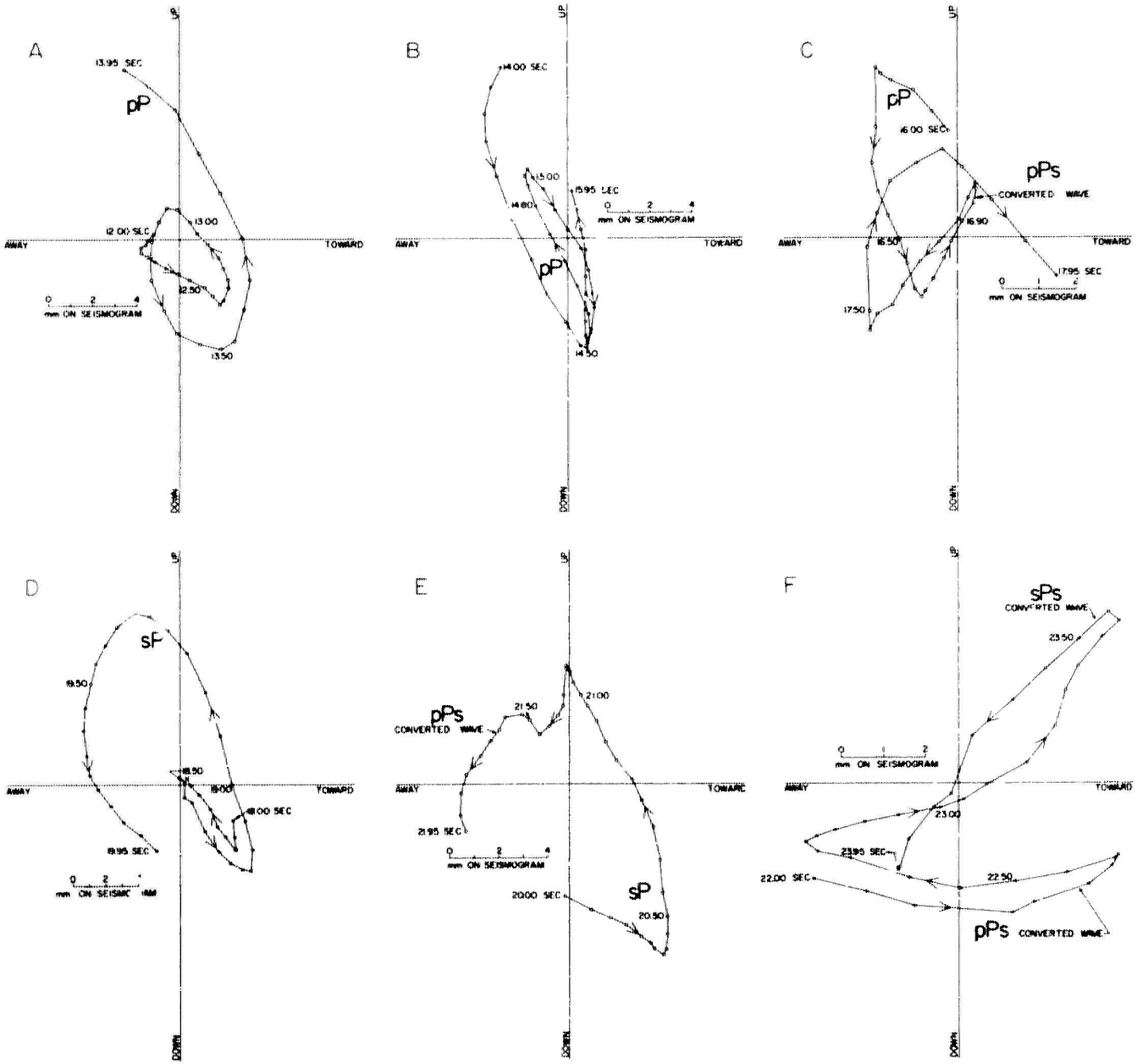

Figure 7-21. Vertical particle-motion diagrams, Kurile Islands earthquake, Feb. 20, 1964, time interval 12.00 to 23.95 sec after first P arrival; 0.00 = 10h 04m 43.6s GCT.

boundaries, respectively, by the pP phase in diagram A. The other PS converted wave in diagram F is apparently generated at the 25-km-depth boundary by the sP phase in diagram D.

Figure 7-22 shows the P- and S-like-motion dot presentation and the digital-to-analog seismogram of this Kurile Islands earthquake. The body phases and the PS converted waves just discussed are shown.

Comparison with Hannon's theoretical results

Figure 7-23C shows one of the theoretical crustal models (designated CAO used by Hannon (1964) in making his synthetic seismograms computed by the Haskell-Thomson matrix method. Although the layering of this model is not strictly applicable to the eastern part of the Basin and Range province, the values of the velocities are sufficiently close to them so that his theoretical results can be compared qualitatively with our observed results. We have added to his model the appropriate ray paths for the incident P waves and the PS converted waves generated at the base of the crust. His theoretical results are for two angles of incidence, namely 53° and 33°, which are shown in diagram C. Hannon's computations included the effect of a layered half-space.

Figures 7-23A and B show Hannon's (1964) theoretical synthetic seismograms from his theoretical model CAO. The top two traces (A) are the radial-horizontal and vertical traces, respectively, for an angle of incidence of 53°; and the bottom two traces (B) are the corresponding traces for an angle of incidence of 33°.

Two PS converted waves are recognizable: (1) one, generated at the base of the 25.43-km-depth boundary, which arrives with a time interval, Δt, of 3.5 sec after the first P

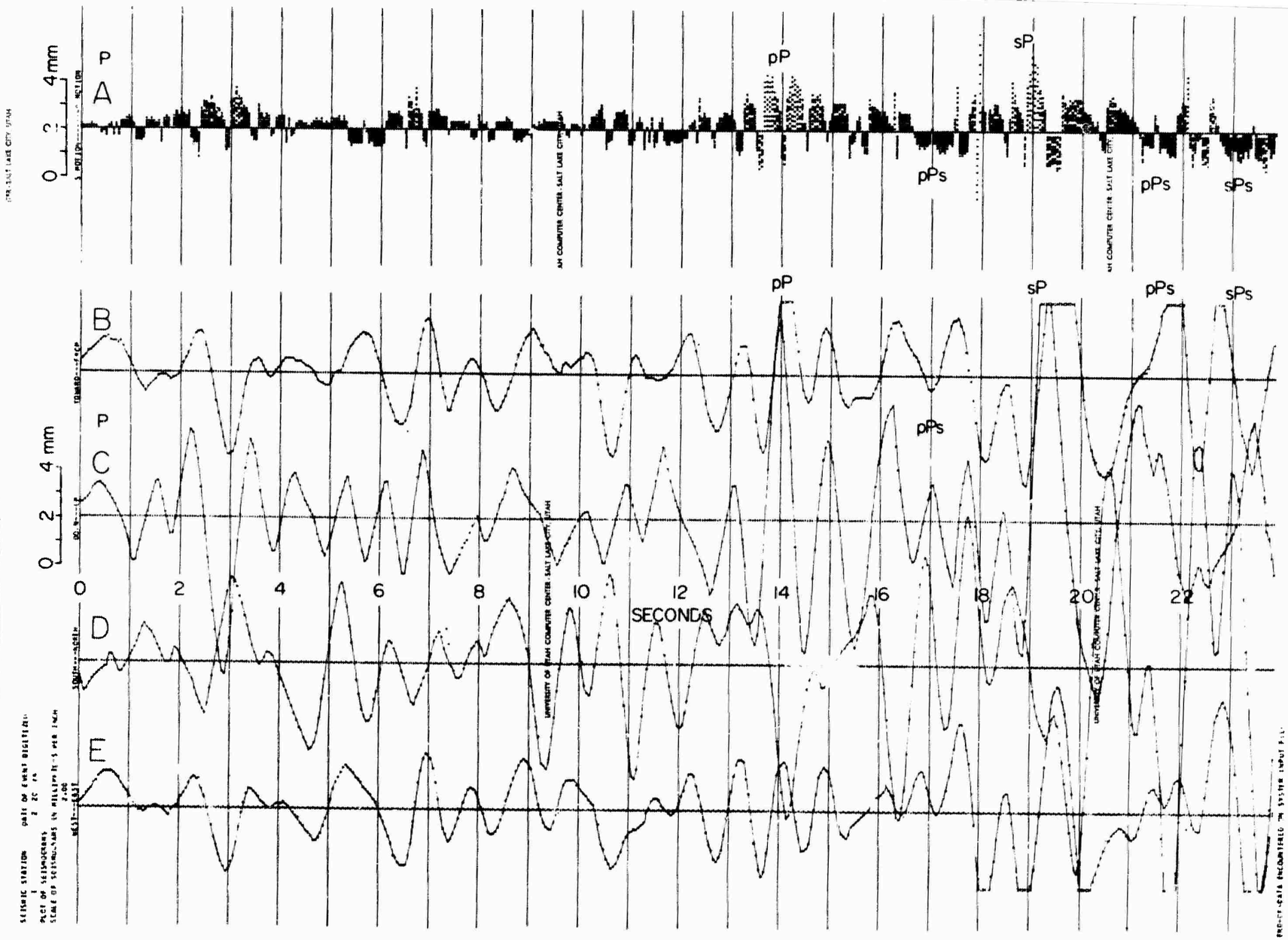

Figure 7-22. (A) P- and S-like motion dot presentation and (B to E) digital-to-analog seismogram of Kurile Islands earthquakes, Feb. 20, 1964, time interval 0.00 (approximately) to 23.95 sec after first P arrival; 0.00 = 10h 04m 43.6s GCT.

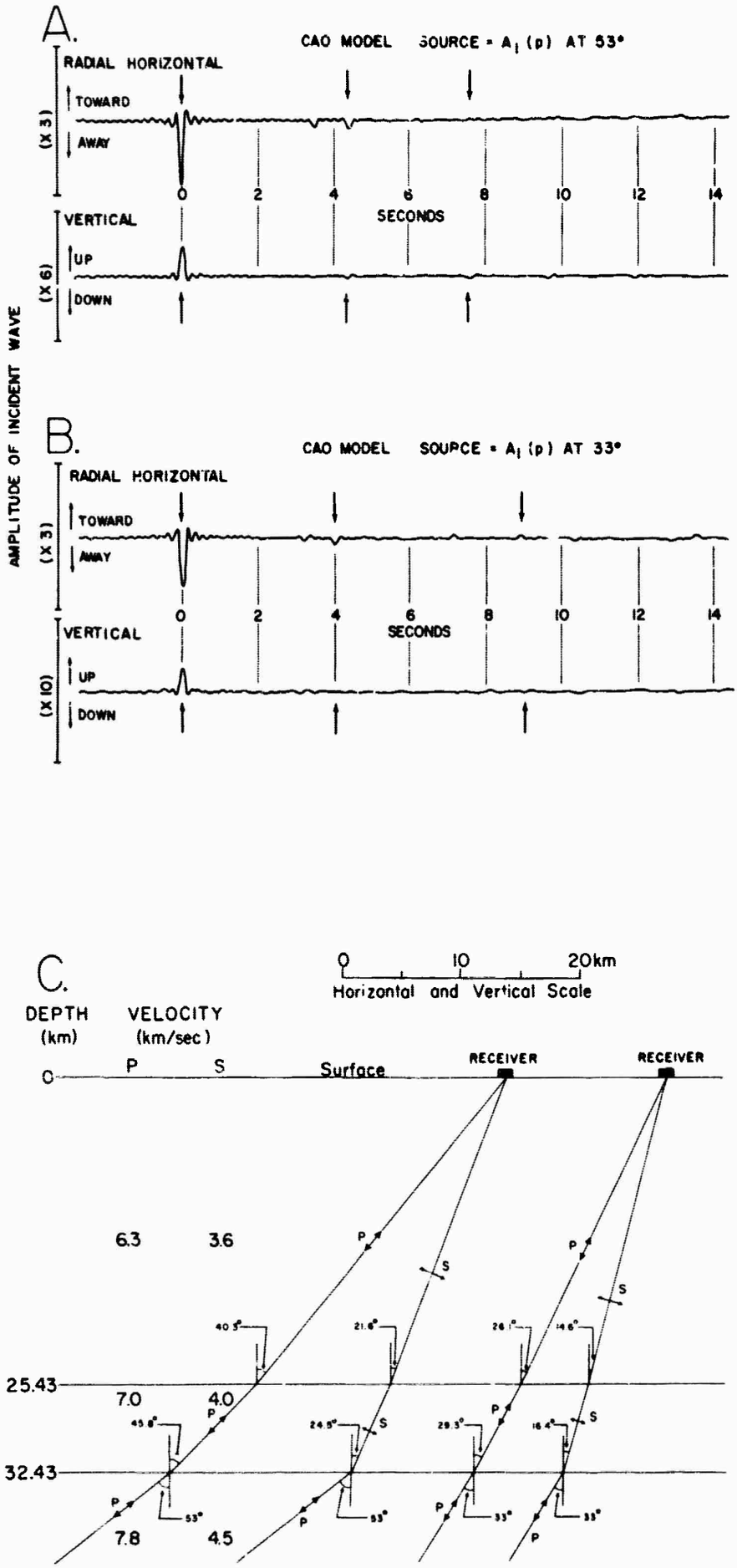

Figure 7-23. Synthetic seismograms of surface motion (Hannon, 1964, his CAO model) for vertical and radial-horizontal components for angles of incidence of (A) 50° and (B) 33° at base of crust for (C) earth crustal model of Gutenberg, on which are drawn P waves and PS converted waves generated at base of crust.

arrival; and (2) another (with the arrow after Hannon), generated at the 32.43-km-depth boundary (i.e., at the base of the crust), which arrives with a time interval, $\triangle t$, of about 4 1/2 sec (actually 4.4 sec after the first P arrival. These time intervals are for the incident P waves with an angle of incidence of 53° at the base of the crust; the time interval $\triangle t$ is 0.4 to 0.4 sec smaller in each case for the P waves with an angle of incidence of 33° at the base of the crust.

The theoretical amplitudes of the PS converted waves generated at the 25.43-km-depth boundary and at the 32.43-km-depth boundary (base of the crust), as measured on the radial-horizontal-component trace, are about 10 to 20 percent of the amplitudes of the first P arrival, similarly measured. The theoretical amplitudes of the PS converted waves, as measured on the vertical-component traces, are small.

In conclusion, our observed results give excellent experimental support of Hannon's (1964) theoretical results for his model CAO. Our work was initiated several years ago and was done quite independently of that of Hannon.

Underground explosions in Semipalatinsk area, USSR

Figure 7-24 shows the vertical particle-motion diagrams for the first 10 sec after the first P arrival for the underground explosion in the Semipalatinsk area, USSR, on July 19, 1964. The emergence is very steep. It is possible that the PcP wave, which should arrive about 1 sec after P, may be "phased in" with the P and is giving an erroneous impression of the steepness of P. The motion phases into S-like motion at about 2.00 sec and continues thus until 3.25 sec; but this value of 2.00 sec is somewhat earlier than could be expected for a PS converted wave generated at

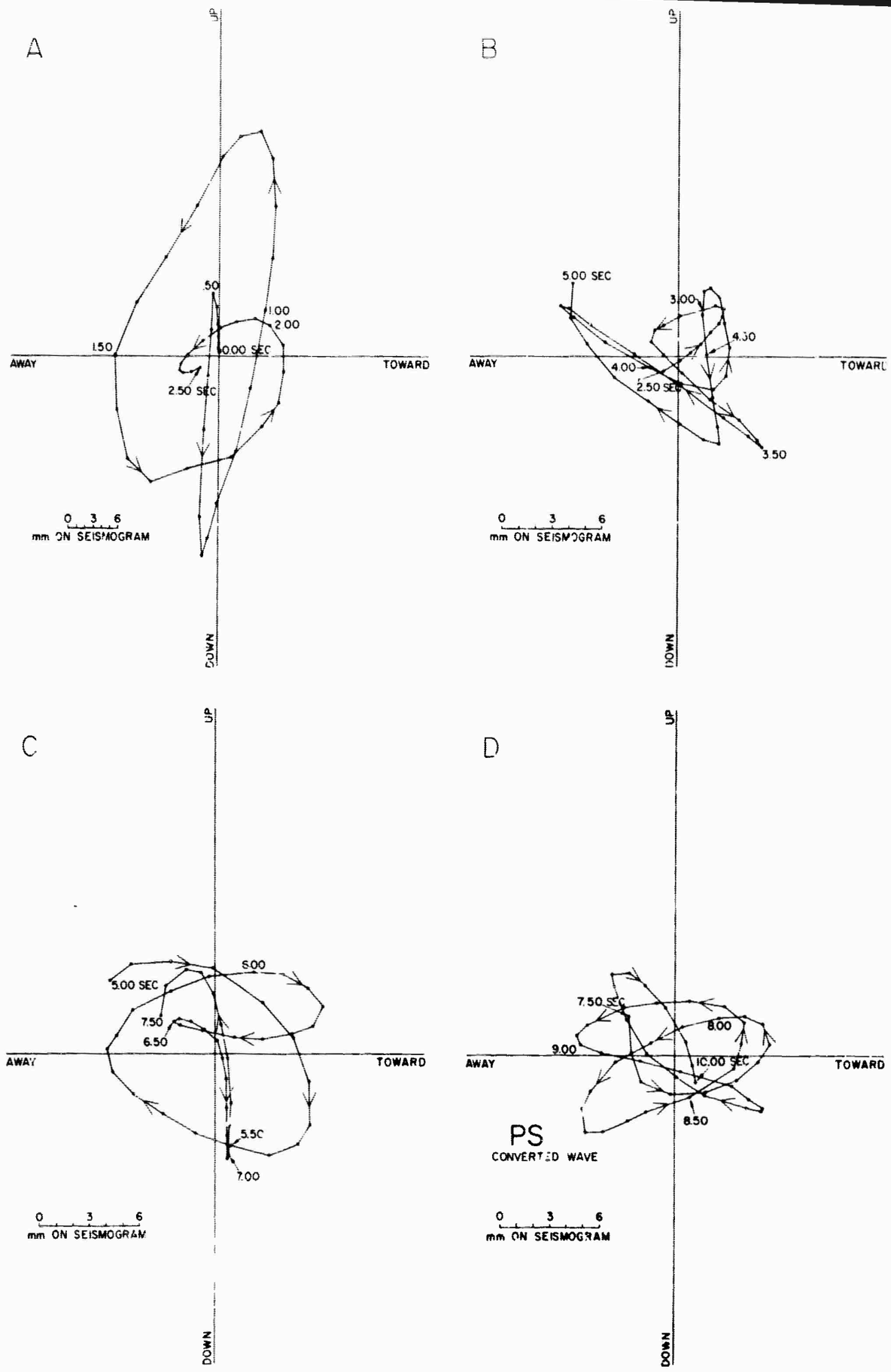

Figure 7-24. Vertical particle-motion diagrams, probable underground explosion in the Semipalatinsk area, USSR, July 19, 1964, time interval 0.00 to 10.00 sec after first P arrival; 0.00 = 06h 13m 01.4s GCT.

the 25-km-depth boundary. S-like motion starting at 7 3/4 sec and lasting about 1 1/4 sec is believ' to be a PS converted wave generated at the 72-km-depth boundary.

The angle of incidence of the P wave at the 25-km-depth boundary is apparently too small to generate PS converted waves in this case.

Figure 7-25 shows the P- and S-like motion dot-presentation of the same Soviet explosion. Note the excellent S-like motion at 2 to 3 sec and at 7 3/4 to 9 sec.

Figure 7-14 shows the digital to-analog seismogram for the same Soviet explosion. Note the excellent S-like motion at 2 to 3 sec and at 7 3/4 to 9 sec.

Figure 7-26 shows the vertical particle-motion diagrams for the first 9.7 sec after the first P arrival for the underground explosion in the Semipalatinsk area, USSR, on March 15, 1964. The character of these particle-motion diagrams is almost identical to those of the ones just shown. The S-like motion is present at about 2 to 2 1/2 sec, and also at 7.3 to 8.2 sec. In this case, however, about half a second should be added to these values because the digitizing was started half a second late.

Figure 7-27 shows the digital-to-analog seismogram of this same Soviet explosion.

Summary

We have shown that PS converted waves have been observed at various probable teleseismic distances from various earthquakes and from certain Soviet / underground explosions. From Mexican earthquakes--that is, at epicentral distances of about 2,000 km, PS converted waves generated at both the

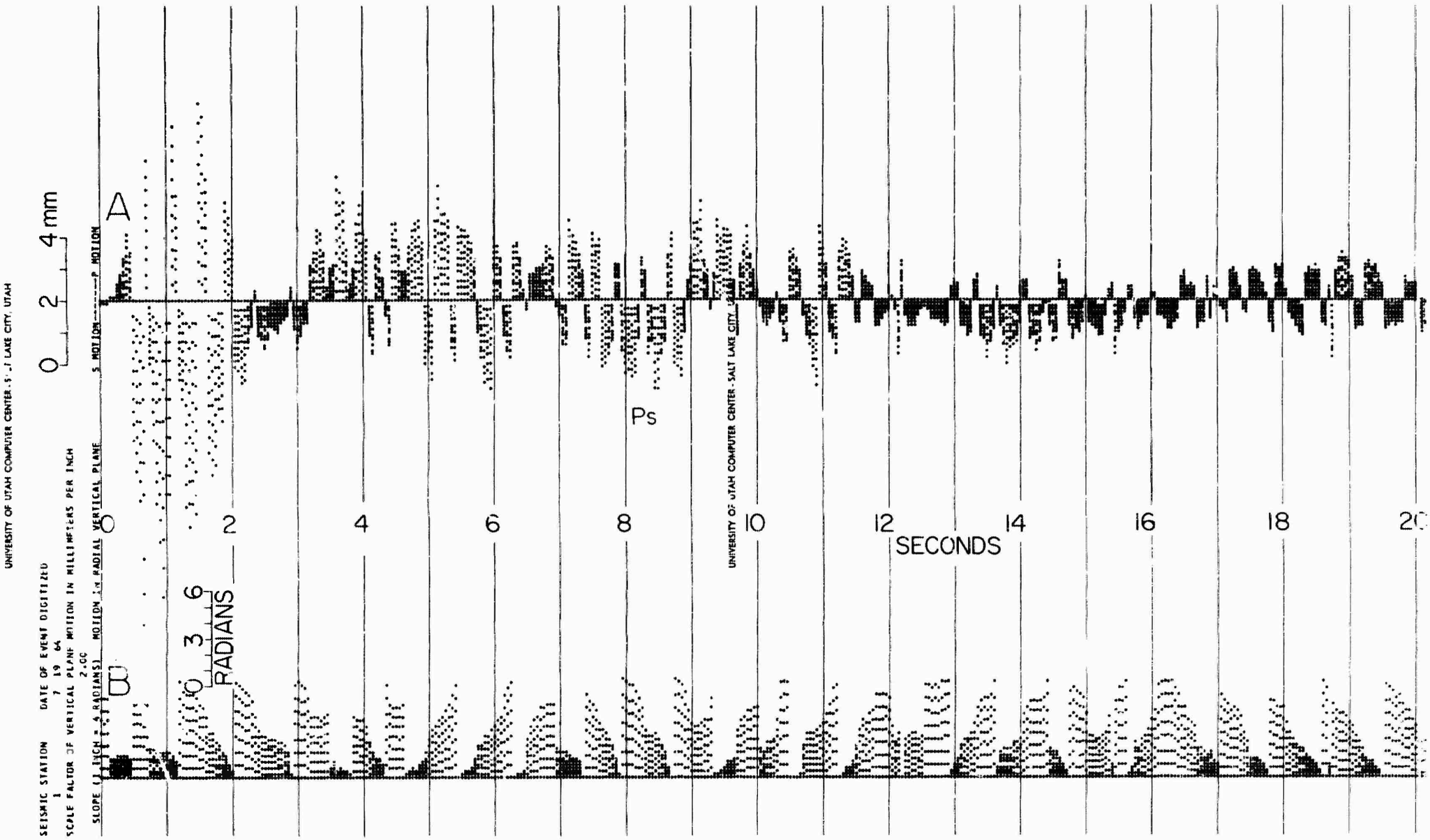

Figure 7-25. (A) P- and S-like-motion dot presentation and (B to E) digital-to-analog seismogram of probable underground explosion in the Semipalatinsk area, USSR, July 19, 1964, time interval 0.00 to 20.00 sec; 0.00 = 06h 13m 01.4s GCT.

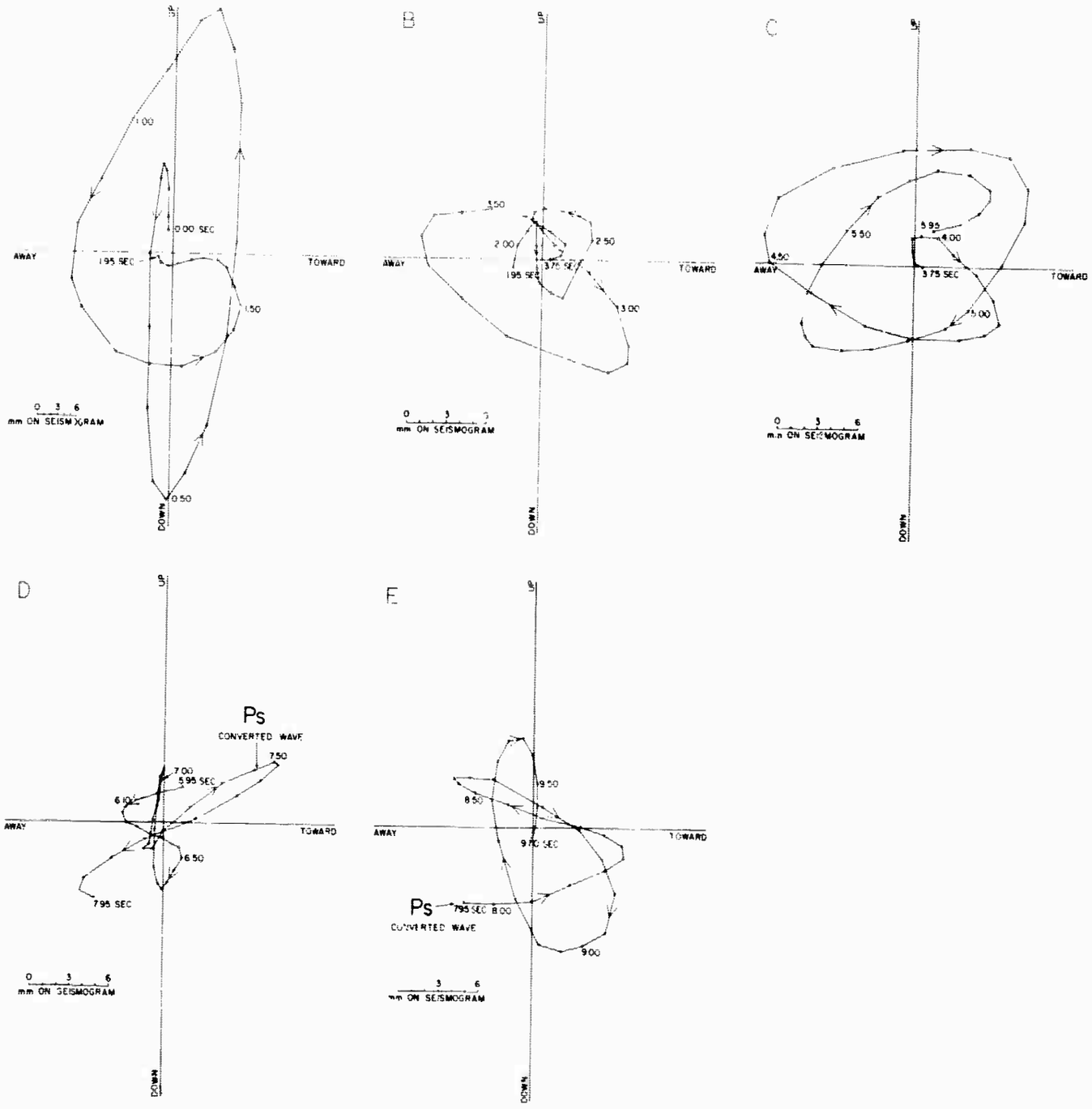

Figure 7-26. Vertical particle-motion diagrams, probable underground explosion in the Semipalatinsk area, USSR, March 15, 1964, time interval 0.00 (approximately) to 9.70 sec after first P arrival; 0.00 - 08h 13m 01.7s GCT.

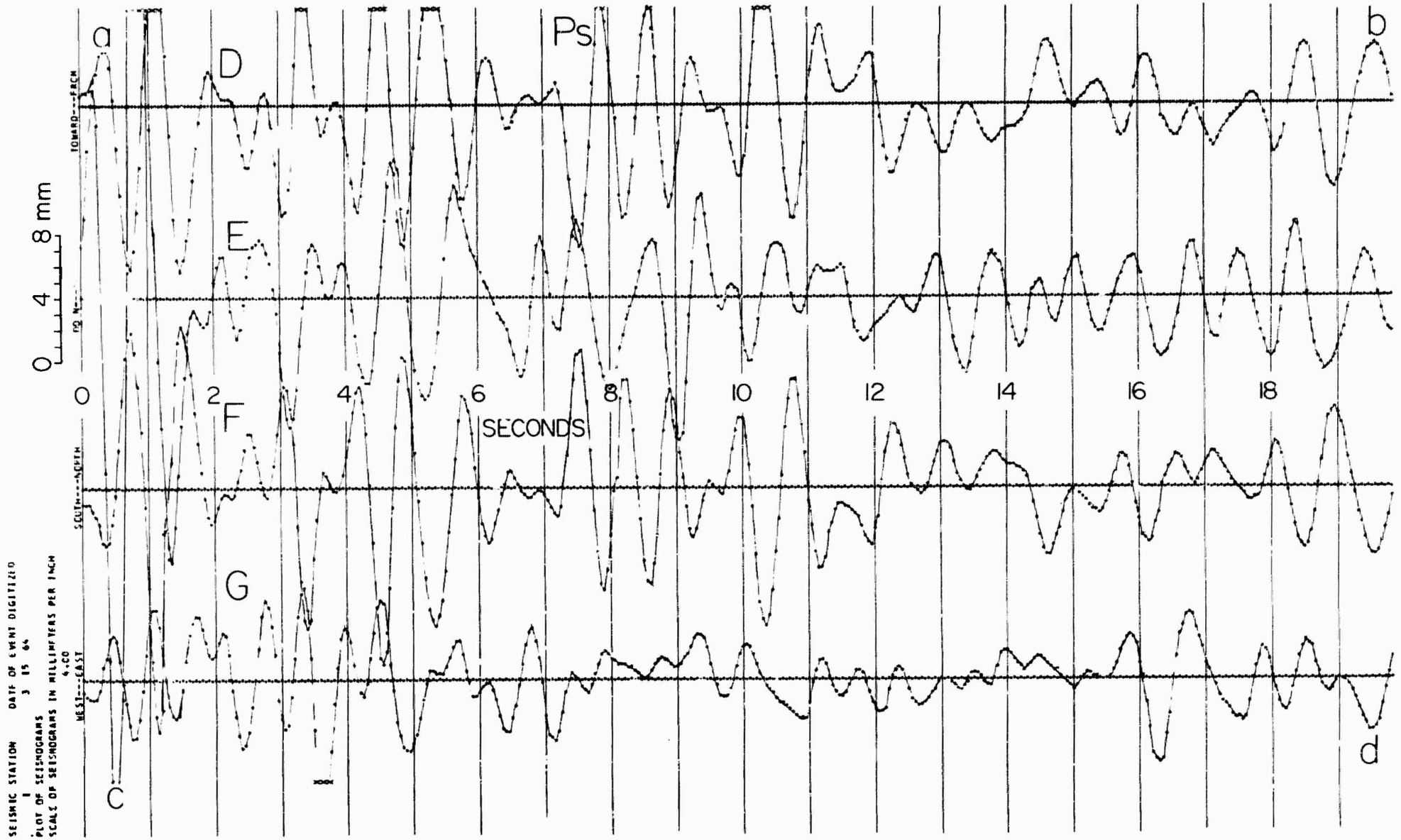

Figure 7-27. Digital-to-analog seismogram of probable underground explosion in the Semipalatinsk area, USSR, March 15, 1964; 0.00 = 08h 13m 01.7s GCT.

25-km-depth boundary and the postulated 72-km-depth boundary have been observed. At intermediate epicentral distances of 50°, PS converted waves generated from both these boundaries are also observed. At an epicentral distance of 90° (10,000 km), PS converted waves generated from the 72-km-depth boundary are observed; but the PS converted waves from the 25-km-depth boundary were not clearly observed. The observed amplitudes of the PS converted waves were generally about one-fifth to one-third of that of the parent P phases that generate the PS converted waves. The PS converted waves from earthquakes at teleseismic distances were observed following the phases P, pP, sP, and PcP. Thus, for earthquakes, the PS converted waves add to the complexity of the coda of P in addition to the phases P, pP, sP, and PcP. The PS converted waves from the Soviet probable underground explosions were apparently generated from the 72-km-depth boundary only and for the P arrival only; however, in this case also, the PS converted waves add somewhat to the complexity of the coda of P.

We consider that our observed results have given experimental support to Hannon's theoretical seismograms using the Haskell-Thomson matrix formulation for ground motion for his model CAO; in particular, the PS converted waves have been observed, as predicted by him theoretically.

Last--but by no means least--we consider that our results give added support to the existence of a velocity discontinuity at a depth of about 72 km beneath the eastern part of the Basin and Range province, as first postulated by Berg and others (1960).

CHAPTER VIII

SUMMARY AND CONCLUSIONS

S-like motion appears on many of the particle-motion diagrams at approximately the expected arrival time for PPS and SPS. Usually, no other S-like motion is apparent on the particle-motion diagrams in the first ten seconds except at these times, approximately 4.0 and 8.0 sec for PPS and SPS, respectively.

The most consistent arrival of large amplitude in the early part of the seismogram is an event which we have called $P_{M_1}P$ in Chapter 5. The arrival time of this event on the seismograms usually coincides very well with the theoretical arrival time of a reflection from the Mohorovicic discontinuity. The arrival is consistent in both time and character, as may be seen from examining the various digital-to-analog CalComp plots in Chapter 5. This phase may be a guided wave in the crust, usually called $\bar{P}$, and not a simple reflection from the base of the crust. However the travel-times of either $P_{M_1}P$ or $\bar{P}$ would probably be very nearly the same. The large amplitudes following $P_{M_1}P$ are attributed to multiple reflections of $P_{M_1}P$ or $\bar{P}$ in the crustal waveguide.

Some evidence for an SPP transmission path is suggested by large amplitude P-motion at the expected time of arrival of this event.

Hannon (1964) showed that SV motion may be accentuated by the presence of thin low-velocity layering beneath the recording site. This would effectively raise the signal-to-noise ratio where S converted waves are concerned and may, for example, partly explain large amplitudes for PPS.

The characteristics of the S-like motion defining PPS and SPS, and other arrivals, will need to be studied further in order to define the differences in explosion-generated shear and earthquake-generated shear, and to use these differences to aid in distinguishing between underground

nuclear explosions and earthquakes. In particular, the signal-to-noise ratio on the seismograms of underground nuclear explosions as recorded at a given station can be increased by "stacking" the seismograms of several blasts, thus obtaining an average seismic signature which may be characteristic of the local blast site. Also, by stacking seismograms and using a reference time measured with respect to P_n, shear arrivals such as PPS and SPS which arrive after P_n at a time independent of the epicentral distance, will have their signal-to-noise ratio increased over what it was for a single recording. This can be done for many of the LRSM Geotech stations for regions over which the crustal section does not change very much. Such a stacking procedure would cause other arrivals, whose arrival time as measured after P_n is a function of the epicentral distance, to become less coherent on the particle-motion diagrams. The signal-to-noise ratio of PPS and SPS should therefore be increased at the expense of distance-dependent arrivals.

Average seismic signatures obtained by stacking same-site explosions as recorded at the same station can then be cross-correlated using the first 20 to 30 seconds, say, of the entire average signature, with a single event recorded at a later time. A cross-correlation index will then aid in confirming the later event as an underground nuclear explosion.

The recordings of the LRSM Geotech stations do confirm that a large amount of shear energy, at least equal to the compressional energy, is generated by some underground nuclear explosions. At the expected time of arrival of the body S-wave (SSS) large amplitudes are observed on many of the LRSM recordings. A few underground nuclear explosions were examined out at this time interval, and the particle-motion diagrams showed shear motion, beginning at the correct time for the SSS trans-

mission path. The large amount of original shear also tends to support the identification of SPP.

Seismograms obtained from 27 confirmed underground nuclear explosions of Richter magnitudes 3.9 to 5.8 at the Nevada test site (NTS) and 4 probable underground explosions in the Semipalatinsk area, USSR of Richter magnitude 5.5 or greater were recorded by the Benioff short-period matched seismometers (magnification 400,000) at Dugway, Utah, hand-digitized, and analyzed (using particle-motion diagrams and digital-to-analog seismograms) during the first 15 to 25 sec after the first arrival of P. The epicentral distances were about 450 and 9,800 km, respectively. Provided the explosions occurred in the same area, a striking consistency of the body-wave phases was observed from some (but not universally from all) underground explosions within that area. The characteristics of the body-wave patterns vary for three different areas of detonation within NTS, presumably because of different source functions (depending on rock type, geologic environment, degree of coupling, yield, etc.) This striking consistency of body-wave phases has been used successfully for the positive detection and identification of certain underground nuclear explosions detonated at NTS and recorded at Dugway, Utah and to correctly determine, within a few kilometers, the area of the detonation within NTS. The following phases were tentatively identified: $P_{III}P$ and/or PPPPPPP, SSPPP, SSPSS, $P_{II}P$ (or $\overline{P}$) and/or PPP, PPS, SPP, SPS, and $\overline{P}'$ (or multiple P reflection)[a]; the times of arrivals of these phases agree moderately well with the crustal model of the area determined by the refraction method.

Seismograms obtained from (a) 10 earthquakes of Richter magnitudes 5 to 7 in the Kurile and Tonga Islands, Japan, and Mexico and (b) the same probable explosions in the USSR mentioned above, were recorded at Dugway, Utah at epicentral distances of (a) 2,300 to 9,700 km and (b) about 9,800 km, respectively, and similarly digitized and analyzed during the first 20 or 40 sec after the first P arrival. PS converted waves were generally observed from both the earthquakes and underground explosions. These converted waves were apparently generated at both the 25- and/or 72-km-depth boundaries; and the time intervals Δt, after the first arrival of P, were about 3 to 3 1/2 sec and 7 1/2 to 8 1/2 sec, respectively. These time-interval values are in excellent accord with the crustal model of Berg and others (1960). Similar PS converted waves with approximately the same Δt values were generally observed following other large phases, including pP, sP, and PcP, from the earthquakes. The time interval, Δt, was generally somewhat less for earthquakes with greater epicentral distances because of the smaller angles of incidence of the incident P waves at the base of the crust. The observed maximum amplitudes of the PS converted waves as measured on the seismograms are usually one-fifth to one-third of that of the parent P phases that generate the PS converted waves. These results give experimental support to the theoretical synthetic seismograms for the CAO model of Hannon (1964). Moreover, the observed PS converted waves give added support to the existence of a velocity discontinuity at a depth of about 72 km beneath the eastern part of the Basin and Range province, as first postulated by Berg and others (1960).

An important consequence of these results is that (1) for the Soviet probable underground nuclear explosions in the Semipalatinsk area, the PS converted waves add somewhat to the complexity of the coda of P, and (2) for earthquakes at teleseismic distances, the PS converted waves add to the complexity of the coda of P in addition to the phases P, pP, sP, and PcP.

ACKNOWLEDGMENTS

Financial support was provided from research contract No. AF19(628)-201 with Air Force Cambridge Research Laboratories of the U. S. Air Force under project VELA UNIFORM of the Advance Research Projects Agency of the Department of Defense. The assistance of Dr. S. T. Algermissen during the early part of the project is gratefully acknowledged. The following Research Assistants in the Department of Geophysics at the University of Utah made various contributions to the project: V. A. Finlayson, D. J. Green, G. M. Hathaway, A. P. Heinen, R. H. Senn, L. C. Wood, and J. R. Wood. The U.S. Coast and Geodetic Survey furnished seismograms and calibration data from several of the permanent seismograph stations under its supervision, and also assisted in many problems that arose incident to (1) the building of the seismograph vaults at Carbon College, Price, Utah and Dugway, Utah and (2) the installation and calibration of the seismographs and allied instrumentation at these two stations, as well as the permanent seismograph station at Salt Lake City, Utah. Dr. J. Stewart Williams, Utah State University, Logan, Utah, made available seismograms from the seismograph station at Logan, Utah. Officials of the following private companies or organizations, assisted in various ways: Gaertner Scientific Corporation, Chicago, Illinois; Hercules Powder Co., Salt Lake City, Utah; Space Technology Laboratories, Redondo Beach, California; The Geotechnical Corporation, Dallas, Texas; and United ElectroDynamics, Incorporated, Alexandria, Virginia. The staff of the Computer Center of the University of Utah assisted in many problems.

BIBLIOGRAPHY

Andreev, S. S., 1957, A study of the plutonic structure of the earth's crust using PS exchange waves recorded during earthquakes: Bull. Acad. Sci. USSR, Geophys. Ser. (English Transl.), no. 1, p. 22-31.

Berg, J. W., Jr., Cook, K. L., Narans, H. D., Jr., and Dolan, W. M., 1960, Seismic investigation of crustal structure in the eastern part of the Basin and Range province: Seismol. Soc. Amer. Bull., v. 50, p. 511-535.

Caless, T. W. (Editor), 1964, Proceedings of the Vesiac conference on variations of the earth's crust and upper mantle, VESIAC Report No. 4410-75-X.

Caless, T. W. (Editor), 1965, U. S. underground nuclear explosions: VELA UNIFORM Periodic Information Digest, v. 1, no. 1, Jan. 1, p. I-1.

Cook, K. L., Algermissen, S. T., and Costain, J. K., 1962, The status of PS converted waves in crustal studies: Jour. Geophys. Research, v. 67, p. 4769-4778.

Costain, J. K., Cook, K. L., and Algermissen, S. T., 1963, Amplitude, energy, and phase angles of plane SV waves and their application to earth crustal studies: Seismol. Soc. Amer. Bull., v. 53, p. 1039-1074.

Costain, J. K., Cook, K. L., and Algermissen, S. T., 1963, Tables of amplitude and energy ratios: VESIAC Special Report 4410-68-X, Acoustics and Seismic Lab., Inst. Science & Technology, Univ. Michigan, Ann Arbor, Mich., 176 p.

Costain, J. K., Cook, K. L., and Algermissen, S. T., 1965, Corrigendum to "Amplitude, energy and phase angles of plane SV waves and their application to earth crustal studies", Seismol. Soc. Amer. Bull., April 1965, in press.

Costain, J. K., and Cook, K. L., 1965, Tables of energy ratios, amplitude ratios, and phase angles for plane SV waves: VESIAC Special Report No. 4410-96-X, Acoustics and Seismics Lab., Inst. Science & Technology, Univ. Michigan, Ann Arbor, Mich., 106 p., in press.

Diment, W. H., Stewart, S. W., and Roller, J. C., 1961, Crustal structure from the Nevada test site to Kingman, Arizona, from seismic and gravity observations: Jour. Geophys. Research, v. 66, p. 201-214.

Eaton, J. P., 1963, Crustal structure from San Francisco, California, to Eureka, Nevada, from seismic refraction measurements: Jour. Geophys. Research, v. 68, p. 5789-5806.

Glasstone, Samuel, 1964, The effects of nuclear weapons: published by the U. S. Atomic Energy Commission, U. S. Gov't. Printing Office, Washington, D. C., 730 p. (Original edition April 1962; revised edition reprinted February 1964).

Hall, D. H., 1964, Converted waves in refraction surveys over markers of variable depth: Geophysics, v. 29, p. 733-744.

Hannon, W. J., 1964, Some effects of a layered system on dilitational waves: Report AFCRL-64-614, Air Force Cambridge Research Lab., U. S. Air Force, Bedford, Mass., 68 p.

Hannon, W. J., 1964, An application of the Haskell-Thomson matrix method to the synthesis of the surface motion due to dilitational waves: Seismol. Soc. Amer. Bull., v. 54, no. 6, p. 2067-2079.

Haskell, N. A., 1960, Crustal reflection of plane SH waves: Jour. Geophys. Research, v. 65, p. 4147-4150.

Haskell, N. A. 1962, Crustal reflection of plane P and SV waves: Jour. Geophys. Research v. 67, p. 4751-4767.

Jackson, W. H., Stewart, S W., and Pakiser, L. C., 1963, Crustal structure in eastern Colorado from seismic-refraction measurements: Jour. Geophys. Research, v. 68, p. 5767-5776.

Kuz'mina, N. V., 1959, The use of converted waves in the study of the structure of the earth's crust in the southeastern portion of the main Caucasus Range: Bull. Acad. Sci. USSR, Geophys. Ser. (English Transl.), no. 7, p. 734-743.

McCamy, K., Meyer, R. P., and Smith, T. J., 1962, Generally applicable solutions of Zoeppritz' amplitude equations: Seism. Soc. Amer. Bull., v. 52, p. 923-955.

Nuttli, Otto, 1959, The particle motion of the S wave: Seismol. Soc. Amer. Bull., v. 49, p. 49-56.

Nuttli, Otto, 1961, The effect of the earth's surface on the S wave particle motion: Seismol. Soc. Amer. Bull., v. 51, p. 237-246.

Nuttli, Otto, 1964a, Some effects of the crust and free surface on the amplitudes of P and S waves, in Proceedings of the VESIAC conference on variations of the earth's crust and upper mantle: VESIAC Report 4410-75-X, Acoustics and Seismics Lab., Inst. Science & Technology, Univ. Michigan, Ann Arbor, Mich., p. 5-18.

Nuttli, Otto, 1964b, The determination of S-wave polarization angles for an earth model with crustal layering: Seismol. Soc. Amer. Bull., v. 54, p. 1429-1440.

Nuttli, Otto, and Whitmore, J. D., 1961, An observational determination of the variation of the angle of incidence of P waves with epicentral distance: Seismol. Soc. Amer. Bull., v. 51, p. 269-276.

Nuttli, Otto, and Whitmore, J. D., 1962, On the determination of the polarization angle of the S wave: Seimol. Soc. Amer. Bull., v. 52, p. 95-107.

Pakiser, L. C., 1963, Structure of the crust and upper mantle in the western United States: Jour. Geophys. Research, v. 68, no. 20, p. 5747-5756.

Press, Frank, 1960, Crustal structure in the California-Nevada region: Jour. Geophys. Research, v. 65, p. 1039-1051.

Richter, C. F., 1958, Elementary Seismology: W. H. Freeman and Co., San Francisco, 768 p.

Roller, J. C., and Healy, J. H., 1963, Seismic-refraction measurements of crustal structure between Santa Monica Bay and Lake Mead: Jour. Geophys. Research, v. 68, p. 5837-5849.

Ryall, Alan, and Stuart, D. J., 1963, Travel times and amplitudes from nuclear explosions, Nevada test site to Ordway, Colorado: Jour. Geophys. Research, v. 68, p. 5821-5835.

Schwind, J. J., Berg, J. W., Jr., and Cook, K. L. 1960, PS converted waves from large explosions: Jour. Geophys. Research, v. 65, p. 3817-3824.

Stewart, S. W., and Pakiser, L. C., 1962, Crustal structure in eastern New Mexico interpreted from the GNOME explosion: Seism. Soc. Amer. Bull., v. 52, p. 1017-1030.

Van Nostrand, R. G., 1964, Reverberation effects on signal amplitude: United Electrodynamics Inc. Seismic Data Laboratory Report No. 110 prepared for AFTAC, 6. p.

Pakiser, L. C., and Hill, D. P., 1963, Crustal structure in Nevada and southern Idaho from nuclear explosions: Jour. Geophys. Research, v. 68, p. 5757-5766.

APPENDIX A

Publications to date on this project

The following publications have resulted from this project to date:

1. "Amplitude, energy, and phase angles of plane SV waves and their application to earth crustal studies", J. K. Costain, K. L. Cook, and S. T. Algermissen: Seismol. Soc. Amer. Bull., v. 53, no. 5, p. 1039-1074, October 1963.

2. "Tables of amplitude and energy ratios of plane SV waves" J. K. Costain, K. L. Cook, and S. T. Algermissen: VESIAC Special Report 4410-68-X, Acoustics and Seismics Lab., Inst. of Science and Technology, Univ. of Michigan, Ann Arbor, Michigan, 176 p., December 1963.

3. "Tables of energy ratios, amplitude ratios, and phase angles for plane SV waves", J. K. Costain and K. L. Cook: VESIAC Special Report, No. 4410-96-X, Acoustics and Seismics Lab., Inst. of Science and Technology, Univ. of Michigan, Ann Arbor, Michigan, 106 p., in press.

4. "PS converted waves from earthquakes and large underground nuclear explosions at epicentral distances of 2,000 to 10,000 kilometers", K. L. Cook and J. K. Costain. Program of papers submitted at annual meeting of Seismological Society of America, St. Louis, Mo., April 12-14, 1965, p. 50-51. Paper in preparation for publication.

5. "The consistency of the character of body-wave phases from large underground explosions", K. L. Cook and J. K. Costain. Program of papers submitted at annual meeting of Seismological Society of America, St. Louis, Mo., April 12-14, 1965, p. 49-50. Paper in preparation for publication.

6. Corrigendum to "Amplitude, energy and phase angles of plane SV waves and their application to earth crustal studies", J. K. Costain, K. L. Cook, and S. T. Algermissen: Seismol. Soc. Amer. Bull., April 1965, in press.

APPENDIX B

Computer Programs
Theoretical Programs

PROGRAM DR-13 (FORTRAN- IBM 7040)
Generalized P and/or S refraction time-distance curves for up to seven layers; also layer thickness determination from P-wave refraction data using intercept times.

PROGRAM X-1 (FORTRAN)
Effect of free surface on incident plane SV wave. (Jeffreys treatment)

PROGRAM 1 (FORTRAN)
Computes Zvolinskii head-wave coefficients for a PPP head wave.

PROGRAM 5 (FORTRAN)
Computes reflection travel times of a wave converted from P to S on reflection from a single dipping interface for varying angles of incidence.

PROGRAM 6 (FORTRAN)
Computes reflection travel times for a P wave reflected from a single dipping interface.

PROGRAM 7 (FORTRAN)
Computes arrival time for a PS converted wave formed at the base of the n^{th} crustal layer.

PROGRAM 9 (FORTRAN)
Zoeppritz equations applied to a multilayered crust. Computes amplitude ratios of PS converted waves. Effects of wave length not included.

PROGRAM 9A (FORTRAN)
Zoeppritz equations applied to a multilayered crust with free surface effects included. Computes amplitude ratios of PS converted waves. Effects of wave length not included.

PROGRAM 11 (FORTRAN)
Computes travel times for refracted PPP, PPS, SPS, and SSS head waves from a single dipping interface.

PROGRAM 18 (FORTRAN - IBM 7040)
Energy ratios, amplitude ratios, and phase angles for an incident P wave. Uses Zoeppritz equations and Knott's energy equation applied to a single interface.

PROGRAM 19 (FORTRAN - IBM 7040)
Energy ratios, amplitude ratios, and phase angles for an incident SV wave. Uses Zoeppritz equations and Knott's energy equation applied to a single interface.

PROGRAM 21 (FORTRAN - IBM 7040)
Computes reflected time-distance curves for up to twenty layers with plane parallel interfaces.

Utility Programs

PROGRAM UP-1 (AUTOCODER - IBM 1401)
BCD (HER) tape to cards or print (IBM 1403 printer).

PROGRAM UP-2 (AUTOCODER - IBM 1401)
Digital to analog plot of HER data (IBM 1403 printer, 20 lines/inch).

PROGRAM UP-4 (AUTOCODER - IBM 1401)
Binary (STL) tape to cards or print (IBM 1403 printer).

PROGRAM UP-5 (AUTOCODER - IBM 1401)
Digital-to-analog trace plot using card input with two sets of data per card (IBM 1403 printer and plotting chain, 20 lines/inch).

PROGRAM UP-6 (AUTOCODER -IBM 1401)
Binary (UED) tape to cards or print (IBM 1403 printer).

PROGRAM UP-7 (AUTOCODER - IBM 1401)
Digital to analog trace plot using card input. One set of data per card. (IBM 1403 printer and plotting chain, 20 lines/inch).

PROGRAM DR-15D (FORTRAN - MAP - IBM 7040)
Punches cards from binary (STL) extract tapes written with FORTRAN.

PROGRAM DR-16B (FORTRAN - MAP - IBM 7040)
Lists binary (STL) tapes.

PROGRAM DR-16C (FORTRAN - MAP - IBM 7040)
Writes a binary extract tape using FORTRAN from binary (STL) tapes.

PROGRAM DR-18TC (FORTRAN - MAP - IBM 7040)
Punches cards from BCD (HER) tapes.

PROGRAM DR-22 (FORTRAN - MAP -IBM 7040)
Punches cards from binary (UED) tapes.

PROGRAM DR-2 (FORTRAN)
Forms an L-Z product trace to accentuate shear and compressional wave arrivals.

PROGRAM DR-7 (FORTRAN)
Scans BCD (HER) data for shear motion.

PROGRAM DR-10B (FORTRAN - IBM 7040)
Composition of vertical motion from east-west and north-south directions to a vertical plane containing the azimuth to the epicenter.

PROGRAM DR-12B (FORTRAN - IBM 7040)
Autocorrelation and power density spectrum.

PROGRAM DR-15B (FORTRAN - MAP - IBM 7040)
Digital-to-analog plot; program lists data using extract tapes written with FORTRAN from binary (STL) tapes; uses plotting chain (10 lines/inch) of IBM 1403 printer.

PROGRAM DR-18C (FORTRAN - MAP - IBM 7040)
Digital-to-analog plot - Program lists data from binary (STL) tapes; uses plotting chain (10 lines/inch) IBM 1403 printer.

PROGRAM DR-18H (FORTRAN - MAP - IBM 7040)
Digital-to-analog plot - Program lists data from BCD (HER) tapes uses plotting chain (20 lines/inch) of IBM 1403 printer)

PROGRAM DR-18F (FORTRAN - MAP - IBM 7040) digital to analog plot.
Program lists data from BCD (HER) tapes using a faster plot subroutine but having less resolution (uses plotting chain (10 lines/inch) of 1403 printer)

PROGRAM DR-18P (FORTRAN - IBM 7040)
Digital-to-analog plot using card input (uses IBM 1403 printer, 10 lines/inch).

PROGRAM DR-18FC (FORTRAN - IBM 7040)
Alphanumeric particle-motion plot and listing from card input (uses IBM 1403 printer, 20 lines/inch).

PROGRAM DR-18FP (FORTRAN - MAP - IBM 7040)
Alphanumeric particle-motion plot-listing for BCD (HER) tapes (used IBM 1403 printer, 20 lines/inch).

PROGRAM DR-18FP1 (FORTRAN - MAP -IBM 7040)
Alphanumeric particle-motion plot for BCD (HER) tapes using faster tape reading subroutine SKIPPD also gives data listing (uses IBM 1403 printer, 20 lines/inch).

PROGRAM DR-18FP2 (FORTRAN - IBM 7040)
Same as DR-18FP1, but with card input. Normalizes the digitized input data for the alphanumeric particle motion plot. Uses IBM 1403 printer, 20 lines/inch.

PROGRAM DR-18RHS (FORTRAN - IBM 7040)
L-Z product trace using IBM 7040 U. of U. Computer Center FORTRAN plot (uses IBM 1403 printer, 20 lines/inch).

PROGRAM DR-24B (FORTRAN - IBM 7040)
Computes epicenter-to-station distance using Richter's method.

PROGRAM DJG-12 (FORTRAN - IBM 7040)
Prints out digital to analog trace plot of east-west, north-south, vertical and radial components, the latter composed from east-west and north-south seismograms. Differentiates the seismogram traces, and plots the differentiated traces. Shows by another plot whether differentiated motion is compression or shear. The program then resolves the horizontal vector of motion into a component parallel to the azimuth and a component perpendicular to the azimuth, and plots the resolved components.

PROGRAM CC-1 (FORTRAN - IBM 7040)
CalComp particle-motion plot for use with Phillips Petroleum Co. plot facilities at Idaho Falls, Idaho.

PROGRAM CC-2 (FORTRAN - IBM 7040)
CalComp particle-motion plot for card input (HER) - uses IBM 1627 plotter at U. of U. Computer Center.

PROGRAM CC-3 (FORTRAN - IBM 7040)
CalComp particle-motion plot for card input (UED) - uses IBM 1627 plotter.

PROGRAM CC-5 (FORTRAN - IBM 7040)
CalComp digitial to analog trace plot of seismograms using card input (HER) and IBM 1627 plotter.

EXHIBIT A

AMPLITUDE, ENERGY, AND PHASE ANGLES OF PLANE SV WAVES AND THEIR APPLICATION TO EARTH CRUSTAL STUDIES

by

John K. Costain, Kenneth L. Cook, and S. T. Algermissen

(See attached reprint from the Bulletin of the Seismological Society of America, v. 53, no. 5, p. 1039-1074, October, 1963)

EXHIBIT B

TABLES OF ENERGY RATIOS, AMPLITUDE RATIOS, AND PHASE ANGLES FOR PLANE SV WAVES*

by

John K. Costain and Kenneth L. Cook

ABSTRACT

This report presents tabulations of energy ratios from Knott's energy equation, amplitude ratios from the Zoeppritz equations, and phase angles computed from the complex amplitude ratios for a plane SV wave incident on a plane elastic discontinuity. All computations were programmed in FORTRAN for an IBM 7040 digital computer. For a Poisson's ratio of 0.250, incident angles were varied from 0° to 88° in increments of 2°, except near phase changes of 180° in the real domain and near the critical angles where the ratios were calculated in increments of 0.25°. For a Poisson's ratio of 0.400, incident angles were varied from 0° to 85° in increments of 5°. Both real and imaginary coefficients were considered in the calculations. The varying parameters were the velocity ratio and density ratio across each interface, and the angle of incidence. Compressional velocity ratios (transmitted/incident) of 0.700, 0.800, and 0.900, and density ratios (transmitted/incident) of 0.700, 0.800, 0.900, and 1.000 were used. The data are presented in 24 tables.

* Contribution No. 57, Dept. of Geophysics, Univ. of Utah, Salt Lake City, Utah; to be published as VESIAC Special Report No. 4410-96-X; 106 p. incl. illus., tables, refs; in press.

Bulletin of the Seismological Society of America. Vol. 53, No. 5, pp. 1039–1074. October, 1963

AMPLITUDE, ENERGY, AND PHASE ANGLES OF PLANE *SV* WAVES AND THEIR APPLICATION TO EARTH CRUSTAL STUDIES

By John K. Costain, Kenneth L. Cook, and S. T. Algermissen

ABSTRACT

Energy ratios from Knott's energy equation and amplitude ratios and phase angles from the Zoeppritz equations were calculated for a plane *SV* wave incident on a plane elastic discontinuity. All computations were programmed in FORTRAN for an IBM 1620 digital computer. Incident angles were varied from 0° to 90° in increments of two degrees except near the critical angles, where the ratios were calculated in increments of 0.25 degree generally. Both real and imaginary coefficients were considered in the calculations. The varying parameters were the velocity ratio and density ratio across each interface and the angle of incidence. Poisson's ratio was kept constant at 0.25. Compressional velocity ratios (transmitted/incident) of 0.7, 0.8, and 0.9, and density ratios (transmitted/incident) of 0.7, 0.8, 0.9, and 1.0 were used. The data are presented in an integrated album which consists of a total of 144 curves (48 curves for each of the 3 characteristics studied). The theoretical amplitudes of *PS* converted waves, which are seismic body waves resulting from the conversion of an incident parent *P* wave at a boundary within the earth's crust to a refracted vertically polarized *SV* wave, were computed (using a FORTRAN program on an IBM 1620 digital computer) for several multi-layered hypothetical and actual crustal models. Preliminary results indicate that the amplitudes of successive *PS* converted waves arriving from successively deeper layers will continually increase provided that the velocity *ratios* (upper medium/lower medium) continually *decrease* with depth. The effects of the wave period have not yet been considered. Particle-motion diagrams obtained from seismograms of two underground nuclear explosions show some shear motion in the first ten seconds which is provisionally interpreted to be from *PS* converted waves.

Introduction

The general properties of plane *SV* (vertically polarized shear) seismic body waves as they impinge upon a plane elastic discontinuity and are subsequently reflected and transmitted, have long been known. Recent studies indicate the desirability, however, of having available a more complete album of curves and tables, than published heretofore, of specific characteristics of *SV* waves to assist in the solution of many current problems in seismology. The purpose of this paper is to present an integrated album of curves for the energies, amplitudes, and phase angles of waves derived from plane *SV* waves which are incident upon a plane elastic discontinuity, and to show how such information can be applied to studies of earth crustal structure, as an example. It is believed that the album of curves will have widespread use in other types of seismic problems in which a quantitative evaluation of the characteristics is desirable.

Previous Work

Theoretical studies of the partition of energy incident at an elastic interface and the amplitudes of the resulting refracted and reflected waves relative to the incident wave have been made by many investigators. These include Knott (1899), Zoeppritz (1919), Jeffreys (1926), Muskat (1933), Slichter (1933), Slichter and Gabriel (1933),

Muskat and Meres (1940), Gutenberg (1944a), Heelan (1953a, b), Nafe (1957), Schwind (1960), Richards (1960, 1961), Steinhart and others (1961), Haskell (1962), and McCamy and others (1962).

The published data pertaining to incident *SV* waves only are summarized in table 1. Although the table does not given an exhaustive list of data and curves that have been published, it is believed to summarize most of the recent data and curves available for incident *SV* waves.

General Method of Computation and Accuracy of Data

The determination of the relative energies and amplitudes of waves derived from a plane *SV* wave incident on a plane interface involves the solution of four simultaneous linear equations (Knott, 1899; Zoeppritz, 1919) with real or imaginary coefficients. The equations were solved in the real and complex domains by the Crout method (Crout, 1941) which was programmed in FORTRAN I and FORTRAN II for use on an IBM 1620 digital computer. The variable field length capability of the 1620 FORTRAN II system provided a means of checking the accuracy of the solutions, most of which were obtained using a floating-point precision of eight decimal places. Those solutions which were obtained in FORTRAN II using a floating point precision of sixteen decimal places differed from those obtained using a precision of eight decimal places only in the seventh decimal place. A conservation of energy check on all solutions was satisfied in every set of computations to at least the sixth decimal place in FORTRAN I, and to the fourteenth decimal place when the higher precision was used in FORTRAN II.

Parameters Investigated

Velocity and Density Ratios

The angle of incidence of plane *SV* waves on a plane interface separating two semi-infinite media of different velocity and density was varied in increments of two degrees from zero to ninety degrees. In the neighborhood of the critical angles, the increment ranged from 0.01 to 0.25 degree, but generally was held at 0.25 degree. The values of the density ratios (density, ρ_1, of medium with transmitted waves/ density, ρ_2, of medium with incident wave) were taken as 0.700, 0.800, 0.900 and 1.000. For each of these density contrasts, the values of the velocity ratios (longitudinal velocity, V, of medium with transmitted waves longitudinal velocity, U, of medium with incident wave) were taken as 0.700, 0.800 and 0.900. In all the calculations, Poisson's ratio, σ, was assigned the value 0.250 for media on each side of the interface. The subscripts 2 and 1 refer to properties of the medium with *incident* waves and medium with *transmitted* waves, respectively (see, for example, figure 2).

In addition to the systematic variations of velocity and density, various hypothetical and actual crustal sections were examined. The density and velocity ratios involved in these sections are shown on figures 19 and 20.

Critical Angles

Figure 1 shows the reflected and transmitted waves derived from a plane *SV* wave incident on a plane interface.

According to Snell's law

$$\frac{\sin\theta}{V} = \frac{\sin b}{V} = \frac{\sin c}{U} = \frac{\sin d}{V} = \frac{\sin e}{Y} = \frac{\sin f}{Z}$$

For Poisson's ratio equal to 0.250, $U/V = Y/Z = \sqrt{3}$, and

$$e = \sin^{-1}(\sqrt{3}\sin\theta)$$

For the sine of the angle e (angle of reflected P wave) to be less than or equal to one, θ should not exceed $\sin^{-1}(1/\sqrt{3}) = 35.264$ degrees. This is the first critical angle. For a velocity ratio of Y/U

$$e = \sin^{-1}[(Y/V)\sin\theta] = \sin^{-1}[(Y/U)\cdot(U/V)\sin\theta] = \sin^{-1}[(\sqrt{3})\cdot(Y/U)\sin\theta]$$

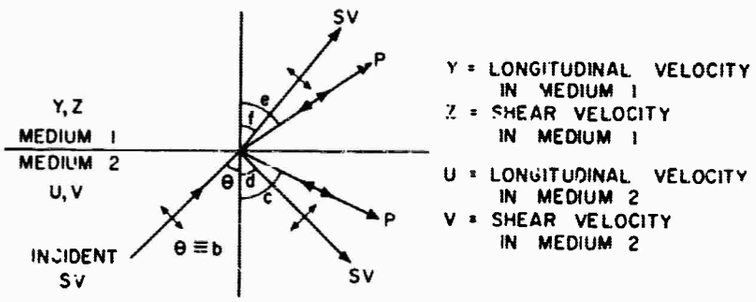

FIG. 1. Reflected and transmitted waves derived from a plane SV wave incident on a plane interface at an angle θ.

For the sine of the angle e (angle of transmitted P wave) to be less than or equal to one, the angle θ should not exceed $\sin^{-1}\{1/[(\sqrt{3})\cdot(Y/U)]\}$. For velocity ratios Y/U equal to 0.700, 0.800 and 0.900, this corresponds to values of the incident angle, θ, of 55.567, 46.194 and 39.904 degrees, respectively. These are the second critical angles. Physically, this means the energy of the reflected P wave becomes zero when the angle of incidence of the SV wave reaches 35.264 degrees, and the energy of the transmitted P wave becomes zero when the angle of incidence of the SV wave reaches 55.567, 46.194 and 39.904 degrees for velocity ratios Y/U of 0.700, 0.800 and 0.900, respectively.

Amplitude Ratios

The Zoeppritz equations for a plane SV wave of amplitude B incident on a plane interface are (Richter, 1958, pp. 670–673):

$$(B + D)\sin b + C\cos a - E\cos e - F\sin f = 0$$

$$(B - D)\cos b + C\sin a + E\sin e - F\cos f = 0$$

TABLE 1

Summary of Energy and Amplitude Ratios Calculated for an Incident *SV* Wave

V_2 and V_1 are compressional velocities in incident and transmitted media, respectively. ρ_2 and ρ_1 are densities in incident and transmitted media, respectively. Poisson's ratio $\sigma = 0.25$ for each medium unless otherwise noted, in which case σ_2 and σ_1 are Poisson's ratios for the incident and transmitted media, respectively.

B_E = Energy of incident *SV* wave
C_E = Energy of reflected *P* wave
D_E = Energy of reflected *SV* wave
E_E = Energy of refracted *P* wave
F_E = Energy of refracted *SV* wave

B_A = Amplitude of incident *SV* wave
C_A = Amplitude of reflected *P* wave
D_A = Amplitude of reflected *SV* wave
E_A = Amplitude of refracted *P* wave
F_A = Amplitude of refracted *SV* wave

No. of curves (C) or tables (T)	Ratios determined	Density ratios ρ_1/ρ_2	Velocity ratios V_1/V_2	Remarks	Reference
4 T	$\frac{C_E}{B_E}, \frac{D_E}{B_E}, \frac{E_E}{B_E}, \frac{F_E}{B_E}$	2/3	1.225	Only real domain was considered.	Knott (1899, p. 84).
4 T	$\frac{C_E}{B_E}, \frac{D_E}{B_E}, \frac{E_E}{B_E}, \frac{F_E}{B_E}$	3/2	0.816		
4 T, C	$\frac{C_E}{B_E}, \frac{D_E}{B_E}, \frac{E_E}{B_E}, \frac{F_E}{B_E}$	1.00	0.85	Only real domain was considered. Slate ($\sigma_2 = 0.16$) to granite ($\sigma_1 = 0.28$)	Knott (1899, p. 84; Fig. 1, p. 86)
4 T, C	$\frac{C_E}{B_E}, \frac{D_E}{B_E}, \frac{E_E}{B_E}, \frac{F_E}{B_E}$	1.00	1.18	Only real domain was considered. Granite ($\sigma_2 = 0.28$) to slate ($\sigma_1 = 0.16$)	Knott (1899, p. 85; Fig. 2, p. 86)
4 T	$\frac{C_E}{B_E}, \frac{D_E}{B_E}, \frac{E_E}{B_E}, \frac{F_E}{B_E}$	0.400	1.000	Only real domain was considered.	Jeffreys (1926, p. 332)
4 C, T	$\frac{C_E}{B_E}, \frac{D_E}{B_E}, \frac{E_E}{B_E}, \frac{F_E}{B_E}$	0.965	0.935	Both real and complex domains were considered.	Slichter and Gabriel (1933, Case I-4)
4 C, T	$\frac{C_E}{B_E}, \frac{D_E}{B_E}, \frac{E_E}{B_E}, \frac{F_E}{B_E}$	1.103	1.286	Both real and complex domains were considered.	Slichter and Gabriel (1933, Case II-3)
4 C, T	$\frac{C_E}{B_E}, \frac{D_E}{B_E}, \frac{E_E}{B_E}, \frac{F_E}{B_E}$	0.906	0.76	Both real and complex domains were considered. $\sigma = 0.275$	Slichter and Gabriel (1933, Case II-4)

1 C, T	$\frac{C_E}{B_E}, \frac{D_E}{B_E}, \frac{E_E}{B_E}, \frac{F_E}{B_E}$	0.8	0.75	Both real and complex domains were considered.	Slichter and Gabriel (1933, Case III 1)
196 T	$\frac{C_E}{B_E}, \frac{D_E}{B_E}, \frac{E_E}{B_E}, \frac{F_E}{B_E}$	0.7 to 1.3 (in steps of 0.1)	0.5 to 2.0 (in steps of 0.25)	Only real domain was considered. Results are limited to four angles of incidence only not exceeding 16°46'45" in each case. Four separate tabulations (i.e. four separate angles of incidence) for each of the values of density contrasts and each of the values of velocity contrasts.	Muskat and Meres (1940)
32 C	$\frac{C_E}{B_E}, \frac{D_E}{B_E}, \frac{E_E}{B_E}, \frac{F_E}{B_E}$	1.036 1.09 1.00 1.103	1.07 1.10 1.14 (1.30) 1.286	Only real domain was considered. Poisson's ratio differed slightly from 0.25 for some computations.	Gutenberg (1944)
24 C	$\frac{C_E}{B_E}, \frac{D_E}{B_E}, \frac{E_E}{B_E}, \frac{F_E}{B_E}$	0.82 1.2	0.20 0.33 0.40 2.5 3.0 3.5	Only real domain was considered.	Nafe (1957)
2	See remarks	0.830	0.5	Normalized (1) vertical and (2) horizontal components of ground displacements for varying ratios of epicentral distances to depth of incident *SV* waves impinging from the bottom layer of a two-layer crustal model. $\sigma_1 = \sigma_2 = \frac{1}{4}$.	Richards (1961, p. 2[illegible])

TABLE I—*Continued*

No. of curves (C) or tables (T)	Ratios determined	Density ratios ρ_1/ρ_2	Velocity ratios V_1/V_2	Remarks	Reference
5 Contour	See remarks	0.852	0.790	Normalized (1) vertical and (2) horizontal components of ground displacement and (3) phase difference between vertical and horizontal components of surface displacement for various periods and angles of incidence of incident *SV* waves impinging from the mantle to the base of the crust in a two-layer earth crustal model.	Haskell (1962)
48 C	$\frac{C_E}{B_E}, \frac{D_E}{B_E}, \frac{E_E}{B_E}, \frac{F_E}{B_E}$	0.700 0.800 0.900 1.000	0.700 0.800 0.900	Both real and complex domains are considered.	This paper
196 T	$\frac{C_A}{B_A}, \frac{D_A}{B_A}, \frac{E_A}{B_A}, \frac{F_A}{B_A}$	0.7 to 1.3 (in steps of 0.1)	0.5 to 2.0 (in steps of 0.25)	Only real domain was considered. Results are limited to angles of incidence not exceeding 16°46′45″. Four separate tabulations (i.e. four separate angles of incidence) for each of the values of density contrasts and each of the values of velocity contrasts.	Muskat and Meres (1940)
24 C	$\frac{C_A}{B_A}, \frac{D_A}{B_A}, \frac{E_A}{B_A}, \frac{F_A}{B_A}$	0.907	0.700 0.754 0.828 0.905 0.912 0.940	Only real domain was considered. Poisson's ratio = 0.24	Schwind (1960)

162 C	$\frac{C_A}{B_A}, \frac{D_A}{B_A}, \frac{E_A}{B_A}, \frac{F_A}{B_A}$	1.65 (o 0.61 (in 44 steps)	0.25 (o 4.00 (in 44 steps)	Both real and complex domains were considered. The effec(of changes in Poisson's ratio on amplitude coefficients was shown.	McCamy and others (1962)
48 C	$\frac{C_A}{B_A}, \frac{D_A}{B_A}, \frac{E_A}{B_A}, \frac{F_A}{B_A}$	0.700 0.800 0.900 1.000	0.700 0.800 0.900	Both real and complex domains are considered.	This paper

$$(B + D)\cos 2b - C\left(\frac{V}{U}\right)\sin 2a + EK\left(\frac{Z^2}{VY}\right)\sin 2e - FK\left(\frac{Z}{V}\right)\cos 2f = 0$$

$$-(B - D)\sin 2b + C\left(\frac{U}{V}\right)\cos 2b + EK\left(\frac{Y}{V}\right)\cos 2f + FK\left(\frac{Z}{V}\right)\sin 2f = 0$$

where the angles are as defined in figure 1. The angle a is the angle of incidence of a compressional wave of velocity U which would generate four waves with the same reference angles as shown in figure 1. K is the density contrast, equal to ρ_1/ρ_2, where ρ_1 and ρ_2 are the densities of the upper and lower media, respectively.

The equations were solved for C, D, E and F, the amplitudes of the reflected P reflected S, transmitted P and transmitted S waves, respectively. A similar set of equations with C, D, E and F as the unknown amplitudes exists for a plane P wave of amplitude A, incident on a plane interface. The equations are not given here but are given by Richter (1958, pp. 670–673). For the analysis of PS converted waves, it was necessary to consider the conversion of a P wave incident on a plane interface. A FORTRAN program with the basic structure of that used for the incident SV wave was employed. When only a single interface was involved, the amplitude of the incident waves, A or B, was set equal to unity.

The quantities C, D, E and F are complex when the angle of incidence of an SV wave is greater than 35.264 degrees for the parameters used in this study. Both the real and imaginary parts of the complex amplitudes were printed out to facilitate the determination of the phase shifts associated with the complex domain. The quantity having physical significance is the modulus of the complex amplitude, which is the square root of the sum of the squares of the real and imaginary parts of the complex amplitude.

Figures 2b through 17b show the amplitude ratios as computed from the Zoeppritz equations for an SV wave incident on a single interface. The dashed portions of the curves refer to angles of incidence for which some of the coefficients of that particular reflected or refracted wave amplitude are imaginary, that is, the angle of reflection or refraction is imaginary. The wave whose angle of reflection or refraction is imaginary does not exist, and no physical significance should be attached to the modulii of the amplitudes (or energies) within these regions.

Inspection of the amplitude ratio curves on figures 2b through 17b shows the amplitudes to be relatively insensitive to changes in the density ratio. Changes in the velocity ratio, however, cause marked changes in the amplitudes. For the most part, the greater the velocity contrast (lower velocity ratio of V/U), the greater will be the amplitude of the reflected or refracted derived wave. At and near the critical angles the amplitudes change rapidly, sometimes passing through zero and resulting in phase changes of 180 degrees. Curve 3 on figure 10b, for example, shows a phase change of 180 degrees near the first critical angle. The critical angles are easily identified with the sharp peaks and troughs on the curves.

Small changes in Poisson's ratio have little effect on the amplitude ratios. For Poisson's ratio equal to 0.400 for both media, the greatest changes were noticed for transmitted P waves, whose amplitudes were decreased. More variation occurs if the upper (transmitted wave) medium has Poisson's ratio equal to 0.400, and the

lower medium is assigned a value of 0.250. However, because of the relative insensitivity of the amplitude ratios to changes in Poisson's ratio for conversions of interest in this study (incident P to transmitted P and transmitted S; and incident S to transmitted P and transmitted S), Poisson's ratio was assigned the value 0.250 for all calculations presented herein.

Energy Ratios

The distribution of energy among the four waves derived from an incident SV wave can be obtained from Knott's energy equation for an incident SV wave, which is (Macelwane, 1932, p. 173, Equation 7.80):

$$1 = \frac{(\cot c)C'^2}{(\cot d)B'^2} + \frac{D'^2}{B'^2} + \frac{\rho_1 (\cot e)E'^2}{\rho_2 (\cot d)B'^2} + \frac{\rho_1 (\cot f)F'^2}{\rho_2 (\cot d)B'^2} \tag{1}$$

where the angles c, d, etc. are defined as in figure 1, and ρ_1 and ρ_2 are the densities of the upper and lower media, respectively. The quantities B', C', D', E' and F' are the amplitudes of the displacement potentials of the incident SV wave and the reflected P, reflected S, transmitted P and transmitted S waves, respectively. These quantities are replaced by BV, CU, DV, EY and FZ, respectively, where B, C, D, E and F are the amplitudes of the particle displacements as defined in the Zoeppritz equations. Equation 1 then becomes

$$1 = \frac{(\cot c)C^2U^2}{(\cot d)B^2V^2} + \frac{D^2V^2}{B^2V^2} + \frac{\rho_1 (\cot e)E^2Y^2}{\rho_2 (\cot d)B^2V^2} + \frac{\rho_1 (\cot f)F^2Z^2}{\rho_2 (\cot d)B^2V^2}$$

or

$$1 = \frac{(\cot c)C^2U^2}{(\cot d)V^2} + D^2 + \frac{\rho_1 (\cot e)E^2Y^2}{\rho_2 (\cot d)V^2} + \frac{\rho_1 (\cot f)F^2Z^2}{\rho_2 (\cot d)V^2} \tag{2}$$

The terms on the right side of equation 2 represent the energies of the reflected P, reflected S, transmitted P and transmitted S waves, respectively, with respect to the energy of an incident SV wave of amplitude B (B set equal to unity). The energy ratios are obtained by determining the amplitudes C, D, E and F from the Zoeppritz equations, inserting these values in equation 2, and then evaluating each term in the equation. These individual terms were then printed out as the ratios of the energy of the reflected P, reflected S, transmitted P and transmitted S waves, respectively, to the energy of an incident SV wave.

Equation 2 serves as a useful conservation of energy check on the accuracy of the amplitudes determined from the Zoeppritz equations, and energy ratios as computed from this equation. In all cases, the sum of the terms on the right hand side of equation 2 differed from unity only in the seventh decimal place at worst, when a floating point precision of eight decimal places was used in the computations.

A similar conservation of energy equation exists for an incident plane P wave on a plane interface (Macelwane, 1932, p. 167, Equation 7.62). Where conversion of incident P to transmitted P or S was desired, as in the multilayer case, the conservation of energy equation for a P wave was similarly applied to check the

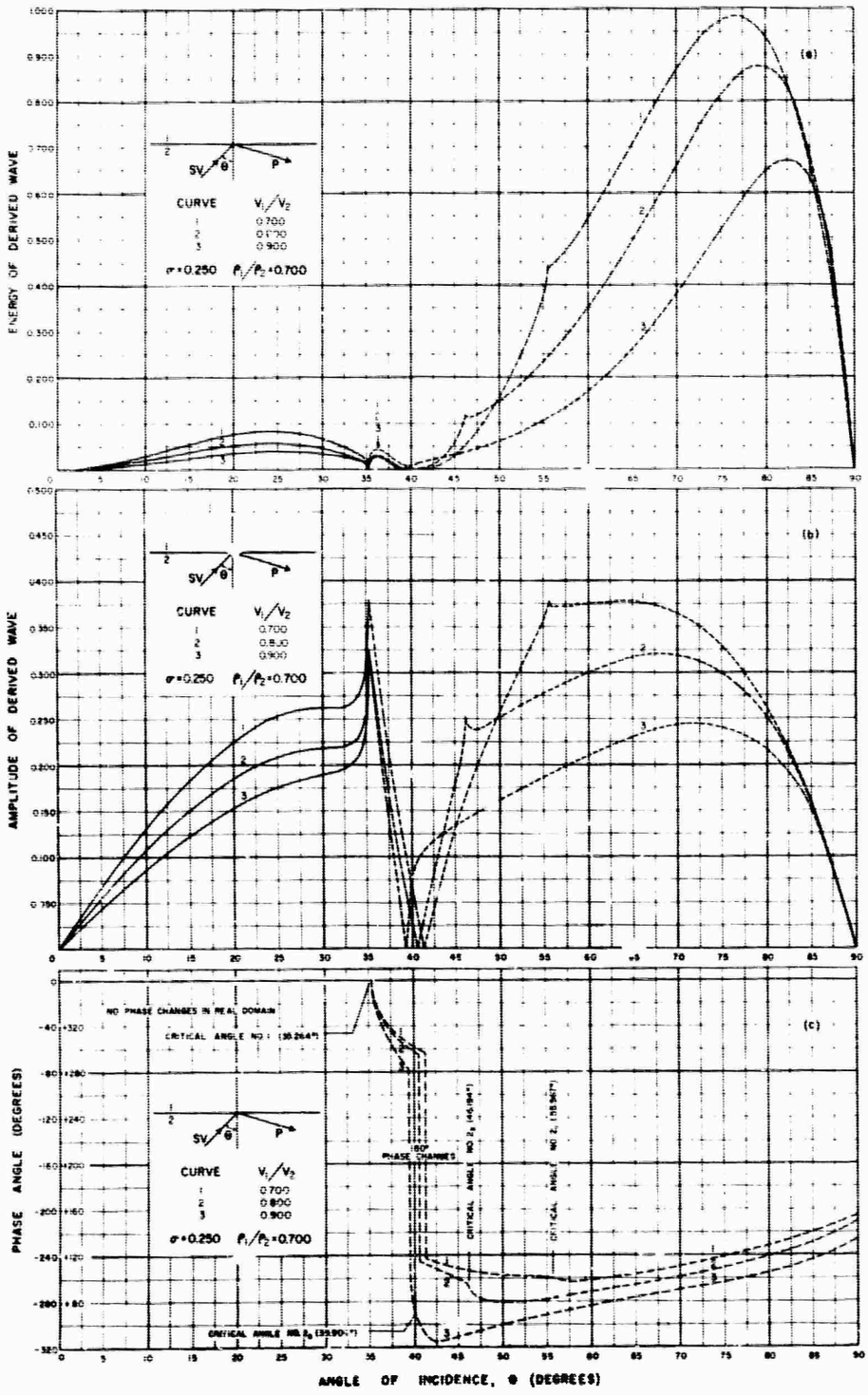

FIG. 2. Plane SV wave incident on a plane interface for a density ratio (transmitted/incident) of 0.700 and velocity ratios (transmitted/incident) of 0.700, 0.800 and 0.900. (a) Ratio of energy of reflected P wave to energy of incident SV wave. (b) Ratio of amplitude of reflected P wave to amplitude of incident SV wave. (c) Phase angle of reflected P wave.

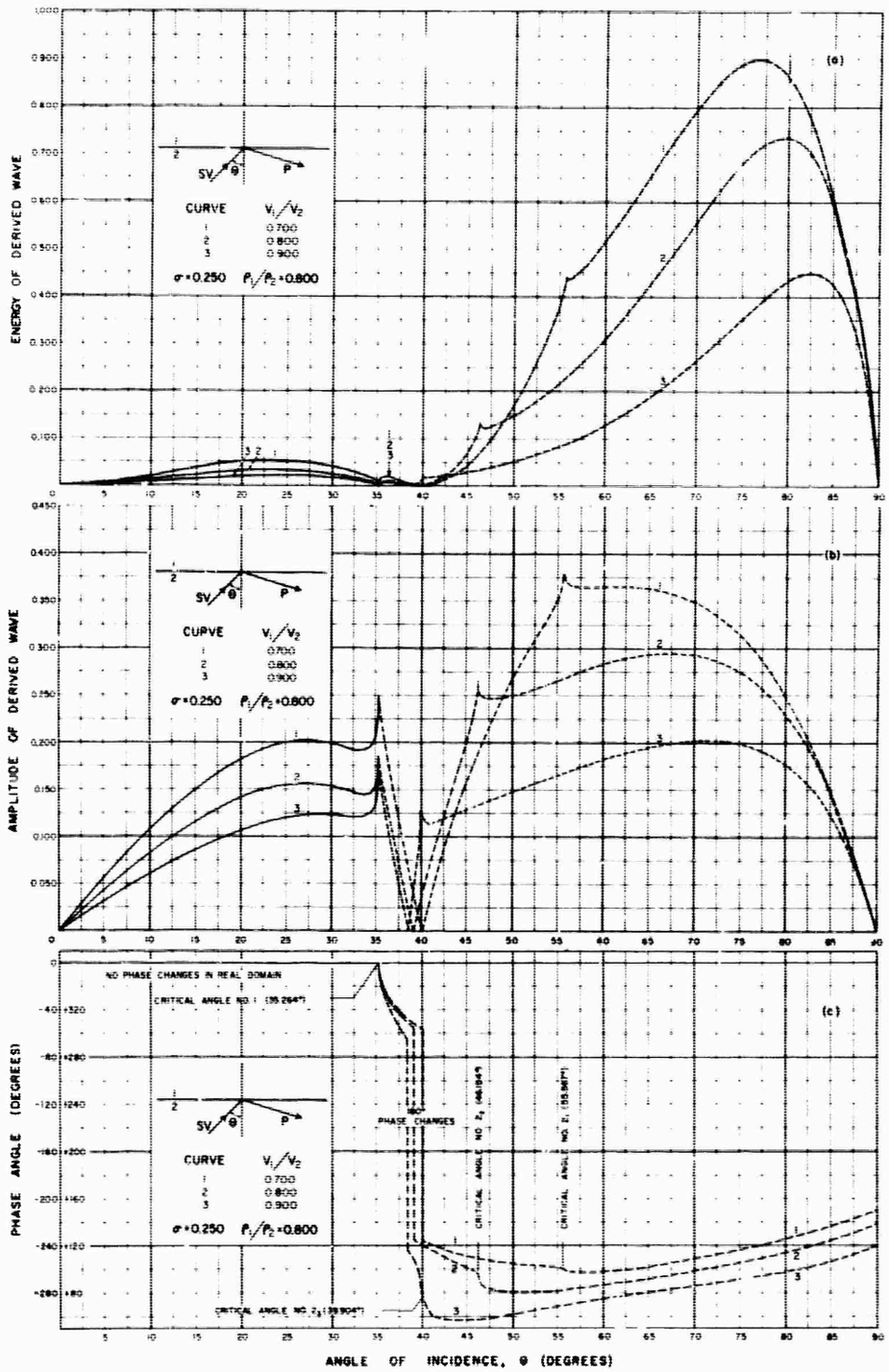

FIG. 3. Plane SV wave incident on a plane interface for a density ratio (transmitted/incident) of 0.800 and velocity ratios (transmitted/incident) of 0.700, 0.800 and 0.900. (a) Ratio of energy of reflected P wave to energy of incident SV wave. (b) Ratio of amplitude of reflected P wave to amplitude of incident SV wave. (c) Phase angle of reflected P wave.

accuracy of the amplitudes as determined from the Zoeppritz equations for an incident P wave.

The same generalizations hold for the energy ratio curves shown on figures 2a through 17a as for the amplitude ratios. Generally, increasing the velocity contrast

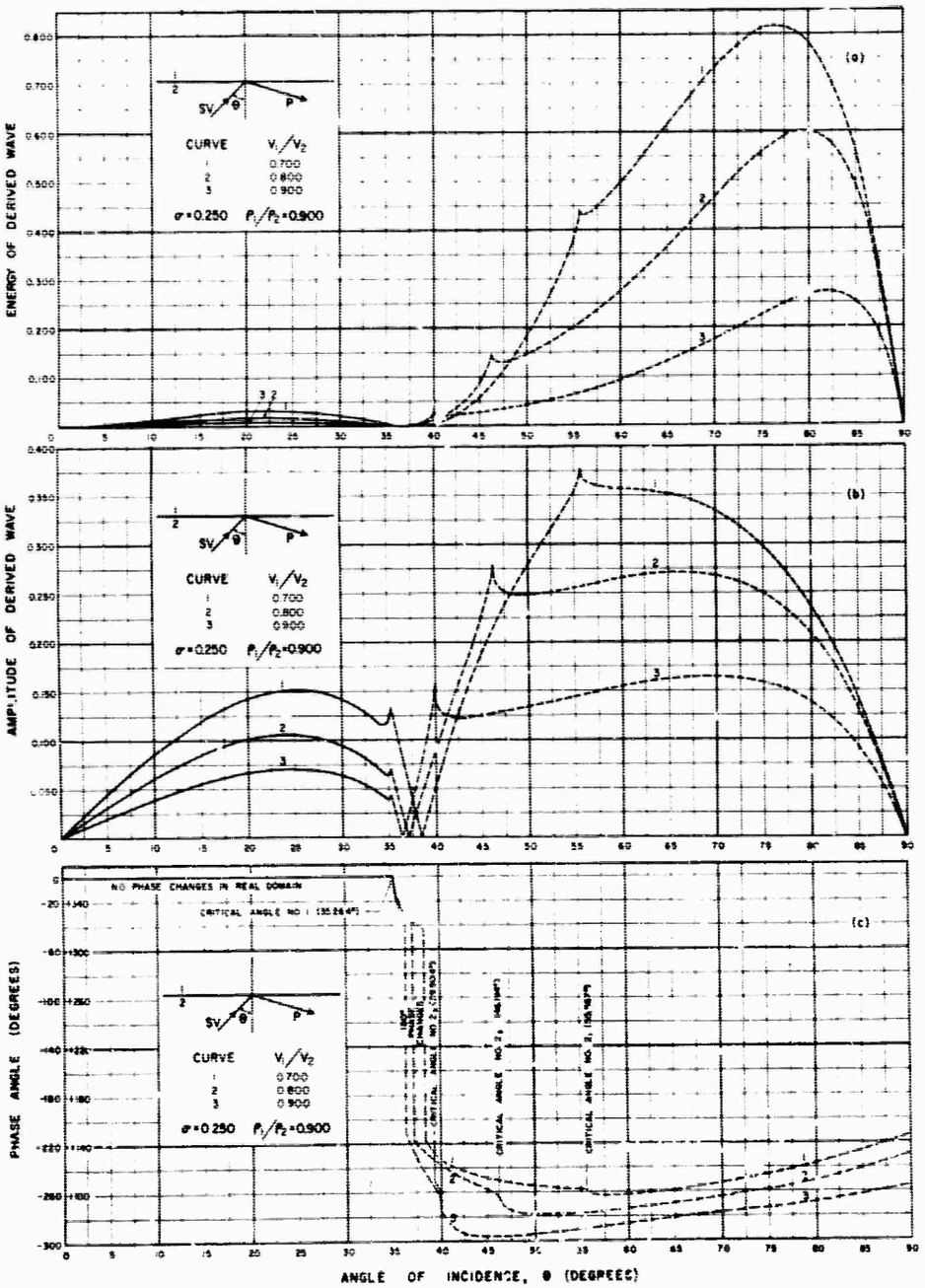

FIG. 4. Plane SV wave incident on a plane interface for a density ratio (transmitted/incident) of 0.900 and velocity ratios (transmitted/incident) of 0.700, 0.800 and 0.900. (a) Ratio of energy of reflected P wave to energy of incident SV wave. (b) Ratio of amplitude of reflected P wave to amplitude of ineident SV wave. (c) Phase angle of reflected P wave.

will increase the energy of the derived wave with respect to the incident wave. The dashed portions of the curves correspond to those incident angles for which certain of the angles of reflection or refraction of a particular derived wave are imaginary. No physical significance is to be attached to these regions. No energy is carried away from the interface by these waves at these angles of incidence.

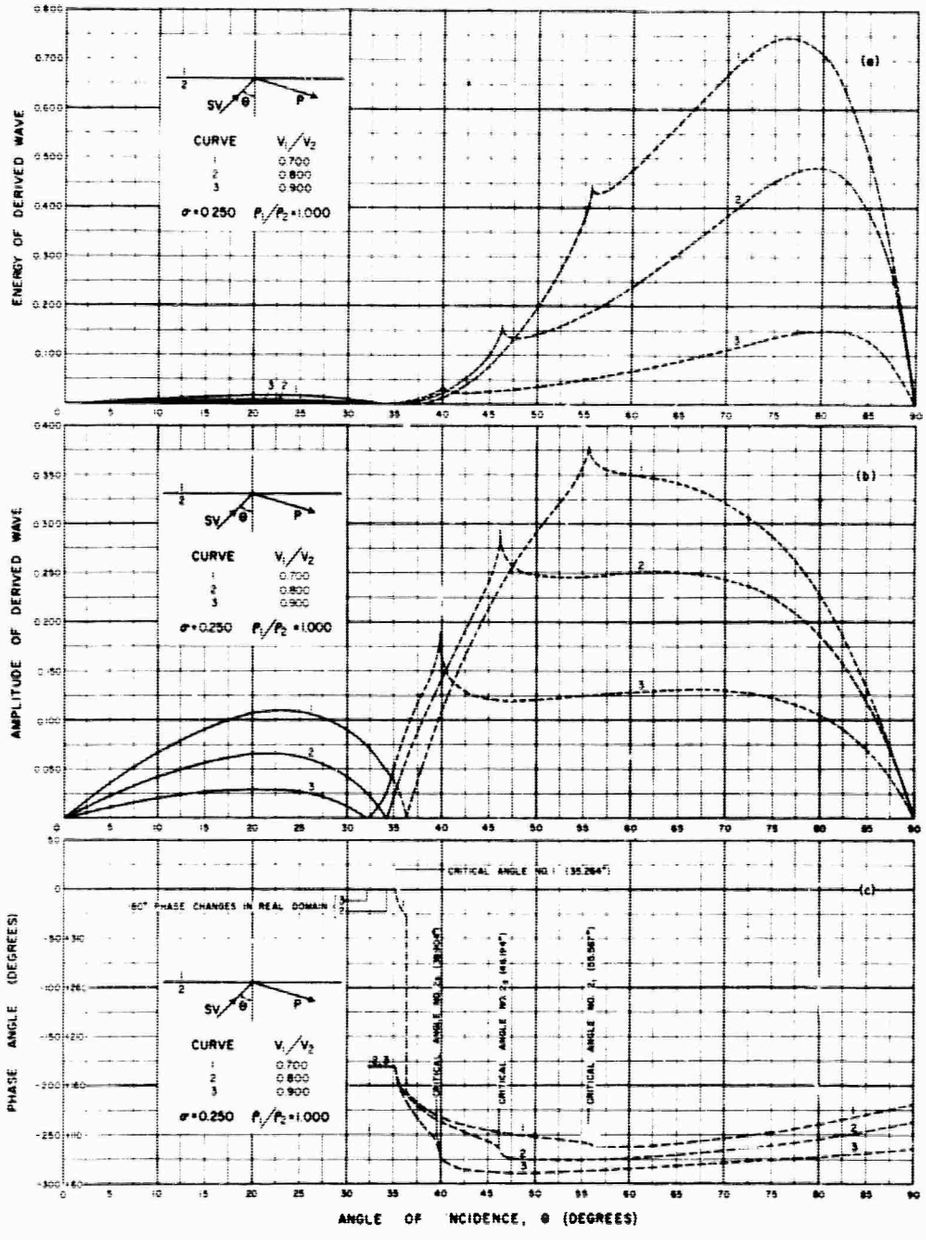

FIG. 5. Plane SV wave incident on a plane interface for a density ratio (transmitted/incident) of 1.000 and velocity ratios (transmitted/incident) of 0.700, 0.800 and 0.900. (a) Ratio of energy of reflected P wave to energy of incident SV wave. (b) Ratio of amplitude of reflected P wave to amplitude of incident SV wave. (c) Phase angle of reflected P wave.

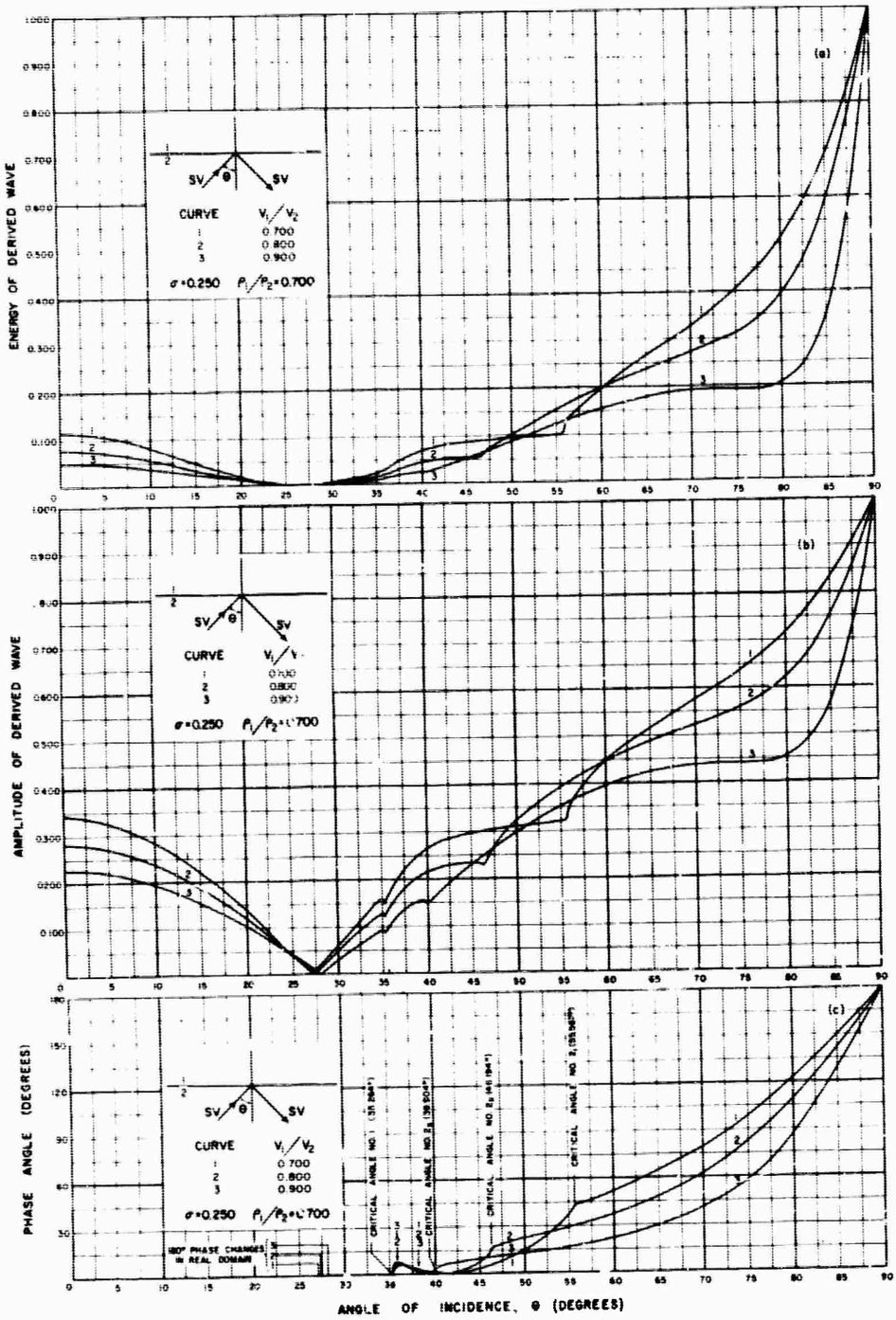

FIG. 6. Plane SV wave incident on a plane interface for a density ratio (transmitted/incident) of 0.700 and velocity ratios (transmitted/incident) of 0.700, 0.800 and 0.900. (a) Ratio of energy of reflected SV wave to energy of incident SV wave. (b) Ratio of amplitude of reflected SV wave to amplitude of incident SV wave. (c) Phase angle of reflected SV wave.

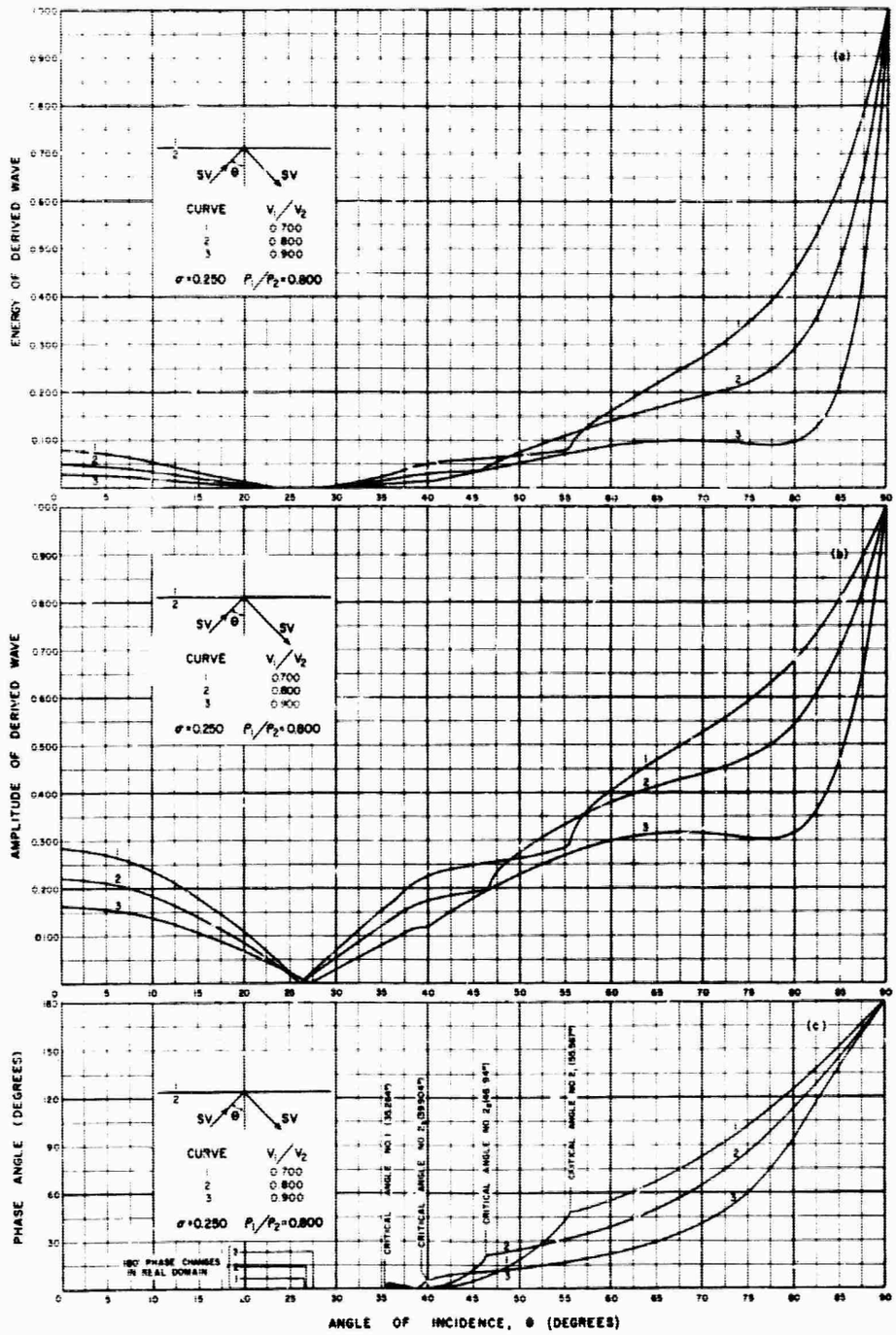

FIG. 7. Plane SV wave incident on a plane interface for a density ratio (transmitted/incident) of 0.800 and velocity ratios (transmitted/incident) of 0.700, 0.800 and 0.900. (a) Ratio of energy of reflected SV wave to energy of incident SV wave. (b) Ratio of amplitude of reflected SV wave to amplitude of incident SV wave. (c) Phase angle of reflected SV wave.

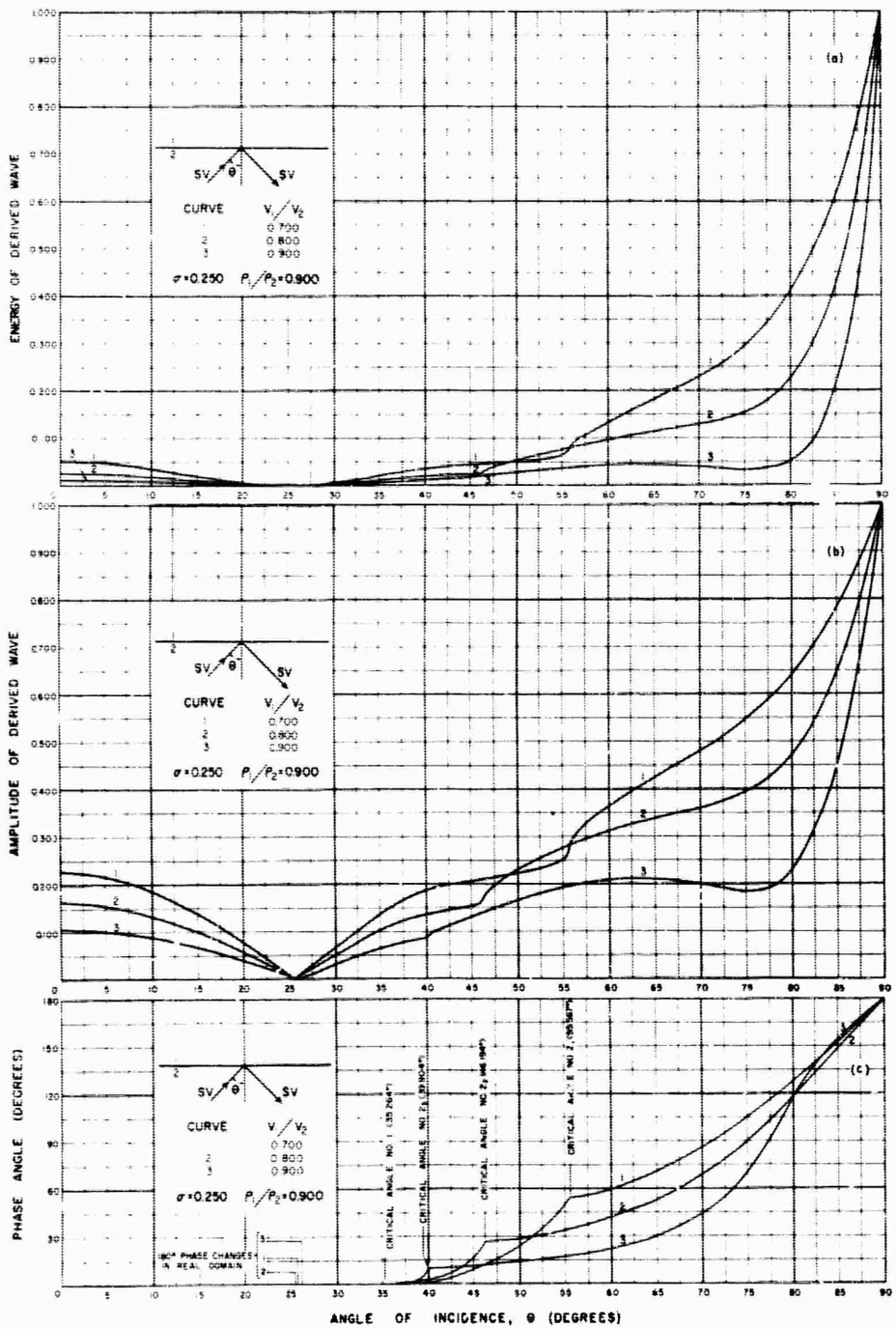

FIG. 8. Plane *SV* wave incident on a plane interface for a density ratio (transmitted/incident) of 0.900 and velocity ratios (transmitted/incident) of 0.700, 0.800 and 0.900. (a) Ratio of energy of reflected *SV* wave to energy of incident *SV* wave. (b) Ratio of amplitude of reflected *SV* wave to amplitude of incident *SV* wave. (c) Phase angle of reflected *SV* wave.

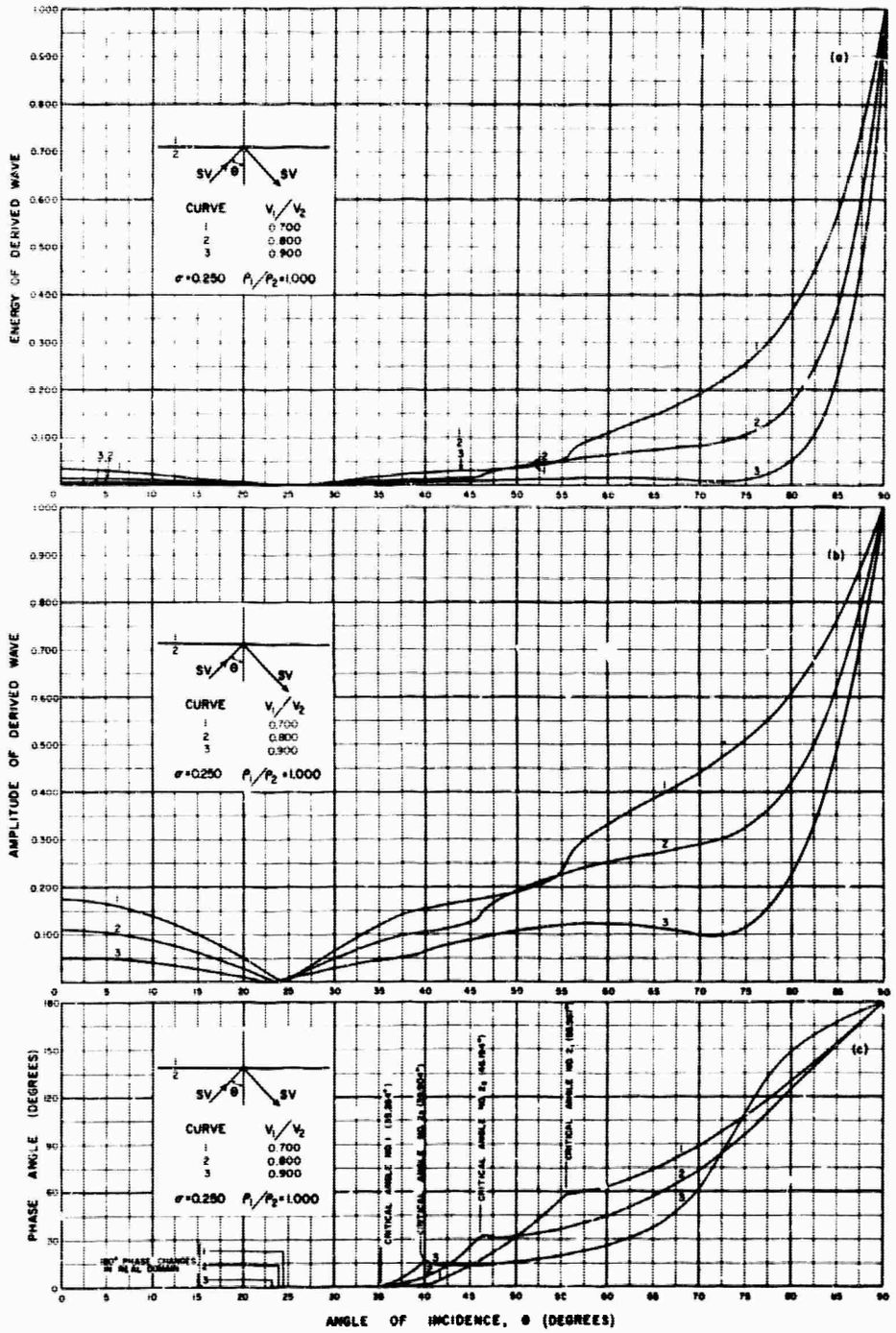

FIG. 9. Plane *SV* wave incident on a plane interface for a density ratio (transmitted/incident) of 1.000 and velocity ratios (transmitted/incident of 0.700, 0.800 and 0.900. (a) Ratio of energy of reflected *SV* wave to energy of incident *SV* wave. (b) Ratio of amplitude of reflected *SV* wave to amplitude of incident *SV* wave. (c) Phase angle of reflected *SV* wave.

At the critical angle beyond which the angle of reflection or refraction of a particular derived wave becomes imaginary, the energy of this wave becomes zero. In applying the conservation of energy equation after 35.264 degrees, for the parameters used in this study, the terms in energy equation 2 are complex. The imaginary parts of all of these terms must add up to zero and the real parts to unity, in all cases. The

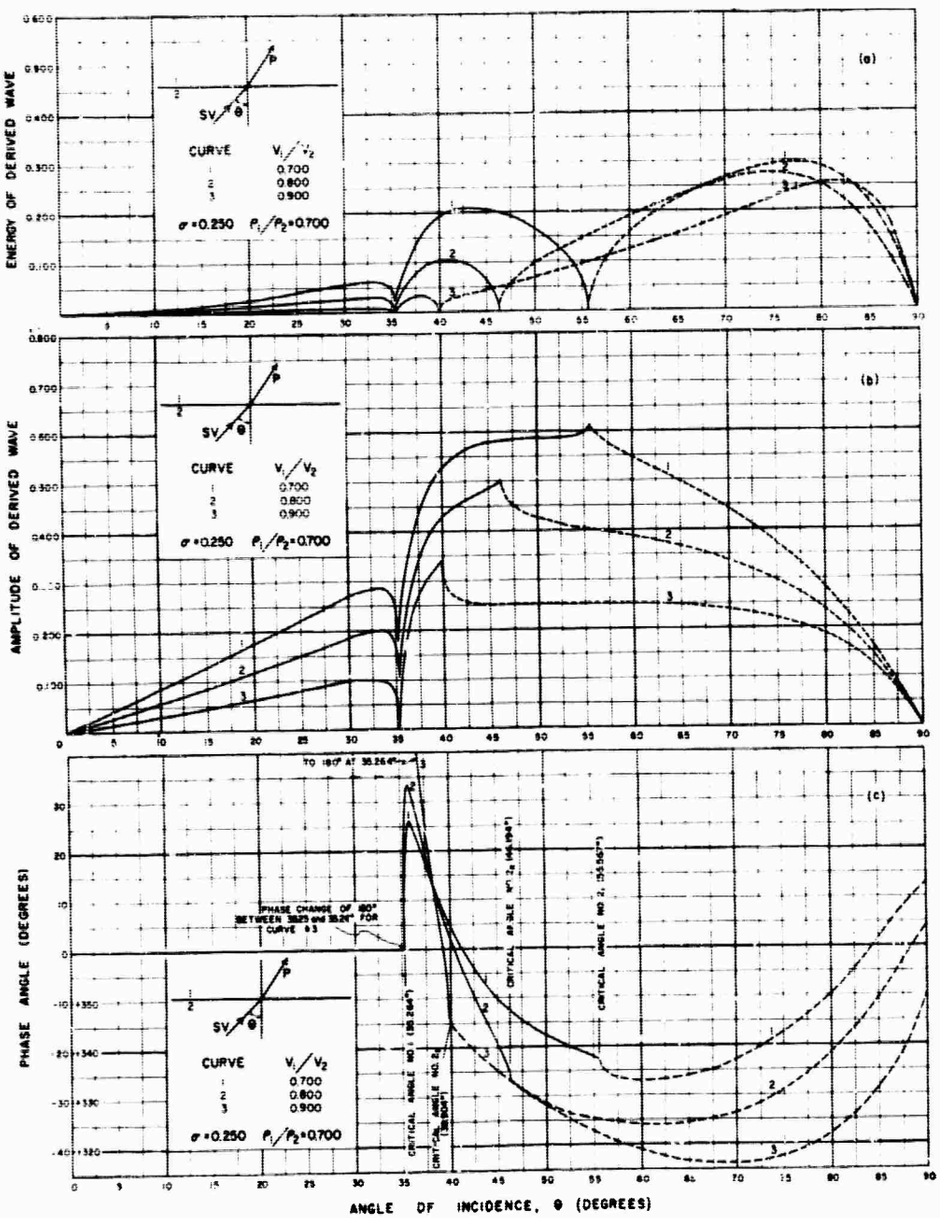

FIG. 10. Plane SV wave incident on a plane interface for a density ratio (transmitted/incident) of 0.700 and velocity ratios (transmitted/incident) of 0.700, 0.800 and 0.900. (a) Ratio of energy of transmitted P wave to energy of incident SV wave. (b) Ratio of amplitude of transmitted P wave to amplitude of incident SV wave. (c) Phase angle of transmitted P wave.

sum of the modulii of the complex energies of those derived waves whose angles of reflection or refraction are not imaginary will be unity. The modulii of those waves whose angles of reflection or refraction are imaginary are not included in the summation.

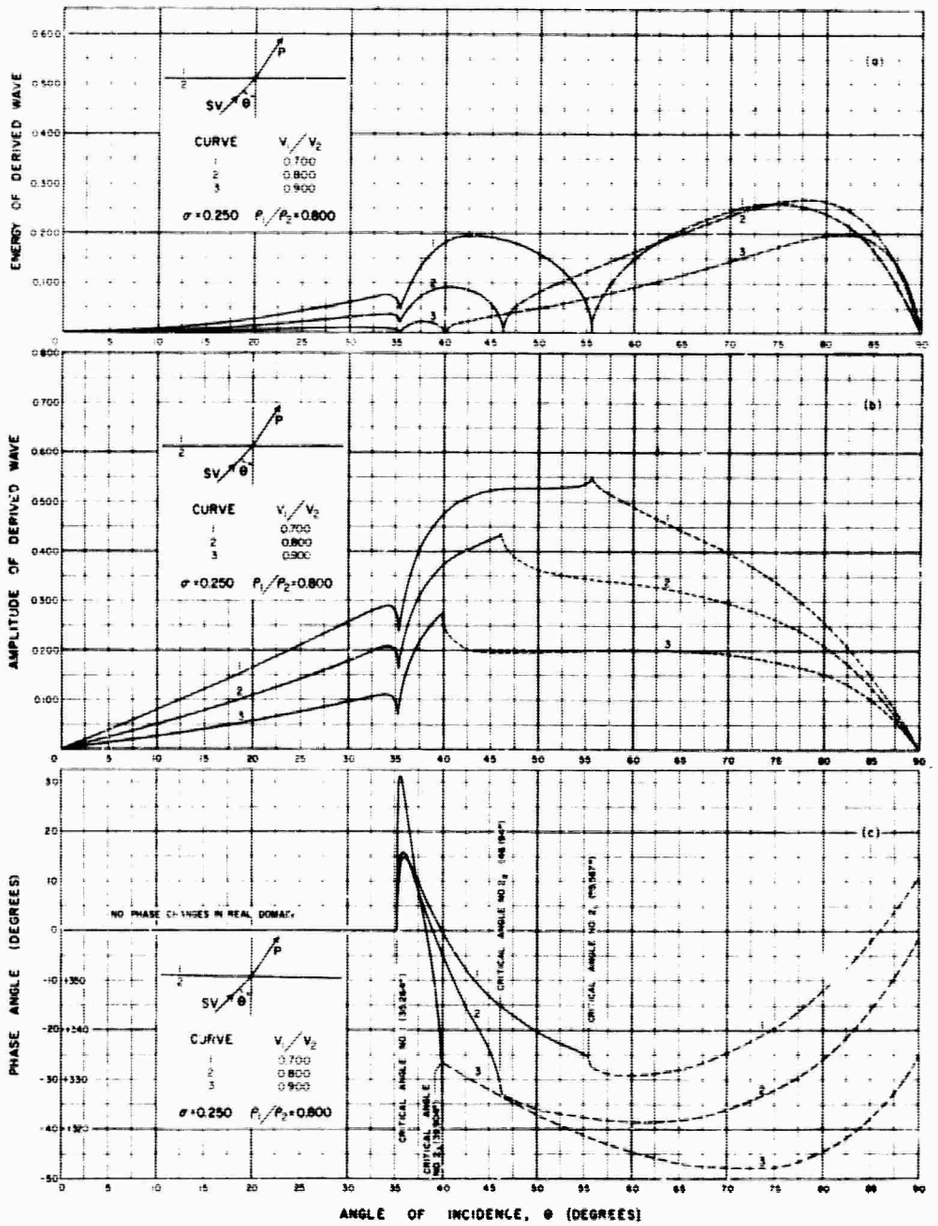

FIG. 11. Plane *SV* wave incident on a plane interface for a density ratio (transmitted/incident) of 0.800 and velocity ratios (transmitted/incident) of 0.700, 0.800 and 0.900. (a) Ratio of energy of transmitted *P* wave to energy of incident *SV* wave. (b) Ratio of amplitude of transmitted *P* wave to amplitude of incident *SV* wave. (c) Phase angle of transmitted *P* wave.

Phase Angles

Beyond the first critical angle, the amplitudes of the derived waves are complex, and all wave amplitudes will generally undergo phase changes. The complex amplitudes computed from the Zoeppritz equations were printed out in the form $a + ib$. The phase angle, ϕ, of the derived wave is given by

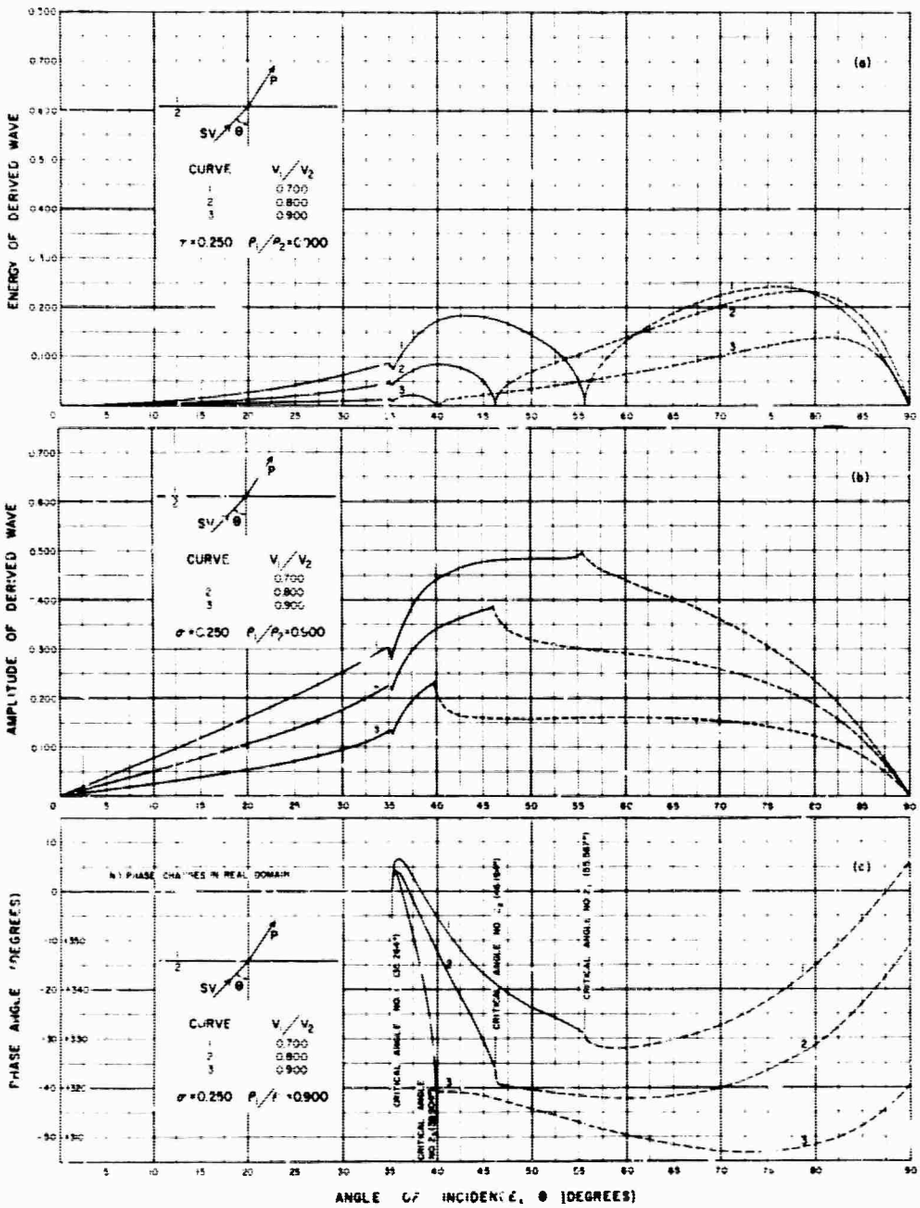

Fig. 12. Plane SV wave incident on a plane interface for a density ratio (transmitted/incident) of 0.900 and velocity ratios (transmitted/incident) of 0.700, 0.800 and 0.900. (a) Ratio of energy of transmitted P wave to energy of incident SV wave. (b) Ratio of amplitude of transmitted P wave to amplitude of incident SV wave. (c) Phase angle of transmitted P wave.

$$\phi = \tan^{-1}\frac{b}{a}$$

The quantities a and b identify the quadrant and thus the phase angle of the derived wave.

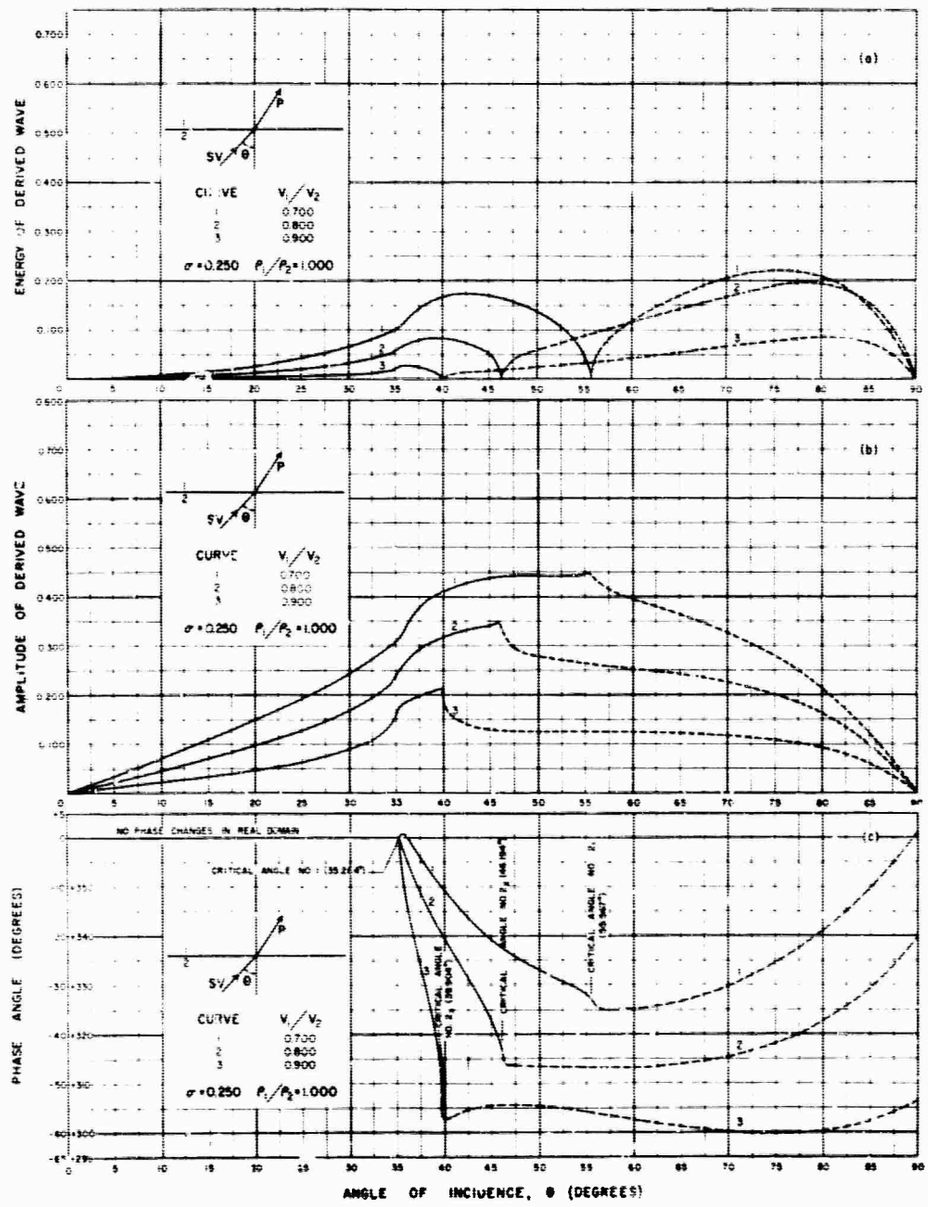

FIG. 13. Plane SV wave incident on a plane interface for a density ratio (transmitted/incident) of 1.000 and velocity ratios (transmitted/incident) of 0.700, 0.800 and 0.900. (a) Ratio of energy of transmitted P wave to energy of incident SV wave. (b) Ratio of amplitude of transmitted P wave to amplitude of incident SV wave. (c) Phase angle of transmitted P wave.

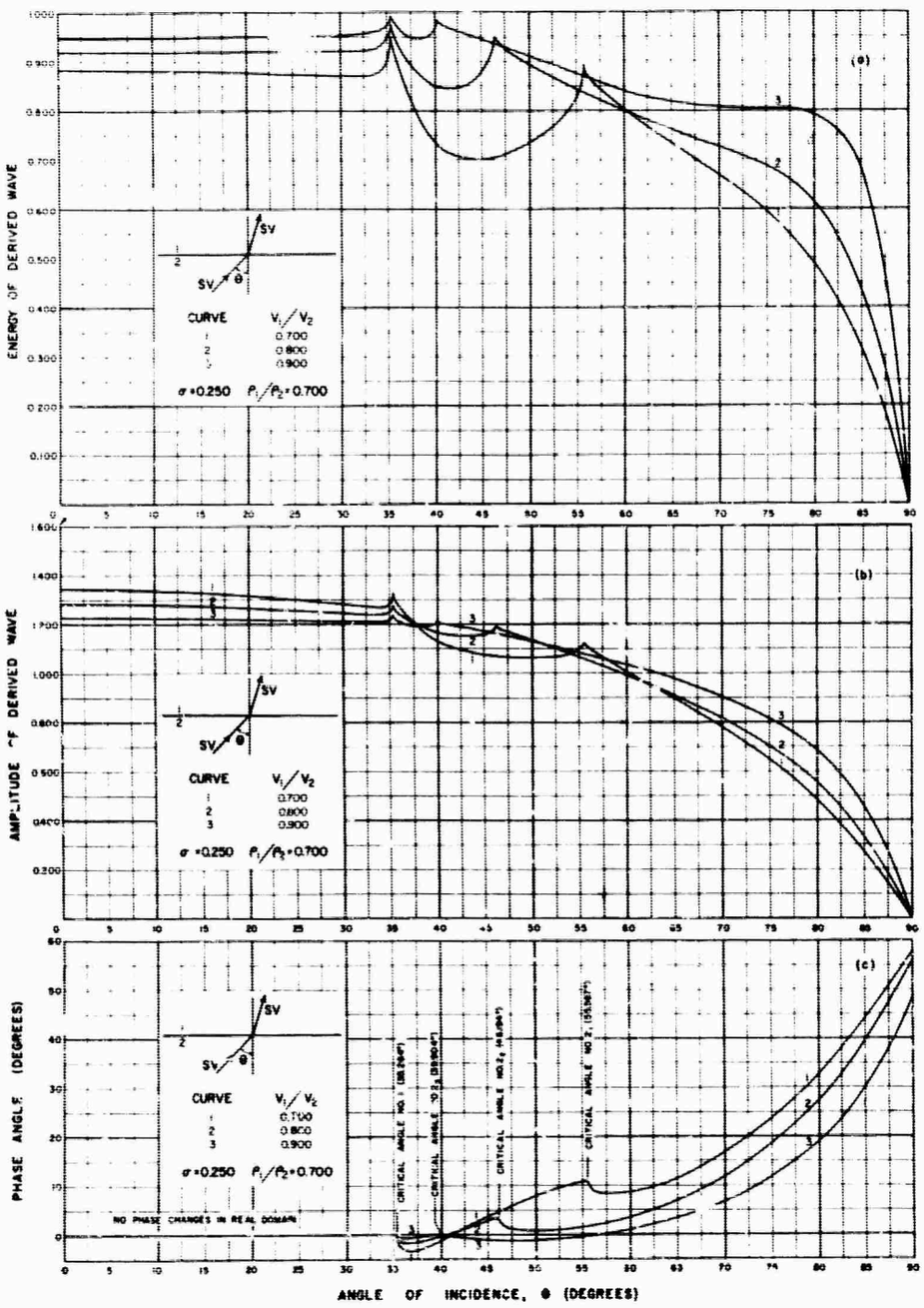

FIG. 14. Plane *SV* wave incident on a plane interface for a density ratio (transmitted/incident) of 0.700 and velocity ratios (transmitted/incident) of 0.700, 0.800 and 0.900. (a) Ratio of energy of transmitted *SV* wave to energy of incident *SV* wave. (b) Ratio of amplitude of transmitted *SV* wave to amplitude of incident *SV* wave. (c) Phase angle of transmitted *SV* wave.

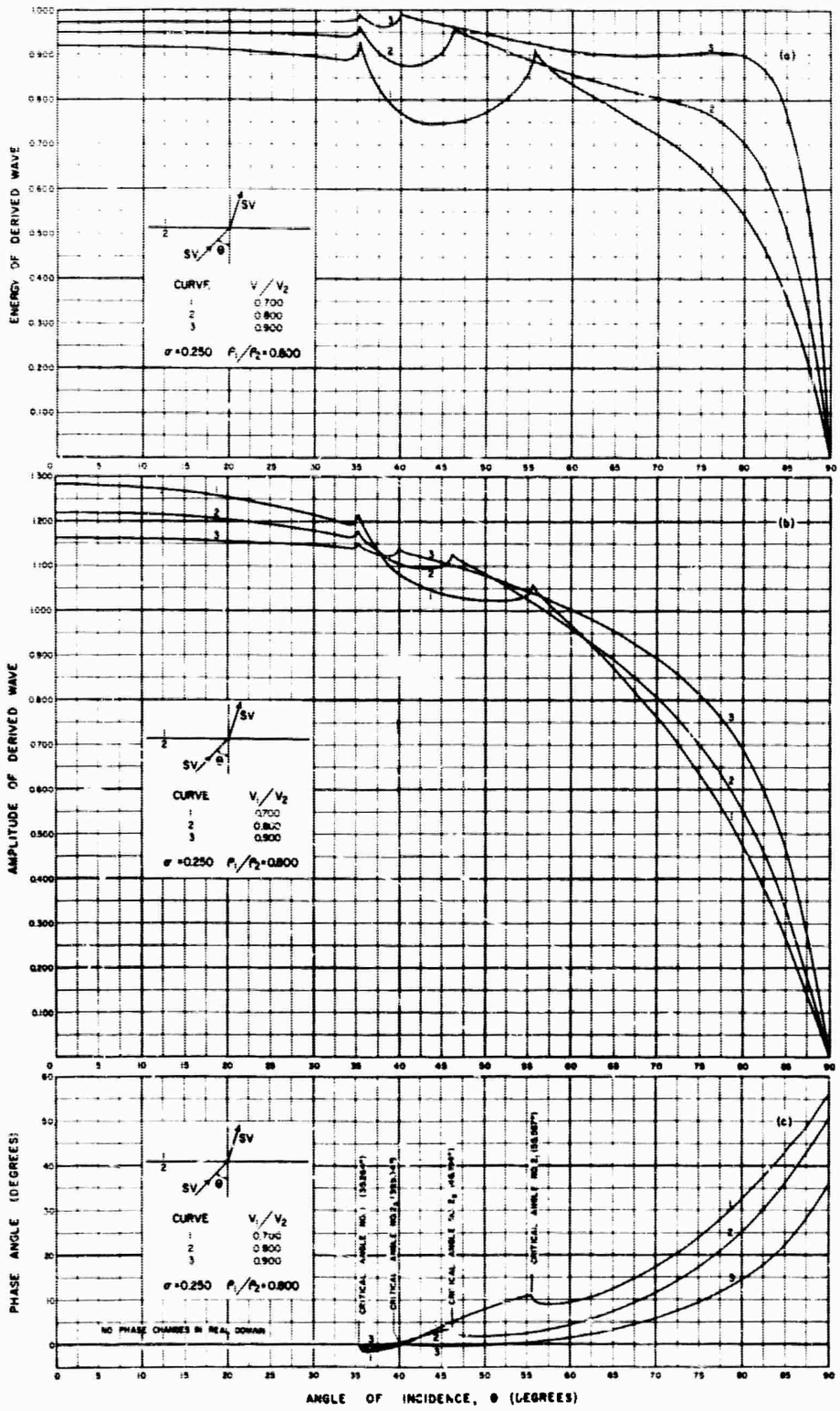

FIG. 15. Plane SV wave incident on a plane interface for a density ratio (transmitted/incident) of 0.800 and velocity ratios (transmitted/incident) of 0.700, 0.800 and 0.900. (a) Ratio of energy of transmitted SV wave to energy of incident SV wave. (b) Ratio of amplitude of transmitted SV wave to amplitude of incident SV wave. (c) Phase angle of transmitted SV wave.

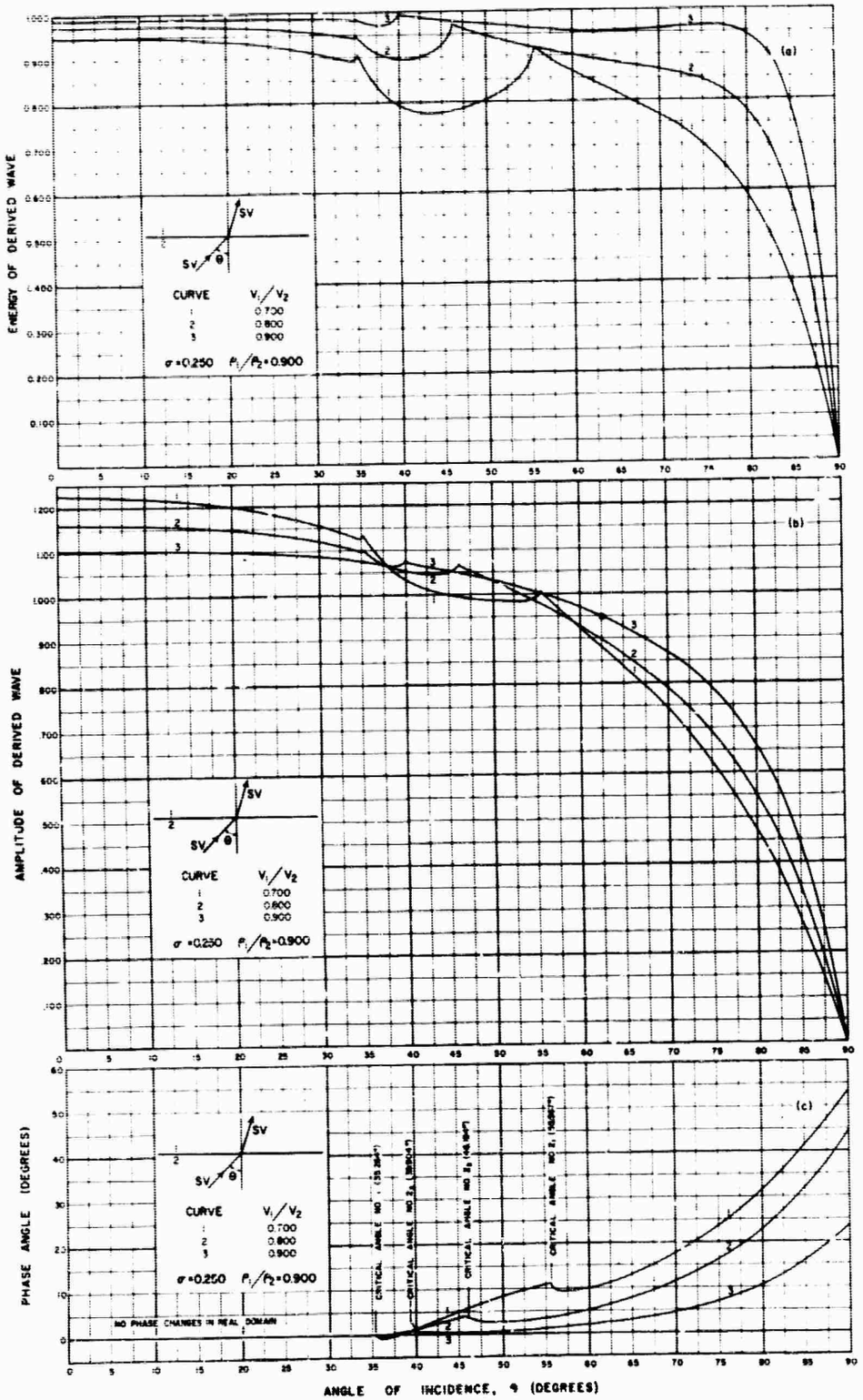

FIG. 16. Plane SV wave incident on a plane interface for a density ratio (transmitted/incident) of 0.900 and velocity ratios (transmitted/incident) of 0.700, 0.800 and 0.900. (a) Ratio of energy of transmitted SV wave to energy of incident SV wave. (b) Ratio of amplitude of transmitted SV wave to amplitude of incident SV wave. (c) Phase angle of transmitted SV wave.

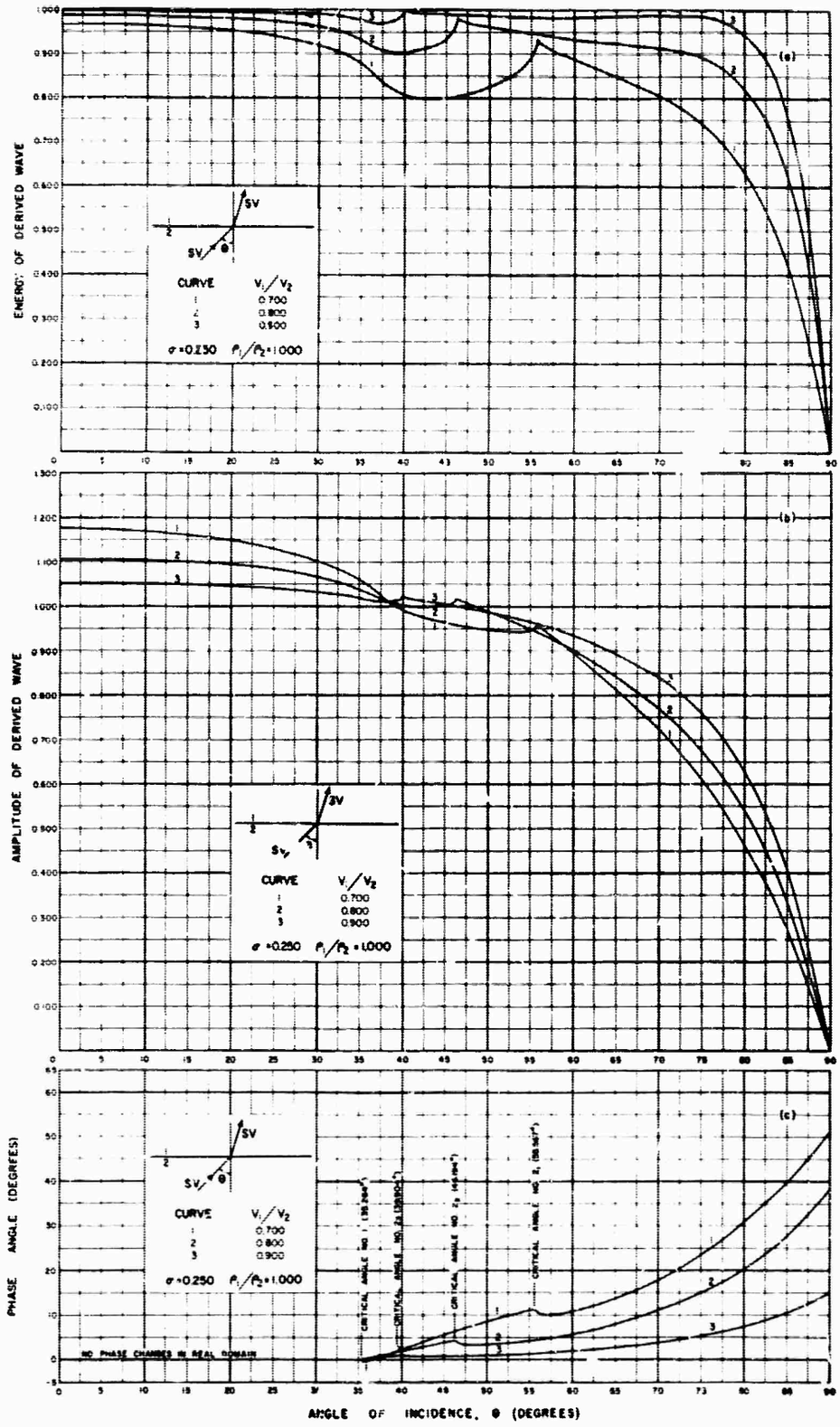

FIG. 17. Plane SV wave incident on a plane interface for a density ratio (transmitted/incident) of 1.000 and velocity ratios (transmitted/incident) of 0.700, 0.800 and 0.900. (a) Ratio of energy of transmitted SV wave to energy of incident SV wave. (b) Ratio of amplitude of transmitted SV wave to amplitude of incident SV wave. (c) Phase angle of transmitted SV wave.

The significance of a phase change in a derived wave is to change the arrival time of a peak or trough of the wave by an amount $\Delta t = (\phi T)/(2\pi)$, where T is the period of the wave. If the phase angle, ϕ, is negative, the peak or trough is delayed an amount Δt; if the phase angle is positive, it is advanced in time this amount. For example, a transmitted SV wave of period one second with a phase angle of 100 degrees will arrive approximately 0.27 second early because of the phase shift. Practical application of phase angles would include the correction of observed travel

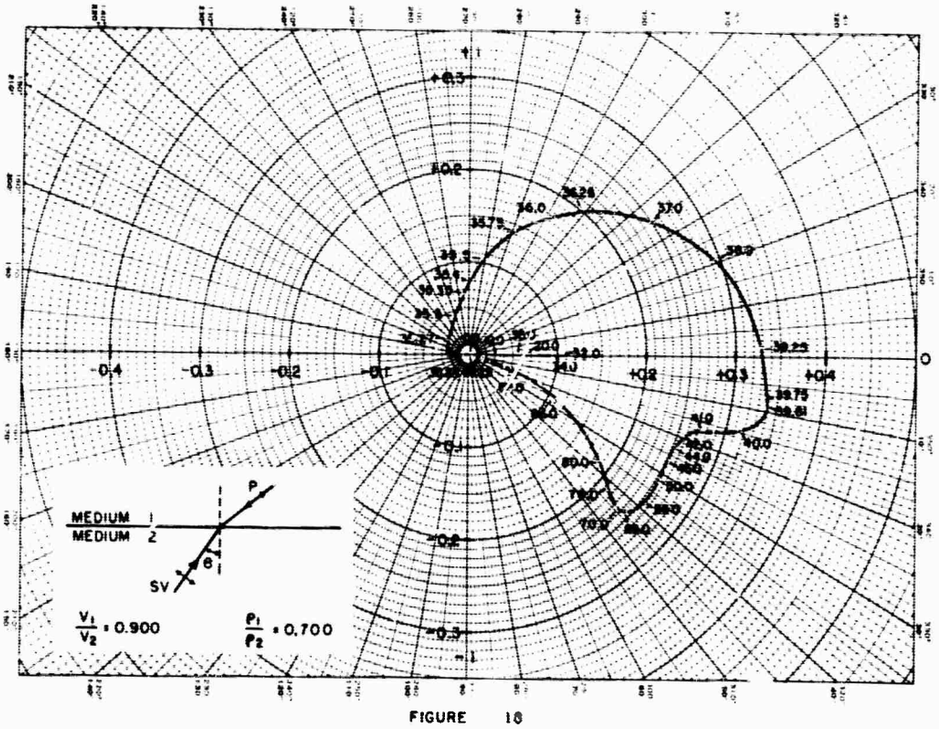

FIGURE 18

FIG. 18. Polar coordinate diagram of amplitudes and phase angles of a transmitted P wave derived from an incident SV wave for a velocity ratio (transmitted/incident) of 0.900 and a density ratio (transmitted/incident) of 0.700. Numbers along the curve refer to the angle of incidence, θ, of the incident SV wave at a plane interface. The curve is dashed after 39.9 degrees, at which point the transmitted P wave vanishes.

times by the appropriate time lead or lag determined from the phase angle, in order to locate more precisely the depths to the interfaces which generate the derived waves (see e.g., Richards, 1961).

Figures 2c through 17c give the phase angles associated with the complex amplitudes computed from the Zoeppritz equations. Phase changes of 180 degrees in the real domain are also noted on the curves where they occur. It will be noted that the phase changes near the critical angles are often large and rapid (figure 10c). The dashed portions of the curves have no physical significance; they are associated with incident angles of derived waves whose angles of reflection or refraction are imaginary. At grazing incidence ($\theta = 90$ degrees), for all velocity ratios, the phase angle of a reflected SV wave reaches 180 degrees, as shown on figures 6c through 9c.

Figure 18 is an alternate method of displaying the data shown, for example, on figure 10b and 15c, curve 3. In particular, the polar coordinate diagram shows how the amplitude of a wave must pass through zero when a phase change of 180 degrees takes place. This is, of course, true in either the complex domain or the real domain. In figure 18, the real part of the complex amplitude is plotted along the abscissa, and the imaginary part along the ordinate. The phase angle is then read directly from the graph. Numbers plotted along the curve refer to the angle of incidence, θ. In the real domain, the amplitudes pass through zero with a phase change of 180 degrees, as also shown, for example, on figure 6b and 6c, curves 1, 2 and 3.

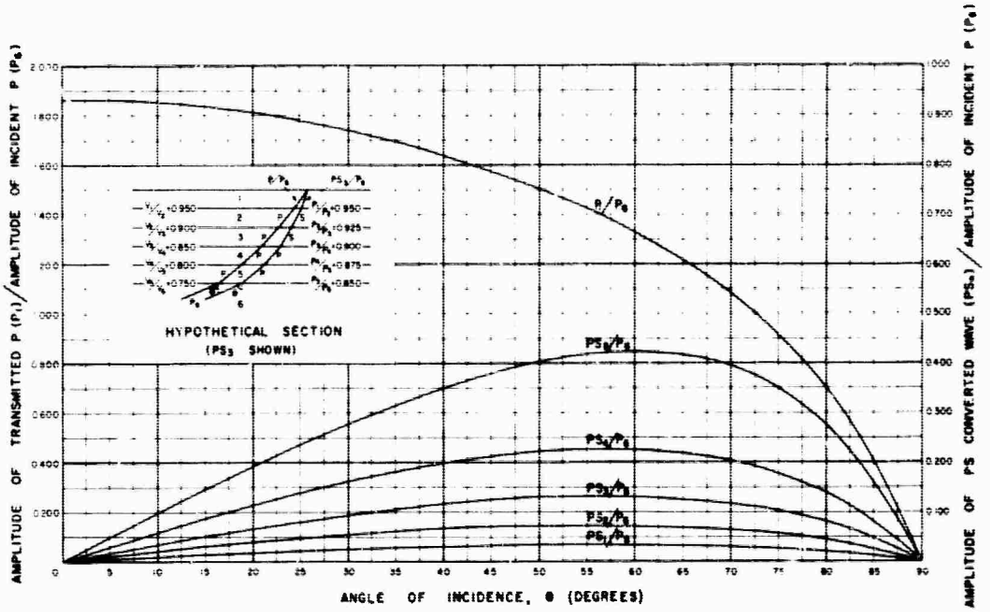

FIG. 19. Hypothetical crustal section in which the velocity ratio (transmitted/incident) decreases with depth. The amplitudes of successive *PS* converted waves successively increase with increasing depth to the interface. Free surface effects are not included. Arrival of PS_3 converted wave is shown in insert.

APPLICATIONS OF DATA

The thickness of a single crustal layer can theoretically be determined by observing, with suitable instrumentation at a single station, the difference in time of arrival of the first *P* wave and the arrival of an *S* wave (a *PS* converted wave) derived from this *P* wave at the base of the layer (Andreev, 1957; Cook and others, 1962). For a multilayered crust, *PS* converted wave arrivals corresponding to each interface will theoretically exist. If the compressional and shear velocities in each of the different layers are known, the thickness of each layer can be computed from the differences in time of arrivals of the parent *P* wave and of the individual *PS* converted waves.

Using seismograms from both earthquakes and blasts, Russian workers (Andreev, 1957, Andreev and Shebalin, 1957, Kuz'mina, 1959) have observed that the amplitudes of the various successive *PS* converted wave arrivals increase with successively increasing depth to the interface where the conversion took place. Bulin

(1960), as well as Schwind and others (1960, p. 3823), find that this is not always true.

A preliminary investigation of the theoretical amplitudes to be expected from *PS* converted waves shows that if the velocity *ratios* (upper medium lower medium) continually decrease with depth, then the amplitudes of successive *PS* converted waves arriving from successively deeper layers *will* continually increase with depth. Figure 19 shows this situation for a hypothetical five-layered crust. The curves were obtained by repeatedly applying the Zoeppritz equations at each interface to obtain

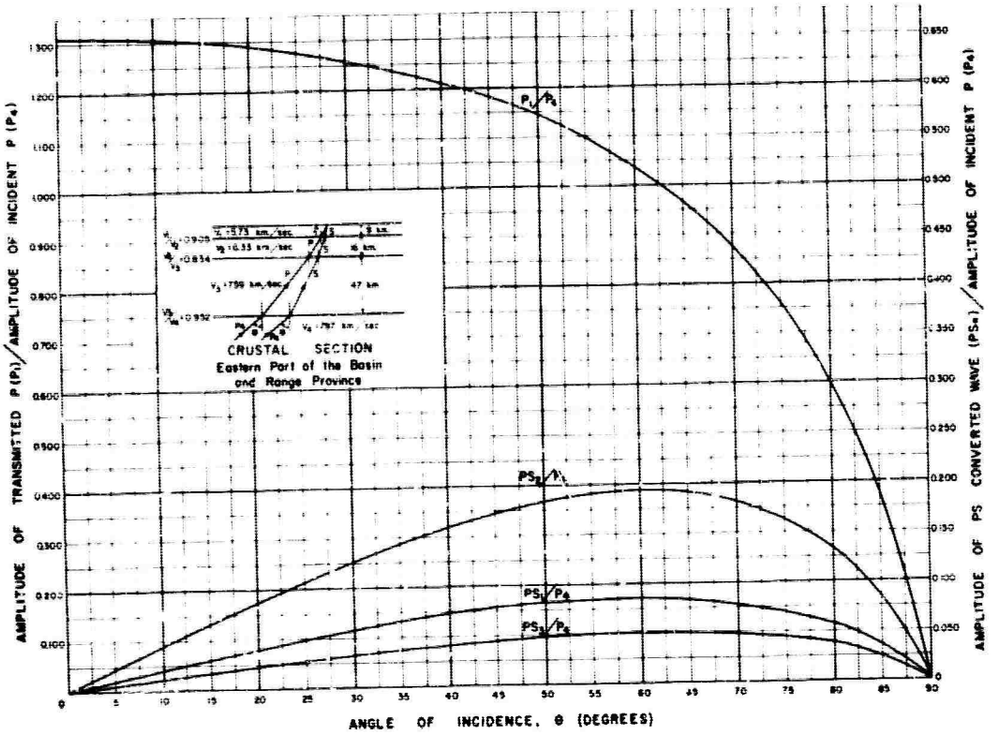

FIG. 20. Crustal section in the eastern part of the Basin and Range province, according to Berg and others (1960). The amplitudes of successive *PS* converted waves do not successively increase with increasing depth to the interface. Free surface effects are not included.

the amplitudes of the various converted waves.[1] The results show that the various *PS* converted wave arrivals should have the largest amplitude when the angle of incidence (θ) of the parent *P* wave at the base of the crustal section is approximately 60 degrees, as indicated in figure 19.[2] Figure 20 shows that for the crustal section as interpreted by Berg and others (1960, figure 10) in Utah, where the velocity ratios do *not* continually decrease with depth, the amplitudes of the PS_2 converted waves are theoretically larger than the amplitudes of the PS_1 waves which in turn are larger than the amplitudes of the PS_3 waves. Figures 19 and 20 do not

[1] In traveling to the surface from the bottom layer (layer 4), the wave designated PS_1 continues as a *P* wave through layers 3 and 2, and converts to an *SV* wave in passing from layer 2 to layer 1 (surface layer); the wave designated PS_3 converts from a *P* to an *SV* wave at the boundary between layers 4 and 3 and continues through layers 3, 2, and 1 as an *SV* wave (See figures 19 and 20).

[2] Additional studies are in progress to ascertain the range of parameters for which this generalization may hold.

include the effects of a free surface on the P and PS arrivals. The general conclusions would remain the same, however, with the amplitudes of both the P and PS arrivals being approximately doubled.

Figures 21 and 22, which include the effects of a free surface, show the ratios of the

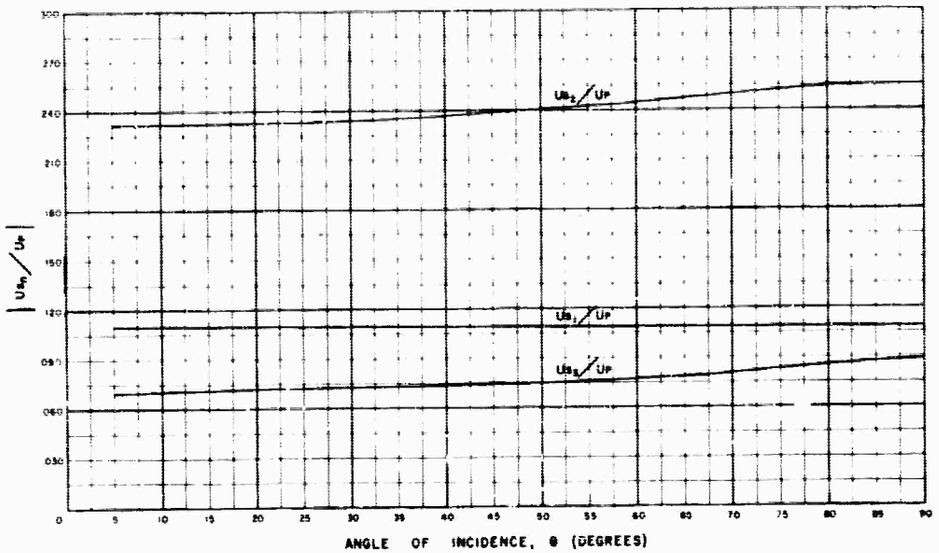

FIG. 21. Ratio of the horizontal component of the ground motion, (U_{s_n}), due to the arrival of PS_n converted waves to the horizontal component of the untransformed transmitted P wave, (U_p), for the crustal section in the eastern part of the Basin and Range province, according to Berg and others (1960), as shown in figure 20. Free surface effects are included.

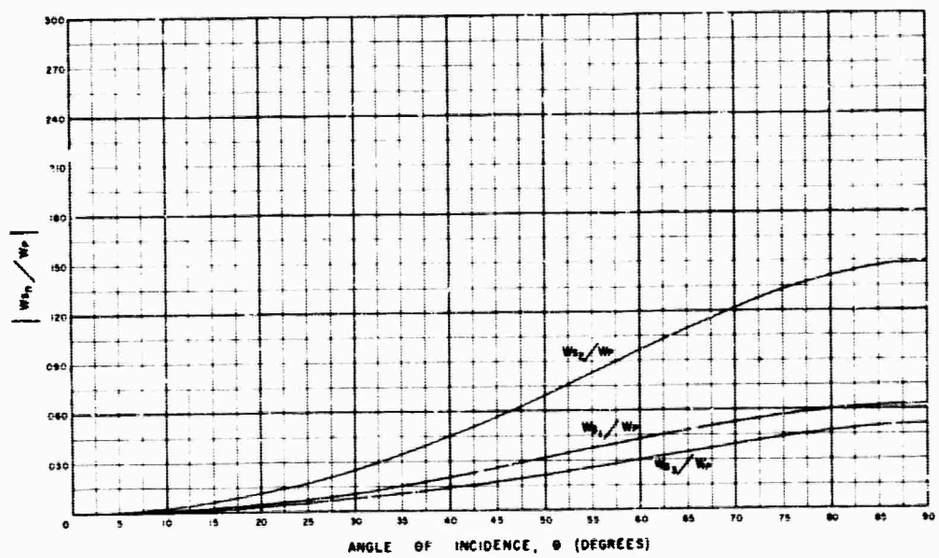

FIG. 22. Ratio of the vertical component of the ground motion, (W_{s_n}), due to the arrival of PS_n converted waves to the vertical component of the untransformed transmitted P wave, (W_p), for the crustal section in the eastern part of the Basin and Range province, according to Berg and others (1960), as shown in figure 20. Free surface effects are included.

magnitudes of the horizontal and vertical components of the ground motion due to the arrivals of the various PS converted waves, to the horizontal and vertical components, respectively, of the untransformed transmitted P wave, for the three-layer crustal section of Berg and others (1960, figure 10). As Slichter (1933, p. 246,

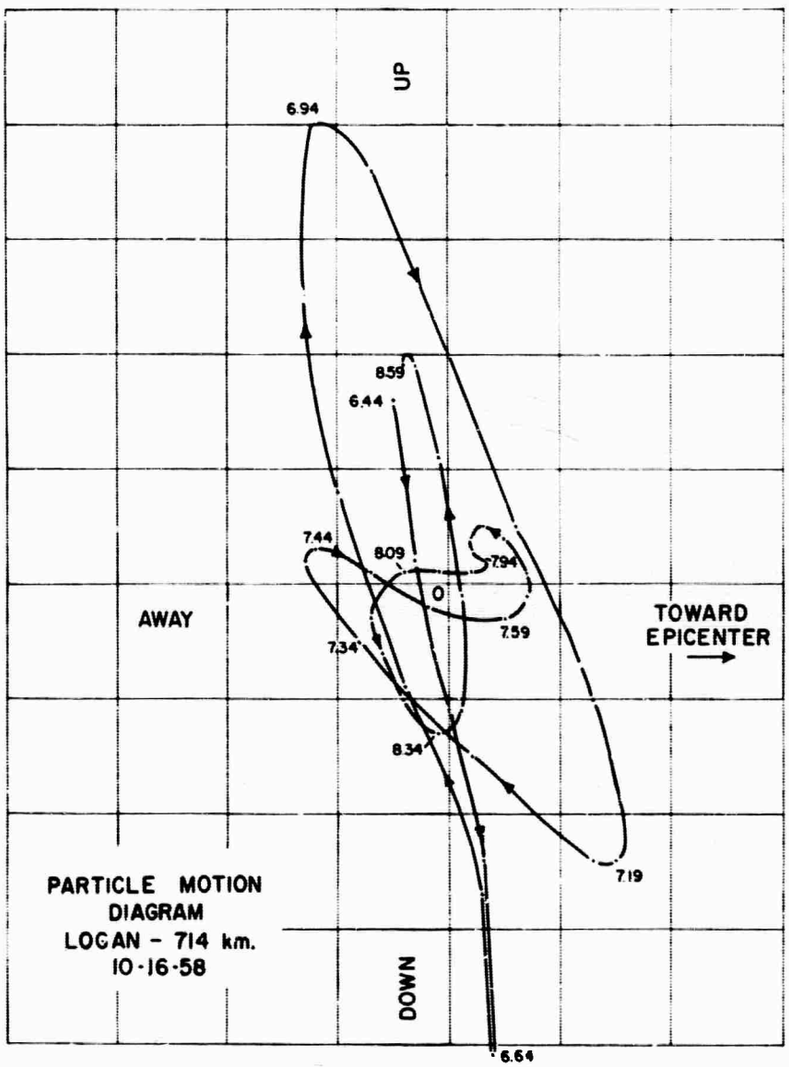

FIG. 23. Particle-motion diagram of the LOGAN nuclear explosion recorded at a distance of 714 km in northern New Mexico with short-period Benioff seismometers. Interval shown is from 6.44 to 8.59 sec after the first motion. Digitizing interval is 0.05 sec.

figure 5, and p. 248) points out, the horizontal ground motion of the PS converted wave with respect to the horizontal ground motion due to the transmitted untransformed parent P wave may be prominent at all epicentral distances, as also shown for PS_2 in figure 21. For the crustal section assumed, the resultant magnitude of these PS converted waves, however, is greatest for angles of incidence of ap-

BLANK PAGE

proximately 60 degrees, corresponding to earthquakes at an epicentral distance of approximately 18 degrees. Bulin (1960, p. 519) noted that *PS* converted waves of maximum amplitude were observed on seismograms of local, deep-focus earthquakes for which the average value of the angle of incidence, θ, at the base of the crust was 56 degrees.

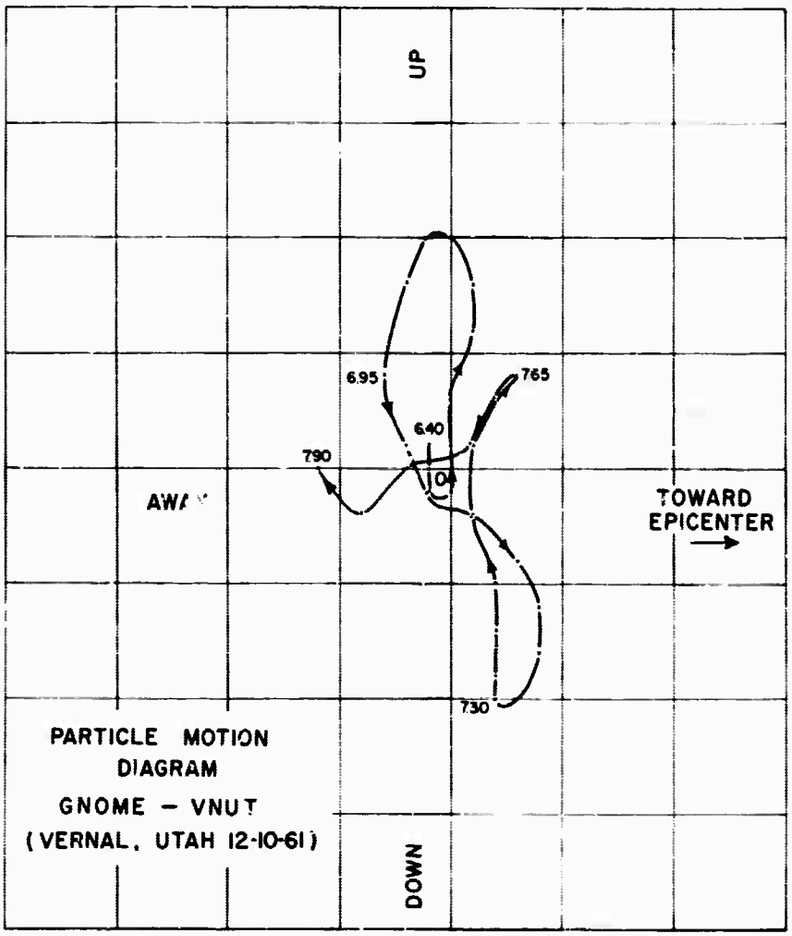

FIG. 24. Particle motion diagram of the GNOME nuclear explosion recorded at Vernal, Utah (VNUT). Interval shown is from 6.40 to 7.90 sec after the first motion. Digitizing interval is 0.05 sec.

Vasil'ev (1956) discusses various *PS* converted waves recorded as a result of explosion seismic work by the Geophysical Institute of the Academy of Sciences of the U.S.S.R. conducted in 1954 in the Tatar A.S.S.R. Vasil'ev found that the wave $P_{123432}S_1$ has slightly lower amplitude than the wave which travelled along the entire path as a longitudinal wave. The indices 1, 2, etc. refer to each layer. He found the amplitude of the converted wave $P_{1234}S_{321}$ to be "at least twice the value of the amplitude of the corresponding longitudinal wave." He noted that these large amplitudes are "to a certain extent" in contradiction with calculated amplitude

values and attributed this to a "partial screening and weakening" of the pure longitudinal waves.

Selected copies of three-component seismograms (made available by Dr. Carl F. Romney) from the underground nuclear explosion LOGAN, near Mercury, Nevada,

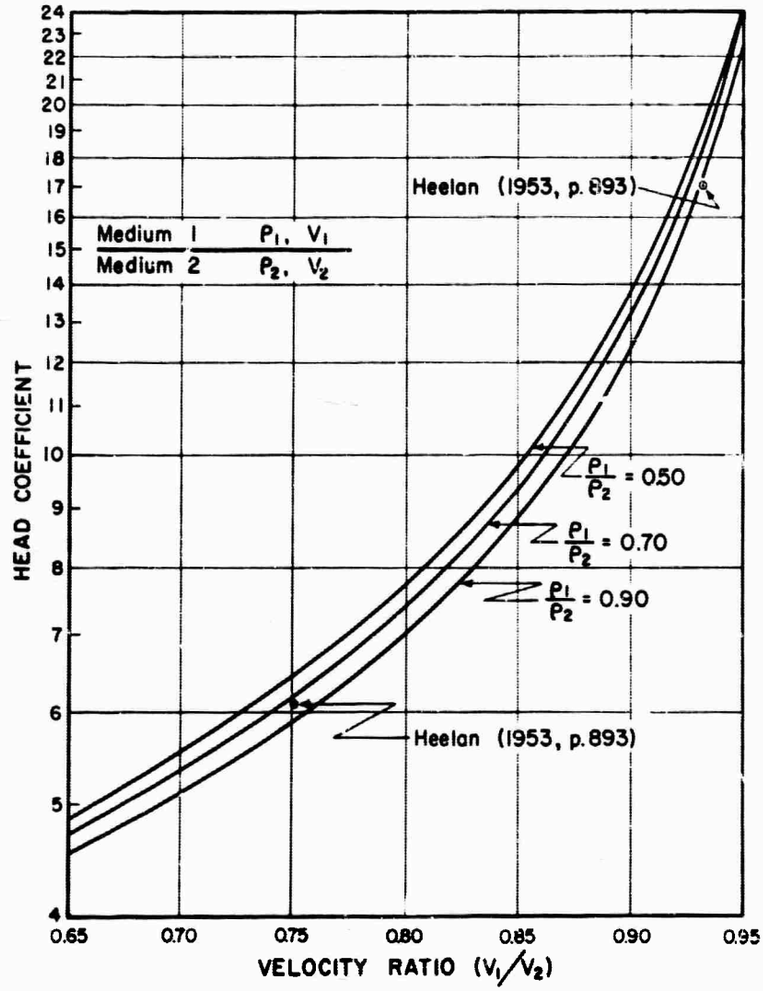

FIG. 25. Head wave coefficients for compressional waves for density ratios (upper medium/lower medium) of 0.50, 0.70 and 0.90 for velocity ratios (upper medium/lower medium) from 0.65 to 0.95, as computed by the method of Zvolinskii (1957, 1958). Two coefficients given by Heelan (1953b, p. 893) are shown for comparison.

which were recorded at temporary field stations out to epicentral distances of 2000 km, were enlarged, and selected intervals were digitized for the study of *PS* converted waves. For the analysis of particle motion, the records were enlarged to a scale of 1 mm = 0.05 sec. These enlargements were then digitized at 1 mm intervals. The resulting data were used to plot particle-motion diagrams in both (1) the vertical plane in a radial direction from the epicenter and (2) the vertical plane transverse to this direction. On a seismogram obtained in northeastern New Mexico

from the LOGAN explosion at an epicentral distance of 714 km, the first ten seconds of arrivals show *P* motion except for an interval of approximately 0.6 sec (see figure 23) which begins 7.5 sec after the first arrival. This interval shows shear motion (predominantly *SV*). Various crustal models used by other workers (Steinhart and Woollard, 1959, p. 347; Werth and others, 1962, p. 1589) in northern Arizona and New Mexico place the Mohorovičić discontinuity at depths ranging from 34 to 57 km. Using velocities found by these investigators for the crust beneath northern Arizona and New Mexico, the time interval of 7.5 sec between the first arrival and the shear arrival could coincide with the arrival of a *PS* converted wave generated at the base of the crust at a depth of approximately 45 km.

Selected events from three-component recordings by the Geotech field recording teams of the underground nuclear explosion GNOME, made available by Dr. Carl F. Romney, were digitized at intervals of 0.05 sec. Particle-motion diagrams were prepared from the data. Station VNUT (Vernal, Utah) shows a single interval of shear motion, which is provisionally interpreted as the arrival of a *PS* converted wave, in the first 10 seconds (7.50 to 7.85 sec) from the GNOME explosion. (See figure 24.)

PS converted waves generated from head waves will have amplitude coefficients as given by Heelan (1953b) and Zvolinskii (1957, 1958). The Zvolinskii method of determining *P*-wave head coefficients was programmed in FORTRAN, and head wave coefficients for density ratios of 0.700, 0.800, and 0.900 were calculated for velocity ratios (compressional velocity in upper medium/compressional velocity in lower medium) ranging from 0.50 to 0.95. These data are shown in figure 25. They suggest that there might be some inherent difficulty in correlating crustal sections as indicated from *PS* converted waves, with those interpreted from conventional seismic refraction travel-time curves. For example, figure 25 shows that the lower the velocity contrast (higher the numerical value of the velocity ratio), the larger will be the amplitude of the head wave. However, high velocity ratios are less efficient for the conversion of *P* to *SV* waves. Conceivably, an interface across which the velocity contrast is low might generate a large amplitude head wave, but result in a *PS* converted wave of amplitude too small to be detected. It might, therefore, be difficult to expect the same information about depths to, and number of, interfaces from both methods.

ACKNOWLEDGMENTS

Messrs. Bongil Jeong and Roy E. Willie, Jr., graduate students in the Department of Geophysics, University of Utah, assisted in the compiling and execution phases of the computer programs. Financial support was provided from research contract No. AF19(628)-201 with the Air Force Cambridge Research Laboratories of the U. S. Air Force under project VELA UNIFORM of the Advance Research Projects Agency of the Department of Defense.

REFERENCES

Andreev, S. S.

1957. "A Study of the Plutonic Structure of the Earth's Crust Using *PS* Exchange Waves Recorded During Earthquakes", *Bull. Akad. Sci USSR*, Geophys. Ser. (*English Transl.*) 1: 22-31.

Andreev, S. S., and N. V. Shebalin

1957. "The Use of Short-period Seismographs for Isolating Exchange Waves on Traces of

Distant Earthquakes", *Bull. Akad. Sci. USSR, Geophys. Ser. (English Transl.)* 7: 109–112.

Berg, J. W., Jr., K. L. Cook, H. D. Narans, Jr., and W. M. Dolan
1960. "Seismic Investigation of Crustal Structure in the Eastern Part of the Basin and Range Province", *Bull. Seism. Soc. Amer.* 50: 511–535.

Berlage, H. P.
1930. "Näherungsformeln zur Berechnung der Amplituden der elastischen Wellen, die beim Durchgang einer gegebenen Welle durch eine Unstetigkeitsfläche entstehen", *Gerlands Beitr. z. Geophysik* 26: 131–140.

Bulin, N. K.
1960. "Determination of the Depth of the Folded Basement with the Aid of Transmitted Exchange Waves of Type PS Recorded in Earthquakes", *Bull. Akad. Sci. USSR, Geophys. Ser. (English Transl.)* 6: 518–521.

Chekin, B. S.
1957. "Wave Form Changes on Reflection and Refraction", *Bull. Akad. Sci. USSR, Geophys. Ser. (English Transl.)* 4: 36–46.

Cook, K. L., S. T. Algermissen, and J. K. Costain
1962. "The Status of PS Converted Waves in Crustal Studies", *J. Geophys. Res.* 67: 4769–4778.

Crout, P. D.
1941. "A Short Method for Evaluating Determinants and Systems of Linear Equations with Real or Complex Coefficients", *Trans. Am. Inst. Elec. Eng.* 60: 1235–1240.

Epinat'eva, A. M.
1957. "Reflected Waves Produced at Angles of Incidence Greater than Critical", *Bull. Akad. Sci. USSR, Geophys. Ser. (English Transl.)* 6: 16–40.

Gutenberg, B.
1944a. "Energy Ratio of Reflected and Refracted Seismic Waves", *Bull. Seism. Soc. Amer.* 34: 85–102.
1944b. "Reflected and Minor Phases in Records of Near-by Earthquakes in Southern California", *Bull. Seism. Soc. Amer.* 34: 137–160.
1952. "*SV* and *SH*", *Trans. Am. Geophys. Union* 33: 573–584.

Haskell, N. A.
1962. "Crustal Reflection of Plane *P* and *SV* Waves", *J. Geophys. Res.* 67: 4751–4767.

Heelan, P. A.
1953a. "Radiation From a Cylindrical Source of Finite Length", *Geophysics* 18: 685–696.
1953b. "On the Theory of Head Waves", *Geophysics* 18: 871–893.

Jeffreys, H.
1926. "The Reflexion and Refraction of Elastic Waves", *Monthly Notices Roy. Astron. Soc. London, Geophys. Suppl.* 1: 321–334.

Jeong, Bongil
1962. *A Study of the Amplitude and Energy of Converted Waves*, M.S. thesis, University of Utah, 45 pp.

Knopoff, L., R. W. Fredricks, A. F. Gangi, and L. D. Porter
1957. "Surface Amplitudes of Reflected Waves", *Geophysics* 22: 842–847.

Knott, C. G.
1899. "Reflexion and Refraction of Elastic Waves, with Seismological Applications", *Phil. Mag. London* 48: 64–97; 567–569.
1910. "Seismic radiations", *Proc. Roy. Soc. Edinb.* 30: 23–37.

Kuz'mina, N. V.
1959. "The Use of Converted Waves in the Study of the Structure of the Earth's Crust in the Southeastern Portions of the Main Caucasus Range", *Bull. Akad. Sci. USSR, Geophys. Ser. (English Transl.)* 7: 734–743.

Macelwane, J. B.
1932. *Introduction to Theoretical Seismology, Part 1: Geodynamics*, St. Louis University, St. Louis, 336 pp.
McCamy, K., R. P. Meyer, and T. J. Smith
1962. "Generally Applicable Solutions of Zoeppritz' Amplitude Equations", *Bull. Seism. Soc. Amer.*, 52: 923–955.
Muskat, M., and M. W. Meres
1940. "Reflection and Transmission Coefficients for Plane Waves in Elastic Media", *Geophysics* 5: 115–148.
Nafe, J. E.
1957. "Reflection and Transmission Coefficients at a Solid-solid Interface of High Velocity Contrast", *Bull. Seism. Soc. Amer.* 47: 205–219.
Richards, T. C.
1960. "Wide Angle Reflections and Their Applications to Finding Limestone Structures in the Foothills of Western Canada", *Geophysics* 25: 385–407.
1961. "Motion of the Ground on Arrival of Reflected Longitudinal and Transverse Waves at Wide-angle Reflection Distances", Geophysics, 26: 277–297.
Richter, C. F.
1958. *Elementary Seismology*, W. H. Freeman and Co., San Francisco, 768 pp.
Schwind, J. J.
1960. *Converted Waves, PS-type, Resulting From Large Explosions*, M. S. thesis, University of Utah, 124 pp.
Schwind, J. J., J. W. Berg, Jr., and K. L. Cook
1960. "*PS* Converted Waves from Large Explosions", *J. Geophys. Res.* 65: 3817–3824.
Slichter, L. B.
1933. "Studies in Reflected Seismic Waves. Part II. Surface Motions Due to Reflections in a Layered Crust", *Gerlands Beitr. z. Geophysik* 38: 239–256.
Slichter, L. B., and V. G. Gabriel
1933. "Studies in Reflected Seismic Waves. Part 1. Some Computations of the Reflection of Seismic Waves at Solid Boundaries", *Gerlands Beitr. z. Geophysik* 38: 228–238.
Steinhart, J. S., T. J. Smith, and R. P. Meyer
1959. "Theoretical Background", *in* "Explosion Studies of Continental Structure", *Carnegie Inst. Washington Pub.* 622, 409 pp.
Steinhart, J. S., and G. P. Woollard
1959. "Seismic Evidence Concerning Crustal Structure", *in* "Explosion Studies of Continental Structure", *Carnegie Inst. Washington Pub.* 622, 409 pp.
Talwani, M., G. H. Sutton, and J. L. Worzel
1959. "A Crustal Section Across the Puerto Rico Trench", *J. Geophys. Res.* 64: 1545–1555.
Vasil'ev, Yu. I.
1957. "Study of Alternating Refracted Waves in Seismic Prospecting", *Bull. Akad. Sci. USSR, Geophys. Ser. (English Transl.)* 3: 30–55.
Wanner, E.
1931. "Beitrage zum Studium der PS-Phase und Mächtigkeit der Molasse unterhalb Zürich", *Gerlands Beitr. z. Geophysik* 32: 231–341.
Werth, G. C., R. F. Herbst, and D. L. Springer
1962. "Amplitudes of Seismic Arrivals from the M. Discontinuity", *J. Geophys. Res.* 67: 1587–1610.
Zoeppritz, Karl
1919. "Über Erdbebenwellen VIIB: Über Reflexion und Durchgang seismischer Wellen durch Unstetigkeitsflaschen", *Nachr. der Königlichen Gesell. d. Wissen. Göttingen math.-phys. Kl.*: 66–84.

Zvolinskii, N. V.
1957. "Reflected and Head Waves Emerging at a Plane Interface of Two Elastic Media—I", *Bull. Akad. Sci. USSR, Geophys. Ser. (English Transl.)* 10: 1–21.
1958. "Reflected Waves and Head Waves Arising at a Plane Interface Between Two Elastic Media—II", *Bull. Akad. Sci. USSR, Geophys. Ser. (English Transl.)* 1: 1–7.

Department of Geophysics
University of Utah
Salt Lake City, Utah
Contribution No. 49

Manuscript received March 28, 1963.

DISCLAIMER NOTICE

THIS DOCUMENT IS THE BEST QUALITY AVAILABLE.

COPY FURNISHED CONTAINED A SIGNIFICANT NUMBER OF PAGES WHICH DO NOT REPRODUCE LEGIBLY.